ANALYSIS OF COMPLEX ELASTIC STRUCTURES BY A RAYLEIGH-RITZ COMPONENT MODES METHOD USING LAGRANGE MULTIPLIERS

by

Larisse Rosentweig Klein

April 1974

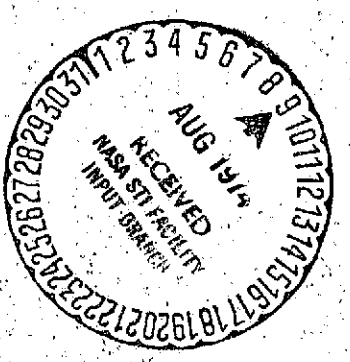

PRINCETON UNIVERSITY

Department of Aerospace and Mechanical Sciences

Aeroelastic and Magnetoelastic Laboratory

AMS Report No. 1159
(NASA Grant 31-001-146)
(Langley Research Center)

I

ANALYSIS OF COMPLEX ELASTIC STRUCTURES BY A RAYLEIGH-RITZ COMPONENT MODES METHOD USING LAGRANGE MULTIPLIERS

by

Larisse Rosentweig Klein

A DISSERTATION
PRESENTED TO THE
FACULTY OF PRINCETON UNIVERSITY
IN CANDIDACY FOR THE DEGREE
OF DOCTOR OF PHILOSOPHY

RECOMMENDED FOR ACCEPTANCE BY THE
DEPARTMENT OF
AEROSPACE AND MECHANICAL SCIENCES

April 1974

ACKNOWLEDGEMENTS

The author wishes to express her deepest appreciation to her faculty advisor, Professor Earl H. Dowell, for his advice and encouragement during the entire course of this study. She also gratefully acknowledges the assistance and valuable comments of Professor Robert H. Scanlan and Dr. Francis C. Moon who are the readers of this dissertation. The author wishes to thank the Zonta International Organization for supporting her research through the Amelia Earhart Fellowship Award of which she was three times a recipient.

The mechanical work in the experimental part was ably carried out by Mr. Michael Hibbs, whose help is very much appreciated. Last but not least the author wishes to express her appreciation to Mrs. Elfriede Takats for her expert typing of the manuscript and to Mr. T. Poly, Miss A. Sichil and Mr. M. Freeman for the drafting of the figures. The thesis carries number 1159 in the records of the Department of Aerospace and Mechanical Sciences. This work was supported in part by NASA Grant NGL-31-001-146, Langley Research Center.

TABLE OF CONTENTS

Chapter		Page
	ACKNOWLEDGEMENTS	i
	TABLE OF CONTENTS	ii
	LIST OF FIGURES	viii
	NOMENCLATURE	xi
I	INTRODUCTION	
	1. Purpose of the study	1
	2. Historical background	2
	3. Statement of the problems	4
II	MODAL BEHAVIOR OF BEAMS WITH NON-UNIFORM PROPERTIES	
	1. Statement of the problem and basic assumptions	8
	2. Theoretical background	9
	3. Derivation of the frequency equation	10
	4. Numerical analysis	22
	a) A simply supported beam of variable geometry	22
	b) A non-uniform helicopter rotor blade (cantilivered beam)	28
	5. Discussion on accuracy and convergence of the method	30
III	MODAL BEHAVIOR OF A SYMMETRIC FLEXIBLE AIRPLANE WITH HIGH ASPECT RATIO BEAM-LIKE COMPONENTS	
	1. Statement of the problem and basic assumptions	34
	2. Rigid body analysis (small amplitude motion about the initial configuration)	35

Chapter		Page
	3. Elastic modal behavior; derivation of the frequency equation	37
	a) Statement of the elastic problem: degrees of freedom, derivation of the constraint equations	37
	b) Derivation of the frequency equation	41
	c) Accuracy of the method	54
	d) Results and convergence study in a check case	63
	4. Experimental work	69
	a) Introduction	69
	b) Experimental model	70
	c) Choice of the optimum supports	71
	d) Experimental setting	72
	e) Frequency measurements	74
	5. Numerical analysis for the experimental model; theoretical results, comparison with the experimental results	
	6. A modal analysis of the Lockhead model L-100 Hercules	82
	a) Presentation of the model	82
	b) Numerical results	83
IV	MODAL BEHAVIOR OF A HIGH ASPECT RATIO AIRPLANE WITH OBLIQUE WING AND TAIL	
	1. Statement of the problem and basic assumptions	89
	2. Rigid body dynamics in the linearized theory	90
	3. Elastic modal behavior, derivation of the frequency equation	92

Chapter		Page
	a) Statement of the elastic problem: degrees of freedom, derivation of the constraint equations	92
	b) Derivation of the frequency equation	94
	c) Remarks on the sensitivity of the natural frequencies with respect to small changes in α from the symmetric configuration	109
	4. Numerical analysis: a pivoting-wing version of the Lockhead model L-100 Hercules	114
	5. Discussion	118
V	THE RAYLEIGH-RITZ COMPONENT MODES METHOD USING LAGRANGE MULTIPLIERS APPLIED TO PLATE PROBLEMS	
	1. Statement of the problem and basic assumptions	120
	2. Lateral vibrations of cantilivered plates	121
	a) Principle of the Method	121
	b) Problem of the constraint conditions	123
	c) Theoretical development; frequency equation	125
	d) Natural frequencies of a square cantilivered plate	134
	3. Vibrations of a rectangular plate with an internal support	136
	a) Principle of the method	137
	b) Lagrangian formulation of the problem, frequency equation	138
	c) Numerical results	141
	d) Conclusion	143

Chapter		Page
V	CONCLUSION AND RECOMMENDED FUTURE WORK	
	1. Conclusions	144
	2. Recommended future work	145
APPENDIX I:	MODAL BEHAVIOR OF NON-UNIFORM CONTINUOUS BEAMS BY A PERTURBATION-GALERKIN METHOD	
	1. Introduction	148
	2. Theoretical development	148
	3. Beams with linear bending stiffness and mass distribution along the span	155
	4. Tapered truncated cantiliver beams with elliptical cross section	159
	5. Conclusion and discussion on the limitations of the method	162
APPENDIX II:	ANALYSIS OF MODAL DAMPING BY COMPONENT MODES METHOD USING LAGRANGE MULTIPLIERS	
	1. Introduction	164
	2. Theoretical development	164
	3. Example	167
	4. Discussion and conclusions	168
APPENDIX III:	FREE VIBRATIONS OF A BEAM CLAMPED IN ITS MIDDLE BY A RAYLEIGH-RITZ METHOD USING LAGRANGE MULTIPLIERS	
	1. Introduction; statement of the problem	169
	2. Modal analysis using even modes of an unconstrained beam	170

Chapter		Page
	3. Modal analysis using antisymmetric modes of an unconstrained beam	172
	4. Discussion	174
APPENDIX IV:	MODAL ANALYSIS OF A FLEXIBLE AIRPLANE WITH LOW ASPECT RATIO WING AND TAIL	
	1. Introduction	176
	2. Modal analysis for motions of the rolling type	177
	3. Modal analysis for motions of the pitching type	185
	4. Discussion of the convergence of the method	191
APPENDIX V:	EFFECT OF THE ELASTIC SUPPORTS ON THE NATURAL FREQUENCIES OF THE EXPERIMENTAL MODEL CONSIDERED IN CHAPTER III	
	1. Introduction	194
	2. Theoretical Development	194
	3. Remark	200
APPENDIX VI:	EFFECT OF THE MASSES AND INERTIAS OF THE ENGINES ON THE NATURAL FREQUENCIES OF THE LOCKHEED L-100 MODEL CONSIDERED IN CHAPTER III	
	1. Introduction	202
	2. Effect of the engines on the rolling natural frequencies	202
	3. Effect of the engines on the pitching natural frequencies	203
	4. Conclusion	207
APPENDIX VII:	EVALUATION OF INTERNAL FORCES (SHEAR AND BENDING MOMENTS) ILLUSTRATED FOR A CANTILIVERED BEAM	

Chapter		Page
	1. Introduction	208
	2. Convergence of $\overline{W}''$ and $\overline{W}'''$ illustrated for a cantiliver beam	209
	3. Generalization and conclusions	211
APPENDIX VIII:	EFFECTS OF FINITE CROSS-SECTIONAL DIMENSIONS ON BEAM INERTIAS AND CONSTRAINT CONDITIONS	213
REFERENCES		217
FIGURES		221
ABSTRACT		273

LIST OF FIGURES

1. Simply supported Beam of Variable Geometry

2. Uniform Beam, First Mode. Convergence of the "Rayleigh-Ritz" Type

3. Uniform Beam. Convergence of the "Rayleigh-Ritz" Type (2nd. Mode).

4. Uniform Beam, Third Mode. Convergence of the "Rayleigh-Ritz" Type.

5. Uniform Beam. Convergence of the "Finite-Element" Type.

6. Uniform Beam. Comparative Convergence in the Fundamental Mode.

7. Simply Supported Uniform Beam. Deflection in the Fundamental Mode.

8. Simply Supported Uniform Beam. Deflection in the Second Mode.

9., 9 bis Stepped Beam Simply Supported at Both Ends. Variation in the Fundamental Frequency with the Thickness Ratio

10. Non-Uniform Cantilivered Helicopter Blade. Fundamental Mode ω_1=4.4 cps.

11. Non-Uniform Cantilivered Helicopter Blade. Second Mode ω_2=24.6 cps.

12. Non-Uniform Cantilivered Helicopter Blade. Third Mode ω_3=61 cps.

13. Check Case of a Cantilivered Beam, Antisymmetric Vibrations. Convergence in the Fundamental Frequency Versus Nb. of Modes Used.

14. Limiting Case ν_1=0, $3.49 \leq \omega_1 \leq 3.66$. First Bending Mode.

15. Limiting Case ν_1=0, $22.11 \leq \omega_2 \leq 22.97$. Second Bending Mode

16. Limiting Case ν_1=0, $61.63 \leq \omega_3 \leq 64.5$. Third Bending Mode.

17. Check Case of a Cantilivered Beam, Symmetric Vibrations and Twisting. Convergence in the Fundamental Mode.

18. Check Case of a Cantiliver Beam in Twisting. Convergence in the Fundamental Mode (extended).

19. Experimental Model.

20. Experimental Model with Supports.

21. Experimental Apparatus

22. Types of Oscillations α and β .

23. Theoretical Results for the Experimental Model. ω = 36.7 cps. Physical Displacements of the Components.

24. Theoretical Results for the Experimental Model. ω = 69 cps. Physical Displacements of the Components.

25. Theoretical Results for the Experimental Model. ω = 125.6 cps. Physical Displacements of the Components.

26. Theoretical Results for the Experimental Model. ω = 295.5 cps. Physical Displacements of the Components.

27. Theoretical Results for the Experimental Model. ω = 404.8 cps. Physical Displacements of the Components.

28. Theoretical Results for the Experimental Model. ω = 536.2 cps. Physical Displacements of the Components.

29. Theoretical Results for the Experimental Model. ω = 546.5 cps. Physical Displacements of the Components.

30. Theoretical Results for the Experimental Model. ω = 643.3 cps. Physical Displacements of the Components.

31. Theoretical Results for the Experimental Model. ω = 648.2 cps. Physical Displacements of the Components.

32. Lockheed L-100 (Civil Hercules)

33. Lockheed L-100 Hercules. Physical Deformations of the Components in the First Mode.

34. Lockheed L-100 Hercules. Physical Deformations of the Components in the Second Mode.

35. Lockheed L-100 Hercules. Physical Deformations of the Components in the Third Mode.

36. Lockheed L-100 Hercules. Physical Deformations of the Components in the Fourth Mode.

37. Concept of a Pivoting-Wing SST for Commercial Operations.

38. Pivoting-Wing Version of the Lockheed L-100 Hercules. Change in the Natural Frequencies Versus Oblicity Angle α.

39. Pivoting-Wing Version of the L-100 Hercules. Physical Displacements in the Fundamental Mode.

40. Pivoting-Wing Version of the L-100 Hercules, Second Mode. Change in the Physical Deformations with the Angle α.

41. Pivoting-Wing Version of the L-100 Hercules, Third Mode.

42. Cantilivered Plate in Transverse Vibrations.

43. Point Clamped Square Plate. Convergence of the Natural Frequencies Towards Those of a Cantiliver Plate.

44. Point Clamped Square Plate. Convergence of the Fundamental Natural Frequency Towards that of a Cantilivered Plate.

45. Point Clamped Square Plate. Convergence of the Second Natural Frequency Towards That of a Cantilivered Plate.

46. Point Clamped Square Plate. Convergence of The Third Natural Frequency Towards That of a Cantilivered Plate.

47. Simply Supported Square Plate with a Line of Internal Support. Change in the Fundamental Frequency With The Support Length.

48. Tapered Cantiliver Beam. Percentage Error in the Fundamental Natural Frequency versus ε.

49. Tapered Cantiliver Beam. Percentage Error in the Second Natural Frequency Versus ε.

50. Tapered Cantiliver Beam. Percentage Error in the Third Natural Frequency Versus ε.

51. Cantilivered Beam. Convergence of the Internal Bending Moment At the Point of Constraint.

52. Cantiliver Beam. Convergence of the Internal Shear Force At the Point of Constraint.

NOMENCLATURE

α	- taper parameter in Appendix I
$A(\xi)$	- cross sectional area of a beam at station ξ
$b(\xi)$	- width of a beam at station ξ
c, c_1, c_2	- half chords of components in Chapters III and IV
D	- bending stiffness of a plate, or damping dissipation function (when specified so)
e	- taper parameter in Appendix I
E	- Young Modulus of Elasticity
$E_i(\varepsilon), F_i(\varepsilon)$	- Functions defined in Appendix I
$f(\xi), g(\xi)$	- Functions defined in Appendix I
G	- shear modulus of elasticity
$h, h(\xi)$	- thickness of a beam or plate structure
H	- thickness ratio of a stepped beam
$\vec{H}$	- angular momentum vector
$\mathbf{I}, \mathbf{I}_1, \mathbf{I}_2$	- mass moments of inertia
I, I_1, I_2	- structural moments of inertia
J, J_1, J_2	- constants, GJ = torsional stiffness
k_i	- bending natural frequency parameter of a free-free beam
k_{mn}	- bending natural frequency parameter of a plate simply supported along all edges
k_n	- bending natural frequency parameter of an unconstrained plate
L, l, l_1, l_2	- linear dimensions of a beam or plate
$\mathcal{L}$	- Lagrangian of the structure
M, M_1, M_2	- masses of beams or plates
$M(\varepsilon), N(\varepsilon)$	- functions defined in Appendix I

N	- number of components of a structure, or number of degrees of freedom considered (when specified so)
$o(1)$, $O(1)$	- Landau's notation
P_n, $P_n^{(1)}$, $P_n^{(2)}$	- generalized coordinates in twisting
$P(\omega)$, $Q(\omega)$	- functions defined in Chapter III
$Q_n, q_n(1), q_n^{(2)}$	- generalized coordinates in bending
R	- number of points at which the constraints are applied
s	- aspect ratio of a plate
S	- structure
t	- time variable
T	- kinetic energy
U	- potential energy
x, y, z	- spatial coordinates
$X_n(x), Y_n(y)$	- bending natural modes of a beam with span along x or y axis, used in Chapter V and Appendix IV
$W(x,t), W(x,y,t)$	- transverse displacement of a beam of plate
α	- oblicity angle in Chapter IV, or type of mode in Chapter III
β	- type of mode (Chapter III)
γ_1, γ_2	- length ratios between components
$\vec{\Gamma}$	- acceleration vector
δ_{np}	- Kronecker symbol
$\delta(x-x_o)$	- Dirac function
$\mathbf{\Delta}(\omega)$	- eigenvalue tensor
$\Delta_{ij}(\omega)$	- elements of the eigenvalue matrix
ϵ	- small parameter
ζ_j	- damping coefficients

ξ, η, ζ	- non-dimensional coordinantes
$\Theta, \Theta_1, \Theta_2$	- twisting angles of the components
$\theta_n(\xi)$	- torsional natural modes of a free-free beam
λ_i	- Lagrange Multipliers
μ_i	- Lagrange Multipliers, or mass ratios (when specified so)
ν	- Poisson ratio
ν_1, ν_2, ν_3	- inertia ratios
ξ_1, ξ_2	- points of connection between fuselage and wing, fuselage and tail
ρ	- mass density of the material
$\phi_n(\xi)$	- bending natural modes of an unconstrained beam
$\Phi_n(x,y)$	- bending natural modes of an unconstrained plate
ψ, θ, ϕ	- Euler angles
Ω, ω	- frequencies of vibration
ω^*	- defined as $\omega/2\pi^2$ (Chapter V)
$(\dot{})$	- time derivative
$(')$, $(''')$	- spatial derivative
$(\bar{})$	- quantity no longer time dependent after harmonic motion has been assumed.
Convergence	of the Rayleigh-Ritz type - convergence analysis for a fixed number of components and a variable number of modes per component.
Convergence	of the Finite Element type - convergence analysis with a fixed number of modes per component; the convergence parameter is the number of components considered.

CHAPTER I

INTRODUCTION

1. Purpose of the study.

The analysis of the modal behavior of an elastic structure, i.e. the determination of its natural frequencies and corresponding normal modes is an important part of the actual design of the structure. The calculation of normal modes is important for several reasons. First, by examining the normal modes obtained and particularly the positions of the nodal lines, it may be possible to tell whether flutter is likely or not, and in any case such an examination will indicate what types of flutter should be investigated. It may also be possible to predict whether there is any likelihood of resonant response vibration, due to the proximity of the natural frequencies to the forcing frequencies of the power plant, gust fields, etc. Further, the normal modes are commonly used for the actual flutter and response calculations. Theoretically, any set of independent, complete deformation modes can be used as degrees of freedom in setting up the flutter equations, but from practical considerations it is suitable to select those modes which give an accurate flutter speed when the number of chosen modes is small. This is more likely to be the case when the modes are related to the actual structure, as the normal modes are, than when arbitrary modes are chosen. An additional reason for using normal modes is that they can later be compared with the resonance - test modes.

It is then understandable that the modal analysis of elastic systems has been given extensive attention in the literature. The

list of the various methods developed for this purpose is much too large to be included here, therefore the next paragraph will review only the main conventional methods that have been used in modal analysis.

2. Historical Background.

The first half of this century has seen a large development of approximate methods for solving the eigenvalue problem for which analytic solutions were impossible. In 1921 Holzer [1] developed a step-by-step method for solving the differential equation of beams in pure torsion; this method was later extended to the case of flexural vibrations by Myklestad [2] in 1944. At about the same time Stodola [3] developed a method of iterative integration for solving the differential equation, while White [4] and Crout [5] focused their interest on finding solutions to the integral equations by numerical integration and collocation [4] or by collocation with assumed functions [5]. In 1939 Grammel [6] developed the Complementary Energy Method which was later introduced by Westergaard [7] and Reissner [8]. Alternatively, Duncan [9, 10] applied Galerkin and Rayleigh-Ritz method to the eigenvalue problems with special polynomial functions used in the series expansions. Various matrix methods were developed in the process: matrix iteration [11], relaxation methods [12], etc.

Some of the aforementioned methods failed to apply to the problems of complex elastic structures: For instance, in a Galerkin method the comparison functions depending upon the spatial coordinates must satisfy the boundary conditions associated with the problem

and this choice would be particularly difficult in the case of a structure such as an airplane. In any case, all the methods that have been mentioned so far suffer from the defects inherent in replacing a structure by a disc te mass system. Duncan has shown by considering the torsion of a uniform cantilever that the error in the frequency, obtained by means of the discrete mass method is inversely proportional to the square of the number of degrees of freedom used. To obtain an accuracy of one per cent it is necessary to use six times as many degrees of freedom as there are desired modes. The accuracy for flexure may be a little better. If an accuracy to within two per cent is to be achieved, then at least four times as many degrees of freedom as there are desired modes should be used for either flexure or torsion.

As a consequence, in the second half of this century most of the effort has been directed towards developing new methods in which the structures will no longer have discrete representations but will be approximated in a continuous manner. Hurty [13, 14] has developed a component modes approach for complex structures through the use of various types of modes: "rigid body modes", "constraint modes" and "normal modes", the latter being usually those of some (artificially) restrained component. Gladwell [15] speaks of "branch modes" which are again those of an artificially restrained component. Wittrick and Williams [37] present an algoritum for computing the natural frequencies of elastic structures if their dynamic stiffness matrix $K(w)$ corresponding to any finite set of

displacements is known. Walton and Steeves [16] present an interesting alternative analysis which deals directly with the equations of motion and constraint. Buckling problems, which are of course, mathematically analogous to free vibration problems,have been investigated by Budiansky [17] and Reissner [18]. Most recently, Dowell has treated the free vibrations of a linear structure with arbitrary support conditions by a Rayleigh-Ritz method introducing the use of Lagrange Multipliers [19], and he applied a similar approach to the free vibrations of an arbitrary structure in terms of component modes [20]. The theoretical analysis presented in this study is developed from the works of Dowell aforementioned.

3. Statement of the Problems.

The intention of the present work is to point out the generality of the Rayleigh-Ritz Component Modes approach using Lagrange Multipliers, by illustrating this method for different types of problems.

In some cases, the problems treated have already been considered in the literature by ad-hoc methods, and their choice was intentional in order to check the method for accuracy. This is the case of the problems treated in Chapters II and V; in other cases the theoretical results obtained are checked with experimental results (e.g. rotor blade problems of Chapter II, beam-like configuration of Chapter III).

Finally, as the method is being proved accurate, new problems are investigated, as the oblique wing configuration of

Chapter IV.

A more detailed statement of the problems is now discussed.

The free vibrations of beams with non uniform properties are the object of Chapter II; in addition to the conventional discrete mass methods already mentioned, almost all the methods developed for this type of problems have been ad-hoc methods. For instance, Cranch and Adler [23] offer an analytic solution for some classes of cantilever beams with rectangular cross section by means of Bessel functions, Conway and Dubil [24] used a similar approach for the study of truncated cone and wedge beams, and many other examples can be found through the literature. The theory presented in Chapter II is valid as well for an arbitrary variation in the beam properties along the span as for an arbitrary set of constraints, or boundary conditions, applying at the edges of the beam. For continuous beams with smooth non-uniform characteristics, an alternative method is developed in Appendix I. It is a perturbation - Galerkin method, particularly suitable for the determination of harmonics above the fundamental.

The Rayleigh-Ritz component modes method using Lagrange multipliers is applied in Chapter III to the free vibrations of a flexible airplane with high aspect ratio components. The earliest theoretical treatments of this problem have been based upon the representation of the aircraft by a system of rigid masses elastically connected, as show the works of Traill-Nash [25, 26] and Hunn [27]; more recently Przemieniecki [28] used the sub-

structure concept with the boundary interaction forces as unknowns in the analysis. An interesting alternative method was presented by Schmitz [29]; the equations of motion of the flexible airplane are written in the form of a nonself-adjoint system (including structural damping), which is then treated by an eigenfunction expansion. Although the analysis presented in Chapter III does not include structural damping, the method can be readily generalized to the non-conservative case. Appendix II provides in fact an analysis of the modal damping, also a Rayleigh Ritz component modes analysis using Lagrange Multipliers.

The study of Chapter IV is motivated by the increasing interest developed in the past recent years for the concept of a yawed wing aircraft. In a recent article [30], R. T. Jones from the NASA Ames Research Center suggested that an oblique wing configuration can be very suitable from an aerodynamic point of view, and encouraged in a more serious investigation of the problem.

The concept was found interesting and resulted in a large number of research proposals from Universities and Companies. The Boeing Company [31] is already engaged in studies concerning the static aeroelastic phenomena associated with the oblique wing aircraft, and Stanford University has submitted a proposal for the investigation of the effects of asymmetry on the dynamic stability of aircraft . As a first step in the aeroelastic analysis, the study of Chapter IV provides the structural material frequencies and normal mods for such configerations.

For straight-wing airplanes where the high aspect ratio assumption for the wing and the tail is not satisfactory, a theoretical treatment is developed in the Appendix IV; the latter components are represented by plates with uniform properties.

As a preliminary analysis, the study of the Chapter V shows how successfully the method applies for the two-dimensional problems of plate vibrations. Two different examples are chosen for this purpose; the first example treats the problem of a point clamped plate and investigates the convergence of the natural frequencies towards those of a cantilivered plate, as given in Reference [35]. This analysis gives insight into the suitable values to be chosen for the parameters (initial nb. of modes used for the plate in x and y - directions, nb. of points of constraint along the plate) so that the natural frequencies obtained by the analysis of Appendix IV, are within a good degree of accuracy.

The second example, which had a recent treatment in the literature [36] by the use of dual series expansions, is the problem of a simply supported plate with an internal rigid line of support. The present method is proven to be very satisfactory for such problems as shown by the convergence graphs obtained in the analysis.

CHAPTER II

MODAL BEHAVIOR OF BEAMS WITH NON-UNIFORM PROPERTIES

1. Statement of the problem and basic assumptions.

The present chapter deals with structures of the beam type, as illustrated below.

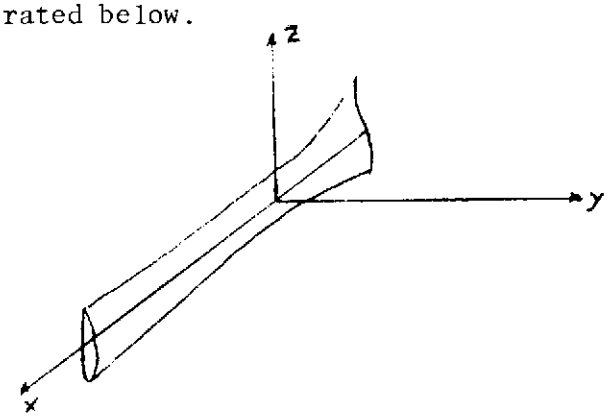

We consider beams of length 2L along the x axis and we denote by E Young modulus of elasticity and by I the structural moment of inertia about the neutral axis,

$$I = \iint_{\text{cross sectional area}} z^2 dy\, dz$$

The bending stiffness EI will be considered variable along the span; the variations can be due to the geometry of the beam (non constant thickness or width), or to variations in the elastic properties (variable E along the span). The theoretical development is general and applies to all the possible cases mentioned above; numerical results are given in some particular cases.

The basic assumptions of the present analysis are the following:

(1) The elastic axis of the unbent beam (as classically defined, Ref. (2)) is a straight line which bends into a plane curve during vibration.

(2) The elastic axis coincides with the line of the centers of gravity of the cross sections, hence bending is uncoupled from twisting.

(3) Initial stress in the axial direction is neglected although conceptually it could be included. An additional term $\frac{T}{2}\int_{-L}^{L} w'^2\,dx$ would appear in the potential energy; the details of the constraint conditions and effects on the distribution of internal shear and bending moment require more study.

(4) The lateral displacements of the beam in vibration are small compared to its thickness and the slope is small compared to unity (this justifies a geometrically linear theory).

(5) The elastic constitutive equations are those of a linear isotropic material, in other words the stress - strain relation is given by Hooke's law.

(6) Shear deflection and rotatory inertia are neglected.

2. Theoretical background.

The problem is considered in a variational formulation ; $w(x,t)$ being the deflection of the beam at time t and station x, its kinetic and potential energies are:

$$T = \frac{1}{2}\int_{-L}^{L} \left(\frac{\partial w}{\partial t}(x,t)\right)^2 dm$$

where dm is the element of mass per unit length.

$$U = \frac{1}{2} \int_{-L}^{L} EI(x) \left(\frac{\partial^2 w}{\partial x^2}(x,t) \right)^2 dx$$

When EI has a complicated dependence on x, the last integral is very difficult to handle.

The present method proposes a solution to the problem by conceptually disassembling the structure into sub-beam components of uniform bending stiffness.

The rigourous justification of this approach is based on the mathematical approximation of a continous function defined on a compact set by step functions, in the following manner:

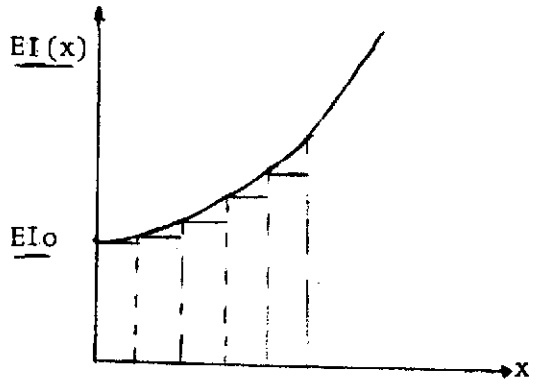

For each of the substructures, the modal displacements are sought in a Rayleigh Ritz expansion and the continuity conditions are enforced by means of Lagrange multipliers.

3. Derivation of the frequency equation.

The following notations are now introduced:

$(EI)^{(n)}$: constant bending stiffness of the nth. component, n=1, N

$M^{(n)}$: half mass of the nth component

$\ell^{(n)}$: half length of the nth component

$dm^{(n)}$: element of mass/unit length relatif to the nth component

$w^{(n)}(x,t)$: bending displacement of the nth component

k_i : non dimensional frequency parameter of a free-free beam of uniform stiffness.

$\phi_i(x)$: corresponding normal mode (free-free beam)

$q_i^{(n)}(t)$: generalized coordinate of the nth component relative to the normal mode number i.

The modal solutions are sought in the form:

$$w^{(n)}(x,t) = \sum_{i=1}^{\infty} q_i^{(n)}(t)\ \phi_i(x) \qquad (1)$$

$$\text{for} \quad -\ell^{(n)} \leq x \leq \ell^{(n)}$$

Subsequently, the total kinetic energy of the structure is:

$$T = \frac{1}{2} \sum_{n=1}^{N} \int_{-\ell^{(n)}}^{\ell^{(n)}} \dot{w}^{(n)2}(x,t)\ dm^{(n)} \qquad (2)$$

By substitution of eq (1) and use of the orthonormal properties of the free-free beam modes, (2) can be written in the form:

$$T = \frac{1}{2} \sum_{n=1}^{N} \sum_{i=1}^{\infty} M^{(n)}\ \dot{q}_i^{(n)2}(t) \qquad (3)$$

Similarly, the potential energy of the entire beam is:

$$U = \frac{1}{2} \sum_{n=1}^{N} (EI)^{(n)} \int_{-\ell^{(n)}}^{\ell^{(n)}} \left(\frac{\partial^2 w^{(n)}}{\partial x^2}(x,t) \right)^2 dx$$

Substitution of eq (1) and use of elementary beam equation yields:

$$U = \frac{1}{2} \sum_{n=1}^{N} \sum_{i=1}^{\infty} \frac{(EI)^{(n)}}{\ell^{(n)3}}\ k_i^4\ q_i^{(n)}(t)^2 \qquad (4)$$

The beam-components are required to satisfy the following continuity conditions:

a) continuity of the bending displacements at the interfaces:

$$w^{(p)}(\ell^{(p)}) = w^{(p+1)}(-\ell^{(p+1)}) \quad (5) \qquad \text{where } \ell^{(p)} = -\ell^{(p+1)}$$

b) continuity of the slopes:

$$\frac{\partial}{\partial x} w^{(p)}(\ell^{(p)}) = \frac{\partial}{\partial x} w^{(p+1)}(-\ell^{(p+1)}) \qquad (6)$$

At this point it has to be pointed out how convenient is the choice of the free-free beam modes as "trial" functions in the Rayleigh Ritz expansion.

In addition to the fact that they allow a great flexibility in expressing the various constraint conditions, their choice satisfies already the continuity of the second and third derivative of the $w^{(n)}$ at the connection points.

In the case in which the initial beam is not free at both ends, corresponding additional constraints have to be added, as illustrated in section 4.b)

For the time being, the initial beam will be considered unconstrained without loss in generality.

Equations (5) and (6) can be written after suitable non-dimensionalization:

$$w^{(p)}(\ell) = w^{(p+1)}(-1)$$

for $p = 1, \ldots .N-1$

$$\frac{1}{\ell^{(p)}} w'^{(p)}(1) = \frac{1}{\ell^{(p+1)}} w'^{(p+1)}(-1)$$

and further, by use of eq (1):

$$\sum_{i=1}^{\infty} q_i^{(p)}(t)\ \phi_i(1) - q_i^{(p+1)}(t)\ \phi_i(-1) = 0 \qquad (7)$$

$$\sum_{i=1}^{\infty} q_i \frac{(p)}{\ell^{(p)}}(t)\ \phi'_i(1) - q_i \frac{(p+1)}{\ell^{(p+1)}}(t)\ \phi'_i(-1) = 0 \qquad (8)$$

$p = 1, \ldots N-1$

Subsequently, the Lagrangian of the structure is:

$$\mathcal{L} = \frac{1}{2} \sum_{n=1}^{N} \sum_{i=1}^{\infty} M^{(n)} \dot{q}_i^{(n)}(t)^2 - \frac{1}{2} \sum_{n=1}^{N} \sum_{i=1}^{\infty} \frac{(EI)^{(n)} k_i^4 q_i^{(n)}(t)^2}{\ell^{(n)3}}$$

$$+ \sum_{n=1}^{N-1} \sum_{i=1}^{\infty} \lambda n \left(q_i^{(n)}(t)\phi_i(1) - q_i^{(n+1)}(t)\ \phi_i(-1)\right) +$$

$$\sum_{n=1}^{N-1} \sum_{i=1}^{\infty} \mu n \left(q_i \frac{(n)}{\ell^{(n)}}(t)\ \phi'_i(1) - q_i \frac{(n+1)}{\ell^{(n+1)}}(t)\ \phi'_i(-1)\right)$$

where λ_n, μ_n are Lagrange multipliers. (9)

It is interesting to note at this point that through the use of the Lagrange multipliers as they appear in (9), the present method gives not only information about the modal behavior of the beam, but in addition provides results for shear forces and bending

moments.

Indeed, it is known in Classical Mechanics that the Lagrange multipliers can be physically interpreted as being the generalized forces demanded for the maintenance of the corresponding constraint conditions. In the present case, the values of the λ_n and μ_n, n=1,...N=1 give respectively the distribution of the shear force and the distribution of the bending moment along the span of the beam at the points of constraint.

The Lagrange's equations derived from (9) are:

- $$M^{(1)} \ddot{q}^{(1)}(t) + \frac{(EI)^{(1)}}{\ell^{(1)\,3}} k_i^4 q_i^{(1)}(t) - \lambda_1 \phi_i(1) - \frac{\mu_1}{\ell^{(1)}} \phi'_i(1) = 0$$

- $$M^{(n)} \ddot{q}_i^{(n)}(t) + \frac{(EI)^{(n)}}{\ell^{(n)3}} k_i^4 q_i^{(n)}(t) - \lambda_n \phi_i(1) +$$

$$\lambda_{n-1} \phi_i(-1) - \frac{\mu_n}{\ell^{(n)}} \phi'_i(1) + \frac{\mu_{n-1}}{\ell^{(n)}} \phi'_i(-1) = 0$$

$$n = 2, \ldots . N-1$$

- $$M^{(N)} \ddot{q}^{(N)}(t) + \frac{(EI)^{(N)}}{\ell^{(N)3}} k_i^4 q_i^{(N)}(t) + \lambda_{N-1} \phi_i(-1) +$$

$$\frac{\mu_{N-1}}{\ell^{(N-1)}} \phi'_i(-1) = 0$$

- $$\sum_{i=1}^{\infty} q_i^{(n)}(t) \phi_i(1) - q_i^{(n+1)}(t) \phi_j(-1) = 0 \qquad n=1,\ldots N-1$$

$$\sum_{i=1}^{\infty} \frac{q_i^{(n)}(t)}{\ell^{(n)}} \phi'_i(1) - \frac{q_i^{(n+1)}(t)}{\ell^{(n+1)}} \phi'_i(-1) = 0 \qquad n=1,\ldots N-1$$

The last two equations are in fact the constraint equations expressing the continuity of the displacements and slopes.

The following harmonic time dependence is assumed in the modal analysis:

$$q_i^{(n)}(t) = \bar{q}_i^{(n)} e^{i\sqrt{\frac{EI^{(1)}}{\mu^{(1)}\ell^{(1)4}}}\omega t}$$

$$\lambda_n(t) = \bar{\lambda}_n \frac{(EI)^{(1)}}{\ell^{(1)3}} e^{i\sqrt{\frac{EI^{(1)}}{\mu^{(1)}\ell^{(1)4}}}\omega t}$$

$$\mu_n(t) = \bar{\mu}_n \frac{(EI)^{(1)}}{\ell^{(1)2}} e^{i\sqrt{\frac{EI^{(1)}}{\mu^{(1)}\ell^{(1)4}}}\omega t}$$

and the following notations are introduced:

$$m_n = \frac{M^{(1)}}{M^{(n)}} \quad ; \quad \gamma_n = \frac{\ell^{(1)}}{\ell^{(n)}}$$

$$\psi_n = \frac{\frac{(EI)^{(n)}}{M^{(n)}\ell^{(n)3}}}{\frac{(EI)^{(1)}}{M^{(1)}\ell^{(1)3}}} \quad ; \quad F_i^{(1)} = \omega^2 - k_i^4$$

$$F_i^{(n)} = \omega^2 - \psi_n k_i^4 \qquad n=2\ldots N$$

As a first step in solving the Lagrange's equations, the generalized coordinates are expressed in terms of the Lagrange Multipliers from the equations of motion per se;

$$\bar{q}_i^{(1)} = - \frac{\bar{\lambda}_1 \phi_i(1) + \bar{\mu}_1 \phi'_i(1)}{F_i^{(1)}} \qquad (10)$$

$$\bar{q}_i^{(n)} = - m_n \left(\frac{\bar{\lambda}_n \phi_i(1) - \bar{\lambda}_{n-1} \phi_i(-1) + \gamma_n \bar{\mu}_n \phi'_i(1) - \gamma_{n-1} \mu_{n-1} \phi'_i(-1)}{F_i^{(n)}} \right) \qquad (11)$$

$$\bar{q}_i^{(N)} = m_N \frac{F_i}{} \left(\bar{\lambda}_{N-1} \phi_i(-1) + \gamma_{N-1} \bar{\mu}_{N-1} \phi'_i(-1) \right) \qquad (12)$$

Then (10), (11), (12) are used in the constraint equations in order to obtain a set of 2N-2 linear algebraic equations in terms of the unknown $\bar{\lambda}_n$ and $\bar{\mu}_n$. This set of eigenvalue equations is now written for convenience in matrix form:

$$\Delta(\omega) \cdot \vec{\lambda} = 0 \qquad (13)$$

where $\vec{\lambda}$ is the 2N-2 dimensional vector having for components $\bar{\lambda}_n$ (n=1, ...N-1) and $\bar{\mu}_n$ (n=1, ...N-1) and $\Delta(\omega)$ is the symmetric matrix of order 2N-2 defined by its elements Δ_{nm} as follows:

• n=1:

$$\Delta_{1\,1} = \sum_{i=1}^{\infty} \left(\frac{\phi_i^2(1)}{F_i(1)} + m_2 \frac{\phi_i^2(-1)}{F_i(2)} \right)$$

$$\Delta_{1\,2} = - \sum_{i=1}^{\infty} m_2 \frac{\phi_i(1)\,\phi_i(-1)}{F_i}$$

$$\Delta_{1\,m} = 0 \qquad 3 \leq m \leq N-1$$

$$\Delta_{1\,N} = \sum_{i=1}^{\infty} \left(\frac{\phi_i(1)\phi'_i(1)}{F_i(1)} + m_2 \gamma_2 \frac{\phi_i(-1)\,\phi'_i(-1)}{F_i(2)} \right)$$

$$\Delta_{1\,N+1} = - \sum_{i=1}^{\infty} m_2 \gamma_2 \frac{\phi'_i(1)\,\phi_i(-1)}{F_i(2)}$$

$$\Delta_{1\,m} = 0 \qquad N+2 \leq m \leq 2N-2 \qquad (N>4)$$

• n = 2, ... N-2

$$\Delta_{n\,m} = 0 \qquad 1 \leq m \leq n-2$$

$$\Delta_{n\,n-1} = - \sum_{i=1}^{\infty} m_n \frac{\phi_i(1)\,\phi_i(-1)}{F_i(n)}$$

$$\Delta_{n\,n} = \sum_{i=1}^{\infty} \left(m_n \frac{\phi_i^2(1)}{F_i(n)} + m_{n+1} \frac{\phi_i^2(-1)}{F_i(n+1)} \right)$$

$$\Delta_{n\ n+1} = -\sum_{i=1}^{\infty} m_{n+1}\ \phi_i\frac{(1)\ \phi_i(-1)}{F_i^{(n+1)}}$$

$$\Delta_{n\ m} = 0 \qquad n+2 < m < N+n\ 3$$

$$\Delta_{n\ N+n-2} = -\sum_{i=1}^{\infty} m_n \gamma_n \frac{\phi_i(1)\phi'_i(-1)}{F_i^{(n)}}$$

$$\Delta_{n\ N+n-1} = \sum_{i=1}^{\infty} \left(m_n \gamma_n\ \phi_i \frac{(1)\phi'_i(1)}{F_i^{(n)}} + m_{n+1}\ \gamma_{n+1}\frac{\phi'_i(-1)\phi_i(-1)}{F_i^{(n+1)}} \right)$$

$$\Delta_{n\ N+n} = -\sum_{i=1}^{\infty} m_{n+1}\ \gamma_{n+1}\frac{\phi'_i(1)\phi_i(-1)}{F_i^{(n+1)}}$$

$$\Delta_{n\ m} = 0 \qquad n+N+1 \le m \le 2N-2$$

- $n = N-1$

$$\Delta_{N-1\ m} = 0 \qquad 1 \le m \le N-3 \qquad (N \ge 4)$$

$$\Delta_{N-1\ N-2} = -\sum_{i=1}^{\infty} m_{N-1}\frac{\phi_i(1)\phi_i(-1)}{F_i^{(N-1)}}$$

$$\Delta_{N-1\ N-1} = \sum_{i=1}^{\infty} \left(m_{N-1}\frac{\phi_i^2(1)}{F_i^{(N-1)}} + m_N\frac{\phi_i^2(1)}{F_i^{(N)}} \right)$$

$$\Delta_{N-1\ m} = 0 \qquad N \le m \le 2N-4$$

$$\Delta_{N-1\ 2N-3} = - \sum_{i=1}^{\infty} m_{N-1}\,\gamma_{N-1}\ \phi_i\frac{(1)\ \phi'_i(-1)}{F_i^{(N-1)}}$$

$$\Delta_{N-1\ 2N-2} = \sum_{i=1}^{\infty}\left(m_{N-1}\,\gamma_{N-1}\,\phi_i\frac{(1)\ \phi'_i(1)}{F_i^{(N-1)}} + m_N\,\gamma_N\phi_i\frac{(-1)\phi'_i(-1)}{F_i^{(N)}}\right)$$

- $\underline{m = N}$

$$\Delta_{N\ m} = \Delta_{m\ N} \quad \text{already defined for } 1\leq m\leq N-1$$

$$\Delta_{N\ N} = \sum_{i=1}^{\infty}\left(\frac{\phi'^{2}_i(1)}{F_i^{(1)}} + m_2\gamma_2^2\ \frac{\phi'^{2}_i(-1)}{F_i^{(2)}}\right)$$

$$\Delta_{N\ N+1} = - \sum_{i=1}^{\infty} m_2\gamma_2^2\ \frac{\phi'_i(1)\phi'_i(-1)}{F_i^{(2)}}$$

$$\Delta_{N\ m} = 0 \qquad N+2<m<2N-2$$

- $\underline{n = N+1,\ \ldots\ 2N-3}$; $p = n-N+1$

$$\Delta_{n\ m} = \Delta_{mn} \quad \text{already defined for } 1<m<N \ ;\ N+1<n<2N-3$$

$$\Delta_{n\ p} = \sum_{i=1}^{\infty}\left(m_p\gamma_p\ \phi_i\frac{(1)\phi'_i(1)}{F_i^{(p)}} + m_{p+1}\gamma_{p+1}\ \frac{\phi_i(-1)\phi'_i(-1)}{F_i^{(p+1)}}\right)$$

$$\Delta_{n\ p+1} = -\sum_{i=1}^{\infty} m_{p+1}\,\gamma_{p+1}\,\frac{\phi_i(1)\phi'_i(-1)}{F_i^{(p+1)}}$$

$$\Delta_{n\ m} = 0 \qquad p+2 < m < p+N-3$$

$$\Delta_{n\ N+p-2} = -\sum_{i=1}^{\infty} m_p\,\gamma_p^2\,\frac{\phi_i(1)\phi'_i(1)}{F_i^{(p)}}$$

$$\Delta_{n\ N+p-1} = \sum_{i=1}^{\infty}\left(m_p\,\gamma_p^2\,\frac{\phi'^2_i(1)}{F_i^{(p)}} + m_{p+1}\,\gamma_{p+1}^2\,\frac{\phi'^2_i(-1)}{F_i^{(p+1)}}\right)$$

$$\Delta_{n\ N+p} = -\sum_{i=1}^{\infty} m_{p+1}\,\gamma_{p+1}^2\,\frac{\phi'_i(1)\ \phi'_i(-1)}{F_i^{(p+1)}}$$

$$\Delta_{n\ m} = 0 \qquad N+p+1 < m < 2N-2$$

$$\Delta_{2N-2\ 2N-2} = \sum_{i=1}^{\infty}\left(m_{N-1}\,\gamma_{N-1}^2\,\frac{\phi'^2_i(1)}{F_i^{(N-1)}} + m_N\,\gamma_N^2\,\frac{\phi'^2_i(-1)}{F_i^{(N)}}\right)$$

Equation (3) leads to the frequency equation

$$\boxed{\det\ (\Delta\ (\omega)\ ) = 0} \qquad (14)$$

which is the necessary and sufficient condition for existence of

solutions $\bar{\lambda}_n$, $\bar{\mu}_n$ $n = 1,....N-1$

This equation cannot be solved analytically except maybe for very small values of N ; numerically, the fastest and simplest method to use is a trial and error approach. The left hand side of the equation (14) is plotted against the variable ω ; if two successive values of ω make the left hand side of (14) change sign, then one of the natural frequencies should be between these two ω's.

This is a quite straight forward operation except for the fact that care should be taken to decide whether the change in sign corresponds to a valid solution (i.e. a natural frquency of the beam) or to a natural frequency of one of the components. Such types of situations are illustrated below:

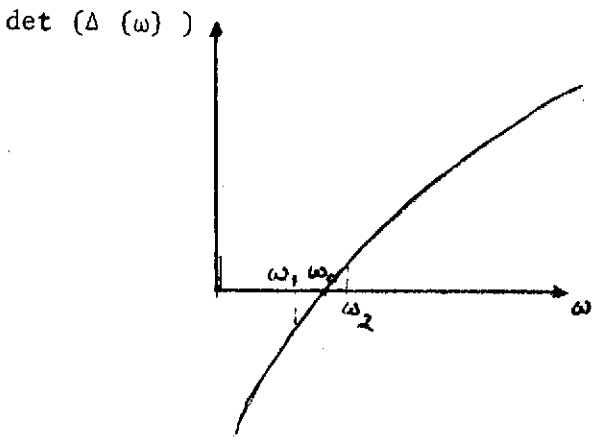

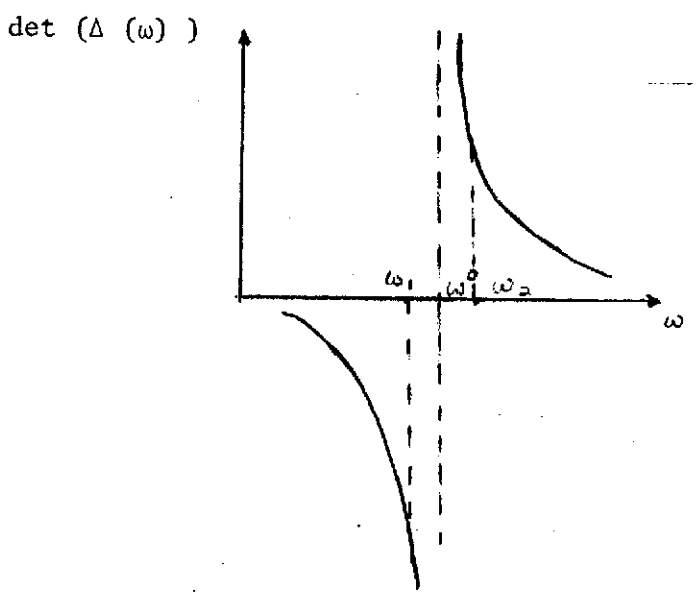

The accuracy of the natural frequency can be made as high as necessary, provided that the 2 successive ω's are close enough and

that the values of the left hand side of equation (14) are close to zero.

For each natural frequency the Lagrange multipliers are then determined from equation (13) up to multiplicity, for instance the ratios $\frac{\chi_n}{\lambda_1}$ n=2,...N-1 and $\frac{\mu_n}{\lambda_1}$ n=1,...N-1

can be determined.

Subsequently the generalized coordinates for each component are determined from eqs. (10), (11), (12) and then the corresponding mode shape as given by equation (1).

4. Numerical analysis.

a) A simply supported beam of variable geometry.

The present analysis treats the case of a stepped beam, simply supported at each end as shown in Figure 1.

The variation in the bending stiffness is due to the variation in the thickness of the beam and the geometry of the problem suggests to consider two components. As mentioned previously, the theory extends to the cases where the initial beam is constrained at the ends; in the present problem two additional constraint conditions have to be reinforced, namely

$$w^{(1)}(-l_1) = 0$$

$$w^{(2)}(l_2) = 0$$

For the sake of simplicity it is assumed that $l_1 = l_2$ and that

the cross - sections of the beam are rectangular, without great loss in the generality of the problem. The analysis is developed in two steps: the first step provides a check on the method for accuracy and convergence, the second step provides the functional dependence of the fundamental frequency with the ratio $\frac{h^{(2)}}{h^{(1)}}$.

In the particular case in which $\frac{h^{(2)}}{h^{(1)}} = 1$, the problem reduces to that of a uniform beam simply supported at the two ends for which the modal behavior is known analytically; in particular the first three non-dimensional frequency parameters are $\omega_1 = \pi^2$, $\omega_2 = 4\pi^2$, $\omega_3 = 9\pi^2$. In a first analysis, the convergence of the natural frequencies of the beam towards the above values versus the number of modes used per component has been investigated, and the numerical results are presented below in tabulated form:

Table 1: First natural frequency

# modes used per component	total # of modes	ω_1	percentage error
3	6	11.94	21.6%
4	8	11.05	12 %
6	12	10.16	3 %
8	16	9.918	0.5%
10	20	9.898	0.2%

Table 2: Second natural frequency

# modes used per component	total # of modes	ω_2	percentage error
3	6	53.68	36.7%
4	8	45.01	14.9%
6	12	41.06	4.7%
8	16	39.835	0.9%
10	20	39.64	0.4%

Table 3: Third natural frequency

# modes used per component	total # of modes	ω_3	percentage error
3	6	151.89	71 %
4	8	103.93	17 %
6	12	94.16	6.3 %
8	16	90.25	1.58%
10	20	89.71	0.87%

The results given in Table 1 are plotted in Figure 2; it can be seen that the first natural frequency converges rapidly towards π^2 and that the rate of convergence is very steep especially at the begining. Figure 3 represents a graph of the percentage error in ω_2 versus the number of modes used per component; it can be seen by extrapolation that in order to reach the accuracy in ω_1 corresponding to 10 modes per component, it is necessary to consider in

this case two additional modes for each segment.

Figure 4 provides a picture of the rate of convergence in the third mode; in this case 14 modes are needed per component in order to reach an accuracy of 0.2%.

This analysis is somewhat similar to the convergence analysis in the classical Rayleigh Ritz method; moreover all the numerical natural frequencies obtained are higher that the exact frequencies. Another important convergence parameter is N (the number of components into which the structure is conceptually disassembled); the rate of convergence versus N in the fundamental mode has been investigated in the check case of the uniform beam. The results are shown in Figure 5; 3 free-free modes are used for each component. Although the graph shows rapid convergence, the results cannot be interpreted in a self-contained manner. The reason is that even with a fixed number of modes per component, the fact of increasing N has the effect of increasing the total number of modes considered and hence of improving the convergence.

As a consequence, the total number of modes considered has to be chosen as a common parameter although it is not controlled directly in the method. The comparative rate of convergence is shown in Figure 6; it can be seen that for the same total number of modes, better results are obtained when for a fixed number of components (N=2) the number of free-free modes per component gets larger. The reason in this case is that there is "no need" in fact to increase the number of components and thus making N>2 adds no physical improve-

ment. From the numerical point of view, increasing the number of modes corresponds to simpler operations than increasing the number of components. By considering additional modes per component we are only increasing the number of terms in the series giving the $\Delta ij\ (\omega)$, while an additional number of components correspond to an increase in the size of the matrix $\Delta\ (\omega)$.

Operations of the first type are handled by computer with higher accuracy than computations of determinants for instance, for large size matrices.

It should be mentioned that the present convergence analysis applies only to this check case and therefore gives only an insight to how the convergence problem should be handled; general conclusions about convergence will be developed in the next paragraph.

The study of the case $\frac{h^{(2)}}{h^{(1)}} = 1$ is completed by Figure 7 and 8. Figure 7 shows the first mode shape and the orders of magnitude of the shear force per unit length and bending moment per unit length at the mid-point; Figure 8 shows similar results for the second mode. There is very good agreement with the classical sinusoidal shapes. This concludes the study of the check case; in the second part of the analysis the change in the fundamental frequency with the thickness ratio is investigated.

The values of the non-dimensional frequency parameter ω_1 are plotted versus the ratio $H = \frac{h^{(1)}}{h^{(2)}}$ in Figure 9.

For $h^{(1)} > h^{(2)}$ the frequency parameter is based on the character-

istics of the first component, for $h^{(1)} < h^{(2)}$ ω_1 is based on the characteristics of the second component. The reason for this choice will appear clearly as we proceed.

The Figure shows that for $h^{(1)} > h^{(2)}$, as H increases the fundamental frequency decreases from the value 9.898 (i.e. π^2) to zero. The first value correspond to the previous analysis, the second value correspond to the limiting case of a uniform beam simply supported at one end and free at the other. In this limiting case the fundamental frequency is zero and corresponds to a rigid body rotation of the structure. The monotonic variation of ω_1 with H checks our physical intuition; given the two beams illustrated below:

it is expected that the resonant frequencies of the right-most beam be lower than the frequencies of the beam at its left. The configurations for which $h^{(1)} < h^{(2)}$ correspond to the previous configurations by mirror-symmetry and hence the physical resonant frequencies should be the same for two beams of respectives thickness ratios Ho and $\frac{1}{Ho}$.

If we switch the "reference beams" on which the material frequencies are based, the same argument holds for the non-dimensional frequency parameters and this provides additional checking for the method and numerical work. This is the reason for which the fundamental frequency parameter ω_1 is based on different components in Figure 9.

The Figure shows very good correspondence of the frequencies in the mapping of [1, ∞] into [1, o].

An additional checking of the quantitative results of Figure 9 can be made by considering Figure 9 (bis). The variation in ω_1 based on $h^{(1)}$ is represented as function of $H = \frac{h^{(1)}}{h^{(2)}}$ and it is seen that for H = 0 the obtained uniting value for ω_1 is 15.6. This limiting case is that of a uniform beam simply supported at one end and clamped at the other, for which the first natural frequency has the exact value of 15.418; i.e. only 1.2% lower than the numerical value predicted by the method.

b) A non-uniform helicopter rotor blade (cantilivered beam).

The choice of the present model is related to a more general investigation of the effects of distributed blade properties on the stability of hingeless rotors, done by Professor Dowell and Professor Curtiss at Princeton University for the NASA Ames Research Center.

This project is of recent interest (1973) and includes extensive theoretical and experimental developments.

In the first part of the investigation, the main interest has been focused upon a theoretical study of the structural modeling and determination of natural frequencies of a rotor blade with large changes in stiffness distribution. The classical Rayleigh Ritz method using an assumed Duncan polynomial shape (Ref.(38)) fails to give accurate results if the blade non-uniformity is severe; therefore the results of the method developed in the present chapter will be

compared to the results of a more accurate method developed by Professor Dowell, which is an initial value approach to boundary value problems (IVBV). An experimental value of the fundamental natural frequency is also available. The non-uniform rotor blade under consideration has the following characteristics:

Total length: 48 inches

Span	bending stiffness	mass per unit length
0 - 4 in	3×10^6 lb x in^2	0.52×10^{-3} lb x sec^2/in^2
4 -14 in	24,400 lb x in^2	0.66×10^{-4} lb x sec^2/in^2
14 -48 in	3,276 lb x in^2	0.35×10^{-4} lb x sec^2/in^2

The fundamental natural frequency of this blade predicted by different methods is given below:

	Rayleigh Ritz method using Duncan polynomials	Myklestad	IVBV (Ref. (49))	Component modes using Langrange mult.	Experiment
ω_1	6.7 cps.	4.45 cps.	4.36 cps.	4.37 cps.	4.4 cps.

The IVBV and component modes method using Lagrange multipliers are seen to provide the most accurate results and shall be considered for further comparing the next two resonant frequencies. A summary of the numerical results is given below in tabulated form.

Natural frequency	Prediction of the component modes-Lagrange	Prediction of IVBV (Ref.(49))	Percentage disagreement
fundamental	4.37 cps.	4.36 cps.	0.23%
second	24.6 cps.	24.2 cps.	0.16%
third	61 cps.	59.3 cps.	1.12%

The fundamental mode shape is shown in Figure 10 as predicted by both IVBV and CML methods; the figure shows good quantitative agreement - the largest deviation of 0.07% occurs at around 31 in. from the clamped end. Similar results are shown in Figures 11 and 12 for the second and the third mode.

5. Discussion on accuracy and convergence of the method.

The question which most naturally arises when the method is to be applied to an engineering problem is that of the optimal choice of the number of components and of the number of modes per component, in order to obtain good numerical results with minimum computational effort. It is obvious that no general answer including all possible cases can be given to this question; furthermore the complexity of the problem is such that for most of the cases of interest there is no analytical answer.

The purpose of this paragraph is to develop a two-step procedure that can be called "modes-component selection" in order to provide a satisfactory answer to the above question.

The procedure is illustrated on an arbitrary case.

The stiffness distribution along the beam span is assumed to vary as follows:

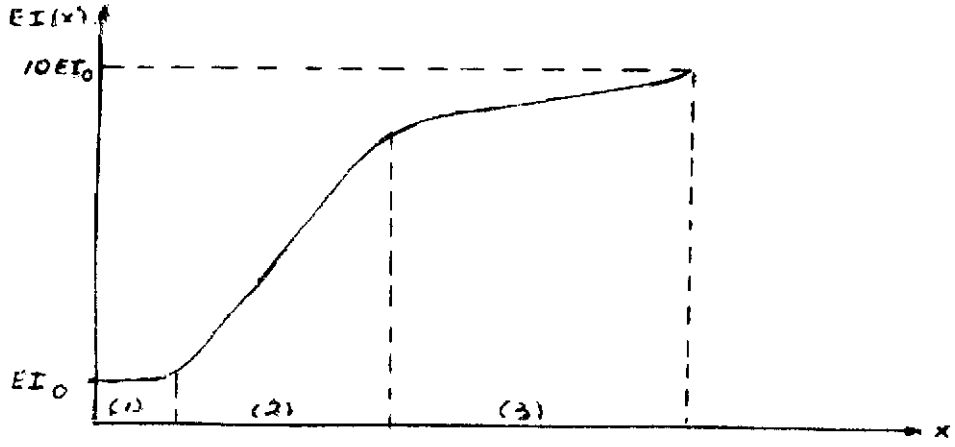

The method consists in:

(1) Determining first an order of magnitude of the natural frequencies.

For this purpose few components are considered (in order to keep the size of the eigenvalue matrix small) with no restriction on the number of modes per component. The number of components is directly related to the rate of change of $EI(x)$; for instance region (1) can very well be represented by only one component, region (3) could have similar representation within reasonable approximation, but more than one component should be used in region (2).

For the purpose of obtaining only orders of magnitude of the frequencies, two or three components should suffice in region (2). Thus in a first analysis a 4 or 5 components approximation is taken for the initial beam, which keeps the size of the matrix $\mathbf{A}$ of the order of 6 or 8.

Additional saving in computer time can be made by noticing that the component in region (3) is much stiffer than the other components Thus most of the bending will occur in regions (1) and (2); region (3) is expected to have predominantly rigid behavior. As a consequence, less free-free modes need to be used for that component than for the others.

The orders of magnitude of the natural frequencies are now determined, and we proceed to the second step.

(2) Improving the solution in the neighborhood of each natural frequency.

This is realized by first improving the modelling of the beam,

i.e. increasing the number of components in regions (2) and (3) for instance.

A reasonable way of improvement would be for example to consider about **six** components in region (2) and two components in region (3). At this point the size of the eigenvalue matrix is increased and thus more computer time is needed. A way of compensating for this disadvantage is to make use of the information provided in the previous analysis in order to decrease the number of modes used per component to the strict minimum needed.

The selection of the modes which are to be used for each component is made on the basis of the order of magnitude of the corresponding natural frequencies compared to the orders of magnitude found in the previous analysis.

Such a selection can decrease the number of modes used quite considerably without any significant loss in accuracy.

Mathematically, this selection can be justified by the fact that only the reasonably small $F_i^{(n)}$ are to be kept in the analysis. Their inverses provide the main contribution for the expression of the $\Delta_{ij}(\omega)$ and hence for the frequency equation.

It can be anticipated that if problems of non-uniform plates were to be treated, a more accurate solution would be obtained by increasing the number of components rather than the number of modes per component. The reason is that generally only approximate numerical solutions are known for the modes of an unconstrained plate and that the precision decreases as the modes get higher. Therefore it

is better to increase the total number of degrees of freedom for the plate by increasing the number of componens rather than considering higher (approximate) modes.

CHAPTER III

MODAL BEHAVIOR OF A SYMMETRIC FLEXIBLE AIRPLANE WITH HIGH ASPECT RATIO BEAM-LIKE COMPONENTS.

1. Statement of the problem and basic assumptions

The type of structure considered in this chapter is a flexible airplane with a high aspect ratio wing.

There are many various possible models which can represent such a structure, every one of these presents advantages and inconveniences. When the problem is modeled very close to reality, the components are represented by fairly complicated elastic structures for which the normal modes and frequencies are only known with a certain degree of approximation. These initial errors propagate up to the final result and there is no guarantee that the modal behavior is determined more accurately in such analysis. On the other hand if a simpler mathematical model is chosen to represent the structure, the natural frequencies and mode shapes can be determined more accurately but the resemblance between the physical and the mathematical problem may be slight. The choice between the two alternatives has been made on the basis of simplicity and clarity of the formulation and taking into account the fact that the errors due to physical simplifying assumptions are easier to determine than mathematical errors propagating with the computations. Therefore a simple mathematical model has been chosen to represent the problem. The aircraft is considered to be made of substructures (fuselage, wing, tail) which have been approximated by beams of uniform stiffness as illustrated in the following

figure:

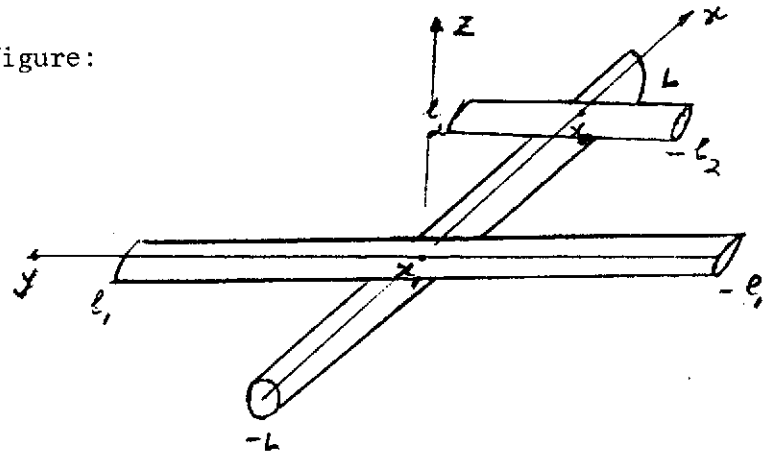

If "yawing-type" motions (i.e. bending in the y-direction) were to be considered the rudder should be included as well; for our purpose (transversal bending of the structure), it has been neglected.

The basic assumptions are summarized below:

(1) The airplane structure is considered to be of the beam type.

(2) The displacements of the beam components are governed by the classical one-dimensional equations (in particular, Bernoulli-Euler equation for the lateral bending).

(3) The geometrical and elastic characteristics are constant along the span for each component. This last assumption can be relieved using the approach of Chapter II.

2. Rigid body analysis (small amplitude motion about the initial configuration)

Notations:

R_o: Gallilean frame of reference

G: Center of gravity of the structure

$\vec{\Gamma}(G/R_o)$: Acceleration of the center of gravity with respect to R_o

ψ: yaw angle in the rigid motion

θ: roll angle in the rigid motion

ϕ: pitch angle in the rigid motion

(ψ, θ, ϕ are the classical Euler angles)

$\vec{H}$ $((S)/R_o)$: angular momentum of the structure with respect to R_o

I_1, I_2, I_3: principal moments of inertia

In absence of exterior forces Newton's law yields.

$$(\text{total mass}) \cdot \vec{\Gamma}\,(G/R_o) = \vec{0} \tag{15}$$

This relation decouples the translations in the three directions from the rotation motion abound the center of gravity.

For zero exterior torque the angular momentum equation is simply:

$$\frac{d}{dt} \vec{H}\,((S)/R_o) = \vec{0} \tag{16}$$

Because of the symmetry of the structure, $\vec{x}$ $\vec{y}$ $\vec{z}$ are principal axis of inertia with respectif moments of intertia I_1, I_2, I_3 and therefore the linearized equations of motion of the rigid body are:

$$I_1 \ddot{\theta} = 0 \tag{17}$$

$$I_2 \ddot{\phi} = 0 \tag{18}$$

$$I_3 \ddot{\psi} = 0 \tag{19}$$

This set of equations shows that the roll, yaw and pitch motions are all decoupled from each other and that the corresponding natural frequencies are zero.

The same type of considerations apply in the elastic domain because of the symmetry, as will be seen in paragraph 3.

The study of the decoupled motion of "yaw-type" is not included in the present analysis, as mentioned before.

3. Elastic modal behavior ; derivation of the frequency equation

a) Statement of the elastic problem:

degrees of freedom, derivation of the constraint equations

As the motions investigated are of both roll and pitch type, each of the substructures has to be allowed to undergo transverse bending and twisting as well. Although it is sufficient to consider only rigid twisting for each component, the analysis will be developed for the general case in which the torsional stiffness of each conponent is finite. The previous case will then be a simplification of the latter.

We develop a Rayleigh Ritz analysis by defining:

- for the fuselage: $-L \leq x \leq L$

The bending displacement $W(x, t)$ sought in the form:

$$W(x, t) = \sum_{n=1}^{\infty} Q_n(t)\, \phi_n(x) \tag{20}$$

The twisting angle $\Theta(x, t)$ sought likewise:

$$\Theta(x, t) = \sum_{n=1}^{\infty} P_n(t)\, \theta_n(x) \tag{21}$$

- for the wing: $-\ell_1 \leq y \leq \ell_1$

The bending displacement $W_1(y, t)$:

$$W_1(y, t) = \sum_{n=1}^{\infty} q_n^{(1)}(t)\, \phi_n(y) \tag{22}$$

The twisting angle $\Theta_1 (y, t)$:

$$\Theta_1 (y, t) = \sum_{n=1}^{\infty} P_n^{(1)} (t) \quad \theta_n (y) \tag{23}$$

- <u>for the tail</u>: $\quad -\ell_2 \leq y \leq \ell_2$

The bending displacement $W_2 (y, t)$:

$$W_2 (y, t) = \sum_{n=1}^{\infty} q_n^{(2)} (t) \quad \phi_n (y) \tag{24}$$

The twist angle $\Theta_2 (y, t)$:

$$\Theta_2 (y, t) = \sum_{n=1}^{\infty} P_n^{(2)} (t) \; \theta_n (y) \tag{25}$$

The physical displacement of each component, respectively at $y = + c$, $x = x_1 + c_1$, $x = x_2 - x_1 + c_2$, is given by:

$$W_{phys} (x, t) = W (x, t) + c \; \Theta (x, t) \tag{26}$$

$$W_{phys} (y, t) = W_1 (y, t) + c_1 \quad \Theta_1 (y, t) \tag{27}$$

$$W_{phys} (y, t) = W_2 (y, t) + c_2 \quad \Theta_2 (y, t) \tag{28}$$

Where c, c_1, c_2 are the half chords of the respectif components.

With suitable non-dimensionalization $x = L \xi$ eq. (26) yields:

$$\underline{W_{phys\ (\xi,t)}}_{L} = \underline{W_{(\xi,t)}}_{L} + \underline{c}_{L} \quad \Theta (\xi, t) \tag{29}$$

and by similar changes of variables

$y = \ell_1 \eta$ and $y = \ell_2 \eta$ for equations (27) and (28) respectively, they become:

$$\frac{W_{1\,\mathrm{phys}}(\eta, t)}{\ell_1} = \frac{W_1(\eta, t)}{l_1} + \frac{c_1}{l_1}\,\Theta_1(\eta, t) \qquad (30)$$

and

$$\frac{W_{2\,\mathrm{phys}}(\eta, t)}{\ell_2} = \frac{W_2(\eta, t)}{l_2} + \frac{c_2}{l_2}\,\Theta_2(\eta, t) \qquad (31)$$

In agreement with the one-dimensional treatment of each substructure, it can be assumed that $\frac{c}{L}$, $\frac{c_1}{l_1}$ and $\frac{c_2}{l_2}$ are negligibly small,

in fact small enough so that

$$\frac{c}{L}\,\Theta(\xi, t) \ll 1 \quad \text{for any } \xi \qquad -1 \leq \xi \leq 1$$

$$\frac{c_1}{l_1}\,\Theta_1(\eta, t) \ll 1 \quad \text{for any } \eta \qquad -1 \leq \eta \leq 1$$

$$\frac{c_2}{l_2}\,\Theta_2(\eta, t) \ll 1 \quad \text{for any } \eta \qquad -1 \leq \eta \leq 1$$

As a consequence, the corresponding second terms will be neglected on the right hand side of equations (29), (30), (31). The physical displacements at the joints between the components must be equal, and this leads mathematically to the constraint conditions:

$$W_{\mathrm{phys}}(\xi_1, t) = W_{1\,\mathrm{phys}}(0, t) \qquad (32)$$

$$W_{phys}\ (\xi_2,\ t) = W_{2\ phys}\ (0,\ t) \tag{33}$$

or, by using (29), (30), (31):

$$W\ (\xi_1,\ t) = W_1\ (0,\ t) \tag{34}$$

$$W\ (\xi_2,\ t) = W_2\ (0,\ t) \tag{35}$$

The equality between the slopes in the $\vec{x}$ and $\vec{y}$ directions has also to be enforced as part of the constraint conditions and leads to the equations:

$$\Theta\ (\xi_1,\ t) = \frac{1}{\ell_1}\ \frac{\partial W_1}{\partial \eta}\ (o,\ t) \tag{36}$$

$$\Theta\ (\xi_2,\ t) = \frac{1}{\ell_2}\ \frac{\partial W_2}{\partial \eta}\ (0,\ t) \tag{37}$$

for the continuity of the slope in the x - direction, and similarly

$$\frac{1}{L}\ \frac{\partial W}{\partial \xi}\ (\xi_1,\ t) = -\ \Theta_1\ (0,\ t) \tag{38}$$

$$\frac{1}{L}\ \frac{\partial W}{\partial \xi}\ (\xi_2,\ t) = -\ \Theta_2\ (0,\ t) \tag{39}$$

for the continuity of the slope in the y - direction.

b) Derivation of the frequency equation

The total kinetic energy of the structure is

$$T = \frac{1}{2}\left(\int_{-L}^{L} \dot{W}^2(x, t)\, dm + \int_{-L}^{L} \mathbf{I}\, \dot{\Theta}^2(x, t)\, dx + \int_{-\ell_1}^{\ell_1} \dot{W}_1^2(y, t)\, dm_1\right.$$

$$+ \int_{-\ell_1}^{\ell_1} \mathbf{I}_1\, \dot{\Theta}_1^2(y, t)\, dy + \int_{-\ell_2}^{\ell_2} \dot{W}_2^2(y, t)\, dm_2$$

$$\left. + \int_{-\ell_2}^{\ell_2} \mathbf{I}_2\, \dot{\Theta}_2^2(y, t)\, dy\right) \qquad (40)$$

where $\mathbf{I}$, $\mathbf{I}_1$, $\mathbf{I}_2$ are the fuselage, wing and tail mass moments of inertia per unit length about the torsional axis. In particular

$$\mathbf{I} = \rho_{fus} \iint_{\substack{\text{fuselage}\\ \text{cross-section}}} (y^2 + z^2)\, dy\, dz$$

$$\mathbf{I}_1 = \rho_{wing} \iint_{\substack{\text{wing}\\ \text{cross-section}}} (x^2 + z^2)\, dx\, dz$$

$$\mathbf{I}_2 = \rho_{tail} \iint_{\substack{\text{tail}\\ \text{cross-section}}} (x^2 + z^2)\, dx\, dz$$

By substitution of the corresponding expansions for each of the bending and angular displacements and because of the orthonormal

property of the bending and twisting modes, equation (40) becomes:

$$T = \frac{1}{2}\left(M \sum_{n=1}^{\infty} \dot{Q}_n^2(t) + I L \sum_{n=1}^{\infty} \dot{p}_n^2(t) + M_1 \sum_{n=1}^{\infty} \dot{q}_n(1)^2(t)\right.$$

$$\left. + I_1 \ell_1 \sum_{n=1}^{\infty} \dot{p}_n(1)^2(t) + M_2 \sum_{n=1}^{\infty} \dot{q}_n(2)^2(t) + I_2 \; 2 \sum_{n=1}^{\infty} \dot{p}_n(2)^2(t)\right) \quad (41)$$

where

M, M_1, M_2 are the half masses of the fuselage, wing and tail respectively (i. e. mass/unit length x half length)

Likewise, the total potential energy is the sum of the potential energies of the components:

$$U = \frac{1}{2}\left[EI \int_{-L}^{L} \left(\frac{\partial^2 W}{\partial x^2}\right)^2 dx + GJ \int_{-L}^{L} \left(\frac{\partial \Theta}{\partial x}\right)^2 dx + \right.$$

$$(EI)_1 \int_{-\ell_1}^{\ell_1} \left(\frac{\partial^2 W_1}{\partial y^2}\right)^2 dy + (GJ)_1 \int_{-\ell_1}^{\ell_1} \left(\frac{\partial \Theta_1}{\partial y}\right)^2 dy +$$

$$\left. (EI)_2 \int_{-\ell_2}^{\ell_2} \left(\frac{\partial^2 W_2}{\partial y^2}\right)^2 dy + (GJ)_2 \int_{-\ell_2}^{\ell_2} \left(\frac{\partial \Theta_2}{\partial y}\right)^2 \right] \quad (42)$$

where

I, I_1, I_2 are the corresponding structural moments of inertias about the neutral axes given by

$$I = \iint_{\substack{\text{fuselage} \\ \text{cross section}}} z^2 \, dy \, dz$$

$$I_1 = \iint_{\substack{\text{wing}\\ \text{cross-section}}} z^2 \, dx \, dz$$

$$I_2 = \iint_{\substack{\text{tail}\\ \text{cross-section}}} z^2 \, dx \, dz$$

E and G are the Young and shear modulus of elasticity (related by $G = \frac{E}{2(1+\nu)}$) and J is a constant which value depends upon the shape of the beam's cross-section.

In particular, useful values of J are tabulated in Ref. (39). (GJ) is the classical twisting stiffness.

By expansion of the bending and angular displacements and use of the corresponding beam equation, equation (42) leads to:

$$U = \frac{1}{2}\left(\frac{EI}{L^3} \sum_{n=1}^{\infty} k_n^4 Q_n^2(t) + \frac{GJ}{L} \sum_{n=1}^{\infty} (n-1)^2 \frac{\pi^2}{4} P_n^2(t) + \right.$$

$$\frac{(EI)_1}{\ell_1^3} \sum_{n=1}^{\infty} k_n^4 q_n^{(1)2}(t) + \frac{(GJ)_1}{\ell_1} \sum_{n=1}^{\infty} (n-1)^2 \frac{\pi^2}{4} P_n^{(1)2}(t) +$$

$$\left. \frac{(EI)_2}{\ell_2^3} \sum_{n=1}^{\infty} k_n^4 q_n^{(2)2}(t) + \frac{(GJ)_2}{\ell_2} \sum_{n=1}^{\infty} (n-1)^2 \frac{\pi^2}{4} P_n^{(2)2}(t) \right) \quad (43)$$

The constraint conditions have been previously derived and they are given by equations (34), (35), (36), (37), (38), (39). Substitution

of the displacements in terms of the component modes yields:

$$\sum_{n=1}^{\infty} \left(Q_n(t)\, \phi_n(\xi_1) - q_n^{(1)}(t)\, \phi_n(0)\right) = 0 \tag{44}$$

$$\sum_{n=1}^{\infty} \left(Q_n(t)\, \phi_n(\xi_2) - q_n^{(2)}(t)\, \phi_n(0)\right) = 0 \tag{45}$$

$$\sum_{n=1}^{\infty} \left(P_n(t)\, \theta_n(\xi_1) - q_n \frac{^{(1)}(t)}{\ell_1}\, \phi'_n(0)\right) = 0 \tag{46}$$

$$\sum_{n=1}^{\infty} \left(P_n(t)\, \theta_n(\xi_2) - q_n \frac{^{(2)}(t)}{\ell_2}\, \phi'_n(0)\right) = 0 \tag{47}$$

$$\sum_{n=1}^{\infty} \left(\frac{Q_n(t)}{L} \phi'_n(\xi_1) + P_n^{(1)}(t)\, \theta_n(0)\right) = 0 \tag{48}$$

$$\sum_{n=1}^{\infty} \left(\frac{Q_n(t)}{L}\, \phi'_n(\xi_2) + P_n^{(2)}(t)\, \theta_n(0)\right) = 0 \tag{49}$$

The Lagrangian of the total elastic system is then:

$$L = T - U + \sum_{i=1}^{6} \lambda_i \times (i^{\text{th}} \text{ constr. equation}) \tag{50}$$

where T and U are given by equations (41) and (43).

As mentioned in Chapter II, the Lagrange Multipliers provide effective information, namely:

λ_1 and λ_2 give the shear forces developed at the joint between the fuselage and wing and at the joint between the fuselage and tail respectively, in motions of plunging type.

λ_3 and λ_4 give the torque developed at the two joints respectively,

in motions of rolling type.

λ_5 and λ_6 provide similar information for motions of pitching type.

By use of equations (41), (43), (44) - (49), equation (50) leads to the Lagrange's equations

$$M \ddot{Q}_n(t) + \frac{EI}{L^3} k_n^4 Q_n(t) - \lambda_1 \phi_n(\xi_1) - \lambda_2 n(\xi_2) - \frac{\lambda_5}{L} \phi'_n(\xi_1) - \frac{\lambda_6}{L} \phi'_n(\xi_2) = 0 \qquad (51)$$

$$I L \ddot{P}_n(t) + \frac{(GJ)}{L} (n-1)^2 \frac{\pi^2}{4} P_n(t) - \lambda_3 \Theta_n(\xi_1) - \lambda_4 \Theta_n(\xi_2) = 0 \qquad (51 \text{ bis})$$

$$M_1 \ddot{q}_n^{(1)}(t) + \frac{(EI)_1}{\ell_1^3} k_n^4 q_n^{(1)}(t) + \lambda_1 \phi_n(0) + \frac{\lambda_3}{\ell_1} \phi'_n(0) = 0 \qquad (52)$$

$$I_1 \ell_1 P_n^{(1)}(t) + \frac{(GJ)_1}{\ell_1} (n-1)^2 \frac{\pi^2}{4} P_n^{(1)}(t) - \lambda_5 \theta_n(0) = 0 \qquad (53)$$

$$M_2 \ddot{q}_n^{(2)}(t) + \frac{(EI)_2}{\ell_2^3} k_n^4 q_n^{(2)}(t) + \lambda_2 \phi_n(0) + \frac{\lambda_4}{\ell_2} \phi'_n(0) = 0 \qquad (54)$$

$$I_2 \ell_2 \ddot{P}_n^{(2)}(t) + \frac{(GJ)_2}{\ell_2} (n-1)^2 \frac{\pi^2}{4} P_n^{(2)}(t) - \lambda_6 \theta_n(0) = 0 \qquad (55)$$

The harmonic time dependence in the normal analysis is taken in the following form:

$$\left.\begin{matrix} Q_n(t) \\ q_n^{(1)}(t) \\ q_n^{(2)}(t) \\ P_n(t) \\ P_n^{(1)}(t) \\ P_n^{(2)}(t) \end{matrix}\right\} = \left\{\begin{matrix} \overline{Q}_n \\ \overline{q}_n^{(1)} \\ \overline{q}_n^{(2)} \\ P_n \\ P_n(1) \\ P_n^{(2)} \end{matrix}\right\} \times e^{i \left(\frac{(EI)_1}{M_1 l_1^3}\right)^{1/2} \omega t}$$

$$\left.\begin{matrix} \lambda_1(t) \\ \lambda_2(t) \end{matrix}\right\} = \left\{\begin{matrix} \overline{\lambda}_1 \\ \overline{\lambda}_2 \end{matrix}\right\} \times \frac{(EI)_1}{l_1^3} \, e^{i \left(\frac{(EI)_1}{M_1 l_1^3}\right)^{1/2} \omega t}$$

$$\left.\begin{matrix} \lambda_3(t) \\ \lambda_4(t) \\ \lambda_5(t) \\ \lambda_6(t) \end{matrix}\right\} = \left\{\begin{matrix} \overline{\lambda}_3 \\ \overline{\lambda}_4 \\ \overline{\lambda}_5 \\ \overline{\lambda}_6 \end{matrix}\right\} \times \frac{(EI)_1}{l_1^2} \, e^{i \left(\frac{(EI)_1}{M_1 l_1^3}\right)^{1/2} \omega t}$$

and the following notations are introduced:

$$\mu_1 = \frac{M_1}{M} \quad ; \quad \mu_2 = \frac{M_2}{M} \quad ; \quad \gamma_1 = \frac{l_1}{L} \quad ; \quad \gamma_2 = \frac{l_2}{L}$$

$$\nu_1 = \frac{M_1 l_1}{I} \quad ; \quad \nu_2 = \frac{M_1 L}{I_1} \quad ; \quad \nu_3 = \frac{M_1 L}{I_2}$$

$$\psi_1 = \frac{\frac{EI}{ML^3}}{\frac{(EI)_1}{M_1 \ell_1^3}} \quad ; \quad \psi_2 = \frac{\frac{GJ}{I L^2}}{\frac{(EI)_1}{M_1 \ell_1^3}} \quad ; \quad \psi_3 = \frac{\frac{(GJ)_1}{I_1}}{\frac{(EI)_1}{M_1 \ell_1}}$$

$$\psi_4 = \frac{\frac{(EI)_2}{M_2 \ell_2^3}}{\frac{(EI)_1}{M_1 \ell_1^3}} \quad ; \quad \psi_5 = \frac{\frac{(GJ)_2}{I_2 \ell_2^2}}{\frac{(EI)_1}{M_1 \ell_1^3}}$$

$$F_n^{(1)} = \omega^2 - \psi_1 k_n^4$$

$$F_n^{(2)} = \omega^2 - \psi_2 (n-1)^2 \frac{\pi^2}{4}$$

$$F_n^{(3)} = \omega^2 - k_n^4$$

$$F_n^{(4)} = \omega^2 - \psi_3 (n-1)^2 \frac{\pi^2}{4}$$

$$F_n^{(5)} = \omega^2 - \psi_4 k_n^4$$

$$F_n^{(6)} = \omega^2 - \psi_5 (n-1)^2 \frac{\pi^2}{4}$$

The generalized coordinated are then expressed in terms of the Lagrange multipliers as follows:

$$\bar{Q}_n = -\mu_1 \left(\frac{\bar{\lambda}_1 \phi_n(\xi_1) + \bar{\lambda}_2 \phi_n(\xi_2) + \bar{\lambda}_5 \gamma_1 \phi'_n(\xi_1)}{F_n^{(1)}} + \right.$$

$$\left. \frac{\bar{\lambda}_6 \gamma_1 \phi'_n(\xi_2)}{F_n^{(1)}} \right) \tag{56}$$

$$\bar{P}_n = -\gamma_1 \nu_1 \left(\frac{\bar{\lambda}_3 \theta_n(\xi_1) + \bar{\lambda}_4 \theta_n(\xi_2)}{F_n^{(2)}} \right) \tag{57}$$

$$\bar{q}_n^{(1)} = \frac{\bar{\lambda}_1 \phi_n(0) + \bar{\lambda}_3 \phi'_n(0)}{F_n^{(3)}} \tag{58}$$

$$\bar{P}_n^{(1)} = -\nu_2 \gamma_1 \frac{\bar{\lambda}_5 \theta_n(0)}{F_n^{(4)}} \tag{59}$$

$$\bar{q}_n^{(2)} = \mu_2 \left(\frac{\bar{\lambda}_2 \phi_n(0) + \bar{\lambda}_4 \gamma_2 \phi'_n(0)}{F_n^{(5)}} \right) \tag{60}$$

$$\bar{P}_n^{(2)} = - \gamma_1 \gamma_2 \nu_3 \frac{\bar{\lambda}_6 \theta_n(0)}{F_n^{(6)}} \tag{61}$$

Note that $P_n^{(1)}$ and $P_n^{(2)}$ are proportional to $\theta_n(0)$ and hence they have zero value for all the odd modes; as a consequence the angular twist for the wing and tail has an even distribution along the span as expected from the geometrical symmetry.

The eigenvalue equations are found by substitution of equations (56) - (61) into the constraint conditions (44) - (49) and form a set of six linear algebraic equations in the $\bar{\lambda}_i$ given by:

$$\sum_{n=1}^{\infty} \left(\mu_1 \left(\frac{\bar{\lambda}_1 \phi_n^2(\xi_1) + \bar{\lambda}_2 \phi_n(\xi_1) \phi_n(\xi_2) + \bar{\lambda}_5 \gamma_1 \phi_n(\xi_1) \phi'_n(\xi_1)}{F_n^{(1)}} \right.\right.$$

$$\left.\left. + \frac{\bar{\lambda}_6 \gamma_1 \phi_n(\xi_1) \phi'_n(\xi_2)}{F_n^{(1)}} \right) + \frac{\bar{\lambda}_1 \phi_n^2(0)}{F_n^{(3)}} \right) = 0 \tag{62}$$

$$\sum_{n=1}^{\infty} \left(\mu_1 \left(\frac{\bar{\lambda}_1 \phi_n(\xi_1) \phi_n(\xi_2) + \bar{\lambda}_2 \phi_n^2(\xi_2) + \bar{\lambda}_5 \gamma_1 \phi'_n(\xi_1) \phi_n(\xi_2)}{F_n^{(1)}} + \right.\right.$$

$$\left.\left. \frac{\bar{\lambda}_6 \gamma_1 \phi_n(\xi_2) \phi'_n(\xi_2)}{F_n^{(1)}} \right) + \mu_2 \frac{\bar{\lambda}_2 \phi_n^2(0)}{F_n^{(5)}} \right) = 0 \tag{63}$$

$$\sum_{n=1}^{\infty} (\gamma_1\nu_1 \left(\frac{\overline{\lambda}_3\, \theta_n^{\,2}(\xi_1) + \overline{\lambda}_4\, \theta_n(\xi_1)\, \theta_n(\xi_2)}{F_n^{(2)}} \right) + \overline{\lambda}_3 \frac{\phi'^{\,2}_n(0)}{F_n^{(3)}}) = 0 \quad (64)$$

$$\sum_{n=1}^{\infty} (\gamma_1\nu_1 \left(\frac{\overline{\lambda}_3\theta_n(\xi_1)\, \theta_n(\xi_2) + \overline{\lambda}_4\theta_n^{\,2}(\xi_2)}{F_n^{(2)}} \right) +$$

$$\mu_2\gamma_2^{\,2} \frac{\overline{\lambda}_4\, \phi'^{\,2}_n(0)}{F_n^{(5)}}) = 0 \quad (65)$$

$$\sum_{n-1}^{\infty} (\mu_1\, \gamma_1 \left(\frac{\overline{\lambda}_1\, \phi_n(\xi_1)\, \phi'_n(\xi_1) + \overline{\lambda}_2\, \phi_n(\xi_2)\, \phi'_n(\xi_1) + \overline{\lambda}_5\gamma_1}{F_n^{(1)}} \right.$$

$$\left. \frac{\phi'^{\,2}_n(\xi_1) + \overline{\lambda}_6\gamma_1\, \phi'_n(\xi_1)\, \phi'_n(\xi_2)}{F_n^{(1)}} \right) + \gamma_1\nu_2 \frac{\overline{\lambda}_5\, \theta_n^{\,2}(0)}{F_n^{(4)}}) = 0 \quad (66)$$

$$\sum_{n=1}^{\infty} (\mu_1\, \gamma_1 \frac{\overline{\lambda}_1\, \phi_n(\xi_1)\, \phi'_n(\xi_2) + \overline{\lambda}_2\, \phi_n(\xi_2)\, \phi'_n(\xi_2) + \overline{\lambda}_5\, \gamma_1}{F_n^{(1)}}$$

$$\left. \frac{\phi'_n(\xi_1)\, \phi'_n(\xi_2) + \overline{\lambda}_6\gamma_1\, \phi'^{\,2}_n(\xi_2)}{F_n^{(1)}} \right) + \gamma_1\gamma_2\nu_3 \frac{\overline{\lambda}_6\theta_n^{\,2}(0)}{F_n^{(6)}}) = 0 \quad (67)$$

or, in tensional form

$$\Delta(\omega) \cdot \vec{\lambda} = \vec{0} \tag{68}$$

where $\vec{\lambda}$ is the six-dimensional vector of components $\overline{\lambda}_i$ and $\Delta(\omega)$ is a symmetric tensor of order six which elements in matrix representation are:

$$\Delta_{11} = \sum_{n=1}^{\infty} \left(\mu_1 \frac{\phi_n^{\,2}(\xi_1)}{F_n^{(1)}} + \frac{\phi_n^{\,2}(0)}{F_n^{(3)}} \right)$$

$$\Delta_{12} = \sum_{n=1}^{\infty} \mu_1 \frac{\phi_n(\xi_1)\, \phi_n(\xi_2)}{F_n^{(1)}}$$

$$\Delta_{13} = \Delta_{14} = 0$$

$$\Delta_{15} = \sum_{n=1}^{\infty} \mu_1 \gamma_1 \frac{\phi_n(\xi_1)\phi'_n(\xi_1)}{F_n^{(1)}}$$

$$\Delta_{16} = \sum_{n=1}^{\infty} \mu_1 \gamma_1 \frac{\phi_n(\xi_1)\, \phi'_n(\xi_2)}{F_n^{(1)}}$$

$$\Delta_{22} = \sum_{n=1}^{\infty} \left(\mu_1 \frac{\phi_n^{\,2}(\xi_2)}{F_n^{(1)}} + \mu_2 \frac{\phi_n^{\,2}(0)}{F_n^{(5)}} \right)$$

$$\Delta_{23} = \Delta_{24} = 0$$

$$\Delta_{25} = \sum_{n=1}^{\infty} \mu_1 \gamma_1 \frac{\phi'_n(\xi_1)\, \phi_n(\xi_2)}{F_n^{(1)}}$$

$$\Delta_{26} = \sum_{n=1}^{\infty} \mu_1 \gamma_1 \frac{\phi_n(\xi_2)\, \phi'_n(\xi_2)}{F_n^{(1)}}$$

$$\Delta_{33} = \sum_{n=1}^{\infty} \left(\gamma_1 \nu_1 \frac{\theta_n^2(\xi_1)}{F_n^{(2)}} + \frac{\phi'^2_n(0)}{F_n^{(3)}} \right)$$

$$\Delta_{34} = \sum_{n=1}^{\infty} \gamma_1 \nu_1 \frac{\theta_n(\xi_1)\, \theta_n(\xi_2)}{F_n^{(2)}}$$

$$\Delta_{35} = \Delta_{36} = 0$$

$$\Delta_{44} = \sum_{n=1}^{\infty} \left(\gamma_1 \nu_1 \frac{\theta_n^2(\xi_2)}{F_n^{(2)}} + \mu_2 \gamma_2^2 \frac{\phi'^2_n(0)}{F_n^{(5)}} \right)$$

$$\Delta_{45} = \Delta_{46} = 0$$

$$\Delta_{55} = \sum_{n=1}^{\infty} \left(\mu_1 \gamma_1^2 \frac{\phi'^2_n(\xi_1)}{F_n^{(1)}} + \nu_2 \gamma_1 \frac{\theta_n^2(0)}{F_n^{(4)}} \right)$$

$$\Delta_{56} = \sum_{n=1}^{\infty} \mu_1 \gamma_1^2 \frac{\phi'_n(\xi_1)\, \phi'_n(\xi_2)}{F_n^{(1)}}$$

$$\Delta_{66} = \sum_{n=1}^{\infty} \left(\mu_1 \gamma_1^2 \frac{\phi'^2_n(\xi_2)}{F_n^{(1)}} + \gamma_1 \gamma_2 \nu_3 \frac{\theta_n^2(0)}{F_n^{(6)}} \right)$$

Equation (68) has solutions only for the values of ω for which

$$\boxed{\det\ (\ \Delta(\omega)\ ) = 0} \qquad (69)$$

and these values are precisely the non-dimensional resonant frequencies of the structure.

Eq (69) can be written more explicitely,

$$\begin{vmatrix} \Delta_{11} & \Delta_{12} & 0 & 0 & \Delta_{15} & \Delta_{16} \\ \Delta_{12} & \Delta_{22} & 0 & 0 & \Delta_{25} & \Delta_{26} \\ 0 & 0 & \Delta_{33} & \Delta_{34} & 0 & 0 \\ 0 & 0 & \Delta_{34} & \Delta_{44} & 0 & 0 \\ \Delta_{15} & \Delta_{25} & 0 & 0 & \Delta_{55} & \Delta_{56} \\ \Delta_{16} & \Delta_{26} & 0 & 0 & \Delta_{56} & \Delta_{66} \end{vmatrix} = 0$$

or, by simple algebraic manipulation,

$$(\Delta_{33}\, \Delta_{44} - \Delta_{34}^2) \begin{vmatrix} \Delta_{11} & \Delta_{12} & \Delta_{15} & \Delta_{16} \\ \Delta_{12} & \Delta_{22} & \Delta_{25} & \Delta_{26} \\ \Delta_{16} & \Delta_{26} & \Delta_{56} & \Delta_{66} \end{vmatrix} = 0 \qquad (70)$$

The decoupling between the rolling and pitching type of motion found where the rigid behavior was investigated is also valid in the elastic domain as shows equation (50) and therefore the two types of motions are to be studied separately.

The natural frequencies of the motions of rolling type are solutions of the equation

$$(\Delta_{33} \Delta_{44} - \Delta_{34}^{2}) = 0 \quad ; \qquad (71)$$

In such motions the fuselage undergoes only angular twisting and the wing and tail undergo anti-symmetric bending.

The pitching type of motion has natural frequencies given by :

$$\begin{vmatrix} \Delta_{11} & \Delta_{12} & \Delta_{15} & \Delta_{16} \\ \Delta_{12} & \Delta_{22} & \Delta_{25} & \Delta_{26} \\ \Delta_{15} & \Delta_{25} & \Delta_{55} & \Delta_{56} \\ \Delta_{16} & \Delta_{26} & \Delta_{56} & \Delta_{66} \end{vmatrix} = 0$$

The fuselage bends only, while the wing and tail bend and twist as well.

c) Accuracy of the method

As part of the analysis relies on numerical computations, the question of accuracy is a consequence of precisely these computational errors.

The sources of error are:

1) The fact of considering a finite number of modes for each component

in the Rayleigh-Ritz analysis

2) the fact of solving with approximation the frequency equation, $\det\ (\Delta\ (\omega)\ ) = 0$

3) the fact that the various computer subroutines used in the numerical analysis have errors inherent to the way in which they have been written.

This last type of error can be eliminated by using Double Precision in the computation or Extended Precision if needed, and hence will not be accounted for in the accuracy analysis.

Let $\det\ \Delta_{ij}^{(N)}(\omega)$ be the approximation of $\Delta_{ij}\ (\omega)$ when N modes per component are considered. Then

$$\Delta_{ij}\ (\omega)\ = \Delta_{ij}^{(N)}\ (\omega) + \varepsilon_{ij}\ (\omega) \qquad (73)$$

where $\varepsilon_{ij}(\omega)$ is mainly the next-order term in the serie giving $\Delta_{ij}\ (\omega)$ i.e. the term due to considering the $N^{th} + 1$ component modes. These errors propagate into the determinant in a way which can be determined by substituting equation (73) into equations (71) and (72) respectively. For the motions of the rolling type this substitution yields:

$$(\Delta_{33}^{(N)}\ \Delta_{44}^{(N)} - \Delta_{34}^{(N)2}) + \Delta_{33}^{(N)}\ \varepsilon_{44} + \Delta_{44}^{(N)}\ \varepsilon_{33} - 2\Delta_{34}^{(N)}\varepsilon_{34} +$$

higher order terms $= 0$

which can be written in the form:

$$\text{Det}^{(N)} + E^{(N)} = 0 \qquad (74)$$

where

$$\text{Det}^{(N)} = \Delta_{33}^{(N)} \Delta_{44}^{(N)} - \Delta_{34}^{(N)}$$

is the determinant actually computed in the finite mode - approximation and

$$E^{(N)} = \Delta_{33}^{(N)} \varepsilon_{44} + \Delta_{44}^{(N)} \varepsilon_{33} - 2\Delta_{34}^{(N)} \varepsilon_{44}$$

is the truncation error.

Hence, instead of solving the exact frequency equation, one solves in fact

$$\text{Det}^{(N)}(\omega) = 0 \tag{75}$$

Furthermore, the numerical solutions ω_n do not satisfy equation (75) exactly, but satisfy in fact

$$\text{Det}^{(N)}(\omega) = \varepsilon \tag{76}$$

where the values of ε are known and inherent to the trial and error process. Therefore the question that naturally arises is: given the numerical errors listed above, how different is the exact solution $\omega_n^{(e)}$ from the solution ω_n actually computed?

Let $\omega_o^{(e)}$ be an exact natural frequency satisfying equation (71), ω_o the approximated value of $\omega_o^{(e)}$.

Let

$$\text{Det}(\omega) = \Delta_{33}(\omega)\Delta_{44}(\omega) - \Delta_{34}^2(\omega) = \text{Det}^{(N)}(\omega) + E^{(N)}(\omega)$$

A 1-term Taylor expansion of $\text{Det}(\omega_o^{(e)})$ gives:

$$\text{Det}(\omega_o^{(e)}) = \text{Det}(\omega_o) + (\omega_o^{(e)} - \omega_o) \left| \frac{\partial \text{Det}}{\partial \omega} \right|_{\omega = \omega_o}$$

and since $\text{Det}\ (\omega_o^{(e)}) = 0$,

$$\omega_o^{(e)} - \omega_o = \frac{\text{Det}\ (\omega_o)}{\left| \frac{\partial \text{Det}}{\partial \omega} \right|_{\omega = \omega_o}}$$

$$\omega_o^{(e)} - \omega_o = - \frac{\text{Det}^{(N)}(\omega_o) + E^{(N)}(\omega_o)}{\left| \frac{\partial \text{Det}^{(N)}}{\partial \omega} \right|_{\omega=\omega_o} + \left| \frac{\partial E^{(N)}}{\partial \omega} \right|_{\omega=\omega_o}} \qquad (77)$$

All terms in the right hand side of equation (77) are known: ε, as mentioned before is known in the trial and error process of solving $\text{Det}^{(N)}(\omega) = o$,

$$E^{(N)}(\omega_o) = \Delta_{33}^{(N)}(\omega_o)\ \varepsilon_{44}(\omega_o) + \Delta_{44}^{(N)}(\omega_o)\varepsilon_{33}(\omega_o) - 2\Delta_{34}^{(N)}(\omega_o)$$

$$\varepsilon_{34}(\omega_o)$$

can be explicitely computed from the values of the $\Delta_{ij}^{(N)}$ and ε_{ij} which are known,

$$\left| \frac{\partial \text{Det}^{(N)}}{\partial \omega} \right|_{\omega=\omega_o} = \left| \frac{\partial \Delta_{33}^{(N)}}{\partial \omega} \right|_{\omega=\omega_o} \Delta_{44}^{(N)}(\omega_o) + \Delta_{33}^{(N)}(\omega_o) \left| \frac{\partial \Delta_{44}^{(N)}}{\partial \omega} \right|_{\omega=\omega_o}$$

$$-2\ \Delta_{34}^{(N)}\ (\omega_o) \left| \frac{\partial \Delta_{34}^{(N)}}{\partial \Delta} \right|_{\omega=\omega_o}$$

is then explicitely known, and so is

$$\left|\frac{\partial E^{(N)}}{\partial \omega}\right|_{\omega=\omega_o} = \left|\frac{\partial \Delta_{33}^{(N)}}{\partial \omega}\right|_{\omega=\omega_o} \varepsilon_{44}(\omega_o) + \Delta_{33}^{(N)}(\omega_o)\left|\frac{\partial \varepsilon_{44}}{\partial \omega}\right|_{\omega=\omega_o}$$

$$+ \left|\frac{\partial \Delta_{44}^{(N)}}{\partial \omega}\right|_{\omega=\omega_o} \varepsilon_{33}(\omega_o) + \Delta_{44}^{(N)}(\omega_o)\left|\frac{\partial \varepsilon_{33}}{\partial \omega}\right|_{\omega=\omega_o}$$

$$- 2\left|\frac{\partial \Delta_{34}^{(N)}}{\partial \omega}\right|_{\omega=\omega_o} \varepsilon_{34}(\omega_o) - 2\,\Delta_{34}^{(N)}(\omega_o)\left|\frac{\partial \varepsilon_{34}}{\partial \omega}\right|_{\omega=\omega_o}$$

Thus, equation (77) gives an analytic determination of the first order error for the natural frequencies in motions of the rolling type.

It is interesting to note that equation (76) also shows that $|\omega_n^{(e)} - \omega_n|$ increases with n, i.e. the lower modes are obtained with higher accuracy for a given number of modes per component. This fact is expected, in a way similar to the convergence in a pure Rayleigh Ritz analysis.

This statement is proven as follows:

The $\Delta_{ij}^{(N)}(\omega)$ can be written in the following form:

$$\Delta_{ij}^{(N)}(\omega) = \sum_{n=1}^{N} \frac{C_n^{ij}}{\omega^2 - D_n^{ij}} \quad \text{with} \quad D_n^{ij} > 0$$

hence $\Delta_{ij}^{(N)}(\omega)$ are of the order of $\frac{1}{\omega^2}$ for any i, j. and same

conclusion is valid for the

$$\varepsilon_{ij}(\omega) = \frac{C^{ij}_{N+1}}{\omega^2 - D^{ij}_{N+1}}$$

The respective derivatives $\frac{\partial \Delta^{(N)}_{ij}}{\partial \omega}$ and $\frac{\partial \varepsilon_{ij}}{\partial \omega}$ are then of the order of $\frac{1}{\omega^3}$. Hence $\mathrm{Det}^{(N)}(\omega)$ and $E^{(N)}(\omega)$ are of the order of $\frac{1}{\omega^4}$, and $\frac{\partial \mathrm{Det}^{(N)}}{\partial \omega}$ and $\frac{\partial E^{(N)}}{\partial \omega}$ are of the order of $\frac{1}{\omega^5}$.

From equation (77) it follows that $| \omega_n^{(e)} - \omega_n |$ is of the order of ω_n, thus increasing with ω_n.

The initial truncation errors and the approximations of equation (76) propagate also in the value of the Lagrange multipliers as follows:

The non-dimensional Lagrange multipliers corresponding to the antisymmetrical rolling motions, $\overline{\lambda}_3$ and $\overline{\lambda}_4$ are solutions of:

$$\Delta_{33}(\omega)\,\overline{\lambda}_3 + \Delta_{34}(\omega)\,\overline{\lambda}_4 = 0 \qquad (78)$$

$$\Delta_{34}(\omega)\,\overline{\lambda}_3 \quad \Delta_{44}(\omega)\,\overline{\lambda}_4 = 0 \qquad (79)$$

By letting $\overline{\lambda}_3 = 1$ in equation (78),

$$\overline{\lambda}_4 = - \frac{\Delta_{33}(\omega)}{\Delta_{34}(\omega)} \qquad (80)$$

and this solution substituded into equation (79) leads to:

$$\bar{\lambda}_3 = \frac{\Delta_{33}(\omega)\ \Delta_{44}(\omega)}{\Delta_{34}^{2}(\omega)}$$

which, for each natural frequency ω_n computed, can be written:

$$\bar{\lambda}_3 = 1 + \frac{\mathrm{Det}(\omega_n)}{\Delta_{34}^{2}(\omega_n)}$$

or, at the first order,

$$\bar{\lambda}_3 = 1 + \frac{\mathrm{Det}^{(N)}(\omega_n) + E^{(N)}(\omega_n)}{\Delta_{34}^{(N)2}(\omega_n) + 2\Delta_{34}^{(N)}(\omega_n)\ \varepsilon_{34}(\omega_n)}$$

It follows that the first order error in the value of $\bar{\lambda}_3$ for the resonant freq. ω_n is:

$$E_{\bar{\lambda}_3} = \frac{\mathrm{Det}^{(N)}(\omega_n) + E^{(N)}(\omega_n)}{\Delta_{34}^{(N)2}(\omega_n) + 2\ \Delta_{34}^{(N)}(\omega_n)\ \varepsilon_{34}(\omega_n)}$$

which can be written also by using a one-term binomial expansion

$$E_{\bar{\lambda}_3} = \frac{\mathrm{Det}^{(N)}(\omega_n)}{\Delta_{34}^{(N)2}(\omega_n)}\left(1 + \frac{E^{(N)}(\omega_n)}{\mathrm{Det}^{(N)}(\omega_n)} - \frac{2\ \varepsilon_{34}(\omega_n)}{\Delta_{34}^{(N)}(\omega_n)}\right)$$

Equation (80) gives explicitely the first order error in the value of $\bar{\lambda}_4$ by similar algebraic manipulations:

$$E_{\overline{\lambda}_4} = - \frac{\varepsilon_{33}(\omega_n)}{\Delta_{34}^{(N)}(\omega_n)} + \frac{\Delta_{33}^{(N)}(\omega_n)\ \varepsilon_{34}(\omega_n)}{\left(\Delta_{34}^{(N)}(\omega_n)\right)^2}$$

From equations (58) and (60) it follows that $E_{\overline{q}_n}(1)$ is proportional to $E_{\overline{\lambda}_3}$ and $E_{\overline{q}_n}(2)$ is proportional to $E_{\overline{\lambda}_4}$ for each natural frequency (with obvious notations for $E_{\overline{q}_n}(1)$ and $E_{\overline{q}_n}(2)$), and hence the initial errors are finally propagated into the mode shapes of the wing and tail as follows:

$$E_{w_n}(1)\ (\eta) = \sum_{p=1}^{\infty} \frac{E_{\overline{\lambda}_3}(\omega_n)\ \phi'_p(0)\ \phi_p(\eta)}{F_p^{(3)}(\omega_n)} \qquad (81)$$

$$E_{w_n}(2)\ (\eta) = \sum_{p=1}^{\infty} \frac{E_{\overline{\lambda}_4}(\omega_n)\ \phi'_p(0)\ \phi_p(\eta)}{F_p^{(5)}(\omega_n)} \qquad (82)$$

Of course, $E_{w_n}(1)\ (0) = E_{w_n}(2)(0) = 0$

From equation (57) $E_{\overline{P}_n}$ is explicitely computed:

$$E_{\overline{P}_n} = - \frac{\gamma_1 \nu_1\ \left(E_{\overline{\lambda}_3}\ \theta_n(\xi_1) + E_{\overline{\lambda}_4}\ \theta_n(\xi_2)\right)}{F_n^{(2)}}$$

and thus the error in the angular twist of the fuselage for the natural frequency ω_n is given by:

$$E_{\theta_n}(\xi) = -\gamma_1 \nu_1 \sum_{p=1}^{\infty} \frac{(E_{\lambda_3}(\omega_n)\,\theta_p(\xi_1) + E_{\lambda_4}(\omega_n)\theta_p(\xi_2))\,\theta_p(\xi)}{F_p^{(2)}(\omega_n)} \quad (83)$$

The accuracy on the actual physical displacements can be computed from equations (29), (30), (31) with $\underline{c}_L$, $\underline{c}_{1_1}$ and $\underline{c}_{2_1} = o(1)$ and by using equations (81), (82), (83).

The error analysis for the motions of pitching type is far more complicated as shows equation (72) and it is faster to draw a convergence graph versus the number of modes used for a given natural frequency than to obtain analytical expressions for the errors by the procedure explained previously.

Furthermore, an idea of the order of magnitude of errors of the type given by equation (76) is given at the first step by the process of trial and error itself as follows:

The corresponding det (ω) is plotted versus ω and the regions where det (ω) changes sign are considered. For a case such as the one illustrad below

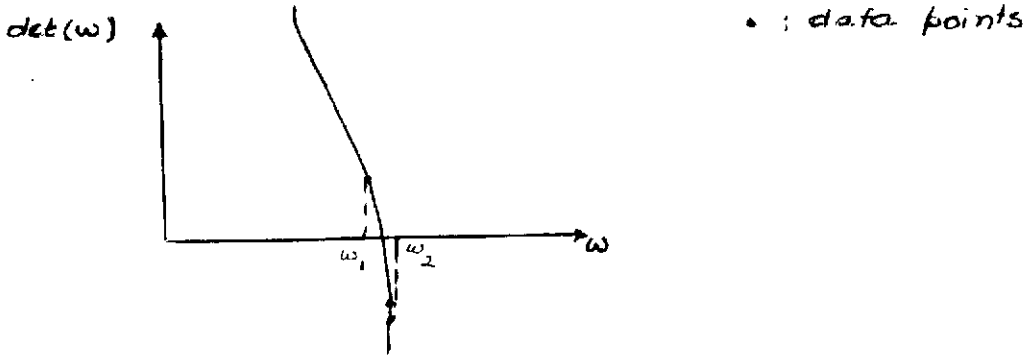

where det (ω) has steep variations in the neighborhood of the natural frequency, values such as ω_1 and ω_2 are a good approximation of ω_n despite the fact that neither det (ω_1) nor det (ω_2) are close to zero.

The frequency solutions in such cases are quite accurate, however the values of the Lagrange multipliers (and hence the modal shapes) are given with less accuracy precisely because of the fact that det (ω_1) or det (ω_2) are not small enough for this purpose.

If the opposite case occurs in the neighborhood of a natural frequency:

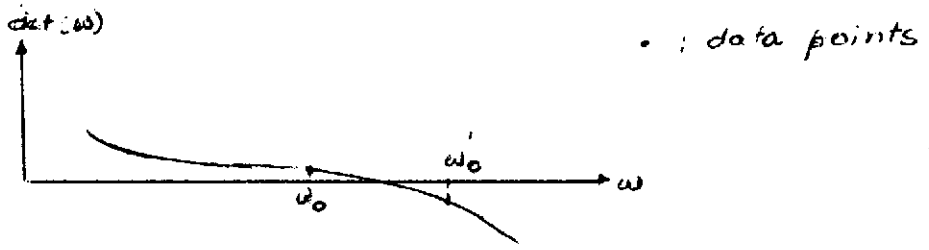

i.e., det (ω) has a locally small slope, even though det (ω_o) and det (ω'_o) are very close to zero, ω_o and ω'_o do not bound the resonant frequency very accurately. However, the mode shape and the information of structural type are given with better precision.

Situations of the first type tend to occur for the lower natural frequencies and smoother variations of det (ω) are seen for the higher frequencies and thus the corresponding conclusions can be drawn.

d) Results and convergence study in a check case

As in the previous chapter, the theoretical and numerical part

of the method are first checked with classical results known analytically.

The reference case is taken to be a cantiliver beam which can be considered a particular case of the airplane - like configuration in the following manner:

Values of the parameters	Physical significance
1) $\xi_1 = \xi_2 = 0$	both the tail and the wing are placed at the middle of the fuselage
2) $\nu_1 \to 0$ for rolling type of motions	the fuselage is given an infinite inertia in twisting
$\mu_1 \to 0$ for pitching type of motions	the fuselage is made infinitely heavy
$\psi_2 \to \infty$ for rolling type of motions	the fuselage is made infinetely rigid in twisting
$\psi_1 \to \infty$ for pitching type of motions	the fuselage is made infinitely rigid in bending

The set of parameters in (2) is such that the fuselage is constrained to stay still, i.e. clamp the wing and the tail in both kinds of motions. In fact, mathematically one could have allowed ψ_1 and ψ_2 to be finite.

For the sake of simplicity the two beams representing the wing and tail are also made identical by taking

$\mu_2 = \gamma_2 = \psi_4 = 1$ for the antisymmetric motions

$\nu_2 = \nu_3 = \psi_4 = \gamma_2 = 1$ for the symmetric motions.

Vibrations of rolling type:

$$\left.\begin{aligned} \nu_1 &= 0 \\ \psi_4 &= 1 \end{aligned}\right\} \rightarrow \left\{\begin{aligned} \Delta_{34} &= 0 \\ \Delta_{33} &= \Delta_{44} = \sum_{n=1}^{\infty} \frac{\phi'_n{}^2(0)}{\omega^2 - k_n^4} \end{aligned}\right.$$

and hence the frequency equation is:

$$\left(\sum_{n=1}^{\infty} \frac{\phi'_n{}^2(0)}{\omega^2 - k_n^4} \right) = 0 \qquad (84)$$

i.e. the frequency equation in the case of a beam clamped in its middle, in an analysis using only antisymmetric free-free modes (see Appendix III).

Of course, all solutions ω of equation (84) are in fact double roots as we have two identical cantilever beams in vibration. Note that in the analysis developed in part b) the non-dimensionalization has been made using half-length of the wing, hence there is no adjusting factor to be computed for the non-dimensional frequencies. Figure 13 shows the rate of convergence of the first natural frequency towards that of a cantilever beam versus the number of antisymmetric modes used; the convergence is very fast for the first few modes. Furthermore the shapes of the first three modes have been obtained using ten antisymmetric modes in the analysis and they are plotted in Figure 14, 15, 16. The frequency bounds are given by the analyses developed in part c); the percentage errors are almost equal for the three natural frequencies (4.1, 4.2 and 4.5 respectively). The values of the slopes

at the origin is given as an indication of the modal shape accuracy.

Vibrations of the pitching type

With the limiting values for the parameters given previously,

$$\Delta_{11} = \Delta_{22} = \sum_{n=1}^{\infty} \frac{\phi_n^2(0)}{\omega^2 - k_n^4}$$

$$\Delta_{12} = \Delta_{15} = \Delta_{16} = \Delta_{25} = \Delta_{26} = \Delta_{56} = 0$$

$$\Delta_{55} = \Delta_{66} = \sum_{n=1}^{\infty} \frac{\theta_n^2(0)}{\omega^2 - (n-1)^2 \frac{\pi^2}{4}}$$

The frequency equation becomes in this case:

$$\left(\sum_{n=1}^{\infty} \frac{\phi_n^2(0)}{\omega^2 - k_n^4} \right)^2 \left(\sum_{n=1}^{\infty} \frac{\theta_n^2(0)}{\omega^2 - (n-1)^2 \frac{\pi^2}{4}} \right)^2 = 0$$

The first factor corresponds to the bending modal behavior of a beam clamped in its middle, the second factor corresponds to the cantiliver beam in twisting (see Appendix III).

As expected, the bending and twisting motions are decoupled from each other. The convergence rates towards the first clamped-free natural frequency respectively for bending and twisting are both shown in Figure 17 so that they can be analysed comparatively.

The percentage error in the first bending frequency computed

using symmetrical modes only decreases very fast to zero in fact much faster than in the case in which only odd modes are used. This result is to be expected as the natural frequencies of the even modes are lower than the ones of the odd modes.

By comparison, there is slower convergence in the torsional modes and Figure 18 which represents a more extensive graph of the twisting convergence shows that in order to get 0.9% error in the non-dimensional frequency (precision attained with only 3 symmetric modes in bending), 21 torsional modes have to be included in the analysis.

This fact is surprising as there is no physical reason for which it could be expected, however, it can be justified on mathematical basis.

Consider the finite N-termes frequency equations:

$$P(\omega) = \sum_{n=1}^{\infty} \frac{\phi_n^2(0)}{\omega^2 - k_n^4} = 0 \qquad (85)$$

and

$$Q(\omega) = \sum_{n=1}^{\infty} \frac{\theta_n^2(0)}{\omega^2 - (n-1)^2\frac{\pi^2}{4}} = 0 \qquad (86)$$

and the first natural frequency corresponding solutions ω_1 and Ω_1.

The problem is that of determining how much will ω_1 and Ω_1 change by considering one more term respectively in the analysis, or equivalently, how much will $P(\omega)$ and $Q(\omega)$ respectively be modified by use

of the additional term.

By separating the rigid body contributions in bending and torsion we can write $P(\omega)$ and $Q(\omega)$ as follows:

$$P(\omega) = \frac{1}{2\omega^2} + \sum_{\substack{n=3 \\ n \text{ odd}}}^{N} \frac{\phi_n^2(0)}{\omega^2 - k_n^4} \tag{87}$$

$$Q(\omega) = \frac{1}{2\omega^2} + \sum_{n=1}^{N} \frac{1}{\omega^2 - n^2\pi^2} \tag{88}$$

The N^{th} + 1 terms in each of the equations (87) and (88) are:

$$\frac{\phi_{N+1}^2(0)}{\omega^2 - k_{N+1}^4}$$

and

$$\frac{1}{\omega^2 - (N+1)^2\pi^2}$$

For $n \geq 5$, $\phi_n(0) > 1$ and $\phi_{n+1}(0) > \phi_n(0)$ $\forall n$, hence for $N \geq 4$,

$$\frac{\phi_{N+2}^2(0)}{\omega^2 - k_{N+2}^4} > \frac{1}{\omega^2 - k_{N+2}^4} \tag{89}$$

Also, $k_{N+2}^4 > (N+1)^2\pi^2$ and hence

$$\frac{1}{\omega^2 - k_{N+2}^4} > \frac{1}{\omega^2 - (N+1)^2\pi^2}$$

By use of this result together with inequality (89) it follows:

$$\boxed{\frac{\phi_{N+2}^2(0)}{\omega^2 - k_{N+2}^4} > \frac{1}{\omega^2 - (N+1)^2\pi^2}} \qquad (90)$$

This inequality shows that an additional bending mode in the analysis provides more contribution (in fact much more contribution) to $P(\omega)$ than an additional twisting mode in $Q(\omega)$.

Thus the value of ω_1 will be more significantly modified by an additional mode than the value of Ω_1.

This explains the relatively slow convergence rate of the torsional frequency by comparison with that of the bending frequency.

Furthermore, this result suggests that for the next investigations more modes should be used in twisting than in bending (in fact quite a large number of modes). This fact does not present any noticable inconvenience however, as it corresponds just to performing more additions; from the point of view of computer work, the additional time and region necessary are negligible.

4. Experimental work

a) Introduction

The idea of a completely unconstrained structure presents no con-

ceptual or theoretical difficulties, however, practical problems arise when such a structure is to be simulated in the laboratory. For experimental purposes the specimen has to be supported, and thus one of the first problems which is to be solved in the design of the experiment is that of finding a suitable type of supports which characteristics will not affect the resonant frequencies of the structure. In particular, for the present analysis care has to be taken that neither the natural frequencies of motions of rolling type, nor the frequencies in the pitching motions will be changed by the type of supports used.

The next subparagraphs describe the experimental model, the type of supports which simulate its free motion and the experimental setting.

b) Experimental model

The beam-like structure on which the experiments have been performed is shown in Figure 19. The components are aluminum alloys beams of rectangular cross-section and following characteristics:

	beams (1) and (2)	beam (3)
length	10 in	10 in
width	0.5 in	0.25 in
thickness	0.1 in	0.05 in
E	10^7 lb/in^2	10^7 lb/in^2
ν	0.33	0.33
ρ	0.1/385 lb/in^3/in/sec^2	0.1/385 lb/in^2/in/sec^2

The values for E, ν, ρ are taken from Ref (40).

Beams (1) and (2) are mounted perpendicular to each other on their middle, beam (3) is mounted parallel to beam (2) at 3 in. distance from it.

Small steel coupons are mounted at one of the tips of each component so that the structure can be excited at various tip locations by a magnetic transducer.

c) Choice of the optimum supports

The experimental model with the two identical supports is shown in Figure 20. The elastic supports at both tips of beam (1) have been perfectly alligned so that they do not affect the rolling of this beam. The constraining effects on the bending motions of the beam have been minimized by a proper choice of the spring constant, proceeding as follows: the idea is to choose the springs soft enough so that the frequency of the rigid body translation of the model resting on the two springs is much lower than the lowest free-free bending frequency of beam (1).

This lowest frequency is found to be of the order of 200 cps. and with the choice of a spring constant equal to 0.5 lb/in, the frequency of the corresponding rigid body translation is of 9.5 cps. The value of the spring constant is related to that of the frequency of the rigid body translation by

$$k = \frac{M\omega^2}{2} \quad , \quad \text{where}$$

M is the mass of the specimen

k is the spring constant

ω is the dimensional frequency (rad/sec) and the factor $\frac{1}{2}$

corresponds to the fact that the two springs are identical.

d) Experimental setting

The set up of the experiment is shown in Figure 21 and more detailed explanation is given in the sketch which follows:

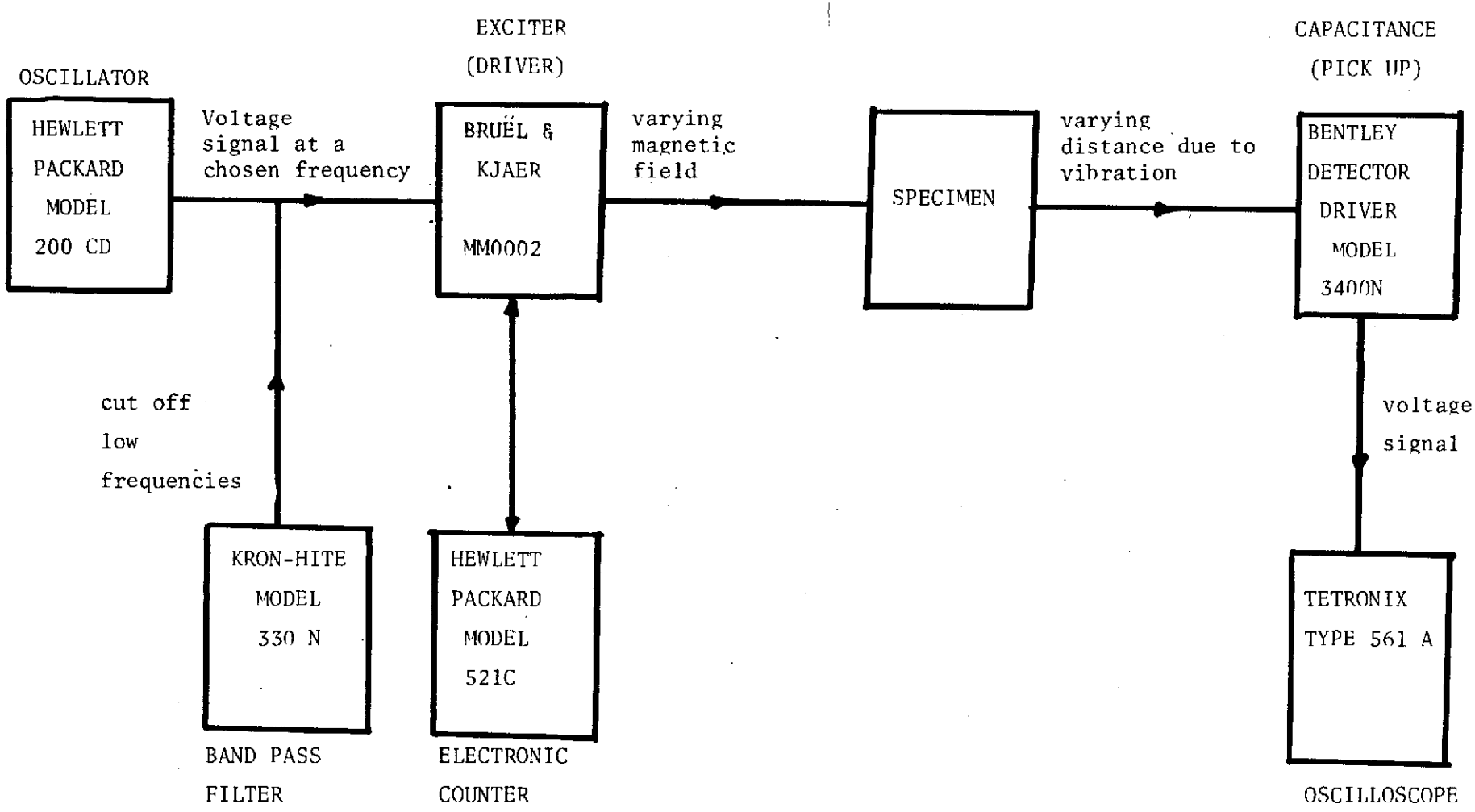
OSCILLATOR
HEWLETT PACKARD MODEL 200 CD
Voltage signal at a chosen frequency
EXCITER (DRIVER)
BRUËL & KJAER MM0002
varying magnetic field
SPECIMEN
varying distance due to vibration
CAPACITANCE (PICK UP)
BENTLEY DETECTOR DRIVER MODEL 3400N
voltage signal
TETRONIX TYPE 561 A
OSCILLOSCOPE
cut off low frequencies
KRON-HITE MODEL 330 N
BAND PASS FILTER
HEWLETT PACKARD MODEL 521C
ELECTRONIC COUNTER

The oscilloscope has a double beam feature and a polaroid camera connected to it, so that the input and output signals can be compared and picture information recorded.

Two types of resonances were found as shown in Figure 22, and labeled type α and β.

The lower part of the Figure 22 shows a resonance of type α: the output signal (lower beam) is seen to be at -90° phase with the input signal.

The upper part of the Figure 22 shows a resonance of type β: the output signal on the lower beam now precedes the input signal by 90°.

e) Frequencies measurements

Three sets of measurements have been performed with the following positions for the driver and pick up:

. set of measurements (1)

Both the driver and pick up are at the tips of beam (1); the driver is positioned farthest away from beam (3), the pick up is placed at the tip closest to beam (3). With this arrangement the following resonant frequencies were detected in increasing value:

62 cps	weak signal	type α
112 cps	weak signal	type α
361.1 cps	strong signal	type α
480 cps	strong signal	type α
575 cps	weak signal	type α

. set of measurements (2)

The arrangement is as shown in Figure 21; the driver and pick up are at each of the tips of beam (2). The measured resonant frequencies are:

32.5 cps	weak signal	type β
62 cps	weak signal	type α
110 cps	weak signal	type α
264 cps	weak signal	type β
489 cps	strong signal	type β
575 cps	weak signal	type α
578.7 cps	strong signal	type β

. set of measurements (3):

The arrangement is similar to the previous case, however, the driver and pick up are positioned now at the tips of beam (3). Because of the larger flexibility of this beam, the resonant frequencies were easier to detect and in fact this set of measurements is considered to be the most satisfactory of the three. The following resonant frequencies were detected:

32.5 cps	strong signal	type β
62 cps	strong signal	type α
112 cps	weak signal	type α
264 cps	strong signal	type β
361.1 cps	strong signal	type α
480 cps	strong signal	type α
489 cps	weak signal	type β

575 cps strong signal type α

578.7 cps strong signal type β

As it can be seen, many natural frequencies were found in more than one set of measurements; very often their value agree exactly from one measurement to the other, for the few frequencies for which this is not the case the data corresponding to the strongest signal on the screen of the oscilloscope have been retained.

Tabulated below is a summary of the measured resonant frequencies, the way in which they have been detected and their type.

natural frequency	driver's position	pick up's position	type
32.5	tip of beam (3)	other tip of beam (3)	β
62	"	"	α
112	tip of any beam	other tip of the same beam	α
264.3	tip of beam (3)	other tip of beam (3)	β
361.1	"	"	α
480	tip of beam (1) or (3)	other tip of the same beam	α
489	tip of beam (2)	other tip of beam (2)	β
575	tip of beam (3)	other tip of beam (3)	α
578.7	tip of beam (2) or (3)	other tip of the same beam	β

The resonant frequencies of this beam-like model have also been investigated theoretically, and the next paragraph deals with the numerical results which have been obtained and the conclusions which can be drawn from the comparison with the experimental work.

5. Numerical analysis for the experimental model: theoretical results, comparison with the experimental results

We remind the reader at this point that although the numerical results are presented with the frequencies in increasing order for easier comparison with experimental data, the frequencies of rolling type and pitching type of motions have been obtained by independent computations as discussed in paragraph 3. This factor will be taken into account however, in the quantitative analysis.

The lowest computed natural frequency is ω_1 = 36.7 cps and the physical deformation of the structure is shown in Figure 23. In this mode beam (1) undergoes only angular twisting; beams (2) and (3) bend antisymmetrically, predominantly in the rigid mode. The value of this resonant frequency can be related to that of 32.5 cps. measured experimentally; as it can be seen in Figure 23 this resonance could not be detected in the first set of measurements. A comparison between the amplitudes of the rigid body rotations of beams (2) and (3) shows that reason for which a stronger response has been obtained where the driver and pick up were both placed at the tips of beam (3).

The value of the second calculated natural frequency is ω_2=69 cps; as shown in Figure 24, the modal behavior is of the pitching type: beam (1) rotates as a rigid body, beam (2) undergoes weak bending in the first symmetric mode, and higher amplitude bending of the same shape (but opposite sign) is observed for beam (3).

The corresponding second resonance measured experimentally occured at a driving frequency of 62 cps (with the strongest response in the third set of measurements); it is interesting to notice that

this resonance has been found experimentally to be of different type than the previous, specifically of the type α. It can be anticipated on these basis that resonance of the type α will correspond to motions with symmetric behavior of beams (2) and (3) while type β resonances will be characteristic of the "rolling motions". In the third mode (for which the computed value of the frequency is ω_3 = 125.6 cps) the deformation of each component is similar in shape and amplitude (see Figure 25); this resonance has been detected in all three sets of measurements, and found to occur at a frequency of 112 cps. Note that indeed it corresponds to a type α deformation.

The next higher natural frequency has a theoretical value of 295.5 cps; Figure 26 shows the deformation of each component and it can be seen that in this second rolling mode both beams (2) and (3) do show an elastic behavior. The corresponding measured value of the frequency is of 264.3 with strongest response picked up on beam (3); indeed it is a resonance of type β.

The next four natural frequencies obtained theoretically and the corresponding modes are shown in Figures 27, 28, 29, 30, 31, respectively; similar analysis show qualitative checking between theoretical and experimental results. As the comparison shows good qualitative agreement, it is of interest to further investigate in a quantitative manner the agreement (or diescrepancies) between theoretical and experimental results. For the time being the quantitative analysis will be done separately for the modes of rolling type and pitching type, as the theoretical results have been obtained by independent computations.

The results are given in tabulated form for clarity, and shown below:

Modes of rolling type:

ω_n theoretical (cps)	ω_n experimental (cps)	percentage error normalized by the experimental data (%)
36.7	32.5	11.5
295.5	264.3	11.8
546.6	489	11.6
648.2	578.7	12.0

At first view the percentage error seems to be too high for being satisfactory; further analysis shows, however, the interesting fact that this error is constant for the four frequencies. This remark suggests that possibly part of the error comes from the difference between the exact and assumed characteristics of the experimental model. If this is true then better agreement should be provided by comparing the two sets of frequencies in a non-dimensional manner. This can be achieved by comparing the ratios (ω_n/ω_1) theoretical and (ω_n/ω_1) experimental as shown in the table:

$\frac{(\omega_n)}{\omega_1 \text{ theoretical}}$	$\frac{(\omega_n)}{\omega_1 \text{ experimental}}$	Percentage error normalized by experimental data
1	1	--
8.05	7.93	1.6
14.89	14.67	1.5
17.66	17.36	1.7

Column 3 illustrates that the previous assumption was correct, but at least two other possible facts have to be taken into account: one is that the components were not welded in the structure but glued together and hence the elastic properties of the glue play a role at the joints, the second fact is that there is a stiffening effect due to the steel coupons, especially on beam (3). It is interesting to notice that, probably because of the facts mentioned previously, all computed values of the frequencies are higher than the measured ones. But, of course, this is also inherent to the Rayleigh Ritz procedure per se.

A simular analysis is now developed for the modes with symmetric behavior.

Modes of pitching type:

ω_n theoretical (cps)	ω_n experimental (cps)	Percentage error normalized by the experimental data (%)
69	62	11.2
125.6	112	12.2
404.8	361.1	12.1
536.2	480	11.7
643.3	575	11.9

Consideration of the percentage error leads to conclusions similar to that of the previous case and thus we develop again a non-dimensional manner of comparing the results, as shown below:

$(\frac{\omega_n}{\omega_1})$ theoretical	$(\frac{\omega_n}{\omega_1})$ experimental	Percentage error normalized by the experimental data
1	1	-
1.82	1.79	1.7
5.87	5.78	0.9
7.77	7.68	1.2
9.32	9.20	1.32

Column 3 shows satisfactory agreement between the non-dimensional frequencies obtained theoretically and experimentally. Furthermore it is of interest to notice that even for different types of modes the percentage errors have almost the same value; this suggests that the analysis performed for the two classes of frequencies applies in fact globally which is an indication of succesfull agreement between theory and experiments.

The global analysis is presented below in tabulated form:

ω_n theoretal (cps)	ω_n experimental (cps)	percentage error (%)	$(\frac{\omega_n}{\omega_1})$ theoretical	$(\frac{\omega_n}{\omega_1})$ experimental	percentage error (%)
36.7	32.5	11.5	1	1	--
69	62	11.2	1.88	1.86	1.1
125.6	112	12.1	3.42	3.36	1.8
295.5	264.3	11.8	8.05	7.93	1.6
404.8	361.1	12.1	11.03	10.83	1.9
536.2	480	11.7	14.61	14.40	1.4
546.6	489	11.6	14.89	14.67	1.5
643.3	575	11.9	17.53	17.25	1.6
648.2	578.7	12.0	17.66	17.36	1.7

For all of the nine resonant frequencies there is less than 2% disagreement between theory and measurements when compared in a non-dimensional manner.

It is important to mention that because of the choice of very soft springs in supporting the model, the frequency of the rigid body translation of the structure resting on springs could be very easily filtered out in the experiment and was not accounted for in the previous discussion.

Even if this had not been the case, a valid comparison between the two types of data should still be possible, and for this purpose the author has developed in Appendix V a theoretical analysis allowing for the effects of the two springs.

6. A modal analysis of the Lockheed model L-100 Hercules

a) Presentation of the model

Following the production of early C-130 military Hercules aircraft, Lockheed - Georgia had decided to offer a commercial version of this heavy transport, and the model L-100 is one of the six models which have been offered for that purpose.

Customers of this aircraft have included Alaska Airlines, Delta Air Lines, Interior Airways and Pacific Western Airlines.

A picture of the airplane is shown in the upper part of Figure 32 and a general arrangement drawing is shown below.

More detailed information can be found in References (32) and (33).

b) Numerical results

The theoretical analysis developed in paragraph 3 has been applied with the following values of the parameters representing the model.

Parameter	Physical significance	Value for L-100
ξ_1	point along the fuselage connected with the wing	0
ξ_2	point along the fuselage connected with the wing	1
μ_1	ratio (mass wing/mass fuselage) - engines not taken into account	1
μ_2	ratio (mass wing/mass tail)	38.97
γ_1	ratio (wing span/fuselage span)	1.36
γ_2	ratio (wing span/tail span)	2.52
ν_1	mass to inertia ratio between wing and fuselage	91.4
ν_2	ratio between mass and inertia of the wing	166.84
ν_3	mass to inertia ratio between wing and tail	2669.44
ψ_1	frequency factor of the fuselage in bending	65.47
ψ_2	frequency factor of the fuselage in torsion	81.05
ψ_3	frequency factor of the wing in torsion	245.67
ψ_4	frequency factor of the tail in bending	39.98
ψ_5	frequency factor of the tail in twisting	1560

The first twelve natural frequencies of the aircraft have been obtained and their values are listed below. A total of 53 modes (38 bending modes and 15 twisting modes) has been considered for the motions of the rolling type; 125 modes in total (50 twisting modes and 75 bending modes) have been used in the analysis of the modes

C - 2

of pitching type in order to compensate for the eventual loss in accuracy in the matrix manipulations especially when they are nearly singular.

non-dimensional frequency ω	frequency Ω (cps)	type of modal behavior
4.20	18	pitching
8.30	36	rolling
12.03	53	rolling
16.78	73	rolling
18.75	82	pitching
21.65	95	pitching
23.5	103	pitching
24.3	106	rolling
25.14	110	pitching
40.09	176	rolling
40.6	179	pitching
45.17	199	rolling
52.55	231	rolling

The deformation of the structure in the first mode is shown in the Figure 33; this mode appears to be mainly a wing mode going only small rigid body translations. In fact the natural frequency of this mode is close to the first free-free bending frequency of the wing alone, more precisely

ω_1 beam cantilivered in the middle $< \omega_1 < \omega_1$ free free beam

The figure shows that the wing translates with the fuselage but mainly bends in the first even mode; the ratio of the corresponding generalized coordinates (bending to translation) which is an indication of the relative contribution of the initial modes, is of 1.6 in absolute value. Structural information obtained from the values of the Lagrange Multipliers is given below (up to multiplication).

Shear force developed at the point of attachment between the wing and the fuselage : 1 lb (taken as reference)

Shear force developed at the point of attachment between the tail and the fuselage : 0.019 lb

Torque developed at the point of attachment between the wing and the fuselage : 0.24 lb x in

Torque developed at the point of attachment between the tail and the fuselage : 0.011 lb x in

As expected, the shear force developed at the point where fuselage and wing join, is predominant in this mode.

The structural deformation of the aircraft in the second mode is shown in Figure 34. This mode is characterised by an antisymmetric behavior of the wing and the tail and only angular deformation of the fuselage. This angular deformation is composed of rigid twisting,

with contributions from the second and first elastic torsional modes by order of importance. For purpose of qualitative information:

$$\left| \frac{\overline{P}_1}{\overline{P}_2} \right| = 5.2 \qquad \left| \frac{\overline{P}_1}{\overline{P}_3} \right| = 3.9$$

The wing rotates with the fuselage and bends in the first antisymmetric mode;

$$\left| \frac{\overline{q}^{(1)}_{\text{bending}}}{\overline{q}^{(1)}_{\text{rotation}}} \right| = 1.3$$

The tail shows practically no elastic behavior.

The value of the torques per unit length developed at the points of connection between fuselage and tail and between fuselage and wing respectively is given by the ratio

$$\left| \frac{\overline{\lambda}_4}{\overline{\lambda}_3} \right| = 0.15$$

The next higher mode presents again antisymmetric behavior of the wing and tail as shows Figure 35, in fact the gross-deformation of the structure is very similar to that of the previous mode except for the fact that in this mode the angular twisting of the fuselage has same direction at the points of connection with the wing and the tail.

Detailed analysis shows that in this mode the behavior of the fuselage is predominantly elastic, in fact mostly in the first elastic

mode with some rigid contribution $\left(\left| \frac{\overline{P}_2}{\overline{P}_1} \right| = 2.1 \right)$ and very little

contribution from the 4th elastic mode

$$\left(\left| \frac{\overline{P}_2}{\overline{P}_5} \right| = 32.1 \right)$$

As previously, the wing bends predominantly in the first antisymmetric mode, but undergoes less rotation than previously and shows also influences due to the second free-free antisymmetric mode.

$$\left| \frac{\overline{q}^{(1)}_{\text{bending}}}{\overline{q}^{(1)}_{\text{rotation}}} \right| = 4.92 \qquad \left| \frac{\overline{q}^{(1)}_{\text{bending}}}{\overline{q}^{(1)}_{\text{bending 2nd mode}}} \right| = 13.6$$

as it can be seen in the lower part of Figure 35 the tail acts mainly rigid, however, slight elastic behavior can be graphically detected (quantitatively, $\left| \frac{\overline{q}^{(2)}_{\text{rotation}}}{\overline{q}^{(2)}_{\text{bending}}} \right| = 18.3$)

The ratio of the torques per unit length developed at the wing and tail is now equal to 0.66 as compared to 0.15 in the previous case.

The modal behavior for the fourth natural frequency is shown in Figure 36 and similar discussion can be developed for this mode.

For a more complex analysis taking into account the masses and inertias of the engines (represented by rigid structures attached to the wing), the author refers the readers to the theoretical development of Appendix VI.

The present model does not provide information about the chordwise bending occuring in the wing and the tail because of the

one-dimensional assumptions for these components. A more sophisticated analysis taking these additional effects into account, is provided in the Appendix IV where the wing and the tail are represented by plate elements with uniform properties.

CHAPTER IV

MODAL BEHAVIOR OF A HIGH ASPECT RATIO AIRPLANE WITH OBLIQUE WING AND TAIL.

1. Statement of the problem and basic assumptions

The present chapter may be considered as a generalization of Chapter III. This analysis has not only a pure academic interest in showing the generality of the method, but also a practical interest. Since the oblique wing configuration was proposed, there has been an increasing concern over the aeroelastic problems arising from such an uncommon geometry. As most of the flutter analysis are based on the structural normal modes, the purpose of the present chapter is to provide precisely these normal modes and frequencies. It is of interest to note that the assumption of a high aspect ratio wing is particularly suitable for such a type of configuration as it can be seen in Reference(34)and Figure 37; the additional assumptions under which the problem is treated are similar to those of Chapter III and are reminded below:

1) the airplane structure is considered to be of beam type
2) the displacements of the beam components are governed by the Bernouilli-Euler equation
3) the geometrical and elastic characteristics are constant along the span for each component.

The geometry of the structure is illustrated in the top view given below:

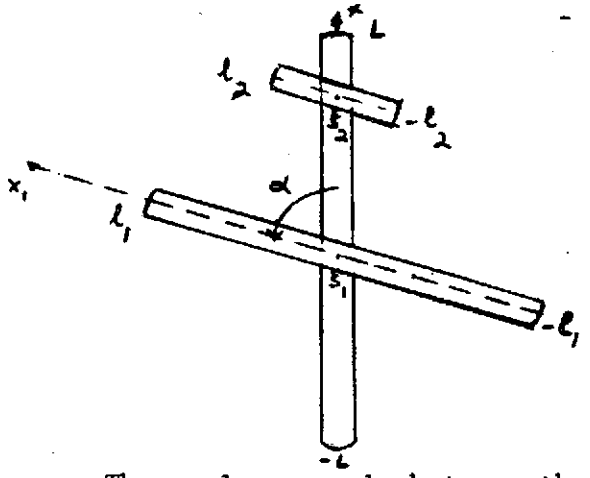

The angle α, angle between the oblique components and the fuselage, is the main new parameter of the problem.

2. Rigid body dynamics in the linearized theory

Notations:

R_o: Gallilean frame of reference

G: Center of gravity of the structure

ψ, Θ, ϕ: Classical Euler angles as defined in Chapter III

$\mathcal{J}$ (G,S): Inertia tensor of the structure at the center of gravity and with respect to its own system of axis

M: Total mass of the structure

$\vec{\Omega}(S/R_o)$: Vector defining the rotations between the frame of the structure and R_o.

$\vec{\Gamma}(G/R_o)$: Acceleration vector as defined in Chapter III.

$\vec{H}((S)/R_o)$: Angular momentum as defined in Chapter III.

In absence of exterior forces Newton's law yields:

$$M \cdot \vec{\Gamma}(G/R_o) = \vec{0} \tag{91}$$

This relation decouples the translations in the three directions

from the rotation motion around the center of gravity.

For zero exterior torque the angular momentum equation is simply:

$$\frac{d}{dt} \vec{H} (S/R_o) = 0 \tag{92}$$

which can be also written as:

$$\frac{d}{dt} (\mathcal{J}(G,S) . \vec{\Omega}(S/R_o)) = o \tag{93}$$

Due to the absence of symetry, the tensor $\mathcal{J}(G,S)$ has a non-diagonal representation and can be written in the following matrix form:

$$\mathcal{J}(G,S) = \begin{pmatrix} I_1(\alpha) & J_1(\alpha) & 0 \\ J_1(\alpha) & I_2(\alpha) & 0 \\ 0 & 0 & I_3 \end{pmatrix}$$

where $J_1 (\pi/2) = 0$.

Hence the linearized equations of the rigid body motion are:

$$(I_1(\alpha) \cos \alpha - J_1(\alpha) \sin\alpha)\ddot{\theta} + (I_1(\alpha) \sin\alpha + J_1(\alpha) \cos\alpha)\ddot{\phi} = 0 \tag{94}$$

$$(J_1(\alpha) \cos\alpha - I_2(\alpha) \sin\alpha)\ddot{\theta} + (J_1(\alpha) \sin\alpha + I_2(\alpha) \cos\alpha)\ddot{} = 0 \tag{95}$$

$$I_3\ddot{\psi} = 0 \tag{96}$$

This set of equations shows that the yawing motion decouples from roll and pitch, but the later two remain coupled unless $\alpha = \pi/2$

This fact introduces a fundamental difference from the types of structures investigated in the previous chapter: indeed, if previously the modal analysis could be done from the onset separately for symmetric

and antisymmetric modes, this is no longer the case for the present problem as it can be seen from the rigid body analysis.

3. Elastic modal behavior, derivation of the frequency equation

a) Statement of the elastic problem: degrees of freedom, derivation of the constraint equations.

The motions investigated are of roll-pitch type; the bending vibrations in the y-direction (yaw-type of motion) are not considered in the present chapter.

Each one of the components is allowed to bend and twist rigidly and elastically and the corresponding modal displacements are sought in the following forms:

- for the fuselage: $-L \leq x \leq L$

bending displacement:

$$W(x,t) = \sum_{n=1}^{\infty} Q_n(t)\phi_n(x) \tag{97}$$

twisting angular displacement:

$$\Theta(x,t) = \sum_{n=1}^{\infty} P_n(t)\,\theta_n(x) \tag{98}$$

- for the oblique wing: $-l_1 \leq x_1 \leq l_1$

bending displacement:

$$w_1(x_1,t) = \sum_{n=1}^{\infty} q_n^{(1)}(t)\,\phi_n(x_1) \tag{99}$$

twisting angular displacement:

$$\Theta_1(x_1,t) = \sum_{n=1}^{\infty} P_n^{(1)}(t)\,\theta_n(x_1) \tag{100}$$

- <u>for the oblique tail:</u> $-l_2 \leq x_1 \leq l_2$

bending displacement:

$$w_2(x_1,t) = \sum_{n=1}^{\infty} q_n^{(2)}(t)\, \phi_n(x_1) \tag{101}$$

twisting angular displacement:

$$\theta_2(x_1,t) = \sum_{n=1}^{\infty} p_n^{(2)}(t)\, \theta_n(x_1) \tag{102}$$

As explained in the previous chapter, the physical displacement of each component is rigorously the sum of the bending displacement and an additional term due to the twisting of that element; however in agreement with the one-dimensional assumption it is reasonable to neglect the contribution due to twisting (based on the fact that the ratio of the chord to the length of the element is considered small). The constraint conditions insuring the equality of the physical displacements at the points of connection between the components can be written then.

$$W(\xi_1,t) = w_1(0,t) \tag{103}$$

$$W(\xi_2,t) = w_2(0,t) \tag{104}$$

after having suitably non-dimensionalized W, W_1 and W_2 so that their domain of definition be $[-1, 1]$.

Another set of constraint conditions is derived from enforcing the equality of the slopes of the components in the $\vec{x}$ and $\vec{y}$ directions and leads to the equations

$$\theta(\xi_1,t) = \theta_1(0,t)\cos\alpha + \frac{1}{l_1}\frac{\partial W_1}{\partial \zeta_1}(0,t)\sin\alpha \tag{105}$$

$$\frac{1}{L}\frac{\partial W}{\partial \xi}(\xi_1, t) = -\Theta_1(0,t)\sin\alpha + \frac{1}{l_1}\frac{\partial w_1}{\partial \zeta_1}(0,t)\cos\alpha \qquad (106)$$

for the wing and fuselage, and

$$\Theta(\xi_2, t) = \Theta_2(0,t)\cos\alpha + \frac{1}{l_2}\frac{\partial w_2}{\partial \zeta_1}(0,t)\sin\alpha \qquad (107)$$

$$\frac{1}{L}\frac{\partial W}{\partial \xi}(\xi_2,t) = -\Theta_2(0,t)\sin\alpha + \frac{1}{l_2}\frac{\partial w_2}{\partial \zeta_1}(0,t)\cos\alpha \qquad (108)$$

for the tail and fuselage.

The slope condition of Chapter III can be found by setting $\alpha = \pi/2$.

b) Derivation of the frequency equation

The total kinetic energy of the structure is

$$T = \frac{1}{2}\left(\int_{-L}^{L} \dot{W}^2(x,t)\,dm + \int_{-l_1}^{l_1} \dot{w}_1^2(x_1,t)\,dm_1 + \int_{-l_2}^{l_2} \dot{w}_2^2(x_1,t)\,dm_2 + \right.$$

$$\left. \int_{-L}^{L} \mathbf{I}\,\dot{\Theta}^2(x,t)\,dx + \int_{-l_1}^{l_1} \mathbf{I}_1\dot{\Theta}^2(x_1,t)\,dx_1 + \int_{-l_2}^{l_2} \mathbf{I}_2\dot{\Theta}^2(x_1,t)\,dx_1\right) \qquad (109)$$

where $\mathbf{I}$, $\mathbf{I}_1$, $\mathbf{I}_2$ are the respective mass moments of inertia per unit length about the torsional axis of the fuselage, wing and tail. Their integral expressions are given in the paragraph 3 section b) of the previous chapter.

Substitution of equations (97) - (102) into equation (109) yields:

$$T = \frac{1}{2}\sum_{n=1}^{\infty} \left(M\dot{Q}_n^2(t) + M_1\,\dot{q}_n^{(1)2}(t) + M_2\,\dot{q}_n^{(2)2}(t) + \right.$$

$$\mathbf{I}\,\ddot{P}_n(t) + \mathbf{I}_1\ddot{P}_n^{(1)}(t) + \mathbf{I}_2\ddot{P}_n^{(2)}(t)\ ) \qquad (110)$$

by virtue of the orthonormality of the free-free component modes.

The total potential energy of the structure in bending and torsion is:

$$U = \frac{1}{2}\left(EI\int_{-L}^{L}\left(\frac{\partial^2 w}{\partial x^2}(x_1 t)\right)^2 dx + EI_1\int_{-l_1}^{l_1}\left(\frac{\partial^2 w_1}{\partial x_1^2}(x_1,t)\right)^2 dx_1 +\right.$$

$$EI_2\int_{-l_2}^{l_2}\left(\frac{\partial^2 w_2}{\partial x^2}(x_1,t)\right)^2 dx_1 + GJ\int_{-L}^{L}\left(\frac{\partial\Theta}{\partial x}(x,t)\right)^2 dx +$$

$$\left.(GJ)_1\int_{-l_1}^{l_1}\left(\frac{\partial\Theta_1}{\partial x_1}(x_1,t)\right)^2 dx_1 + (GJ)_2\int_{-l_2}^{l_2}\left(\frac{\partial\Theta_2}{\partial x_1}(x_1,t)\right)^2 dx_1\right) \qquad (111)$$

where I, I_1, I_2 are the structural moments of inertia about the neutral axis of the fuselage, wing and tail respectively, E and G are the Young and shear modulus of elasticity, and (GJ), $(GJ)_1$ and $(GJ)_2$ are the respectives torsional stiffnesses of each of the components.

Equation (111) can be rewritten by use of (97) - (102) and the free-free beam equations in bending and torsion in the following way:

$$U = \frac{1}{2}\sum_{n=1}^{\infty}\left(\frac{EI}{L^3}k_n^4 Q_n^2(t) + \frac{(EI)_1}{l_1^3}k_n^4 q_n^{(1)2}(t) +\right.$$

$$\left.\frac{(EI)_2}{l_2^3}k_n^4 q_n^{(2)2}(t) + \frac{GJ}{L}(n-1)^2\frac{\pi^2}{4}P_n^2(t) +\right.$$

$$\frac{(GJ)_1}{l_1}(n-1)^2\frac{\pi^2}{4}P_n(1)^2(t) + \frac{(GJ)_2}{l_2}(n-1)^2\frac{\pi^2}{4}P_n^{(2)}(t)^2) \quad (112)$$

Using again the Rayleigh Ritz expansions given in the equations (97) - (102) for substitution into the constraint conditions (103) - (108), the following modal expressions are obtained:

$$\sum_{n=1}^{\infty}(Q_n(t)\phi_n(\xi_1) - q_n^{(1)}(t)\phi_n(0)) = 0 \quad (113)$$

$$\sum_{n=1}^{\infty}(Q_n(t)\phi_n(\xi_2) - q_n^{(2)}(t)\phi_n(0)) = 0 \quad (114)$$

$$\sum_{n=1}^{\infty}(P_n(t)\theta_n(\xi_1) - P_n^{(1)}(t)\theta_n(0)\cos\alpha - \frac{q_n^{(1)}(t)}{l_1}\phi'_n(0)\sin\alpha) = 0 \quad (115)$$

$$\sum_{n=1}^{\infty}(\frac{Q_n(t)}{L}\phi'_n(\xi_1) + P_n^{(1)}(t)\theta_n(0)\sin\alpha - \frac{q_n^{(1)}(t)}{l_1}\phi'_n(0)\cos\alpha) = 0 \quad (116)$$

$$\sum_{n=1}^{\infty}(P_n(t)\theta_n(\xi_2) - P_n^{(2)}(t)\theta_n(0)\cos\alpha - \frac{q_n^{(2)}(t)}{l_2}\phi'_n(0)\sin\alpha) = 0 \quad (117)$$

$$\sum_{n=1}^{\infty}(\frac{Q_n(t)}{L}\phi'_n(\xi_2) + P_n^{(2)}(t)\theta_n(0)\sin\alpha - \frac{q_n^{(2)}(t)}{l_2}\phi'_n(0)\cos\alpha) = 0 \quad (118)$$

These equations weighted by their respective Lagrange multipliers contribute to the formulation of the Lagrangian for the entire elastic structure:

$$\mathcal{L}(t) = T(t) - U(t) + \lambda_1(t) \times \text{eq.}(113) + \lambda_2(t) \times \text{eq.}(114) +$$

$$\lambda_3(t) \times \text{eq.}(115) + \lambda_4(t) \times \text{eq.}(116) + \lambda_5(t) \times \text{eq.}(117) +$$

$\lambda_5(t)$ x eq.(118)

As mentioned in Chapter III the values of the Lagrange multipliers give interesting structural information: $(\lambda_i)_{i = 1,2}$ relative to displacement conditions give a comparative value of the shear force developed at the points of connection between the fuselage and wing and the fuselage and tail; $(\lambda_i)_{i = 3, \ldots 6}$ give a relative value of the bending moments about the x and y axis developed at the points of junction between the components.

Moreover the values of the Lagrange multipliers indicate which type of behavior is predominant in a particular mode before even having actually determined the mode shape. This statement is a little of an anticipation at this point but its proof is clear from equations (125) - (130).

The equations of motion, known as Lagrange's equations for the system are:

$$\bullet\ M\ddot{Q}_n(t) + \frac{EI}{L^3} k_n^4 Q_n(t) - \lambda_1(t)\phi_n(\xi_1) - \lambda_2(t)\phi_n(\xi_2) - \frac{\lambda_4(t)}{L}\phi'_n(\xi_1) - \frac{\lambda_6(t)}{L}\phi'_n(\xi_2) = 0 \qquad (119)$$

$$\bullet\ I_L\ddot{P}_n(t) + \frac{GJ}{L}(n-1)^2\frac{\pi^2}{4} P_n(t)(t) - \lambda_3(t)\theta_n(\xi_1) - \lambda_5(t)\ \theta_n(\xi_2) = 0 \qquad (120)$$

$$\cdot\ M_1\ddot{q}_n(t) + \frac{(EI)_1}{l_1^3}\, k_n^4\, q_n^{(1)}(t) + \lambda_1(t)\phi_n(0) +$$

$$\frac{\lambda_3(t)}{l_1}\,\phi'_n(0)\,\sin\alpha + \frac{\lambda_4(t)}{l_1}\,\phi'_n(0)\cos\alpha = 0 \qquad (121$$

$$\cdot\ \mathbf{I}_1 l_1 \ddot{P}_n^{(1)}(t) + \frac{(GJ)_1}{l_1}\,(n-1)^2\pi^2 P_n^{(1)}(t) + \lambda_3(t)\theta_n(0)\cos\alpha -$$

$$\lambda_4(t)\theta_n(0)\sin\alpha = 0 \qquad (122)$$

$$\cdot\ M_2\ddot{q}_n^{(2)}(t) + \frac{(EI)_2}{l_2^3}\, k_n^4\, q_n^{(2)}(t) + \lambda_2(t)\phi_n(0) + \frac{\lambda_5(t)}{l_2}\,\phi'_n(0)$$

$$\sin\alpha + \frac{\lambda_6(t)}{l_2}\,\phi'_n(0)\,\cos\alpha = 0 \qquad (123)$$

$$\cdot\ \mathbf{I}_2 l_2 \ddot{P}_n^{(2)}(t) + \frac{(GJ)_2}{l_2}\,(n-1)^2\pi^2\, P_n^{(2)}(t) + \frac{\lambda_5(t)}{l_2}\,\theta_n(0)$$

$$\cos\alpha - \lambda_6(t)\theta_n(0)\sin\alpha = 0 \qquad (124)$$

together with the constraint equations (113) - (118).

The harmonic behavior in the modal analysis is taken in a similar form to that of the previous Chapter and is reminded here:

$$\begin{Bmatrix} Q_n(t) \\ P_n(t) \\ q_n^{(1)}(t) \\ P_n^{(1)}(t) \\ q_n^{(2)}(t) \\ P_n^{(2)}(t) \end{Bmatrix} = \begin{Bmatrix} \bar{Q}_n \\ \bar{P}_n \\ \bar{q}_n(1) \\ \bar{P}_n(1) \\ \bar{a}_n(2) \\ \bar{P}_n(2) \end{Bmatrix} \times e^{i \left(\frac{(EI)_1}{M_1 l_1^3}\right)^{1/2} \omega t}$$

$$\begin{Bmatrix} \lambda_1(t) \\ \lambda_2(t) \end{Bmatrix} = \begin{Bmatrix} \bar{\lambda}_1 \\ \bar{\lambda}_2 \end{Bmatrix} \times \frac{(EI)_1}{l_1^3} \, e^{i \left(\frac{(EI)_1}{M_1 l_1^3}\right)^{1/2} \omega t}$$

$$\begin{Bmatrix} \lambda_3(t) \\ \lambda_4(t) \\ \lambda_5(t) \\ \lambda_6(t) \end{Bmatrix} = \begin{Bmatrix} \bar{\lambda}_3 \\ \bar{\lambda}_4 \\ \bar{\lambda}_5 \\ \bar{\lambda}_6 \end{Bmatrix} \times \frac{(EI)_1}{l_1^2} \times e^{i \left(\frac{(EI)_1}{M_1 l_1^3}\right)^{1/2} \omega t}$$

The following non-dimensional parameters are defined:

$$\mu_1 = \frac{M_1}{M} \quad ; \quad \mu_2 = \frac{M_1}{M_2} \; ; \; \gamma_1 = \frac{l_1}{L} \quad ; \quad \gamma_2 = \frac{l_1}{l_2}$$

$$\nu_1 = \frac{M_1 l_1}{I} \; ; \quad \nu_2 = \frac{M_1 L}{I_1} \; ; \quad \nu_3 = \frac{M_1 L}{I_2}$$

$$\psi_1 = \frac{\dfrac{EI}{ML^3}}{\dfrac{(EI)_1}{M_1 l_1^3}} \; ; \quad \psi_2 = \frac{\dfrac{GJ}{IL^2}}{\dfrac{(EI)_1}{M_1 l_1^3}} \; ; \quad \psi_3 = \frac{\dfrac{(GJ)_1}{I_1}}{\dfrac{(EI)_1}{M_1 l_1}}$$

$$\psi_4 = \frac{\dfrac{(EI)_2}{M_2 l_2^3}}{\dfrac{(EI)_1}{M_1 l_1^3}} \; ; \quad \psi_5 = \frac{\dfrac{(GJ)_2}{I_2 l_2^2}}{\dfrac{(EI)_1}{M_1 l_1^3}}$$

$$F_n^{(1)} = \omega^2 - \psi_1 k_n^4$$

$$F_n^{(2)} = \omega^2 - \psi_2 (n-1)^2 \left(\frac{\pi}{4}\right)^2$$

$$F_n^{(3)} = \omega^2 - k_n^4$$

$$F_n^{(4)} = \omega^2 - \psi_3 (n-1)^2 \left(\frac{\pi}{4}\right)^2$$

$$F_n^{(5)} = \omega^2 - \psi_4 k_n^4$$

$$F_n^{(6)} = \omega^2 - \psi_5 (n-1)^2 \frac{\pi}{4}^2$$

In terms of these parameters and of the non-dimensional Lagrange multipliers the generalized coordinates are expressed as follows:

$$\overline{Q}_n = - \mu_1 \frac{(\overline{\lambda}_1 \phi_n(\xi_1) + \overline{\lambda}_2 \phi_n(\xi_2) + \overline{\lambda}_4 \gamma_1 \phi'_n(\xi_1) + \overline{\lambda}_6 \gamma_1 \phi'_n(\xi_2))}{F_n^{(1)}} \tag{125}$$

$$\overline{P}_n = - \gamma_1 \nu_1 \frac{(\overline{\lambda}_3 \theta_n(\xi_1) + \overline{\lambda}_5 \theta_n(\xi_2))}{F_n^{(2)}} \tag{126}$$

$$\overline{q}_n^{(1)} = \frac{\overline{\lambda}_1 \phi_n(0) + \overline{\lambda}_3 \phi'_n(0) \sin\alpha + \overline{\lambda}_4 \phi'_n(0) \cos\alpha}{F_n^{(3)}} \tag{127}$$

$$\overline{P}_n^{(1)} = \nu_2 \frac{(\overline{\lambda}_3 \cos\alpha - \overline{\lambda}_4 \sin\alpha)}{F_n^{(4)}} \theta_n(0) \tag{128}$$

$$\overline{q}_n^{(2)} = \mu_2 \frac{(\overline{\lambda}_2 \phi_n(0) + \overline{\lambda}_5 \gamma_2 \phi'_n(0) \sin\alpha + \overline{\lambda}_6 \gamma_2 \phi'_n(0) \cos\alpha)}{F_n^{(5)}} \tag{129}$$

$$P_n^{(2)} = \gamma_2 \nu_3 \left(\frac{\bar{\lambda}_5 \cos\alpha - \bar{\lambda}_6 \sin\alpha}{F_n^{(6)}} \right) \theta_n(0) \qquad (130)$$

It can be noticed that only even modes contribute to the twisting of the wing and tail as it can be seen from equations (128) and (130).

It is also interesting to point out by the use of two examples how the modal behavior of the structure can be predicted from the value of the Lagrange multipliers directly.

- Example 1:

Assume that for a particular mode the values of the Lagrange multipliers are such that

$$\left| \frac{\bar{\lambda}_i}{\bar{\lambda}_1} \right| << 1 \quad \text{for any } i = 2, \ldots 6$$

Then equations (94) - (99) can be written at zeroth order approximation.

$$\bar{Q}_n = - \frac{\mu_1 \bar{\lambda}_1 \phi_n(\xi_1)}{F_n^{(1)}}$$

$$\bar{P}_n = 0$$

$$\bar{q}_n^{(1)} = \frac{\bar{\lambda}_1 \phi_n(0)}{F_n^{(3)}}$$

$$\bar{P}_n^{(1)} = 0$$

$$\overline{q}_n^{(2)} = 0$$

$$\overline{P}_n^{(2)} = 0$$

for any n.

By substituting these equations into equations (97) - (102) we obtain the expressions of the modal displacements at the lowest order:

$$\overline{W}(\xi) = - \sum_{n=1}^{\infty} \frac{\mu_1 \phi_n(\xi_1)\phi_n(\xi)}{F_n^{(1)}} \tag{131}$$

$$\overline{W}_1(\zeta) = \sum_{n=1}^{\infty} \frac{\phi_n(0)\phi_n(\zeta)}{F_n^{(3)}} \tag{132}$$

$$\overline{\Theta}(\xi) = \overline{\Theta}_1(\zeta) = \overline{W}_2(\zeta) = \overline{\Theta}_2(\zeta) = 0 \tag{133}$$

The modal displacements being defined up to a multiplicative constant, division by $\overline{\lambda}_1$ is justified. Equation (133) shows that the tail does not move almost at all in this mode, nor is there almost any twisting in the fuselage or wing. Equation (132) shows that the wing bends symmetrically about the fuselage; equation (131) gives the mode shape of the fuselage. Such a mode is in fact a plunging mode, totally independent on the angle α and could possibly look as illus-

trated below:

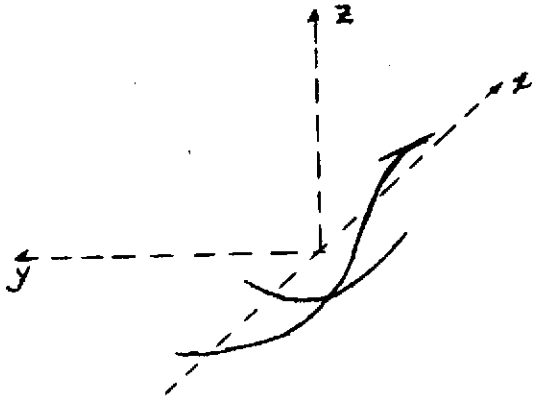

Of course, the analysis has only the value of an example and no claim is made as to the possible existence of such a mode.

- Example 2:

For such a hypothetical mode we assume that the values of $\overline{\lambda}_3$ and $\overline{\lambda}_6$ are much larger than the values of the other Lagrange multipliers. Then equations (125) - (130) give the following zeroth order approximation:

$$\overline{Q}_n = 0 \tag{134}$$

$$\overline{P}_n = - \gamma_1 \nu_1 \frac{\overline{\lambda}_3 \theta_n(\xi_1)}{F_n^{(2)}} \tag{135}$$

$$\overline{q}_n^{(1)} = \frac{\overline{\lambda}_3 \phi'_n(0) \sin\alpha}{F_n^{(3)}} \tag{136}$$

$$\overline{P}_n^{(1)} = \nu_2 \frac{\overline{\lambda}_3 \cos\alpha\ \theta_n(0)}{F_n^{(4)}} \tag{137}$$

$$\overline{q}_n^{(2)} = \mu_2\gamma_2 \frac{\overline{\lambda}_6\phi'_n(0)\cos\alpha}{F_n^{(5)}} \tag{138}$$

$$\overline{P}_n^{(2)} = -\gamma_2\nu_3 \frac{\overline{\lambda}_6\sin\alpha\theta_n(0)}{F_n^{(6)}} \tag{139}$$

It is easily seen that in such a mode the fuselage twists only; an even more refined analysis can be done by comparing $\overline{\lambda}_3$ and $\overline{\lambda}_6$ and hence the generalized coordinates for given values of γ_1,ν_1, γ_2,ν_2, ν_3, μ_2.

It can be noticed that for $\alpha = \frac{\pi}{2}$ such a mode cannot be possibly encountered.

Indeed, equations (134) - (139) reduce to:

$$\overline{0}_n = \overline{P}_n^{(1)} = \overline{q}_n^{(2)} = 0$$

$$\overline{P}_n = -\gamma_1\nu_1 \frac{\overline{\lambda}_3\theta_n(\xi_1)}{F_n^{(2)}}$$

$$\overline{q}_n^{(1)} = \frac{\overline{\lambda}_3\phi'_n(0)}{F_n^{(3)}}$$

$$\overline{P}_n^{(2)} = - \gamma_2 \nu_3 \frac{\overline{\lambda}_6 \theta_n(0)}{F_n^{(6)}} \tag{140}$$

and equation (140) introduces coupling between rolling and pitching modes. In fact the values of $\overline{\lambda}_3$ and $\overline{\lambda}_6$ are obtained by totaly independent analysis.

For the general case, substitution of equations (125) - (130) into the constraint conditions given in equations (113) - (118) leads to the set of linear algebraic equations in terms of $(\overline{\lambda}_i)$ i = 1, ...6 from which the frequency equation will result.

This system of equations can be written in tensorial form

$$\overline{\overline{\Delta}} \cdot \vec{\lambda} = \vec{0} \tag{141}$$

with self explanatory notations for $\vec{\lambda}$ and with the second order symmetric tensor $\overline{\overline{\Delta}}$ defined by its matrix representation as follows:

$$\Delta_{11} = \sum_{n=1}^{\infty} \left(\mu_1 \frac{\phi_n^2(\xi_1)}{F_n^{(1)}} + \frac{\phi_n^2(0)}{F_n^{(3)}} \right) \tag{142}$$

$$\Delta_{12} = \sum_{n=1}^{\infty} \mu_1 \frac{\phi_n(\xi_1)\phi_n(\xi_2)}{F_n^{(1)}} \tag{143}$$

$$\Delta_{13} = \Delta_{15} = \Delta_{23} = \Delta_{25} = \Delta_{36} = \Delta_{45} = 0 \tag{144}$$

$$\Delta_{14} = \sum_{n=1}^{\infty} \mu_1\gamma_1 \frac{\phi_n(\xi_1)\phi'_n(\xi_1)}{F_n^{(1)}} \tag{145}$$

$$\Delta_{16} = \sum_{n=1}^{\infty} \mu_1\gamma_1 \frac{\phi_n(\xi_1)\phi'_n(\xi_2)}{F_n^{(1)}} \tag{146}$$

$$\Delta_{22} = \sum_{n=1}^{\infty} \left(\mu_1 \frac{\phi_n^2(\xi_2)}{F_n^{(1)}} + \mu_2 \frac{\phi_n^2(0)}{F_n^{(5)}}\right) \tag{147}$$

$$\Delta_{24} = \sum_{n=1}^{\infty} \mu_1\gamma_1 \frac{\phi'_n(\xi_1)\phi'_n(\xi_2)}{F_n^{(1)}} \tag{148}$$

$$\Delta_{26} = \sum_{n=1}^{\infty} \mu_1\gamma_1 \frac{\phi_n(\xi_2)\phi'_n(\xi_2)}{F_n^{(1)}} \tag{149}$$

$$\Delta_{33} = \sum_{n=1}^{\infty} \left(\gamma_1\nu_1 \frac{\theta_n^2(\xi_1)}{F_n^{(2)}} + \gamma_1\nu_2 \frac{\theta_n^2(0)\cos^2\alpha}{F_n^{(4)}} + \frac{\phi'^2_n(0)\sin^2\alpha}{F_n^{(3)}}\right) \tag{150}$$

$$\Delta_{34} = \sum_{n=1}^{\infty} \left(-\gamma_1\nu_2 \frac{\theta_n^2(0)}{F_n^{(4)}} + \frac{\phi'^2_n(0)}{F_n^{(3)}}\right)\sin\alpha\cos\alpha \tag{151}$$

$$\Delta_{35} = \sum_{n=1}^{\infty} \gamma_1\nu_1 \frac{\theta_n(\xi_1)\,\theta_n(\xi_2)}{F_n^{(2)}} \tag{152}$$

$$\Delta_{44} = \sum_{n=1}^{\infty} \left(\mu_1\gamma_1^2 \frac{\phi'^2_n(\xi_1)}{F_n^{(1)}} + \gamma_1\nu_2 \frac{\theta_n^2(0)\sin^2\alpha}{F_n^{(4)}} + \frac{\phi'^2_n(0)\cos^2\alpha}{F_n^{(3)}}\right) \quad (153)$$

$$\Delta_{46} = \sum_{n=1}^{\infty} \mu_1\gamma_1^2 \frac{\phi'_n(\xi_1)\phi'_n(\xi_2)}{F_n^{(1)}} \quad (154)$$

$$\Delta_{55} = \sum_{n=1}^{\infty} \left(\gamma_1\nu_1 \frac{\theta_n^2(\xi_2)}{F_n^{(2)}} + \gamma_1\gamma_2\nu_3 \frac{\theta_n^2(0)\cos^2\alpha}{F_n^{(6)}} + \mu_2\gamma_2^2 \frac{\phi'^2_n(0)\sin^2\alpha}{F_n^{(5)}}\right) \quad (155)$$

$$\Delta_{56} = \sum_{n=1}^{\infty} \left(-\gamma_1\gamma_2\nu_3 \frac{\theta_n^2(0)}{F_n^{(6)}} + \gamma_2^2\mu_2 \frac{\phi'_n(0)}{F_n^{(5)}}\right)\sin\alpha\cos\alpha \quad (156)$$

$$\Delta_{66} = \sum_{n=1}^{\infty} \left(\mu_1\gamma_1^2 \frac{\phi'^2_n(\xi_2)}{F_n^{(1)}} + \gamma_1\gamma_2\nu_3 \frac{\theta_n^2(0)\sin^2\alpha}{F_n^{(6)}} + \gamma_2^2\mu_2 \frac{\phi'^2_n(0)\cos^2\alpha}{F_n^{(5)}}\right) \quad (157)$$

It can be pointed out that the elements Δ_{ij} are in fact mathematically Green's functions or in physical language influence coefficients and can be easily understood. For instance Δ_{12} represents the bending displacement of the structure at the connection point between the fuselage and wing due to a unit force applied at the point connecting fuselage and tail.

It is interesting to note that a Green's function approach to eigenvalue problems was suggested by Otakar Danek in 1971, how-

ever no correlations of the work with a variational approach to the problem is mentioned, nor a practical way of actually solving the eigenvalue problems given.

The eigenvalue system (141) leads to the frequency equation

$$\boxed{\det \mathbb{A}(\omega) = 0} \tag{158}$$

necessary and sufficient condition for existence of solutions $\vec{\lambda}$.

Although equation (158) can be reduced to a polynomial equation in ω^2, in order to obtain a reasonably accurate solution for the first few modes, the degree of the polynome has to be high and hence it is impractical and time consuming to obtain the roots by iterative methods. For this reason it is preferable to solve equation (158) by a trial and error method, which besides its simplicity has the advantage of giving information about the slope of the determinant in the vicinity of the natural frequencies.

c) Remarks on the sensitivity of the natural frequencies with respect to small changes in α from the symmetric configuration.

The ultimate purpose of the modal analysis for the oblique airplane is to determine the functional dependence of the natural frequencies upon α and also the changes in the modal shapes due to variations in the oblicity angle. It is by now obvious that these two questions cannot be solved entirely by analytic procedure, in other words it is impossible to express the natural frequencies $\omega_n(\alpha)$ in the form

$$\omega_n(\alpha) = f_n(\alpha)$$

where $f_n(\alpha)$ are known functions of α.

However, particular aspects of the problem can be investigated analytically; for instance it is of interest to determine the order of magnitude of the change in a given natural frequency when the structure is given a small oblicity angle from its symmetric configuration.

Based on physical evidence it is consistent to assume that $\omega_n(\alpha)$ are continuous functions of α ; then, for small values of $|\alpha - \frac{\pi}{2}|$ it is possible to approximate $\omega_n(\alpha)$ as follows:

$$\omega_n(\alpha) = \omega_n(\pi/2) + (\alpha - \pi/2) \left.\frac{d\omega_n}{d\alpha}\right|_{\alpha = \pi/2} \tag{159}$$

provided that $\left.\frac{d\omega_n}{d\alpha}\right|_{\alpha = \pi/2}$ exists and has a finite value.
Using the relation

$$\left.\frac{d\omega_n}{d\alpha}\right|_{\alpha = \pi/2} = \frac{\left.\frac{\partial\, Det(\Delta)}{\partial\alpha}\right|_{\alpha = \pi/2,\ \omega=\omega_n}}{\left.\frac{\partial\, Det\,(\Delta)}{\partial\omega}\right|_{\alpha = \pi/2,\ \omega=\omega_n}} \tag{160}$$

and the expressions of Δ_{ij} given in equations (142) - (157) it can be seen that $\left.\frac{d\omega_n}{d\alpha}\right|_{\alpha = \frac{\pi}{2}}$ exists and it is finite except for situations in which

$$\left.\frac{\partial\, Det\,(\Delta)}{\partial\omega}\right|_{\alpha = \pi/2,\ \omega = \omega_n} \text{ is zero}$$

This type of situation occurs only if ω_n is a double root of the frequency equation for the symmetric configuration (for instance this would be the case if the structure were composed of two identical beams connected at their middle), generally the natural frequencies are only simple roots of the frequency equation.

Substitution of equation (160) into equation (159) yields:

$$\omega_n(\alpha) = \omega_n(\pi/2) + (\alpha - \pi/2) \frac{\left.\frac{\partial \text{ Det } (\Delta)}{\partial \alpha}\right|_{\alpha = \pi/2, \omega=\omega_n}}{\left.\frac{\partial \text{ Det } (\Delta)}{\partial \omega}\right|_{\alpha = \pi/2, \omega=\omega_n}} \tag{161}$$

$\frac{\partial \text{ Det}(\Delta)}{\partial \alpha}$ can be computed as follows:

$$\frac{\partial \text{ Det } (\Delta)}{\partial \alpha} = \sum_{l=1}^{6} \text{Det } (\Delta_l) \tag{162}$$

where Δ_l is the matrix defined as follows:

$$(\Delta_l)_{ij} = \Delta_{ij} \quad \text{if} \quad j \neq l \text{ for all } i$$

$$(\Delta_l)_{il} = \frac{\partial \Delta_{il}}{\partial \alpha} \qquad \text{for all } i$$

This results from the fact that the function determinant is linear with respect to row or column.

By using equation (162) it is found that

$\left.\frac{\partial \text{ Det } (\Delta)}{\partial \alpha}\right|_{\alpha = \frac{\pi}{2}}$ is identically zero in ω.

As a consequence, if the structure is given only a small oblicity angle β from the symmetric configuration there is no change in the natural frequencies at the order β. ($\beta = \alpha - \pi/2$)

A more refined analysis can be done by looking at the second order problem:

$$\omega_n(\alpha) = \omega_n(\pi/2) + \frac{1}{2}(\alpha - \pi/2)^2 \left.\frac{d^2\omega_n}{d\alpha^2}\right|_{\alpha = \pi/2} \tag{163}$$

Because $\left.\frac{\partial \mathrm{Det}(\Delta)}{\partial\alpha}\right|_{\alpha = \pi/2} = 0$ for all ω_n

$$\left.\frac{d^2\omega_n}{d\alpha^2}\right|_{\alpha = \pi/2} = \frac{\left.\frac{\partial^2 \mathrm{Det}(\Delta)}{\partial\alpha^2}\right|_{\alpha = \pi/2, \omega=\omega_n}}{\left.\frac{\partial \mathrm{Det}(\Delta)}{\partial\omega}\right|_{\alpha = \pi/2, \omega=\omega_n}}$$

and hence $\left.\frac{d^2\omega_n}{d\alpha^2}\right|_{\alpha = \frac{\pi}{2}}$ exists under the same conditions as

$$\left.\frac{d\omega_n}{d\alpha}\right|_{\alpha = \frac{\pi}{2}}$$

By substitution into equation (163) it follows that

$$\omega_n(\alpha) - \omega_n(\pi/2) = \frac{1}{2}(\alpha - \pi/2)^2 \frac{\left.\frac{\partial^2 \mathrm{Det}(\Delta)}{\partial\alpha^2}\right|_{\alpha = \pi/2, \omega=\omega_n}}{\left.\frac{\partial \mathrm{Det}(\Delta)}{\partial\omega}\right|_{\alpha = \pi/2, \omega=\omega_n}} \tag{164}$$

$\frac{\partial^2 \text{Det}(\Delta)}{\partial \alpha^2}$ is computed by using again the linearity property:

$$\frac{\partial^2 \text{Det}\ (\Delta)}{\partial \alpha^2} = \sum_{k=1}^{6} \sum_{l=1}^{6} \text{Det}\ (\Delta_{kl})$$

where

$$\Delta_{kl} = (\Delta_k)_l$$

with the previous notations.

As Δ_{i1} and Δ_{i2} are independent of α for all i. The summation above extends in fact only to the subscripts 3, 4, 5, 6.

A practical application of the analysis is given in the example below.

This example assumes a pivoting wing version of the Lockheed L-100 (for which the structural frequencies and modes have been investigated in Chapter III) and by use of equation (132) predicts its first four natural frequencies for an 80° configuration. The results are tabulated below:

$\frac{\partial^2 \text{Det}(\Delta)}{\partial \alpha^2}\Big\vert_{\alpha = \pi/2, \omega=\omega_n}$ / $\frac{\partial^2 \text{Det}(\Delta)}{\partial \omega}\Big\vert_{\alpha = \pi/2, \omega=\omega_n}$	$\omega_{n_{90^\circ}}$	$\omega_{n_{80^\circ}}$
0.00016	4.20	4.200024
0.00206	8.30	8.29969
0.0058	12.03	12.03087
0.8666	16.78	16.65

The results show that for a 10^{o} deviation from the symmetric configuration only the fourth natural frequency changes by a significant amount; moreover it is seen that the first frequency remains virtually unchanged while the second frequency is slightly decreased and the third frequency increased.

4. Numerical analysis: a pivoting - wing version of the Lockheed model L-100 Hercules

The present section provides a more extensive study of the previous example; the modal behavior of such an airplane is investigated for ranges of pivoting angles going from 90^{o} (case of the straight wing) up to 30^{o} (reasonable limiting value for practical purposes). The value of the first four frequencies as functions of the angle α are plotted in Figure 38; for the straight wing case the type of modes is indicated (rolling or pitching).

As predicted by the perturbation theory, it is seen that no significant changes occur up to the fourth natural frequency where α decreases slightly from the 90^{o} value; moreover, the trend of the variation is correctly predicted by the perturbation theory.

It is seen that the first natural frequency is insensitive to values of α; the second natural frequency decreases significantly only when α varies from 60^{o} to 30^{o}; the third frequency can be considered to increase as early as $\alpha = 70^{o}$, and the fourth frequency is seen to decrease even more rapidly.

The fact that the first natural frequency remains constant

through changes in α is not in fact surprising; in the analysis developed in Chapter III it has been pointed out that the corresponding mode is practically a "wing mode"; all other components show rigid behavior.

The values of the ratios $\bar{\lambda}_i/\bar{\lambda}_1$ are tabulated below and give more detailed information about the first mode shape.

α	$\bar{\lambda}_2/\bar{\lambda}_1$	$\bar{\lambda}_3/\bar{\lambda}_1$	$\bar{\lambda}_4/\bar{\lambda}_1$	$\bar{\lambda}_5/\bar{\lambda}_1$	$\bar{\lambda}_6/\bar{\lambda}_1$
90^o	-0.02	-	-	-	-
60^o	-0.02	0.3	0.2	-0.26	0.26
45^o	-0.02	-0.03	-0.03	0.02	0.03
30^o	-0.02	-0.017	-0.03	-0.014	0.03

The results show that for any angle of rotation the non-dimensional Lagrange multipliers $\bar{\lambda}_2$ to $\bar{\lambda}_6$ are small compared to $\bar{\lambda}_1$; as a consequence both the fuselage and the wing will keep a symmetric behavior through changes in α, practically the behavior of the straight configuration. These conclusions follow directly from equations (125) and (127). More specific results can be drawn from the table above for each configuration; in particular, it can be seen that when $\alpha = 60^o$ the value of $\bar{\lambda}_2/\bar{\lambda}_1$ is negligible compared to any $\bar{\lambda}_i/\bar{\lambda}_1, i \neq 2$; in this case equation (129) shows that the tail will undergo mainly antisymmetric vibrations and since ω_1 is less than the first corresponding free free natural frequency of the tail, its modal behavior will be a rigid rotation.

Same argument applies to justify a rigid behavior of the fuselage.

As α decreases further, the values of the ratios $\overline{\lambda}_i/\overline{\lambda}_1$ $i \neq 1$ become comparable and hence the antisymmetric characteristics alternate in the tail's mode.

A more complete picture of the first mode is given in Figure 39. The behavior of the airplane in the second mode can be analysed in similar fashion, given the values of the ratios $\overline{\lambda}_i$ $\overline{\lambda}_1$ $i = 2, \ldots.6$.

α	$\overline{\lambda}_2/\overline{\lambda}_1$	$\overline{\lambda}_3/\overline{\lambda}_1$	$\overline{\lambda}_4/\overline{\lambda}_1$	$\overline{\lambda}_5/\overline{\lambda}_1$	$\overline{\lambda}_6/\overline{\lambda}_1$
90^o	-	-	-	-	-
60^o	-3.56	54.60	36.16	-6.32	-3.04
45^o	-4.0	33.33	39.83	-2.71	-2.11
30^0	-4.94	22.36	48.92	-1.12	-1.30

A first important remark is that the values of $\overline{\lambda}_i/\overline{\lambda}_1$, i = 3,5,6, decrease as the wing and tail pivot from the straight configuration; this shows that the second mode which originates from a mode of the rolling type becomes progressively coupled with pitching.

It is also interesting to notice that $\overline{\lambda}_4/\overline{\lambda}_1$, $\overline{\lambda}_4/\overline{\lambda}_2$ and $\overline{\lambda}_4/\overline{\lambda}_6$ are large compared to unity for the different values of angle α tabulated; as a result, the fuselage will mainly undergo antisymmetric vibrations, in fact rigid rotations in this range of frequencies.

Because $\overline{\lambda}_3/\overline{\lambda}_1$ and $\overline{\lambda}_4/\overline{\lambda}_1$ are large compared to unity, another general feature of this mode is the antisymmetric behavior of the wing.

Finally, it can be seen that the plunging mode becomes increasingly important in the tail as it rotates from the straight position to 30^o.

The evolution of this mode with the pivoting angle is shown in Figure 40; the displacements have been normalized so that the larger generalized coordinate for the wing be equal to 1.

Figure 41 shows the physical displacement of the components in the third mode with same normalization as in Figure 40; this mode is similar in nature to the second natural mode.

The analysis can be pursued for infinitely many modes, but very seldom more than the first 10 or so modes are needed in a flutter investigation; they are very easily provided by the present analysis. As an example, the first 10 natural frequencies are given for the straight wing configuration (Chapter III) and for a 45^{o} oblique wing and tail:

Straight wing		oblique wing	percentage difference:
ω_n	mode type	ω_n	$\left\|\frac{\omega_{n90^o} - \omega_{n45^o}}{\omega_{n90^o}}\right\|$
4.20	pitching	4.20	0%
8.30	rolling	7.87	5.2%
12.03	rolling	12.5	3.9%
16.78	rolling	15.2	9.0%
18.75	pitching	20.51	8.9%
21.65	pitching	21.83	8.3%
23.5	pitching	23.82	14.0%
24.3	rolling	37.54	52%
25.14	pitching	40.41	61%
40.09	rolling	48.50	21%
40.6	pitching	53.88	26%

The results show that the higher frequencies are more subject to change when the wing and tail rotate; moreover the coupling between a particular bending mode and a torsional mode has the effect of making the higher of the two frequencies higher and this trend is shown in the numerical results.

5. Discussion

The validity of the numerical results for such types of problems is generally subject to the assumptions made in their modeling (in the mathematical sense) and also very strongly dependent upon the methods used in handling them.

If the basic assumptions for the problem are suggested by geometric or elastic considerations, it is relatively easy to make a choice giving satisfactory results; a more detailed analysis has to be made concerning the method by which these results are obtained.

For instance, numerical results obtained by a perturbation method can be subject to doubt if it is noticed a posteriori that the small parameter was in fact of the order of unity. The present discussion has the purpose of precisely pointing out the situations in which the results given by the previous analysis have to be considered very critically. It has been mentioned that the important parameter in the problem is the pivoting angle α defined between 0 and 180 degrees. The case where $\alpha = 90^{o}$ is a limiting case of uncoupled motion, case in which both the elements of the eigenvalue matrix Δ_{34} and Δ_{56} vanish because of the factored term $\sin\alpha \cos\alpha$. If this result is similarly true for $\alpha = 0$ or 180 degrees, care should be taken to avoid drawing conclusions

from it. Indeed, the latest situations correspond to a structure made of superimposed beams for which point contraint conditions are unsuitable. The constraint conditions should either apply along the line of contact in the one-dimensional theory, or else in this type of vibrations the beams would perpetually hit each other.

The last remark would be true also when α is close to 0 or 180 degrees; such a type of constraint condition (assuming that its formulation made sense) would be non-holonomic and thus the use of the Lagrange multipliers would be invalid.

It is with this consideration in mind that the previous analysis has not been pursued for oblicity angles of less than 30°; these types of situations are anyway very difficult to realize in practice.

The aforementioned limitation appears thus to be of theoretical rather than practical importance; but it is necessary to have it in mind when the method is used, for a critical analysis of the results.

CHAPTER V

THE RAYLEIGH RITZ COMPONENT MODES METHOD USING LAGRANGE MULTIPLIERS APPLIED TO PLATE PROBLEMS.

1. Statement of the problem and basic assumptions

The problem of the lateral bending of plates is considerably more complex than the one-dimensional problem of the beam theory. While the eigenvalue problems leading to the natural frequencies and modes of vibrations of uniform beams with classical boundary conditions can be solved analytically, this situation is completely different in the two-dimensional theory of thin plates. Analytical solutions are known rigourously only in very few cases (eg. the case of circular plates by use of Bessel functions, or the case of rectangular plates simply supported along at least two opposite edges).

For the other types of boundary conditions numerical methods must be considered; for design purposes they should be general enough so that they still apply when the plate is constrained in a slightly different way. Unfortunately, most of the methods used so far have been ad-hoc methods.

The purpose of the present Chapter is to show that the Rayleigh-Ritz Component Modes Method, through its use of the Lagrange Multipliers, applies to a very large class of problems and gives accurate results for less effort than the corresponding ad-hoc methods. The method requiers mainly basic intuition, (usually suggested by the physics of the problem) and is very flexible in its use.

The bending vibrations which are under consideration correspond to the classical small-deflexion theory of plates based on the following assumptions:

(1) Points which lie on a normal to the mid-plane of the undeflected plate lie on a normal to the mid-plane of the deflected plate. This assumption corresponds to the dual assumption in beam theory that "plane sections remain plane" and "deflections due to shear may be neglected".

(2) The stresses normal to the mid-plane of the plate, arising from the applied loading, are negligible in comparison with the stresses in the plane of the plate.

(3) The slope of the deflected plate in any direction is small so that its square may be neglected in comparison with unity, and the deflections are small in comparison with the thickness of the plate.

(4) The mid plane of the plate is a neutral plane, i.e. any mid plane stresses arising from its deflection may be ignored.

Based upon these assumptions, the following problemes are considered:

2. Lateral vibrations of cantilivered plates

As mentioned in Chapter I, this problem has references in the literature and thus the results obtained by the present method can be checked for accuracy with numerical results already existing.

a) Principle of the Method

The structure under consideration is shown in Figure 42; it consists of a rectangular plate of length L and width 21, clamped along the edge $x = 0$.

Its normal modes are sought in a Rayleigh Ritz expansion in terms of the modes of a completely free plate,with the clamped condition at x = 0 reinforced by means of Lagrange multipliers.

Although the normal modes on an unconstrained plate are themselves given by approximate numerical methods, the foregoing development has been adopted in view of its generality as being valid for any type of support conditions.

These modes themselves are found in a Rayleigh Ritz analysis in the form:

$$\Phi_n(x,y) = \sum_{k=1}^{\infty} \sum_{m=1}^{\infty} A_{km}^{(n)} X_k(x) Y_m(y) \qquad (165)$$

where X_i and Y_i are the natural modes of a free-free beam and the coefficients $A_{km}^{(n)}$ are related to the natural frequencies K_n in the following eigenvalue problem:

$$K_n^2 A_{ij}^{(n)} = A_{ij}^{(n)} (k_i^4 + s^4 k_j^4) + s^2 \sum_{l=1}^{\infty} \sum_{r=1}^{\infty} A_{lr}^{(n)}$$

$$(\nu(\omega_{il}\,\omega_{rj} + \omega_{li}\,\omega_{jr}) + 2(1-\nu)\alpha_{il}\alpha_{jr}) \qquad (166)$$

where

k_i : natural frequency parameter of a free-free beam

s : aspect ratio of the plate

ν : Poisson ratio

$\omega_{ij} = \int X_i''(\xi)\, X_j(\xi)\, d\xi$

non dimensional length of beam

$$\alpha_{ij} = \int_{\text{non dimensional length of beam}} X'_i(\xi)\, X'_j(\xi)\, d\xi = \alpha_{ji}$$

The normal modes of the cantilivered plate are thus sought in the form:

$$W(x,y,t) = \sum_{n=1}^{\infty} \sum_{k=1}^{\infty} \sum_{m=1}^{\infty} Q_n(t)\, A_{km}^{(n)}\, X_k(x) Y_m(y) \qquad (167)$$

b) Problem of the constraint conditions

According to equation (167), W(x,y,t) must satisfy the following boundary conditions:

$$W(x = 0,\ y,t) = 0 \qquad -1 \leq y \leq 1 \qquad (168)$$

$$\frac{\partial W}{\partial x}(x = 0, y, t) = 0 \qquad -1 \leq y \leq 1 \qquad (169)$$

The two boundary conditions above are functional equations.

They can be reduced to one single boundary condition by conceptually considering an unconstrained plate of double aspect ratio in symmetric or antisymmetric vibrations about the y axis, as shown in the lower part of Figure 42.

In the first case the only condition which has to be enforced is

$$W(0, y, t) = 0 \qquad \text{for} \qquad -1 \leq y \leq 1 \qquad (170)$$

in the second case the boundary condition to satisfy is

$$\frac{\partial W}{\partial x}(0,\ y,t) = 0 \qquad \text{for} \qquad -1 \leq y \leq 1 \qquad (171)$$

Because the analysis of Chapter III shows that a more rapid convergence

is obtained when using symmetric free-free beam modes, the first possibility has been chosen. Then the summation in k in equation (167) extends only over the even beam modes.

The additional term in the modified variational integral is:

$$\int_{-1}^{1} \lambda(y)\, W\,(0,y,t)\, dy = 0 \qquad (172)$$

Direct manipulation of this integral is very cumbersome in the Lagrangian method and therefore the integral has to be approximated. Three basic alternatives are considered in the present analysis; the theoretical development is pursued for each one of them and the results compared

* First alternative

The following approximation is taken for the left hand side of equation (172):

$$\int_{-1}^{1} \lambda(y)\, W(0,y,t)\, dy = \lim_{R \to \infty} \sum_{r=1}^{R} \lambda(y) W(0,y,t) \delta(y-y_r) \qquad (173)$$

where

$$-1 = y_1 < y_2 < \text{-------} < y_{R-1} = 1$$

* Second alternative

It is a step function approximation of the integral:

$$\int_{-1}^{1} \lambda(y)W(0,y,t)dy = \lim_{R \to \infty} \sum_{r=1}^{R-1} \lambda(y_r)W(0,y_r,t)(y_{r+1} - y_r) \qquad (174)$$

where the definition of the y_r is the same as in the Dirac approximation.

* Third alternative

This alternative consists in computing the integral by a trapezoidal rule:

$$\int_{-1}^{1} \lambda(y)W(0,y,t)\, dy = \lim_{R \to \infty} \sum_{r=1}^{R-1} \frac{(\lambda(y_r)W(0,y_r,t)+\lambda(y_{r+1})W(0,y_{r+1},t))(y_{r+1}-y_r)}{2} \qquad (175)$$

with same definition of the y_r.

In each one of the cases the following notation is adopted:

$\lambda(y_r) = \lambda_r$.

c) Theoretical development; frequency equation

The kinetic energy of the unconstrained plate which mass density per unit area is ρ , is given by:

$$T = \frac{1}{2} \rho L^2 \int_{-1}^{1} \int_{-1}^{1} \dot{W}^2(\xi,\eta,t)\, d\xi\, d\eta \qquad (176)$$

Since

$$W(\xi,\eta,t) = \sum_{n=1}^{\infty} Q_n(t)\Phi_n(\xi,\eta)$$

and by virtue of the orthonormality of the plate modes it follows:

$$\boxed{T = \frac{1}{2} \rho L 1 \sum_{n=1}^{\infty} \dot{Q}_n^2(t)} \tag{177}$$

If D is the bending stiffness of this plate of thickness h

$(D = \frac{Eh^3}{12(1-\nu^2)})$, the potential energy can be written as:

$$U = \frac{1}{2} D \int_{-1}^{1} \int_{-1}^{1} (\nabla^2 W)^2 + 2(1-\nu)\left(\left(\frac{\partial^2 W}{\partial x \partial y}\right)^2 - \frac{\partial^2 W}{\partial x^2} \frac{\partial^2 W}{\partial y^2}\right) dxdy \tag{178}$$

Substitution of equation (167) into the previous expression yields:

$$U = \frac{1}{2} \frac{D1}{L^3} \sum_{n=1}^{\infty} \sum_{p=1}^{\infty} Q_n(t) Q_p(t) \left(\sum_{k=1}^{\infty} \sum_{m=1,3} A_{km}^{(n)} A_{km}^{(p)}\right.$$

$$(k_k^4 + s^4 k_m^4) + s^2 \sum_{k=1}^{\infty} \sum_{m=1,3} \sum_{1=1}^{\infty} \sum_{r=1,3} A_{km}^{(n)} A_{1r}^{(p)}$$

$$\left.(\nu(\omega_{k1}\ \omega_{rm} + \omega_{1k}\omega_{mr}) + 2(1-\nu)\alpha_{k1}\alpha_{mr})\right) \tag{179}$$

in which $s = L/1$.

By use of equation (166) and the orthonormality of the plate modes it follows that

$$\boxed{U = \frac{1}{2} \frac{D1}{L^3} \sum_{n=1}^{\infty} Q_n^2(t)\ K_n^2} \tag{180}$$

* in the first alternative

The modal expression of the constraint equation is:

$$\lim_{R \to \infty} \sum_{r=1}^{R} \sum_{n=1}^{\infty} \lambda_r \, Q_n(t) \Phi_n(0,\eta_r) = 0$$

so that the Lagrangian of the elastic structure is:

$$\mathcal{L} = \sum_{n=1}^{\infty} \left(\frac{1}{2} \rho L 1 \, \dot{Q}_n^{\,2}(t) + \frac{1}{2} \frac{D1}{L^3} K_n^{\,2} \, Q_n^{\,2}(t) + \right.$$

$$\left. \sum_{r=1}^{\infty} \lambda_r \, Q_n(t) \Phi_n(0,\eta_r) \right) \qquad (181)$$

The subsequent Lagrange's equations are thus:

- $\rho L 1 \ddot{Q}_n(t) + \frac{D1}{L^3} K_n^{\,2} Q_n(t) - \sum_{r=1}^{\infty} \lambda_r \Phi_n(0,\eta_r) = 0 \qquad n = 1,\infty$

- $\sum_{n=1}^{\infty} Q_n(t) \, \Phi_n(0,\eta_r) = 0 \qquad r = 1,\infty$

With the assumed harmonic time dependence of the following form:

$$Q_n(t) = \overline{Q}_n e^{\,i \frac{1}{L^2} \left(\frac{D}{\rho}\right)^{1/2} \omega t}$$

$$\lambda_r(t) = \overline{\lambda}_r \frac{D1}{L^3} e^{\,i \frac{1}{L^2} \left(\frac{D}{\rho}\right)^{1/2} \omega t}$$

The generalized coordinates are solved in terms of the Lagrange multipliers from the first set of equations:

$$\overline{Q}_n = - \frac{\sum_{r=1}^{\infty} \overline{\lambda}_r \, \Phi_n(0,\eta_r)}{\omega^2 - K_n^2} \tag{182}$$

and their substitution into the second set of equations gives the eigenvalue equation:

$$\Delta^{(1)}(\omega) \cdot \vec{\lambda} = \vec{0}$$

where

$$\Delta^{(1)}_{rv} = \sum_{n=1}^{\infty} \frac{\Phi_n(0,\eta_r) \, \Phi_n(0,\eta_v)}{\omega^2 - K_n^2} \tag{183}$$

$r = 1,\ldots\infty \quad ; \quad v = 1,\ldots\infty$

In the numerical analysis both the eigenvalue matrix and its series elements will be given a finite form, i.e:

$n = 1,2\text{---}\ N$	N finite
$r,v = 1,2\text{---}\ R$	R finite

The frequency equation is

$$\det\left(\Delta^{(1)}(\omega)\right) = 0 \tag{184}$$

and its solutions are the natural frequencies of the cantilivered plate initially considered

* in the second alternative

The constraint equation can be written in modal form as:

$$\lim_{R\to\infty} \sum_{r=1}^{R-1} \sum_{n=1}^{\infty} {}^{1}\lambda_r \, Q_n(t) \Phi_n(0,\eta_r)(\eta_{r+1} - \eta_r) \tag{185}$$

and the new expressions of the Lagrange's equations are:

$$\bullet \; \rho L {}^{1}\ddot{Q}_n(t) + \frac{D}{L^3} {}^{1} K_n^2 Q_n(t) - \sum_{r=1}^{\infty} {}^{1}\lambda_r \Phi_n(0,\eta_r)(\eta_{r+1} - \eta_r) = 0 \tag{186}$$

$$n = 1, \infty$$

$$\bullet \sum_{n=1}^{\infty} Q_n(t) \; \Phi_n(0,\eta_r) \; (\eta_{r+1} - \eta_r) = 0 \tag{187}$$

$$r = 1, \infty$$

Same harmonic time dependency is assumed in this case, and

$$\lambda_r(t) = \bar{\lambda}_r \frac{D}{L^3} \; e^{\; i \; \frac{1}{L^2} \; \left(\frac{D}{\rho}\right)^{1/2} \; \omega t}$$

The generalized coordinates are given as functions of the Lagrange multipliers by:

$$\bar{Q}_n = - \frac{\sum_{r=1}^{\infty} \bar{\lambda}_r \, \Phi_n(0,\eta_r)(\eta_{r+1} - \eta_r)}{\omega^2 - K_n^{\; 2}} \tag{188}$$

and the elements of the eigenvalue matrix are in the finite form:

$$\Delta^{(2)}_{rv} = \sum_{n=1}^{N} \frac{\Phi_n(0,\eta_r)\Phi_n(0,\eta_v)(\eta_{r+1}-\eta_r)(\eta_{v+1}-\eta_v)}{\omega^2 - K_n^2} \qquad (189)$$

$$r,v = 1, \text{ --- } R-1$$

It can be further noticed that $\Delta^{(2)}_{rv}$ can be written in fact as:

$$\Delta^{(2)}_{rv} = (\eta_{r+1} - \eta_r)\,(\eta_{v+1} - \eta_v)\,\Delta^{(1)}_{rv}$$

and hence

$$\det\,(\Delta^{(2)}(\omega)) = \prod_{r=1}^{R-1} (\eta_{r+1} - \eta_r)^2 \times \det\,(\Delta^{(1)}(\omega)) \qquad (190)$$

This last equation shows that the difference between the two alternatives is that for the same finite number of plate modes and same accuracy expected in the frequency, it is necessary to take one less point in the subdivision of the y axis. The practical meaning is that the order of the matrixes handled in the numerical computations decreases by one in the second case. Although this fact is an improvement, it is quite negligible compared to the improvement brought by the procedure described in part a) which reduces by half the order of the eigenvalue matrix.

* in the third alternative

The constraint equation can be written in the double serie form as:

$$\lim_{R\to\infty} \sum_{r=1}^{R-1} \sum_{n=1}^{\infty} Q_n(t) 1(\eta_{r+1}-\eta_r) \frac{(\lambda_{r+1}\Phi_n(0,\eta_{r+1})+\lambda_r\Phi_n(0,\eta_r))}{2} = 0 \quad (191)$$

and the subsequent Lagrange's equations are:

$$\bullet\ \rho L1 \ddot{Q}_n(t) + \frac{D1}{L^3} K_n^2 Q_n(t) - 1 \sum_{r=1}^{\infty} \frac{(\eta_{r+1} - \eta_r)}{2}$$

$$(\lambda_{r+1} \Phi_n(0,\eta_{r+1}) - \lambda_r \Phi_n(0,\eta_r)) \quad (192)$$

$$n = 1, \ldots \infty$$

• with $R \to \infty$

$$\sum_{n=1}^{\infty} Q_n(t) \Phi_n(0,\eta_1) (\eta_2 - \eta_1) = 0 \quad (193)$$

$$\sum_{n=1}^{\infty} Q_n(t) \Phi_n(0,\eta_r) (\eta_{r+1}-\eta_{r-1}) = 0 \qquad r = 2,\ldots R-1 \quad (194)$$

$$\sum_{n=1}^{\infty} Q_n(t) \Phi_n(0,\eta_R) (\eta_R - \eta_{R-1}) = 0 \quad (195)$$

With same non-dimensionalization as previously,

$$\bar{Q}_n = - \frac{\sum_{r=1}^{R-1} (\eta_{r+1}-\eta_r) \left(\bar{\lambda}_{r+1}\Phi_n(0,\eta_{r+1}) + \bar{\lambda}_r\Phi_n(0,\eta_r)\right)}{\omega^2 - K_n^2} \qquad (196)$$

and the eigenvalue matrix $\Delta^{(3)}$ of order R is defined by its elements:

$$\Delta_{11}^{(3)} = \sum_{n=1}^{N} \frac{\Phi_n^2(0,\eta_1)(\eta_2 - \eta_1)^2}{\omega^2 - K_n^2}$$

$$\Delta_{r1}^{(3)} = \sum_{n=1}^{N} \frac{\Phi_n(0,\eta_1)\Phi_n(0,\eta_r)(\eta_2 - \eta_1)(\eta_{r+1} - \eta_{r-1})}{\omega^2 - K_n^2}$$

$$r = 1, \ldots. R-1$$

$$\Delta_{R1}^{(3)} = \sum_{n=1}^{N} \frac{\Phi_n(0,\eta_1)\Phi_n(0,\eta_R)(\eta_2-\eta_1)(\eta_R-\eta_{R-1})}{\omega^2 - K_n^2}$$

$$\Delta_{rv}^{(3)} = \sum_{n=1}^{N} \frac{\Phi_n(0,\eta_r)\ \Phi_n(0,\eta_v)(\eta_{r+1}-\eta_{r-1})(\eta_{v+1} - \eta_{v-1})}{\omega^2 - K_n^2}$$

$$r,v = 2, \ldots R-1$$

$$\Delta_{rR}^{(3)} = \sum_{n=1}^{N} \frac{\Phi_n(0,\eta_r)\ \Phi_n(0,\eta_R)(\eta_R-\eta_{R-1})(\eta_{r+1}\ -\ \eta_{r-1})}{\omega^2\ -\ K_n^{\ 2}}$$

$$r = 2, \ \ldots\ R-1$$

$$\Delta_{RR}^{(3)} = \sum_{n=1}^{\infty} \frac{\Phi_n^{\ 2}(0,\eta_R)\ (\eta_R\ -\ \eta_{R-1})^2}{\omega^2\ -\ K_n^{\ 2}}$$

The eigenvalue determinant can be written after factorisation:

$$\det\ (\boldsymbol{\Delta}^{(3)}(\omega)) = \prod_{r=1}^{R-1} (\eta_{r+1}\ -\ \eta_r)^2 \prod_{r=2}^{R-1} (\eta_{r+1}-\eta_{r-1})^2\ \det(\boldsymbol{\Delta}^{(1)}(\omega)) \qquad (197)$$

and hence this approach is seen to be completely equivalent to the first approach considered. This fact is somewhat surprising because generally the trapezoidal rule provides better approximations of integrals than does the Dirac functions method.

It can be noticed that in the process, the present method gives also the natural frequencies of point-clamped plates; the number of points and their location along the edge is completely arbitrary. Furthermore, for each natural frequency the distribution of the shear forces and/or bending moment is given along the constrained edge at the points of constraint.

d) Natural frequencies of a square cantilivered plate

The first three natural frequencies of a square cantilivered plate are computed by the present method using the normal modes and frequencies of an unconstrained plate of aspect ratio 2. The analysis of Chapter III shows that five symmetric modes in the x direction insure good convergence (they correspond to less than 0.1% error in the beam case); the number of free-free beam modes in the y direction is chosen as a function of the number of points at which the constraints are applied along the y axis and as a function of the number of natural frequencies sought. For the present analysis five free-free modes have been taken in the y direction. The changes in the first three natural frequencies with the number of constraint points are shown in Figure 43,both for an approximation by Dirac functions and by characteristic functions. As mentioned earlier, the second alternative gives faster convergence and the results will be discussed for this approach. The asymptotic values corresponding to the square cantilivered plate have been taken from Reference (35).

The lower part of Figure 43 shows that as the number of constraint points increases, the first natural frequency increases monotonically towards that of the cantilivered plate. The results are further analyzed in Figure 44 where the percentage difference with the cantilivered case is plotted versus the number of constraint points.

It can be seen that with as little as three constraint points (one in the middle and two at each extremity) the plate can be considered clamped at the edge x = 0 in the first mode, with an error of

only 1%. This result is to be expected because ω_1 cantilivered = 3.494 is very close to the first natural frequency of a cantilivered beam ω_1 = 3.516 and because in this mode the plate undergoes only translation in the y direction in a "beam-fibers" type of behavior.

The second natural frequency is seen to converge as well towards that of a cantilivered plate when the number of constraint points increase, as shows the middle portion of Figure 43. In this case the variation is not monotonic per se, and this fact will be commented upon later.

The percentage error from the case of the cantilivered plate is plotted in Figure 45; it can be seen that with the characteristic function approach, a square plate clamped at the points $\eta_1 = -1$, $\eta_2 = -0.5$, $\eta_3 = 0$ can be considered as completely clamped along the edge in the second mode, with an error of only 0.7% in the natural frequency. It is interesting to notice that as far as convergence is concerned, there is no improvement in constraining the plate at $\eta_1 = -1$, $\eta_2 = 0$ upon having only the point $\eta_1 = -1$ clamped. This result comes from the fact that the modal behavior of a cantilivered plate in the second mode in the y direction is a combination of plunging and rotation. By imposing zero displacement at $\eta_1 = -1$ we constrain Y_o and Y_1, as for the point $\eta_1 = 0$ it is a redeendant point for this particular type of constraint because $Y_1(0) = 0$.

The method is seen to converge remarkably fast also in the third mode as shows the upper part of Figure 43; this result is even more remarkable considering that only 5 modes are used along

the y axis for as many as 3 points of constraint for instance. For this mode also, the percentage error with the member of constraint points is plotted in Figure 46 and the corresponding mode shape of a squared cantilivered plate is given for reference.

Higher natural frequencies could be obtained provided that more modes are considered in the y-direction in the analysis giving the normal modes and frequencies for the unconstrained plate.

For cantilivered plates with higher aspect ratio, same conclusions are expected to be valid with an even smaller number of constraint points. Also, the method is expected to converge even faster for edge conditions physically closer to the free condition (as simply supported, for instance).

3. Vibrations of a rectangular plate with an internal support

As mentioned in Chapter I, an analytic solution is proposed to the problem of symmetric-symmetric vibrations in Reference (36) for the following configuration:

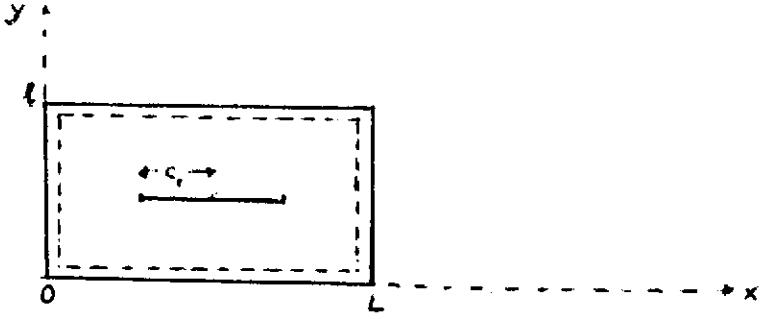

The mixed boundary value problem is formulated in terms of dual series equations; they are first partially solved by means of the Bessel function J_1 and then cast into the form of Abel's integral equation

for which the solution is given explicitely.

Although the method is mathematically interesting, it only applies to the particular foregoing problem and would fail to give results if the line of support were to be displaced in the plate.

a) Principle of the method.

As in the previous paragraph, the mode shapes of the structure are sought in terms of mode shapes of a less constrained plate. The physics of the problem suggest these initial modes to be the modes of a simply supported plate along all four edges; mathematically, they offer the advantage of being known by their analytic expression. Hence the modal solutions are sought in the following serie form:

$$W(x,y,t) = 2 \sum_{m=1}^{\infty} \sum_{m=1}^{\infty} Q_{mn}(t) \sin \frac{m\pi x}{L} \sin \frac{n\pi y}{1} \qquad (198)$$

$$0 \leq x \leq L \; ; \; 0 \leq y \leq 1$$

For motions symmetric about $x = L/2$, $y = 1/2$, the summations in m and n extend to the odd subscripts only.

The boundary conditions at the edges of the plate are already satisfied by the initial choice of the spectral expansion; the only additional constraint to satisfy is that along the internal line of support, i.e.:

$$W(x, \frac{1}{2}, t) = 0 \qquad \text{for} \qquad -c_1 < x \leq c_1$$

when only doubly symmetric modes are sought, this condition further simplifies to:

$$W(x, \frac{1}{2}, t) = 0 \qquad \text{for} \qquad \frac{L}{2} - c_1 < x \leq \frac{L}{2}$$

The above equation requires the function $f(x,t) = W(x,\frac{1}{2},t)$ restricted to $\frac{L}{2} - c_1 \leq x \leq \frac{L}{2}$ to be identically zero in this interval.

Assuming the function to be continuous in x in the interval of definition, if we choose a dense set $(x_r)_{r=1,R}$: $\frac{L}{2} - c_1 = x_1 < x_2 < \ldots\ldots < x_R = \frac{L}{2}$ it is sufficient to require $f(x_R,t) = 0 \qquad r = 1,\ldots.R$
In the limit, equation (199) is equivalent to the set of equations:

$$W(x_r, \frac{1}{2}, t) = 0 \qquad r = 1,R \tag{200}$$

when $R \to \infty$.

The eigenvalue frequency equation will be derived based on this form of the constraint conditon.

b) Lagrangian formulation of the problem; frequency equation.

The total kinetic energy of the structure is:

$$T = \frac{1}{2} \rho L l \int_0^1 \int_0^1 \dot{W}^2(\xi,\eta,t)\, d\xi\, d\eta \tag{201}$$

where ρ is the mass density per unit area of the plate.
By use of equation (198) it follows:

$$T = \frac{1}{2}\rho L l \sum_{m=1,3}^{\infty} \sum_{n=1,3}^{\infty} \dot{Q}_{mn}^2(t) \tag{202}$$

Likewise, D being the bending stiffness of the plate and s its aspect ratio,

$$U = \frac{1}{2} D \int_0^1 \int_0^1 \left(\frac{1}{L^3} \left(\frac{\partial^2 W}{\partial \xi^2} \right)^2 + \frac{L}{l^3} \left(\frac{\partial^2 W}{\partial \eta^2} \right)^2 + \frac{2\nu}{lL} \frac{\partial^2 W}{\partial \xi^2} \frac{\partial^2 W}{\partial \eta^2} + \right.$$

$$\left. \frac{2(1-\nu)}{lL} \left(\frac{\partial^2 W}{\partial \xi \partial \eta} \right)^2 \right) d\xi \, d\eta$$

or, after substitution of equation (198)

$$U = \frac{1}{2} \frac{Dl}{L^3} \sum_{m=1,3}^{\infty} \sum_{n=1,3}^{\infty} Q_{mn}^2(t) \left((m\pi)^2 + s^2 (n\pi)^2 \right)^2$$

In equivalent form,

$$U = \frac{1}{2} \frac{Dl}{L^3} \sum_{m=1,3}^{\infty} \sum_{n=1,3}^{\infty} Q_{mn}^2(t) \, K_{mn}^2 \tag{203}$$

where

$$K_{mn} = (m\pi)^2 + s^2 (n\pi)^2$$

By substitution of (198) into equations (200), the set of constraint conditions is obtained in modal form as follows:

$$\sum_{m=1,3}^{\infty} \sum_{n=1,3}^{\infty} (-1)^{(n-1)/2} Q_{mn}(t) \sin m\pi\xi_r = 0 \qquad r=1,R \tag{204}$$

where $\xi_r = \frac{x_r}{L}$

If λ_r is taken as notation for $\lambda(\xi_r)$, the Lagrangian of the system can be written as

$$\mathcal{L} = \sum_{m=1,3}^{\infty} \sum_{n=1,3}^{\infty} \left(\frac{1}{2} \rho L1 \dot{Q}_{mn}^2(t) - \frac{1}{2} \frac{D1}{L^3} K_{mn}^2 Q_{mn}^2(t) + \right.$$

$$\left. (-1)^{(n-1)/2} Q_{mn}(t) \sum_{r=1}^{R} \lambda_r \sin m\pi\xi_r \right)$$

and the subsequent equations of motion are:

$$\bullet \ \rho L1 \ddot{Q}_{mn}(t) + \frac{D1}{L^3} K_{mn}^2 Q_{mn}(t) - \sum_{r=1}^{R} (-1)^{(n-1)/2} \lambda_r \sin m\pi\xi_r = 0$$

$$n = 1, \ldots \infty \tag{205}$$

$$\bullet \sum_{m=1,3}^{\infty} \sum_{n=1,3}^{\infty} (-1)^{(n-1)/2} Q_{mn}(t) \sin m\pi\xi_r = 0 \qquad r=1,..R \tag{206}$$

In a harmonic time dependent motion of the form:

$$Q_{mn}(t) = \bar{Q}_{mn} \, e^{i \frac{1}{L^2} \left(\frac{D}{\rho} \right)^{1/2} \omega t}$$

$$\lambda_r(t) = \bar{\lambda}_r \frac{D\mathfrak{I}}{L^3} \, e^{i \frac{1}{L^2} \left(\frac{D}{\rho} \right)^{1/2} \omega t}$$

the respective amplitudes of the generalized coordinates are given in function of the Lagrange Multipliers by:

$$\bar{Q}_{mn} = - \frac{\sum_{r=1}^{R} (-1)^{(n-1)/2} \bar{\lambda}_r \sin m\pi\xi_r}{\omega^2 - K_{mn}^2} \tag{207}$$

and the eigenvalue equations are:

$$\Delta_{rv} \bar{\lambda}_v = 0 \tag{208}$$

where

$$\Delta_{rv}(\omega) = \sum_{m=1,3}^{\infty} \sin m\pi\xi_r \, \text{sim} \, m\pi\xi_v \sum_{n=1,3}^{\infty} \frac{1}{\omega^2 - K_{mn}^2} \tag{209}$$

The natural frequencies of the structure are solutions of the equation

$$\det (\Delta (\omega)) = 0$$

c) Numerical results.

The analysis of Reference (36) treats the case of a simply supported square plate and gives the variation of the fundamental

natural frequency with the length of the internal support. For purpose of comparison, the method is applied in the same case. Six symmetric modes are considered in the y direction and five more symmetric modes than constraint points in the x direction.

The results are summarized in the table which follows:

$\frac{2c_1}{L}$	$\omega^*_{Ref(36)}$	$\omega^*_{Present\ Method}$	Percentage disagreement	# constr. points used
0	2.665	2.668	0.9%	ξ = 0,5
0.1	2.898	2.966	2.6%	ξ : (0.45,0.5)
0.2	3.164	3.160	0.13%	ξ : (0.4,0.5)
0.3	3.353	3.360	0.21%	ξ : (0.35,0.5)
0.4	3.451	3.456	0.15%	ξ : (0.3,0.4,0.5)
0.5	3.492	3.480	0.36%	ξ : (0.25,0.325,0.5)
0.6	3.507	3.509	0.06%	ξ :(0.2,0.3,0.4,0.5)
1.0	3.512	3.514	0.06%	ξ :(0.1,0.2,0.3,0.4,0.5)

It can be seen that except for the value $\frac{2c_1}{L} = 0.1$, there is less than 1% disagreement between the fundamental frequencies obtained by the two methods. Moreover, as shows the fifth column, the number of points approximating the line of support is never greater than 5 and hence the corresponding sizes of matrices are being kept small.

The functional dependence of the fundamental frequency upon the length of the line of support is plotted in Figure 47 and indeed the results are in good agreement considering the scale used.

d) Conclusion.

The numerical results tabulated in column four make any comment on the convergence of the method unnecessary.

It has to be pointed out that such a good convergence is due partially to the particular choice of the initial modes which verify the boundary conditions at the edge and which are known in analytic form and hence do not have an intrinsec error.

The problem can be solved alternatively by using unconstrained plate modes, but this choise has for effect in increasing the number of constraint conditions required. More precisely, the analysis of Reference (44) shows that for the first six natural frequencies a simply supported square plate can be approximated to a good degree of accuracy by a point supported plate with four points of support along each edge, and thus the last alternative would include 12 additional ponctual constraint equations.

If the line of support were to be moved in the plate, there the method would still apply with the following modifications.

(1) the sumation in m and n in equation (198) should be extended to both even and odd subscripts

(2) the points of constraint should lie along the entire line of support and no longer be restrained only to its half.

The first modification does not bring any significant increase in the computation time because it corresponds to operations of adding; the second modification would increase the size of the eigenvalue matrices by a factor of two (as their initial size was already small, such a modification does not represent any real inconvenience).

CHAPTER VI

CONCLUSIONS AND RECOMMENDED FUTURE WORK.

1. Conclusions

The Rayleigh-Ritz Component Modes method using Lagrange Multipliers has been shown to predict with good accuracy the modal behavior of linear elastic structures of various degrees of complexity; it has been seen that the analysis offers computational advantages through its convenient matrix formulation and clear physical interpretation.

Good convergence has been obtained in several cases where other analytical results were available. Moreover, for structures with non-uniform properties, because the convergence is based upon several independent parameters, there is more than one procedure for obtaining good accuracy in the solutions. The discussion presented in Chapter II suggests a systematic procedure economical from the point of view of computation time.

The method may be used either as a Rayleigh-Ritz type method or a Finite-Element type method. In the Rayleigh-Ritz option one employs a fixed number of components and systematically increases the number of modes per component; conversely in the Finite-Element option one fixes the number of modes per component and systematically increases the number of components (or elements). Thus, potentically, it is more flexible in its use and has better convergence characteristics than either of the conventional methods.

The main factors upon which the success in the application of the method depends are the following:

1) an adequate mathematical model of the components of the structure

(within the framework of linear elasticity and small deflection theory),

2) an accurate knowledge of the natural modes and frequencies of vibration of the unconstrained components,

3) a suitable formulation of the constraint conditions describing the connections between components and, of course, a suitable choice of the degrees of freedom for each component.

As a consequence of 1), the present theory has the limitations inherent in linear models. The second point mentioned above is particularly critical when one or several components of the overall structure are modeled by shells, for instance, because of the difficulty of obtaining a good modal representation for them. This fact will be commented upon later.

Finally, as is pointed out in Chapter IV, care has to be taken in checking that the constraint equations can be expressed in holonomic form so that the use of the Lagrange Multipliers is valid. The problem of two structures striking each other during vibration for instance, cannot be treated by the present method. For the problems for which the use of the Lagrange Multipliers is justified, the present method is convenient also for computing the internal forces developed at the points of constraint. The analysis of Appendix VII shows that the values of the Lagrange Multipliers are much closer to the actual values of the shear forces and bending moments at those points, than the values directly given by differentiation of the modal shape.

2. Recommended future work

The modal behavior of arbitrarily constrained plates with non-uniform properties can be investigated by extending the analysis developed in Chapters II and V; it is expected that the more sensitive parameter for the convergence of such problems is the number of substructures (or uniform plate elements) considered, rather than the number of unconstrained plate modes used for each component. (The latter depends upon the number of constraint points taken along each edge of the plate elements and their respective bending stiffnesses).

Vibrations of structures with shell components can be also treated by the present method; however, the problem is then of greater complexity. First of all, it is very complicated to formulate and find solutions of the characteristic free vibration equations; while the form of the classical fourth order equations of motion for plates is universally approved, there are numerous shell theories which have been derived for a given shell configuration. Hence, first the theory adopted for obtaining the unconstrained frequencies and mode shapes should be chosen by checking the different assumptions which give rise to that theory. Additional complexity enters into the problem because of the question of the boundary conditions. The classical bending theory of plates requires only two conditions to be specified along an edge, while a corresponding shell theory requires four specified conditions. However, there are already available results, primarily for circular cylindrical shells, as can be seen in Reference (47).

Another problem which is of interest in structural dynamics is that of the determination of the modal damping of a given complex structure.

The analysis presented in Appendix II takes into consideration only the structural damping per se. However, sometimes the damping occurring in structural joints is the major contributor to the total damping of the structure, and hence an open area for further research is that of modeling the joint damping so that it can be incorporated as a constraint condition in the present method. In Reference (48), some experimental attempts are presented for modeling the various types of joint damping occurring in the orbiting Skylab cluster.

In Chapter IV, an analysis for determining the structural modes of an airplane with oblique configuration is developed; the results can be directly used for a flutter or gust response analysis. As a first step, a simple aerodynamic theory could be considered (such as piston theory, or aerodynamic strip theory for instance); then the problem can be pursued with more complex aerodynamic operators.

APPENDIX I

MODAL BEHAVIOR OF NON UNIFORM CONTINUOUS BEAMS BY A PERTURBATION - GALERKIN METHOD.

1. Introduction

The purpose of this Appendix is to present an alternative method to the Rayleigh Ritz component modes method presented in Chapter II, for continuous beams with variable stiffness along the span.

The method previously presented applies with great simplicity to the treatment of stepped or almost - stepped beams, where the number of components is determined by the number of "steps" of the beam. This number is then finite and the convergence problem identifies with the convergence of the Rayleigh-Ritz method. Because of the simplicity and efficiency of the analysis, hardly any other alternative method could be considered for such problems.

For this reason, only the case of beams with continuously varying properties has been investigated by an alternative method.

2. Theoretical development

The variations in the bending stiffness of an elastic beam can be caused by the change in the elastic properties of the material (in particular the Young modulus) and/or variations in the geometry along the span. If changes in E occur, we shall assume them continuous and smooth; as for changes in the geometry, only slowly varying properties along the span are meaningfull within the one-dimensional theory of continuous beams. The previous considerations suggest a "perturbation - type" approach.

Unlike the method presented in Chapter II, this method does not adopt a variational point of view and the starting point is the differential equation and the associated boundary conditions.

a) Notations

$EI(x)$: bending stiffness at station x

EI_o : mean value of $EI(x)$

ρ : mass density

$A(x)$: cross sectional area at station x

A_o : mean value of $A(x)$

$y(x,t)$: transverse displacement of the bent beam

$w(x)$: normal mode shape of the bent beam

δ_{np} : Kroenecker's symbol

b) Development of the problem

The differential equation governing the transversal vibration of a non-uniform beam is:

$$\frac{\partial^2}{\partial x^2}\left(EI(x)\,\frac{\partial^2 y}{\partial x^2}(x,t)\right) + \rho A(x)\,\frac{\partial^2 y}{\partial t^2}(x,t) = 0 \qquad 0 \leq x \leq L \tag{210}$$

and can be written in non-dimensional form as follows:

$$\frac{1}{L^4}\frac{\partial^2}{\partial \xi^2}\left(EI(\xi)\,\frac{\partial^2 y}{\partial \xi^2}(\xi,t)\right) + \rho A(\xi)\,\frac{\partial^2 y}{\partial t^2}(\xi,t) = 0 \tag{211}$$

The normal modes are found by a solution of the form:

$$y(\xi,t) = w(\xi)\, e^{i\Omega t}$$

which when substituted into equation (211) leads to:

$$\frac{1}{L^4}\frac{d^2}{d\xi^2}\left(EI(\xi)\frac{d^2W}{d\xi^2}(\xi)\right) - \rho A(\xi)\Omega^2 W(\xi) = 0 \tag{212}$$

We introduce the following definitions:

$$f(\xi) = \frac{EI(\xi) - EI_o}{(EI(\xi) - EI_o)_{max}} \tag{213}$$

and

$$g(\xi) = \frac{A(\xi) - A_o}{(A(\xi) - A_o)_{max}} \tag{214}$$

The above defined functions satisfy

$$|\, f(\xi)\,| \leq 1 \quad \text{and} \quad |\, g(\xi)\,| \leq 1 \qquad \forall \xi \in [-1, 1]$$

and the quantity

$$\varepsilon = \text{larger of } \left(\frac{|\, EI(\xi) - EI_o\,|_{max}}{EI_o}\,,\ \frac{|\, A(\xi) - A_o\,|_{max}}{A_o}\right) \tag{215}$$

is small compared to unity.

Using (213), (214), (215), $EI(\xi)$ and $A(\xi)$ can be written:

$$EI(\xi) = EI_o\,(1 + N(\varepsilon)\, f(\xi)) \tag{216}$$

$$A(\xi) = A_o\,(1 + M(\varepsilon)\, g(\xi)) \tag{217}$$

with obvious definitions of $N(\varepsilon)$ and $M(\varepsilon)$ from (215).

By substituting (216) and (217) into (212) this equation becomes:

$$\frac{EI_o}{L^4}\left(1 + N(\varepsilon)f(\xi)\right)\frac{d^4W(\xi)}{d\xi^4} + \frac{2EI_o}{L^4}N(\varepsilon)\frac{df(\xi)}{d\xi}$$

$$\frac{d^3W(\xi)}{d\xi^3} + \frac{EI_o}{L^4}N(\varepsilon)\frac{d^2f(\xi)}{d\xi^2} - \rho A_o\left(1+M(\varepsilon)g(\xi)\right)\Omega^2W(\xi) = 0 \qquad (218)$$

So far no specific boundary conditions have been assigned, in fact the method will be developed for any arbitrary type of boundary conditions, noted B.C.

Solutions are sought in the form:

$$W_n(\xi) = \phi_n(\xi) + \sum_{i=1}^{\infty} E_i(\varepsilon)\,\Phi_{in}(\xi) \qquad (219)$$

$$\Omega_n = \omega_n + \sum_{i=1}^{\infty} F_i(\varepsilon)\,\Omega_{in} \qquad (220)$$

with

$$\lim_{\varepsilon\to 0}\frac{E_{i+1}(\varepsilon)}{E_i(\varepsilon)} = \lim_{\varepsilon\to 0}\frac{F_{i+1}(\varepsilon)}{F_i(\varepsilon)} = 0$$

Substitution into (218) yields the perturbation equation:

$$\frac{EI_o}{L^4}\left(1+N(\varepsilon)f(\xi)\right)\left(\frac{d^4\phi_n(\xi)}{d\xi^4} + E_1(\varepsilon)\frac{d^4\Phi_{n1}(\xi)}{d\xi^4} + \right.$$

$$E_2(\varepsilon)\ \frac{d^4\Phi_{n2}(\xi)}{d\xi^4} + \ldots.) + \frac{2EI_o}{L^4}\ N(\varepsilon)\ \frac{df(\xi)}{d\xi}\ ($$

$$\frac{d^3\phi_n(\xi)}{d\xi^3} + E_1(\varepsilon)\ \frac{d^3\Phi_{n1}(\xi)}{d\xi^3} + E_2(\varepsilon)\ \frac{d^3\Phi_{n2}(\xi)}{d\xi^3} + \ldots\ ) +$$

$$\frac{EI_o}{L^4}\ N(\varepsilon)\ \frac{d^2f(\xi)}{d\xi^2}\ (\ \frac{d^2\phi_n(\xi)}{d\xi^2} + E_1(\varepsilon)\ \frac{d^2\Phi_{n1}(\xi)}{d\xi^2} +$$

$$E_2(\varepsilon)\ \frac{d^2\Phi_{n2}(\xi)}{d\xi^2} + \ldots) - \rho A_o\ (1+M(\varepsilon)g(\xi)\ )$$

$$(\omega_n^{\ 2} + 2F_1(\varepsilon)\omega_n\Omega_{n1} + F_1^{\ 2}(\varepsilon)\Omega_{n1}^{\ 2} + 2F_2(\varepsilon)\omega_n\Omega_{n2} + \ldots)$$

$$(\phi_n(\xi) + E_1(\varepsilon)\Phi_{n1}(\xi) + E_2(\varepsilon)\Phi_{n2}(\xi) + \ldots) = 0 \qquad (221)$$

From the boundary conditions B.C. we determine boundary conditions for the functions $\Phi_{ni}(\xi)$.

For example, in the case of a cantilivered beam clamped at the end $\xi = 0$ the boundary conditions are:

$$W(0) = \frac{dW}{d}\ (0) = 0$$

$$EI(1)\ \frac{d^2W}{d\xi^2}\ (1) = \frac{d}{d\xi}\ (EI(\xi)\ \frac{d^2W}{d\xi}\ (\xi)\ )\ (1) = 0$$

from which we determine the boundary conditions on $\Phi_{ni}(\xi)$ using (219)

$$\Phi_{ni}(0) = \frac{d\Phi_{ni}}{d\xi}(0) = 0 \tag{222}$$

$$\frac{d^2\Phi_{ni}}{d\xi^2}(1) = \frac{d^3\Phi_{ni}}{d\xi^3}(1) = 0 \tag{223}$$

The problem is now well defined at each order and solved as follows:

* Zeroth order solution

It is as expected, $\phi_n(\xi)$ satisfying the zeroth order problem:

$$\begin{cases} \dfrac{EI_o}{L^4} \dfrac{d^4\phi_n(\xi)}{d\xi^4} - \rho A_o \omega_n^2 \phi_n(\xi) = 0 \\ \text{B.C.} \end{cases} \tag{224}$$

* First order solution (solution at order $E_1(\varepsilon)$)

For almost all the cases of interest the slow variations in EI (ξ) and A (ξ) have comparable lowest order terms, which can be written using Landau's notation:

$$N(\varepsilon) = O(M(\varepsilon))$$

(i.e. $\lim_{\varepsilon \to 0} (N(\varepsilon)/M(\varepsilon))$ is finite)

Solutions are sought such that:

$$E_1(\varepsilon) = O(N(\varepsilon)) \quad : \quad F_1(\varepsilon) = O(M(\varepsilon)) \tag{225}$$

and hence the first order problem is:

$$\left\{ \begin{array}{l} \dfrac{EI_o}{L^4} \dfrac{d^4\Phi_{n1}(\xi)}{d\xi^4} - \rho A_o \omega_n^2 \Phi_{n1}(\xi) = -\dfrac{d^2}{d\xi^2}\left(f(\xi) \dfrac{d^2\phi_n(\xi)}{d\xi^2}\right) \\ \\ + \rho A_o \left(2\omega_n \Omega_{n1} \phi_n(\xi) + g(\xi)\omega_n^2 \phi_n(\xi)\right) \\ \\ \text{B.C.} \end{array} \right. \tag{226}$$

We denote by $s_{n1}^{(p)}$ the elements of the spectral decomposition of Φ_{n1}, i.e.:

$$\Phi_{n1}(\xi) = \sum_{p=1}^{\infty} s_{n1}^{(p)} \phi_p(\xi) \tag{227}$$

$$s_{n1}^{(p)} = \int_o^1 \Phi_{n1}(\xi)\, \phi_p(\xi)\, d\xi \tag{228}$$

and we apply a Galerkin procedure to equation (226).

It follows, using B.C. that:

$$\rho A_o(\omega_p^2 - \omega_n^2)\, s_{n1}^{(p)} = -\frac{EI_o}{L^4} \int_o^1 \frac{d^2}{d\xi^2}\left(f(\xi) \frac{d^2\phi_n(\xi)}{d\xi^2}\right)\phi_p(\xi)d\xi$$

$$+ \rho A_o\left(2\omega_n \Omega_{n1}\, \delta_{np} + \omega_n^2 \int_o^1 g(\xi)\phi_n(\xi)\phi_p(\xi)d\xi\right)$$

for $n = p$, Ω_{n1} is determined by:

$$\boxed{\Omega_{n1} = \frac{\omega_n}{2}\left[\frac{1}{k_n^4} \int_o^1 f(\xi)\phi''^2_n(\xi)d\xi - \int_o^1 g(\xi)\phi_n^2(\xi)d\xi\right]} \tag{229}$$

where k_n is non-dimensional frequency parameter of the reference beam.

and for $n \neq p$ the $s_{n1}^{(p)}$ are determined by:

$$s_{n1}^{(p)} = \frac{\omega_n^2}{\omega_p^2 - \omega_n^2} \left(- \frac{1}{k_n^4} \int_0^1 f(\xi)\phi''_n(\xi)\phi''_p(\xi)\, d\xi + \right.$$

$$\left. \int_0^1 g(\xi)\phi_n(\xi)\phi_p(\xi) d\xi \right) \qquad (230)$$

From the normalization condition $\int_0^1 W^2(\xi)d\xi = 1$ it follows $s_{n1}^{(n)} = 0$

The solutions at the next order are determined by a similar type of procedure.

3. Beams with linear bending stiffness and mass distribution along the span.

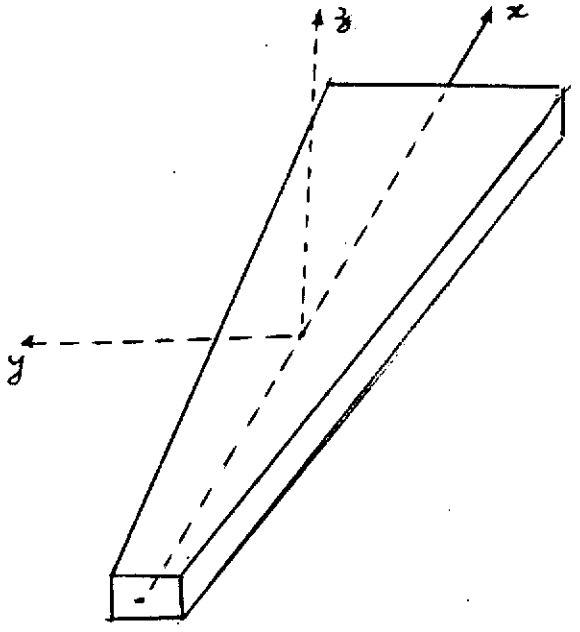

A beam of such type is illustrated above. The width distribution along the span is given by $b(\xi) = b_o(1 + \varepsilon\xi)$ where $\varepsilon = o(1)$

The analysis of the previous paragraph applies with

$$f(\xi) = g(\xi) = \xi \tag{231}$$

$$\mu(\varepsilon) = M(\varepsilon) = \varepsilon \tag{232}$$

and solutions are formed with

$$E_i(\varepsilon) = F_i(\varepsilon) = \varepsilon^i \tag{233}$$

for various types of boundary conditions.

It can be noted that relations (231) and (232) hold not only for the particular type of beams shown in the figure, but are more general (there are multiple ways in which EI(x) and the mass distribution /unit length, m(x) can be made to vary linearly along the span). In fact formula (231) and (232) could have been taken as starting points.

Free-free beams.

The first order corrections to the natural frequencies Ω_{n1} are found to be zero; the corresponding corrections to the mode shapes are:

$$\phi_{n1}(\xi) = \sum_{\substack{p=1 \\ p \text{ different} \\ \text{parity than} \\ n}}^{\infty} \frac{16\alpha_n\alpha_p k_n^5 k_p}{k_p^4 - k_n^4} \phi_p(\xi) \tag{234}$$

where the values of the α_n are given in Reference (21).

On the basis of this result it can be concluded that the natural frequencies of such beams can be considered within a reasonable degree of accuracy as being the same as the natural frequencies of the uniform beams of reference, the degree of accuracy being determined in its major part by the value of Ω_{n2} (the next higher term in the serie (220)). It is also significant to notice from formula (234) that the corrections in the mode shapes at the first order are the corrections due to the fact that there is no longer symmetry about the middle of the beam, and thus although the boundary conditions are symmetrical, the modes are no longer even or odd functions.

Finally, the Ω_{n2} are determined by solving the second order problem and found to be:

$$\Omega_{n2} = -\frac{\omega_n}{2}\left(\alpha_n k_n\left(6 - \frac{1}{2}\alpha_n k_n\right) + \sum_{\substack{k=1 \\ k \neq \text{parity than } n}}^{\infty} \left(k_n^4 - k_p^4\right) \times s_{n1}^{(k)} \; s_{n1}^{(p)}\right) \tag{235}$$

with the notations of paragraph 2.

Clamped - free beams.

The natural frequencies of such cantilivered beams are given at the first order by:

$$\Omega_n = \omega_n \left(1 - 2\varepsilon \frac{\hat{\alpha}_n}{k_n^2}\right) \tag{236}$$

and the associated modes:

$$W_n(\xi) = \phi_n(\xi) - \varepsilon \sum_{\substack{p=1 \\ p\neq n}}^{\infty} \frac{8\alpha_n \alpha_p k_n^3 k_p}{k_p^4 - k_n^4} \left((-1)^{n+p} k_n^2 - k_p^2 \right) \phi_p(\xi)$$

Equation (236) shows that at first order ω_n bounds Ω_n from above if $\varepsilon>0$ and from below if $\varepsilon>0$ and that for a given ε the first order correction decreases in absolute value with n, the order of the natural frequency sought.

Clamped - clamped beams

This type of boundary conditions leads to similar conclusions about the natural modes and frequencies as in the free-free case; such a result is expected because the free-free and the clamped-clamped modes in the constant case are related by:

$$\left(\phi_n(\xi)\right)_{\text{free-free}} = \left(\frac{d^2\phi_n(\xi)}{d\xi^2} \right)_{\text{clamped-clamped}}$$

Beams simply supported at both ends.

The previous conclusions apply again and the natural frequencies up to the second order are found to be:

$$\Omega_n = \omega_n \left(1+\varepsilon^2 \left[\frac{1}{(2n\pi)^2} + \sum_{\substack{p=1 \\ p\neq \text{parity} \\ \text{than n}}}^{\infty} \frac{16\, p^5}{n^5\pi^4(n^2-p^2)^2} \left(\frac{\omega_p^2}{\omega_n^2} - 1 \right) \right] \right)$$

The serie in the right hand side of the equation is convergent, its general term being of the order of $1/p^3$.

The modes shapes are determined at first order by:

$$W_n(\xi) = \sin n\pi\xi - \frac{\varepsilon_n}{\pi^2} \sum_{\substack{p=1 \\ p\neq \text{parity than } n}} \frac{4p^3}{(n^2+p^2)(n_2-p^2)^2} \sin p\pi\xi$$

The other possible types of boundary conditions present no difficulty and the modal characteristics can be found from paragraph 2 in similar fashion.

It is to be noted that for the foregoing class of beams, the natural frequencies are closer to the natural frequencies of the beams of reference when symmetrical boundary conditions apply that for the other types of boundary conditions.

4. Tapered truncated cantiliver beams with elliptical cross section.

This class of beams is a reasonable approximation of high aspect ratio airplane wings and therefore it is of interest to investigate the modal behavior of such structures by the method developed in paragraph 2. The type of configuration considered is the following:

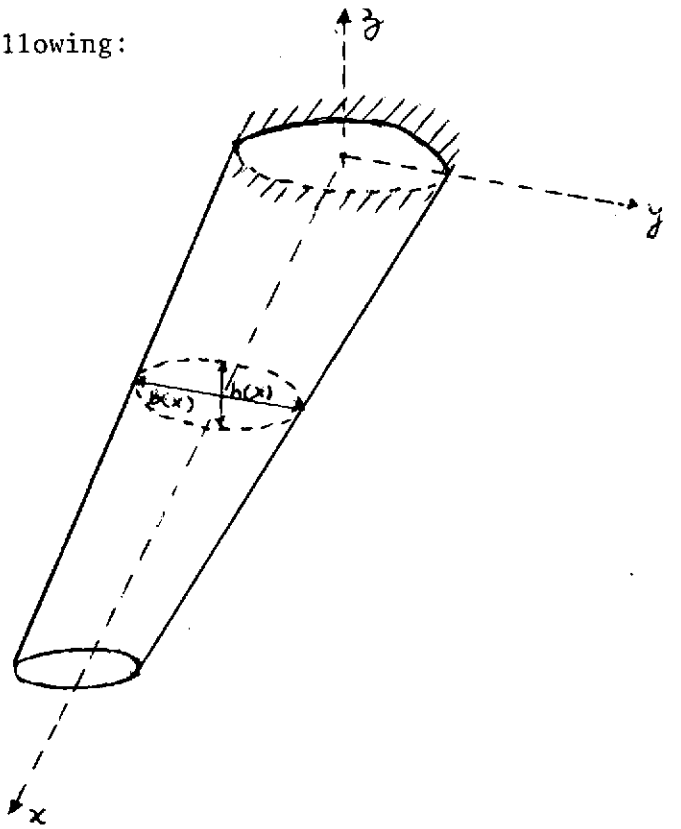

$$h(\xi) = h_o - e\xi \quad ; \quad b(\xi) = b_o - ae\xi$$

$$o<e<<1 \quad ; \quad o \leq \xi \leq 1$$

The corresponding mathematical model is given by the differential equation (212) and the boundary conditions B.C. are:

$$y(o) = \frac{dy}{d\xi}(o) = 0 \tag{237}$$

$$EI(1)\frac{d^2y}{d\xi^2}(1) = \frac{d}{d\xi}\left(EI(\xi)\frac{d^2y}{d\xi^2}(\xi)\right)\Bigg|_{\xi = 1} = 0 \tag{238}$$

The cross sectional area and structural moment of inertia are:

$$A(\xi) = \pi\, b(\xi)\, h(\xi) \tag{239}$$

$$I(\xi) = \frac{\pi}{64} b(\xi)\, h(\xi) \tag{240}$$

and consequently, the method of paragrpah 2 applies for the particular functions:

$$A(\xi) - A_o = -\pi b_o e\xi \left(1 + \frac{ah_o}{b_o} - \frac{ae\xi}{b_o}\right)$$

$$EI(\xi) - EI_o = \frac{E\pi}{64} e\xi \Big[h_o^2 b_o \left(3 - \frac{ah_o}{b_o}\right) +$$

$$3e\xi h_o b_o \left(1 + \frac{ah_o}{b_o}\right) - e^3\xi^3 b_o \left(1 + \frac{3ah_o}{b_o}\right) + ae^4\xi^4 \Big]$$

The first order solutions for the natural frequencies are found to be

$$\Omega_n = \omega_n \left(1 + \frac{e}{h_o} \left(-\frac{1}{2} - \frac{2\alpha_n^2}{k_n^2} \left(4 + \frac{ah_o}{b_o} \right) \right) \right) \tag{241}$$

The first order correction in the right hand side increases linearly with $\frac{ah_o}{b_o}$ the taper ratio between the chord and the thickness; moreover this correction is always negative for the natural frequencies Ω_p for which $k_p > 2\sqrt{4 + \text{taper ratio.}}$

This formula is significant for design purposes because it indicates in which manner to adjust the taper ratio such as to increase the value of a resonant frequency which is within an undesirable range.

This formula shows that the effect of the taper is to increase the fundamental resonant frequency regardless of the taper ratio, but the value of the second natural frequency can be increased by choosing configurations for which $a > 1.5 \frac{bo}{h_o}$.

The first order solutions for the normal modes are found to be:

$$W_n(\xi) = \phi_n(\xi) + \frac{8e}{h_o} \sum_{\substack{p=1 \\ p \neq n}}^{\infty} \frac{\alpha_n \alpha_p k_p}{k_n^2 \left(\frac{k_p^4}{k_n^4} - 1 \right) \left(\frac{k_p^2}{k_n^2} - (-1)^{n+p} \right)} \left(\frac{2(-1)^{n+p}}{\left(\frac{k_p^2}{k_n^2} - (-1)^{n+p} \right)} + 3 + \frac{aho}{b_o} \right) \phi_p(\xi) \tag{242}$$

It can be easily checked (by looking at the order of magnitude of the general term) that the serie on the right hand side of the above equation is convergent.

5. Conclusion and discussion on the limitations of the method.

Like every pertubation method, this analysis is based in large part on the assumption that ε is a small quantity. The term "small" however has no intrinsec meaning; for perturbation problems ε is considered small if the specific perturbation method gives consistent results. Hence the important problem when dealing with such methods is to know what error in the results is associated with a given ε. If this error is acceptable for the specific engineering purpose for which the problem is solved, then ε can be assumed small; if on the contrary, a sufficiently large number of terms in the perturbation serie does not give a satisfactory result, then the value of ε does not justify the validity of that perturbation method.

As an illustration of the above, the method is applied to tapered cantiliver beams for which the theoretical results are given in the paragraph 3 of this Appendix. The accuracy in the first three natural frequency is based on the comparison with analytical results of Reference (22).

One-term perturbation solutions are compared to the exact solutions for different values of ε, and the percentage errors are plotted versus ε for each of the three frequencies in Figures 48, 49, 50.

Figure 48 shows that the one-term solution for the fundamental

frequency is really accurate only for ε small compared to unity. For $\varepsilon = 0.5$ the percentage error in the frequency is 6.03% and increases relatively fast to 9.21% for $\varepsilon = 0.6$.

If a more accurate solution is needed for the fundamental frequency of cantilivered beams which such taper, then it is necessary to proceed to a second order analysis, or to higher order if needed.

However, as it can be seen in Figures 49 and 50 when the second and third natural frequencies are sought, even a one-term solution is highly satisfactory by this method.

For values of ε as high as 0.7 there is only 5% error for the second natural frequency and only 2% error for the third natural frequency.

This perturbation analysis does not present loss in accuracy for higher modes and therefore seems particularly suitable when the determination of the higher harmonics is desired.

APPENDIX II

ANALYSIS OF MODAL DAMPING BY COMPONENT MODES METHOD USING LAGRANGE MULTIPLIERS

1. Introduction

In a rencent note Hallquist and Synder (Reference (42)) formally analysed a linear, damped vibrating system with arbitrary support conditions using Lagrange multipliers. This method is dependent upon determining the coefficients C_{ij} of the Rayleigh dissipation function for damping. Most commonly, in fact, what can be determined experimentally are the damping coefficients relative to the classical undamped normal modes of a structure. In their recent paper (Reference (43)) Kana and Huzar developed an empirical method for predicting the modal damping of a Space Shuttle model by means of damping measurements performed on the individual substructures. As an alternative, presented here is a theoretical analysis which extends that of References (3) and (4) to the determination of the modal behavior of a damped linear elastic structure of arbitrary complexity by a component mode method.

2. Theoretical Development

We conceptually disassemble the structure into N simple components for which we know for each mode:

a) the generalized masses $M_j^{(n)}$ $j = 1,2, \ldots$; $n = 1, \ldots N$

b) the damping coefficients $\zeta_j^{(n)}$ $j = 1,2, \ldots$; $n = 1, \ldots N$

c) the natural undamped frequency $\omega_1^{(n)}$ $j=1,2,\ldots$; $n = 1, \ldots N$

For the total system:

Kinetic energy:

$$T = \frac{1}{2} \sum_{n=1}^{N} \sum_{j=1}^{\infty} M_j^{(n)} \dot{q}_j^{2(n)} \tag{243}$$

Potential energy:

$$U = \frac{1}{2} \sum_{n=1}^{N} \sum_{j=1}^{\infty} M_j^{(n)} \omega_j^{(n)2} q_j^{(n)2} \tag{244}$$

Damping dissipation function:

$$D = \frac{1}{2} \sum_{n=1}^{N} \sum_{j=1}^{\infty} 2\zeta_j^{(n)} \omega_j^{(n)} M_j^{(n)} \dot{q}_j^{(n)2} \tag{245}$$

Here we assume that the damped and undamped modes of components (though not necessarily of overall structure) are indistinguishable.

Interconnecting conditions between the components:

$$f_r = \sum_{n=1}^{N} \sum_{j=1}^{\infty} \beta_{rj}^{(n)} q_j^{(n)} = 0 \quad r=1,....R \tag{246}$$

Lagrangian:

$$L = T + D - U + \sum_{n=1}^{R} \lambda_r f_r$$

where T, D and f_r are given respectively by equations (243), (244), (245) and (246).

Lagrange's equations are thus

$$M_j^{(n)} \left[\ddot{q}_j^{(n)} + 2\zeta_j^{(n)}\omega_j^{(n)} \dot{q}_j^{(n)} + \omega_j^{(n)2} q_j^{(n)} \right] - \sum_{r=1}^{R} \lambda_r \beta_{rj}^{(n)} = 0 \quad (247)$$

Assume time dependent motion of the form,

$$q_j^{(n)}(t) = \bar{q}_j^{(n)} e^{(-\beta\Omega + i\Omega\sqrt{1-\beta^2})t}$$

$$\lambda_r(t) = \bar{\lambda}_r e^{(-\beta\Omega + i\Omega\sqrt{1-\beta^2})t}$$

The Eigenvalue equation is then obtained from (246) and (247), as

$$| \Delta_{pq} | = 0$$

where

$$\Delta_{pq} = \sum_{n=1}^{N} \sum_{j=1}^{\infty} \frac{\beta_{pj}^{(n)} \beta_{pj}^{(n)}}{M_j^{(n)} \{ [\Omega^2(2\beta^2-1) + 2\zeta_j^{(n)}\omega_j^{(n)}\Omega\beta + \omega_j^{(n)2}] + 2i\Omega\sqrt{1-\beta^2}(\zeta_j^{(n)}\omega_j^{(n)} - \Omega\beta) \}} \quad (248)$$

For the case where the damping coefficients of the components are small for each mode, a first order approximation of equation (248) leads to

$$\Delta_{pq} = \sum_{n=1}^{N} \sum_{j=1}^{\infty} \frac{\beta_{pj}^{(n)} \beta_{qj}^{(n)} \left[\omega_j^{(n)2} - \Omega^2)^2 - 2i\Omega(\zeta_j^{(n)} \omega_j^{(n)} - \Omega\beta) \right]}{M_j^{(n)} \left(\omega_j^{(n)2} - \Omega^2 \right)^2} \qquad (249)$$

Thus to first order, for small damping, the natural frequencies, Ω, are the same as for the undamped system.

3. Example:

The utility of the method is now illustrated by a simple example which is that of a structure composed of two identical beams connected at their middle. In particular, for doubly symmetric vibrations, the single constraint condition reduces to the equality of the displacements at the mid-point. The natural frequencies and damping coefficients in each mode are given by (from equation (248) for N = 1)

$$\left\{ \begin{array}{l} \sum_{j=0,2,4}^{\infty} \psi_j^2(0) \dfrac{(\omega_j^2 - \Omega^2)}{(\omega_j^2 - \Omega^2)^2} = 0 \qquad (250) \\ \\ \sum_{j=0,2,4}^{\infty} \psi_j^2(0) \dfrac{\Omega(\zeta_j \omega_j - \Omega\beta)}{(\omega_j^2 - \Omega^2)} = 0 \qquad (251) \end{array} \right.$$

where ψ_j represents an unconstrained beam mode.

The solutions $\Omega_j = \omega_j$; $\beta_j = \zeta_j$ corresponding to $\lambda = 0$ are physically valid and represent modes in which the beams vibrate symmetrically

together, without any constraint force required.

Other solutions for $\lambda \neq 0$ are given by:

$$\sum_{j=0,2,4}^{\infty} \frac{\psi_j^2(0)}{\omega_j^2 - \Omega^2} = 0 \tag{252}$$

$$\sum_{j=0,2,4}^{\infty} \frac{\psi_j^2(0)\,\Omega\,(\zeta_j\omega_j - \Omega\beta)}{(\omega_j^2 - \Omega^2)} = 0 \tag{253}$$

One can show that there is one root of the frequency equation (252) in between each two consecutive unconstrained natural frequencies ω_j. A two-term analysis for the fundamental bending mode gives:

$$\Omega = 0.758\ \omega_2$$

$$\beta = 0.758\ \zeta_2$$

In this mode, the overall structure is more flexible than its individual components and contains less damping.

4. Discussion and Conclusions:

For any arbitrary structure the natural frequencies and modal damping can be predicted from the knowledge of the natural frequencies and damping coefficients of each of the components. All parameters appearing in the analysis can be measured experimentally and the technique is simple and offers physical clarity. Further study needs to be given to the damping which may arise at the connection of the components per se.

APPENDIX III

FREE VIBRATIONS OF A BEAM CLAMPED IN ITS MIDDLE BY A RAYLEIGH RITZ METHOD USING LAGRANGE MULTIPLIERS.

1. Introduction ; statement of the problem.

The present analysis is mainly intended as background for the studies of the limiting cases considered in Chapters III and IV. The problem considered is that of a beam of length 2L, free at both ends and clamped in the middle, as illustrated below:

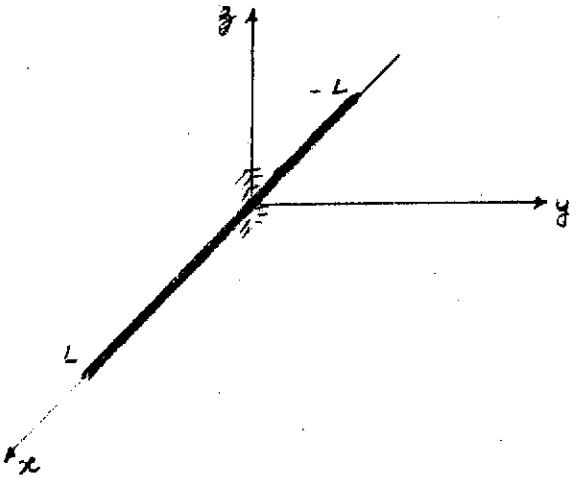

M: half mass of the beam

EI: bending stiffness

$\phi_i(\xi)$: unconstrained beam modes - $-1 \leq \xi \leq 1$

k_i: corresponding non-dimensional frequency parameters.

$W(\xi,t)$: bending displacement of the beam

The kinetic and potential energies of the beam are:

$$T = \frac{1}{2} M \int_{-1}^{1} \dot{W}^2(\xi,t)\, d\xi \qquad (253)$$

$$U = \frac{1}{2} \frac{EI}{L^3} \int_{-1}^{1} W''^2(\xi,t)\, d\xi \tag{254}$$

2. Modal analysis using even modes of an unconstrained beam.

The modal displacements are sought on the form:

$$W(\xi,t) = \sum_{n=1,3}^{\infty} q_n(t)\, \phi_n(\xi) \tag{255}$$

and thus (253) and (254) become

$$T = \frac{1}{2} M \sum_{n=1,3}^{\infty} \dot{q}_n^2(t) \quad ; \quad U = \frac{1}{2} \frac{EI}{L^3} \sum_{n=1,3}^{\infty} k_n^4\, q_n^2(t) \tag{256}$$

by virtue of the orthonormality of the $\phi_i(\xi)$. Because of the choice of even beam modes, the only condition for the beam to be clamped in the middle is:

$$W(0,t) = 0$$

or, by use of (255)

$$\sum_{n=1,3}^{\infty} q_n(t)\, \phi_n(0) = 0 \tag{257}$$

The corresponding Lagrangian is:

$$\mathcal{L} = \sum_{n=1,3}^{\infty} \left(\frac{M}{2} \dot{q}_n^2(t) - \frac{EI}{2L^3} k_n^4\, q_n^2(t) + \lambda q_n(t) \phi_n(0) \right)$$

and the subsequent Lagrange's equations are:

- $M \ddot{q}_n(t) + \frac{EI}{L^3} k_n^4 q_n(t) - \lambda \phi_n(0) = 0 \qquad n=1,\ldots\infty$

- $\sum_{n=1,3}^{\infty} q_n(t)\, \phi_n(0) = 0$

Harmonic solutions are sought in the form:

$$q_n(t) = \bar{q}_n \, e^{i \left(\frac{EI}{ML^3}\right)^{1/2} \omega t}$$

$$\lambda(t) = \bar{\lambda} \frac{EI}{L^3} \, e^{i \left(\frac{EI}{ML^3}\right)^{1/2} \omega t}$$

and thus:

$$\bar{q}_n = - \frac{\bar{\lambda} \phi_n(0)}{\omega^2 - k_n^4} \tag{258}$$

$$\sum_{n=1,3}^{\infty} \frac{\bar{\lambda} \phi_n^2(0)}{\omega^2 - k_n^4} = 0 \tag{259}$$

Equation (259) leads to the frequency equation:

$$\sum_{n=1,3}^{\infty} \frac{\phi_n^2(0)}{\omega^2 - k_n^4} = 0 \qquad (260)$$

and equations (258) determine the generalized coordinates for each natural frequency. The mode shapes are then given by equation (255).

3. Modal analysis using antisymmetric modes of an unconstrained beam.

Only odd free-free beam modes are used in the modal serie:

$$W(\xi,t) = \sum_{n=2,4}^{\infty} q_n(t)\ \phi_n(\xi) \qquad -1 \leq \xi \leq 1 \qquad (261)$$

and equations (253) and (254) become:

$$T = \frac{1}{2} M \sum_{n=2,4}^{\infty} \dot{q}_n^2(t) \qquad (262)$$

$$U = \frac{1}{2} \frac{EI}{L^3} \sum_{n=2,4}^{\infty} k_n^4\ q_n^2(t) \qquad (263)$$

The zero-displacement condition at the middle of the beam is already satisfied by the coice of the antisymmetric modes in the analysis; however the beam has to be constrained so that:

$$\frac{1}{L}\ W'(o,t) = 0$$

or using (261)

$$\frac{1}{L} \sum_{n=2,4}^{\infty} q_n(t)\, \phi'_n(0) = 0 \qquad (264)$$

If μ is the Lagrange Multiplier corresponding to the above constraint, the equations of motion are:

$$M \ddot{q}_n(t) + \frac{EI}{L^3} k_n^4 q_n(t) - \frac{\mu}{L} \phi'_n(0) = 0 \qquad n=1,\ldots\infty$$

$$\sum_{n=2,4}^{\infty} \frac{q_n(t)}{L} \phi'_n(0) = 0$$

Harmonic time dependent input is assumed as follows:

$$q_n(t) = \bar{q}_n\, e^{i \left(\frac{EI}{ML^3}\right)^{1/2} \omega t}$$

$$\mu(t) = \bar{\mu}\, \frac{EI}{L^2}\, e^{i \left(\frac{EI}{ML^3}\right)^{1/2} \omega t}$$

and hence the Lagrange's equations are equivalent to the system:

$$\bar{q}_n = - \frac{\mu\, \phi'_n(0)}{\omega^2 - k_n^4} \qquad (265)$$

$$\sum_{n=2,4}^{\infty} \mu\, \frac{\phi'^2_n(0)}{\omega^2 - k_n^4} = 0 \qquad (266)$$

From the eigenvalue equation (266) we obtain the frequency equation:

$$\sum_{n=2,4}^{\infty} \frac{\phi'_n{}^2(0)}{\omega^2 - k_n^4} = 0 \qquad (267)$$

and equations (265) and (261) determine the corresponding modal displacements.

4. Discussion

Although a more elaborate analysis is presented in Chapter III, a two-modes approximation of the frequency equation can give some insight on the rate of convergence of the fundamental frequency according to the type of modes used.

A two-terms expansion of equation (260) gives:

$$\frac{1}{2\omega^2} + \frac{\phi_3{}^2(0)}{\omega^2 - k_3^4} = 0$$

and yields the following solution for the fundamental frequency:

$$\omega = 3.553$$

with the values of $\phi_3(0)$ and k_3 given in Reference (35). Hence, a two-symmetric-modes analysis is seen to produce an error of about 1% in the fundamental natural frequency.

If two antisymmetric modes are used in equation (267), the fundamental natural frequency is given by

$$\omega = k_4^2 \left(1 + \frac{2}{3} \phi'^2_4(0) \right)^{-1/2}$$

and with the values of k_4 and $\phi'_4(0)$ given in Reference (35), yields the numerical value:

$$\boxed{\omega = 4.709}$$

In the analysis using antisymmetric modes, a two-modes approximation gives a 5.4% error in the fundamental frequency and thus we can anticipate better convergence using symmetric modes.

APPENDIX IV

MODAL ANALYSIS OF A FLEXIBLE AIRPLANE WITH LOW ASPECT RATIO WING AND TAIL

1. Introduction

The present analysis extends the study of Chapter III to the more general case of a flexible airplane with a wing and tail of finite or low aspect ratios.

Such a configuration is illustrated below.

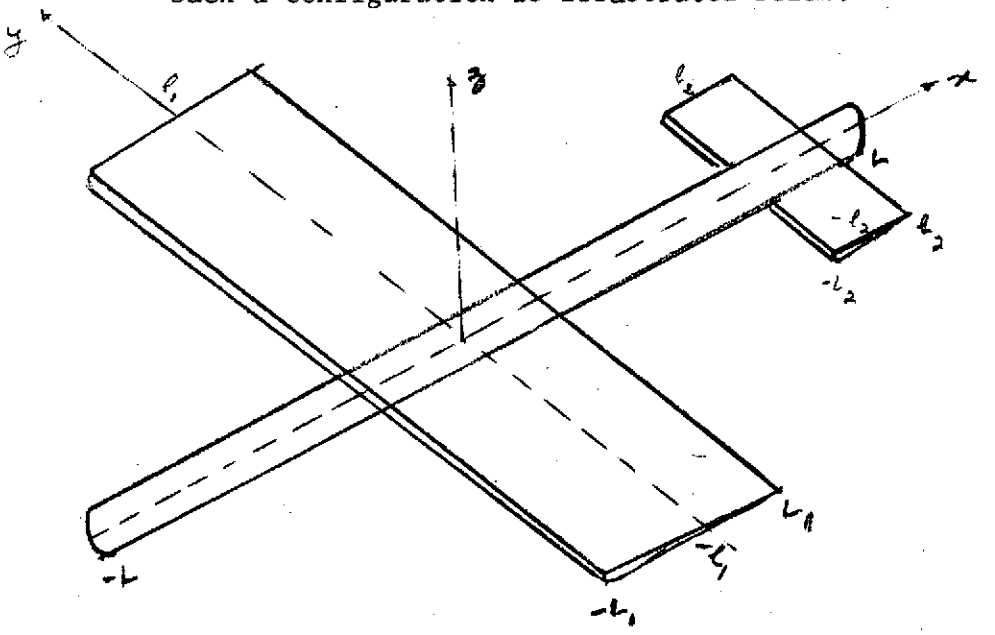

In this analysis the fuselage has a one-dimensional beam representation with freedom in bending and torsion, while the wing and tail are represented by uniform plates undergoing bending in the x and y - directions.

Each one of the components is given a linear treatment, geometrically and elastically.

The rigid body dynamics of this structure are similar in concept to those investigated in Chapter III.

Because of the geometrical symmetry, pitching and rolling motions can be considered independently of each other. Yaw-type of motions are not in the purpose of this analysis.

2. Modal analysis for motions of the rolling type.

Such motions are characterized by pure twisting of the fuselage, and antisymmetric behavior of the wing and tail about the x axis.

The approach is based upon the use of free-free twisting modes for the fuselage and unconstrained plate modes with antisymmetry about the x axis, for the wing and tail. More specifically, the latter modes are of the form:

$$\Phi_n(x,y) = \sum_{k=1}^{\infty} \sum_{m=2,4}^{\infty} A_{km}^{(n)} X_k(x) Y_m(y) \qquad (268)$$

where

X_k and Y_m are free-free beam modes, and the "weighting" coefficients $A_{km}^{(n)}$ are found together with the natural frequencies K_n by solving the eigenvalue problem:

$$A_{km}^{(n)} (k_k^4 + s^4 k_m^4) + s^2 \sum_{l=1}^{\infty} \sum_{r=2,4}^{\infty} A_{lr}^{(n)} [\nu(\omega_{kl}\omega_{rm} + \omega_{lk}\omega_{mr}) +$$

$$2(1-\nu)\alpha_{kl}\alpha_{mr}] = K_n^2 A_{km}^{(n)} \qquad (269)$$

In the above equation:

k_i: natural frequency parameter of free-free beam.

s : ratio length/width plate

ν : Poisson ratio of plate

$$\omega_{ij} = \int_{-1}^{1} X''_i(\xi)\, X_j(\xi) d\xi$$

$$\alpha_{ij} = \int_{-1}^{1} X'_i(\xi) X'_j(\xi) d\xi = \alpha_{ji}$$

The angular displacement of the fuselage $\Theta(x,t)$ is sought given by the following serie:

$$\Theta(x,t) = \sum_{n=1}^{\infty} P_n(t)\ \theta_n(x) \qquad - L \leq x \leq L \tag{270}$$

$\theta_n(x)$: free-free modes in twisting

and the bending displacements of the wing and tail $W_1(x,y,t)$ and $W_2(x,y,t)$ are sought in the forms:

$$W_1(x,y,t) = \sum_{n=1}^{\infty} q_n^{(1)}(t)\ \Phi_n^{(1)}(x,y) \quad - L_1 \leq x \leq L_1 \tag{271}$$

$$- l_1 \leq y \leq l_1$$

$$W_2(x,y.t) = \sum_{n=1}^{\infty} q_n^{(2)}(t)\ \Phi_n^{(2)}(x,y) \quad - L_2 \leq x \leq L_2 \tag{272}$$

$$- l_2 \leq y \leq l_2$$

If the wing and tail have different ratios length/width, then:

$$\Phi_n^{(1)}(x,y) \neq \Phi_n^{(2)}(x,y)$$

The total kinetic energy of the structure is:

$$T = \frac{1}{2}\left[\int_{-L}^{L} I\,\dot{\Theta}^2(x,t)\,dx + \int_{-L_1}^{L_1}\int_{-l_1}^{l_1} \dot{W}_1^2(x,y,t)\,dm_1 + \right.$$

$$\left.\int_{-L_2}^{L_2}\int_{-l_2}^{l_2} \dot{W}_2^2(x,y,t)\,dm_2\right] \qquad (273)$$

where I is the mass moment of inertia per unit length of the fuselage about the x-axis. By sybstitution of (270), (271), (272) and use of the orthonormality of the component modes, equation (273) becomes:

$$\boxed{T = \frac{1}{2}\sum_{n=1}^{\infty} I\dot{L}P_n^2(t) + M_1\,\dot{q}_n^{(1)2}(t) + M_2\,\dot{q}_n^{(2)2}(t)} \qquad (274)$$

In the above equation M_1 and M_2 are one fourth of the masses of the wing and the tail respectively, i.e. relative to half-length and half-width of these components.

The potential energy of the airplane is:

$$U = \frac{1}{2}\left\{\int_{-L}^{L} GJ\left(\frac{\partial\Theta}{\partial x}(x,t)\right)^2 dx + \sum_{i=1}^{2} D_i \int_{-L_i}^{L_i}\int_{-l_i}^{l_i}\left(\frac{\partial^2 W_i}{\partial x^2}+\frac{\partial^2 W_i}{\partial y^2}\right)^2\right.$$

$$\left. + 2(1-\nu_i)\left[\left(\frac{\partial^2 W_i}{\partial x\partial y}\right)^2 - \frac{\partial^2 W_i}{\partial x^2}\,\frac{\partial^2 W_i}{\partial y^2}\right] dxdy\right\} \qquad (275)$$

In a first step equations (270), (271), (272) are substituted into (275), then use is made of the classical beam equation in twisting, and of equation (269) applied respectively to the wing modes and the tail

modes.

After lengthy algebraic manipulations, the potential energy is cast into the form:

$$U = \frac{1}{2} \sum_{n=1}^{\infty} \left(\frac{GJ}{L} (n-1)^2 \frac{\pi^2}{4} P_n^2(t) + \sum_{i=1}^{2} \frac{D_i L_i}{l_i^3} K_n^{(i)2} q_n^{(i)2}(t) \right) \quad (276)$$

Finally, the continuity of the displacements and slopes between the components has to be enforced. The slopes in the x direction and the displacements are already zero because of the choice of antisymmetric modes only, in the y-direction for the plates; as for the slope conditions in the y direction they are:

$$\Theta(x,t) = \frac{\partial W_1}{\partial y}(x,0,t) \qquad -L_1 \leq x \leq L_1$$

$$\Theta(x,t) = \frac{\partial W_2}{\partial y}(x,0,t) \qquad -L_2 \leq x \leq L_2$$

The variational formulation of these conditions is:

$$\int_{-L_1}^{L_1} \lambda^{(1)}(x,t) \left[\Theta(x,t) - \frac{\partial W_1}{\partial y}(x,0,t) \right] dx \quad (277)$$

$$\int_{-L_2}^{L_2} \lambda^{(2)}(x,t) \left[\Theta(x,t) - \frac{\partial W_2}{\partial y}(x,0,t) \right] dx \quad (278)$$

C-3

where $\lambda^{(1)}$ and $\lambda^{(2)}$ are the corresponding Lagrange multipliers. In the present case $\lambda^{(1)}(x,t)$ and $\lambda^{(2)}(x,t)$ are the generalized bending moments per unit length, developed along the widths of the wing and tail respectively and necessary to keep the continuity of slopes.

The integrals (277) and (278) are considered in a Dirac approximation; the alternative procedures discussed in Chapter V are prooved to be equally suitable but give rise to more elaborate computations.

For this purpose, the following notations are introduced:

$(x^{(1)}_r)_{r=1,R}$: partition of the interval $[-l_1, l_1]$

$$\xi'_r = \frac{x^{(1)}_r}{L} \quad ; \quad \xi^{(1)}_r = \frac{x^{(1)}_r}{L_1}$$

$(x^{(2)}_r)_{r=1,R}$: partition of $[-l_2, l_2]$

$$\xi''_r = \frac{x^{(2)}_r}{L} \quad ; \quad \xi^{(2)}_r = \frac{x^{(2)}_r}{L_2}$$

$\lambda^{(1)}_r(t)$, $\lambda^{(2)}_r(t)$: discrete values of $\lambda^{(1)}$ and $\lambda^{(2)}$ at the corresponding points.

Then, the integrals (277) and (278) are approximated by:

$$\sum_{r=1}^{R} \lambda^{(1)}_r \left[\Theta(\xi'_r,t) - \frac{1}{l_1} \frac{\partial W_1}{\partial \eta}(\xi^{(1)}_r,0,t) \right] \qquad (279)$$

$$\sum_{r=1}^{R} \lambda_r^{(2)} \left[\Theta(\xi_r'',t) - \frac{1}{l_1} \frac{\partial W_2}{\partial \eta}(\xi_r^{(2)},0,t) \right] \qquad (280)$$

which can be written in modal form by use of (270), (271), (272) as follows:

$$\sum_{r=1}^{R} \lambda_r^{(1)} \sum_{n=1}^{\infty} \left(P_n(t)\, \theta_n(\xi'_r) - \frac{q_n^{(1)}(t)}{l_1} \frac{\partial \Phi_n^{(1)}}{\partial \eta}(\xi_r^{(1)},0) \right) = 0 \qquad (281)$$

$$\sum_{r=1}^{R} \lambda_r^{(2)} \sum_{n=1}^{\infty} \left(P_n(t)\theta_n(\xi_r'') - \frac{q_n^{(2)}(t)}{l_2} \frac{\partial \Phi_n^{(2)}}{\partial \eta}(\xi_r^{(2)},0) \right) = 0 \qquad (282)$$

The subsequent Lagrange's equations are thus:

$$\cdot\cdot \quad I L P_n(t) + \frac{GJ}{L}(n-1)^2 \pi^2 P_n(t) - \sum_{r=1}^{R} (\lambda_r^{(1)} \theta_n(\xi_r') - \lambda_r^{(2)} \theta_n(\xi_r'')) = 0$$

$$\cdot\cdot \quad M_i q_n^{(i)}(t) + \frac{D_i L_i}{l_i^3} K_n^{(i)2} q_n^{(i)}(t) + \sum_{r=1}^{R} \frac{\lambda_r^{(i)}}{l_i} \frac{\partial \Phi_n^{(i)}}{\partial \eta}(\xi_r^{(i)},0) = 0, i = 1,2$$

together with the continuity conditions (281) and (282)

The following harmonic behavior is assumed in the analysis:

$$\begin{pmatrix} P_n(t) \\ (q_n^{(i)}(t))_{i=1,2} \end{pmatrix} = \begin{pmatrix} \bar{P}_n \\ (\bar{q}_n^{(i)})_{i=1,2} \end{pmatrix} \times e^{i \frac{1}{l_1^2} (D_1/\rho_1)^{1/2} \omega t}$$

$$(\lambda_r^{(i)}(t))_{i=1,2} = \bar{\lambda}_r^{(i)} \times \frac{D_1 L_1}{l_1^2} \times e^{i \frac{1}{l_1^2} (D_1|\rho_1)^{1/2} \omega t}$$

where ρ_1 is the mass density of the wing per unit area.

The following non-dimensional parameters are defined:

$$\gamma_1 = \frac{l_1}{L} \; ; \quad \gamma_2 = \frac{l_1}{L_2} \; ; \quad \mu_1 = \frac{M_1 l_1}{I} \; ; \quad \mu_2 = \frac{M_1}{M_2}$$

$$\psi_1 = \frac{\frac{GJ}{\frac{IL^2}{D_1}}}{\frac{4}{l^1 l_1}} \; ; \quad \psi_2 = \frac{\frac{D_2}{\frac{4}{2 l_2}}}{\frac{D_1}{l^1 l_1}}$$

$$F_n^{(1)} = \omega^2 - (n-1)^2 \frac{\pi^2}{4} \psi_1$$

$$F_n^{(2)} = \omega^2 - K_n^{(1)2}$$

$$F_n^{(3)} = \omega^2 - K_n^{(2)2} \psi_2$$

Then the generalized coordinates are expressed in function of $\lambda_r^{(1)}$ and $\lambda_r^{(2)}$ from the equations of motion as follows:

$$\bar{P}_n = - \gamma_1 \mu_1 \frac{\sum_{r=1}^{R} \bar{\lambda}_r^{(1)} \theta_n(\xi'_r) + \bar{\lambda}_r^{(2)} \theta_n(\xi''_r)}{F_n^{(1)}} \tag{283}$$

$$\bar{q}_n^{(i)} = \frac{\sum_{r=1}^{R} \bar{\lambda}_r^{(i)} \frac{\partial \Phi_n^{(i)}}{\partial \eta} (\xi_r^{(i)}, 0)}{F_n^{(i+1)}} \qquad i=1,2 \tag{284}$$

Substitution of the above equations into the constraint conditions lead to the eigenvalue equation and then to the frequency equation

$$\boxed{\det (\Delta (\omega)) = 0} \tag{285}$$

with the following representation of the eigenvalue tensor:

. $1 \leq r \leq R \quad ; \quad 1 \leq v \leq R$

$$\Delta_{rv}(\omega) = \sum_{n=1}^{\infty} \frac{(\gamma_1 \mu_1 \theta_n(\xi'_r \theta_n(\xi'_v) + \frac{\partial \Phi_n^{(1)}}{\partial \eta} (\xi_r^{(1)}, 0) \frac{\partial \Phi_n^{(1)}}{\partial \eta} (\xi_r^{(2)}, 0))}{F_n^{(2)}}$$

. $1 \leq r \leq R \quad ; \quad R+1 \leq v \leq 2R$

$$\Delta_{rv}(\omega) = \sum_{n=1}^{\infty} \frac{\gamma_1 \mu_1 \theta_n(\xi_r'') \theta_n(\xi_v')}{F_n^{(1)}}$$

. $R+1 \leq r \leq 2R \quad ; \quad R+1 \leq v \leq 2R$

$$\Delta_{rv}(\omega) = \sum_{n=1}^{\infty} \left(\frac{\gamma_1 \mu_1 \theta_n(\xi_r'') \theta_n(\xi_v'')}{F_n^{(1)}} + \frac{\gamma_2 \mu_2 \frac{\partial \Phi_n^{(2)}}{\partial \eta}(\xi_r^{(2)}, 0) \frac{\partial \Phi_n^{(2)}}{\partial \eta}(\xi_v^{(2)}, 0)}{F_n^{(2)}} \right.$$

3. Modal analysis for motions of the pitching type

Such motions are characterized by pure bending of the fuselage and symmetric behavior of the wing and tail about the x axis. The procedure is similar to that of paragraph 2, except for the facts that free-free beam modes in bending are used for the fuselage, and that the unconstrained plate modes are now based on even $\lambda_m(y)$.

Hence, equations (1) and (2) are still valid formally, but the subscripts m and r are 1,3,5,.....

The bending displacements of the three components are sought given by the series:

$$W(x,t) = \sum_{n=1}^{\infty} q_n(t) \phi_n(x) \qquad -L \leq x \leq L \qquad (286)$$

$$W_i(x,y,t) = \sum_{n=1}^{\infty} q_n^{(i)}(t)\ \Phi_n^{(i)}(x,y) \qquad \begin{matrix} -L_i \le x \le L_i \\ -l_i \le y \le l_i \end{matrix} \tag{287}$$

$i = 1,2$

and thus the kinetic and potential energies of the structure are:

$$T = \frac{1}{2} \sum_{n=1}^{\infty} \left(M\dot{q}_n^{\,2}(t) + \sum_{i=1}^{2} M_i\, \dot{q}_n^{(i)}(t)^2 \right) \tag{288}$$

$$U = \frac{1}{2} \sum_{n=1}^{\infty} \left(\frac{EI}{L^3} k_n^4\, q_n^2(t) + \sum_{i=1}^{2} \frac{D_i L_i}{l_i^3} K_n^{(i)2}\, q_n^{(i)}(t)^2 \right) \tag{289}$$

where M is half of the fuselage mass, and EI its bending stiffness.

The above equations are derived in a procedure similar to that of the paragraph 2 and therefore the details of the computations are omitted.

Because symmetric behavior of the wing and tail has been assumed in equation (1), the continuity of slopes in the y-directions between components is automatically satisfied; the continuity of the displacements and slope in the x-direction at the connections between components is expressed by:

$$W(x,t) = W_i(x,0,t) \tag{290}$$

$$\frac{\partial W}{\partial x}(x,t) = \frac{\partial W_i}{\partial x}(x,o,t) \qquad (291)$$

for $-L_i \leq x \leq L_i$ and $i = 1,2$

By following a similar procedure to that of paragraph 2, the following expressions are obtained for equations (29)) and (291) in the variational form:

$$\sum_{r=1}^{R} \lambda_r^{(1)} \sum_{n=1}^{\infty} (q_n(t)\, \phi_n(\xi_r') - q_n^{(1)}(t)\, \Phi_n^{(1)}(\xi_r^{(1)},0)) = 0 \qquad (292)$$

$$\sum_{r=1}^{R} \lambda_r^{(2)} \sum_{n=1}^{\infty} \left(\frac{q_n(t)}{L}\, \phi'_n(\xi_r') - \frac{q_n^{(1)}(t)}{L_1} \frac{\partial \Phi_n^{(1)}}{\partial \xi}(\xi_r^{(1)},0)\right) = 0 \qquad (293)$$

$$\sum_{r=1}^{R} \lambda_r^{(3)} \sum_{n=1}^{\infty} (q_n(t)\phi_n(\xi_r'') - q_n^{(2)}(t)\, \Phi_n^{(2)}(\xi_r^{(2)},0)\ ) = 0 \qquad (294)$$

$$\sum_{r=1}^{R} \lambda_r^{(4)} \sum_{n=1}^{\infty} \left(\frac{q_n(t)}{L}\phi'_n(\xi_r'') - \frac{q_n^{(2)}(t)}{L_2} \frac{\partial \Phi_n^{(2)}}{\partial \xi}(\xi_r^{(2)},0)\right) = 0 \qquad (295)$$

Also, the harmonic analysis in the Lagrange's equations assumes similar harmonic time dependence.

The following non-dimensional parameters are defined here:

$$\delta_1 = \frac{L_1}{L} \quad ; \quad \delta_2 = \frac{L_1}{L_2} \quad ; \quad \mu_1 = \frac{M_1}{M} \quad ; \quad \mu_2 = \frac{M_1}{M_2}$$

$$\psi_1 = \frac{\frac{EI}{ML^3}}{\frac{D_1}{\gamma_1 l_1^4}} \quad ; \quad \psi_2 = \frac{\frac{D_2}{\gamma_2 l_2^4}}{\frac{D_1}{\gamma_1 l_1^4}}$$

$$F_n^{(1)} = \omega^2 - k_n^4 \psi_1$$

$$F_n^{(2)} = \omega^2 - K_n^{(1)\,2}$$

$$F_n^{(3)} = \omega^2 - K_n^{(2)\,2}\,\psi_2$$

The equations of motion are first solved for the generalized coordinates:

$$\bar{q}_n = -\mu_1 \frac{\sum_{r=1}^{R} \bar{\lambda}_r^{(1)} \phi_n(\xi_r') + \delta_1 \bar{\lambda}_r^{(2)} \phi_n'(\xi_r') + \bar{\lambda}_r^{(3)} \phi_n(\xi_r'') + \delta_1 \bar{\lambda}_r^{(4)} \phi_n'(\xi_r'')}{F_n^{(1)}}$$

$$\bar{q}_n^{(1)} = \frac{\sum_{r=1}^{R} \bar{\lambda}_r^{(1)} \phi_n^{(1)}(\xi_r^{(1)},0) + \bar{\lambda}_r^{(2)} \frac{\partial \phi_n^{(1)}}{\partial \xi}(\xi_r^{(1)},0)}{F_n^{(2)}}$$

$$\bar{q}_n^{(2)} = \mu_2 \frac{\sum_{r=1}^{R} \bar{\lambda}_r^{(3)} \Phi_n^{(2)}(\xi_r^{(2)},0) + \delta_2 \bar{\lambda}_r^{(4)} \frac{\partial \Phi_n}{\partial \xi}^{(2)}(\xi_r^{(2)},0)}{F_n^{(3)}}$$

and then the eigenvalue equations are found by substitution into (292) - (295). The eigenvalue matrix is of order 4Rx4R, symmetric, and its elements are:

. $1 \leq r \leq R \quad ; \quad 1 \leq v \leq R$

$$\Delta_{rv}(\omega) = \sum_{n=1}^{\infty} \left(\frac{\mu_1 \phi'_n(\xi'_r)\phi'_n(\xi'_v)}{F_n^{(1)}} + \frac{\Phi_n^{(1)}(\xi_r^{(1)},0)\ \Phi_n^{(1)}(\xi_v^{(1)},0)}{F_n^{(2)}} \right)$$

. $1 \leq r \leq R \quad ; \quad R+1 \leq v \leq 2R$

$$\Delta_{rv}(\omega) = \sum_{n=1}^{\infty} \left(\frac{\mu_1 \delta_1 \phi'_n(\xi'_r)\phi_n(\xi'_v)}{F_n^{(1)}} + \frac{\frac{\partial \Phi_n}{\partial \xi}^{(1)}(\xi_r^{(1)},0)\Phi_n^{(1)}(\xi_v,^{(1)}0)}{F_n^{(2)}} \right)$$

. $1 \leq r \leq R \quad ; \quad 2R+1 \leq v \leq 3R$

$$\Delta_{rv}(\omega) = \sum_{n=1}^{\infty} \mu_1 \frac{\phi_n(\xi''_r)\phi_n(\xi'_v)}{F_n^{(1)}}$$

. $1 \leq r \leq R \quad ; \quad 3R+1 \leq v \leq 4R$

$$\Delta_{rv}(\omega) = \sum_{n=1}^{\infty} \mu_1 \delta_1 \frac{\phi'_n(\xi''_r)\phi_n(\xi'_v)}{F_n^{(1)}}$$

. $R+1 \leq r \leq 2R$; $R+1 \leq v \leq 2R$

$$\Delta_{rv}(\omega) = \sum_{n=1}^{\infty} (\mu_1 \delta_1^2 \frac{\phi'_n(\xi'_r)\phi'_n(\xi'_v)}{F_n^{(1)}} + \frac{\frac{\partial \Phi_n^{(1)}}{\partial \xi}(\xi_r^{(1)},0) \frac{\partial \Phi_n^{(1)}}{\partial \xi}(\xi_r^{(2)},0))}{F_n^{(2)}}$$

. $R+1 \leq r \leq 2R$; $2R+1 \leq v \leq 3R$

$$\Delta_{rv}(\omega) = \sum_{n=1}^{\infty} \mu_1 \delta_1 \frac{\phi_n(\xi''_r)\phi'_n(\xi'_v)}{F_n^{(1)}}$$

. $R+1 \leq r \leq 2R$; $3R+1 \leq v \leq 4R$

$$\Delta_{rv}(\omega) = \sum_{n=1}^{\infty} \mu_1 \delta_1^2 \frac{\phi'_n(\xi''_r)\phi'_n(\xi'_v)}{F_n^{(1)}}$$

. $2R+1 \leq r \leq 3R$; $2R+1 \leq v \leq 3R$

$$\Delta_{rv}(\omega) = \sum_{n=1}^{\infty} (\frac{\mu_1 \phi_n(\xi''_r)\phi_n(\xi''_v)}{F_n^{(1)}} + \frac{\mu_2 \Phi_n^{(2)}(\xi_r^{(2)},0)\Phi_n^{(2)}(\xi_v^{(2)},0))}{F_n^{(3)}}$$

. $2R+1 \leq r \leq 3R \quad ; \quad 3R+1 \leq v \leq 4R$

$$\Delta_{rv}(\omega) \sum_{n=1}^{\infty} \frac{(\mu_1 \delta_1 \phi'_n(\xi''_r)\phi_n(\xi''_v) + \mu_2 \delta_2 \frac{\partial \phi_n^{(2)}(\xi_r^{(2)},0)\phi_n^{(2)}(\xi_{v,}^{(2)}0))}{F_n^{(3)}}}{F_n^{(1)}}$$

. $3R+1 \leq r \leq 4R \quad ; \quad 3R+1 \leq v \leq 4R$

$$\Delta_{rv}(\omega) = \sum_{n=1}^{\infty} \frac{(\mu_1 \delta_1{}^2 \phi'_n(\xi''_r)\phi'_n(\xi''_v) + \frac{\mu_2 \delta_2{}^2 \frac{\partial \Phi_n^{(2)}}{\partial \xi}(\xi_r^{(2)}, 0)\frac{\partial \Phi_n^{(2)}(\xi_v^{(2)},0)}{\partial \xi}}{F_n^{(3)}}}{F_n^{(1)}}$$

Non-trivial solutions for the Lagrange multipliers exist if:

$$\det \ (\ \Delta(\omega) \ ) = 0$$

i.e., for the natural frequencies of the structure.

4. Discussion of the convergence of the method.

The main sources of error for the natural frequencies are the use of a finite number of modes per component and the choice of a finite number of points at which the constraints are applied.

An obvious way of solving the problem would be to give to both parameters very large values form the beginning, but then the computation may be too time consuming for the accuracy desired. A better approach is to aim at optimizing the values of the two parameters based on pre-

vious information acquired in the dissertation.

As a first remark, it can be noticed that the bending or torsional free-free modes of the fuselage are analytically known functions and are used only in elementary operations such as summation. Therefore, a large number of these modes can be used without any loss in accuracy or significant time increase.

The problem is much more complicated, however, for the plate modes. The unconstrained modes are obtained by numerical techniques applied to equation (?69), and therefore neither the $A_{km}^{(n)}$ nor the $K_n^{(2)}$ are rigourously known. As a consequence, it is desireable to avoid using a larger number of modes than is strictly necessary, in order to minimize the initial errors propagating to the final result.

The minimum number of modes necessary is, of course, determined by the number of natural frequencies desired and by the number of constraint points considered. For instance, if five constraint points are considered along the width of the wing and the first three natural frequencies are desired, at least ten degrees of freedom in the x-direction should be used in the analysis, for a reasonably good accuracy. Obviously, a suitable number of modes in the y-direction has to be considered as well.

The purpose of this discussion is to suggest a systematic approach for the optimum choice of plate modes versus points of constraint, for the wing and the tail. The procedure is based upon convergence in a limiting case, i.e. the case in which the fuselage behaves rigidly and therefore the constraints at the connections are most critical.

The analysis of the Chapter V shows that by using five modes $X_k(x)$ and five symmetric modes $Y_k(y)$, an unconstrained plate with aspect ratio 2 can be considered clamped in the middle of the first three natural frequencies with as little as seven constraint points. The fundamental natural frequency is then predicted with less than 0.1% error, similar precision is obtained in the second natural frequency, and an error of only 0.4% is obtained in the third natural frequency. If the plate has higher aspect ratio, an even smaller number of points should suffice for comparable accuracy. Therefore, setting R=7 in the analysis of the pitching modes should be very satisfactory for at least the first three natural frequencies. The order of the eigenvalue matrix would then be 28, which is not unreasonable for computations of such type.

The analysis of Chapter III indicates that for motions of the rolling type, a number of twenty antisymmetric modes should be used in the y-direction in order to obtain same accuracy in the natural frequencies. This disadvantage is compensated by the fact that in this analysis the eigenvalue matrix would be of order 14 only and hence the total computation time should not be higher. Finally, it is also suitable to check the unconstrained plate modes for orthonormality at the beginning of the numerical analysis in order to avoid possible errors comming from an incorrect numerical assumption.

APPENDIX V

EFFECT OF THE ELASTIC SUPPORTS ON THE NATURAL FREQUENCIES OF THE EXPERIMENTAL MODEL CONSIDERED IN CHAPTER III

1. Introduction

As discussed in Chapter III, the effect of the supporting springs on the resonant frequencies of the rolling type can be completely eliminated by a perfect allignment of these supports along beam (1). In the present study this is supposed to be the case and only the corrections to the frequencies of the pitching type are considered.

The springs are supposed to be massless and perfectly elastic.

The analysis is developed by a Component Modes Method using Lagrange Multipliers. The notations of Chapter III are used in the present analysis; some new notations are introduced below:

k_1, k_2 : elastic constants of the two springs (the experiment was performed with $k_1=k_2$ but generally this might not be the case).

$Z_1(t)$, $Z_2(t)$: longitudinal rigid body translations due to the elongations of the springs.

2. Theoretical development

For the total system in which the supports are included, the kinetic and potential energies are:

$$T = \frac{1}{2}\left(\sum_{n=1}^{\infty} M Q_n^{\cdot 2}(t) + \sum_{n=1,3}^{\infty}\sum_{i=1}^{2} M_i q_n^{\cdot (i)2}(t) + \sum_{n=1}^{\infty}\sum_{i=1}^{2} I_i\, l_i\, P_n^{\cdot (i)2}(t)\right) \tag{296}$$

$$U = \frac{1}{2}\left(\sum_{n=1}^{\infty} \frac{EI}{L^3} k_n^4 Q_n(t)^2 + \sum_{n=1,3}^{\infty} \sum_{i=1}^{2} \frac{(EI)_i}{l_i^3} k_n^4 q_n^{(i)2}(t) + \right.$$

$$\left. \sum_{n=1}^{\infty} \sum_{i=1}^{2} \frac{(GJ)_i}{l_i} (n-1)^2 \frac{\pi^2}{4} P_n^{(i)}(t)^2 + \sum_{i=1}^{2} k_i Z_i^2(t) \right) \qquad (297)$$

The new continuity conditions are:

$$\sum_{n=1}^{\infty} Q_n(t)\phi_n(\xi_i) - \sum_{n=1,3}^{\infty} q_n^{(i)}(t)\phi_n(0) = 0 \qquad i=1,2 \qquad (298)$$

$$\sum_{n=1}^{\infty} \left(\frac{Q_n(t)\phi'_n(\xi_i)}{L} + P_n^{(i)}(t)\,\theta_n(0)\right) = 0 \qquad i=1,2 \qquad (299)$$

$$\left(\sum_{n=1}^{\infty} Q_n(t)\phi_n(-1)\right) - Z_1(t) = 0 \qquad (300)$$

$$\left(\sum_{n=1}^{\infty} Q_n(t)\phi_n(1)\right) - Z_2(t) = 0 \qquad (301)$$

Equations (298) and (299) are found in the analysis developed in Chapter III, equations (300) and (301) express the continuity of the displacements between the beam (1) and the supports placed at the tips.

The Lagrange's equations of the system are:

$$\cdot\ M\ \ddot{Q}_n(t) + \frac{EI\ k_n^4}{L^3} Q_n(t) - \lambda_1\phi_n(\xi_1) - \lambda_2\phi_n(\xi_2) - \frac{\lambda_3}{L}\phi'_n(\xi_1)$$

$$- \frac{\lambda_4}{L}\phi'_n(\xi_2) - \lambda_5\,\phi_n(-1) - \lambda_6\,\phi_n(1) = 0 \qquad (302)$$

$$\cdot\ M_i\ \ddot{q}_n^{(i)}(t) + \frac{(EI)_i\ k_n^4}{l_i^3}\ q_n^{(i)}(t) + \lambda_i\phi_n(0) = 0 \qquad (303)$$

for i = 1,2 and n=1,3,5,...

$$\cdot\ I_i l_i\ \ddot{P}_n^{(i)}(t) + \frac{(GJ)_i}{l_i}\ (n-1)^2\frac{\pi^2}{4}\ P_n^{(i)}(t) - \lambda_{2+i}\theta_n(0) = 0 \qquad (304)$$

for i = 1,2

$$\cdot\ k_i Z_i(t) + \lambda_{4+i} = 0 \qquad (305$$

for i = 1,2

. equations (298) - (301)

The physical interpretations of the Lagrange Multipliers λ_1, λ_2, λ_3, λ_4 has been given in Chapter III; λ_5 and λ_6 are the internal forces developed at the tips of beam (1) when connected to its supports (this physical interpretation is particularly obvious from equations (305)).

The equations (302) - (305) are solved for the generalized coordinates, when harmonic time dependent motion is assumed as in Chapter III. In particular:

$$\overline{Q}_n = -\mu_1 \frac{(\overline{\lambda}_1\phi_n(\xi_1) + \overline{\lambda}_2\phi_n(\xi_2)+\overline{\lambda}_3\gamma_1\phi'_n(\xi_1)+\overline{\lambda}_4\gamma_1\phi'_n(\xi_2) + \overline{\lambda}_5\phi_n(-1)+\overline{\lambda}_6\phi_n(1))}{F_n^{(1)}}$$

$$\overline{q}_n^{(1)} = \frac{\overline{\lambda}_1\phi_n(0)}{F_n^{(2)}} \qquad n=1,3,\ldots$$

$$\overline{P}_n^{(1)} = -\frac{\overline{\lambda}_3\nu_1\theta_n(0)}{F_n^{(3)}}$$

$$\overline{q}_n^{(2)} = \frac{\mu_2\overline{\lambda}_2\,\phi_n(0)}{F_n^{(4)}} \qquad n=1,3,\ldots$$

$$\overline{P}_n^{(2)} = -\frac{\gamma_2\nu_2\,\overline{\lambda}_4\theta_n(0)}{F_n^{(5)}}$$

$$\overline{Z}_1 = +\overline{\lambda}_5\psi_5 \quad \text{with} \quad \psi_5 = \frac{M_1}{k_1\omega^2}$$

$$\overline{Z}_2 = \overline{\lambda}_6\psi_6 \quad \text{with} \quad \psi_6 = \frac{M_1}{k_2\omega^4}$$

The resulting tensonial eigenvalue equation is

$$\overline{\overline{\Delta}}\,(\omega)\ .\ \vec{\lambda} = \vec{0} \tag{305}$$

where

$$\vec{\lambda} \ : \ (\ \overline{\lambda}_1,\ \overline{\lambda}_2, \ldots\ldots\ldots,\ \overline{\lambda}_6\ )$$

and $\Delta(\omega)$ is a sixth order symmetric tensor with the following matrix representation:

$$\Delta_{11} = \sum_{n=1}^{\infty} \mu_1 \frac{\phi_n^{\,2}(\xi_1)}{F_n^{(1)}} + \sum_{n=1,3}^{\infty} \frac{\phi_n^{\,2}(0)}{F_n^{(2)}}$$

$$\Delta_{12} = \sum_{n=1}^{\infty} \mu_1 \frac{\phi_n(\xi_1)\phi_n(\xi_2)}{F_n^{(1)}}$$

$$\Delta_{13} = \sum_{n=1}^{\infty} \mu_1\gamma_1 \frac{\phi_n(\xi_1)\phi'_n(\xi_1)}{F_n^{(1)}}$$

$$\Delta_{14} = \sum_{n=1}^{\infty} \mu_1\gamma_1 \frac{\phi_n(\xi_1)\phi'_n(\xi_2)}{F_n^{(1)}}$$

$$\Delta_{15} = \sum_{n=1}^{\infty} \mu_1 \frac{\phi_n(\xi_1)\phi_n(-1)}{F_n^{(1)}}$$

$$\Delta_{16} = \sum_{n=1}^{\infty} \mu_1 \frac{\phi_n(\xi_1)\phi_n(1)}{F_n^{(1)}}$$

$$\Delta_{22} = \sum_{n=1}^{\infty} \mu_1 \frac{\phi_n^2(\xi_2)}{F_n^{(1)}} + \sum_{n=1}^{\infty} \mu_2 \frac{\phi_n^2(0)}{F_n^{(4)}}$$

$$\Delta_{23} = \sum_{n=1}^{\infty} \mu_1\gamma_1 \frac{\phi'_n(\xi_1)\phi_n(\xi_2)}{F_n^{(1)}}$$

$$\Delta_{24} = \sum_{n=1}^{\infty} \mu_1\gamma_1 \frac{\phi'_n(\xi_2)\phi_n(\xi_2)}{F_n^{(1)}}$$

$$\Delta_{25} = \sum_{n=1}^{\infty} \mu_1 \frac{\phi_n(-1)\phi_n(\xi_2)}{F_n^{(1)}}$$

$$\Delta_{26} = \sum_{n=1}^{\infty} \mu_1 \frac{\phi_n(1)\phi_n(\xi_2)}{F_n^{(1)}}$$

$$\Delta_{33} = \sum_{n=1}^{\infty} \left(\mu_1\gamma_1^2 \frac{\phi'_n(\xi_1)^2}{F_n^{(1)}} + \nu_1 \frac{\theta_n^2(0)}{F_n^{(3)}}\right)$$

$$\Delta_{34} = \sum_{n=1}^{\infty} \mu_1\gamma_1^2 \frac{\phi'_n(\xi_1)\phi'_n(\xi_2)}{F_n^{(1)}}$$

$$\Delta_{35} = \sum_{n=1}^{\infty} \mu_1\gamma_1 \frac{\phi_n(-1)\phi'_n(\xi_1)}{F_n^{(1)}}$$

$$\Delta_{36} = \sum_{n=1}^{\infty} \mu_1\gamma_1 \frac{\phi_n(1)\phi'_n(\xi_1)}{F_n^{(1)}}$$

$$\Delta_{44} = \sum_{n=1}^{\infty} \left(\mu_1 \gamma_1^2 \frac{\phi'^2_n(\xi_2)}{F_n^{(1)}} + \nu_2 \gamma_2 \frac{\theta_n^2(0)}{F_n^{(5)}} \right)$$

$$\Delta_{45} = \sum_{n=1}^{\infty} \mu_1 \gamma_1 \frac{\phi_n(-1)\phi'_n(\xi_2)}{F_n^{(1)}}$$

$$\Delta_{46} = \sum_{n=1}^{\infty} \mu_1 \gamma_1 \frac{\phi_n(1)\,\phi'_n(\xi_2)}{F_n^{(1)}}$$

$$\Delta_{55} = \left(\sum_{n=1}^{\infty} \mu_1 \frac{\phi_n^2(-1)}{F_n^{(1)}} \right) + \psi_5$$

$$\Delta_{56} = \sum_{n=1}^{\infty} \mu_1 \frac{\phi_n(1)\phi_n(-1)}{F_n^{(1)}}$$

$$\Delta_{66} = \left(\sum_{n=1}^{\infty} \mu_1 \frac{\phi_n^2(1)}{F_n^{(1)}} \right) + \psi_6$$

For given values of k_1 and k_2, the natural frequencies of the supported structure are solutions of

$$\det \left(\Delta(\omega) \right) = 0$$

3. Remark

The foregoing analysis can be easily extended to the case in which the structure is resting on two beam-like elastic foundations perpendicular to beam (1).

In such a case, $(k_i, Z_i)_{i=1,2}$ are substituted in the analysis by the free-free frequency parameters and combinations of normal modes and the additional generalized masses terms appear in the kinetic energy.

APPENDIX VI

EFFECT OF THE MASSES AND INERTIAS OF THE ENGINES ON THE NATURAL FREQUENCIES OF THE LOCKHEED L-100 MODEL CONSIDERED IN CHAPTER III.

1. Introduction

In the analysis of the L-100 model considered in Chapter III the effects of the engines were ignored. This omission was intended only for the purpose of computational simplicity and the present analysis indicates the modifications to be made in the previous theoretical study in order to take into account the masses and inertias of the engines.

The Lockheed L-100 Hercules is equipped with four 4,050 eshp Allison T 56-A-7A turboprop engines whose characteristics are given in Ref.(32).

A schematic representation of the structure is illustrated below:

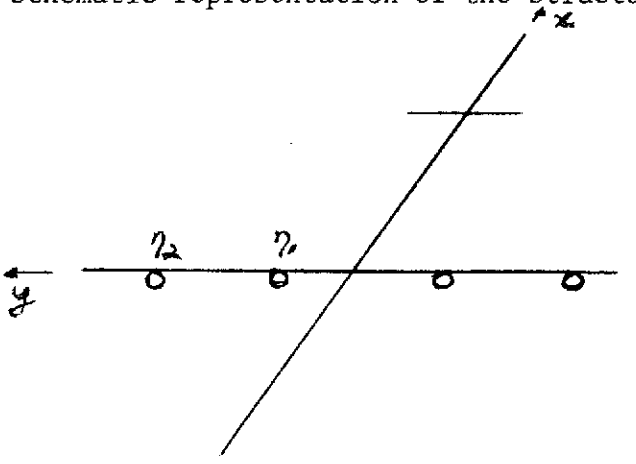

Because the geometrical symmetry of the structure is preserved, motions of the rolling and pitching type can be studied independently.

2. Effect of the engines on the rolling natural frequencies

Additional notations to those of Chapter III are now introduced:

η_1, η_2 : location of the engines along the span of the wing

m_E : mass of each engine

$Z_1(t), Z_2(t)$: plunging displacement of the engines

I_x : moment of inertia of each engine about its axis of symmetry

$\alpha_1(t), \alpha_2(t)$: angular rotation of the engines about the axis previously defined.

The presence of the engines accounts for an additional term in the expression of the kinetic energy given by equation (41);

$$T_{engines} = m_E(\dot{Z}_1^2(t) + \dot{Z}_1^2(t)) + I_x(\dot{\alpha}_1^2(t) + \dot{\alpha}_2^2(t)) \qquad (306)$$

while the expression for potential energy given by equation (43) remains unmodified.

Additional constraint conditions expressing the continuity of displacement and slope at the connection points along the wing span are:

$$\left(\sum_{n=2,4}^{\infty} q_n^{(1)}(t)\phi_n(\eta_1)\right) - Z_1(t) = 0 \qquad (307)$$

$$\left(\sum_{n=2,4}^{\infty} q_n^{(1)}(t)\phi_n(\eta_2)\right) - Z_2(t) = 0 \qquad (308)$$

$$\left(\sum_{n=2,4}^{\infty} \frac{q_n^{(1)}(t)}{l_1}\phi'_n(\eta_1)\right) - \alpha_1(t) = 0 \qquad (309)$$

$$\left(\sum_{n=2,4}^{\infty} \frac{q_n^{(1)}(t)}{l_1}\phi'_n(\eta_2)\right) - \alpha_2(t) = 0 \qquad (310)$$

and $(\Lambda_i)_{i=1,\ldots 4}$ are the corresponding Lagrange Multipliers, or generalized forces developed at the points of constraint. The modified Lagrange's equations are:

$$. \; I \; L \; \ddot{P}_n(t) + \frac{GJ}{L} (n-1)^2 \pi^2 P_n(t) - \lambda_3 \theta_n(\xi_1) - \lambda_4 \theta_n(\xi_2) = 0 \qquad (311)$$

$$. \; M_1 \; \ddot{q}_n^{(1)}(t) + \frac{(EI)_1}{l_1^3} k_n^4 \; q_n^{(1)}(t) + \frac{\lambda_3}{l_1} \phi'_n(0) - \Lambda_1 \phi_n(\eta_1) -$$

$$\Lambda_2 \phi_n(\eta_2) - \frac{\Lambda_3}{l_1} \rho'_n(\eta_1) - \frac{\Lambda_4}{l_1} \phi'_n(\eta_1) = 0 \qquad (312)$$

$$. \; M_2 \; \ddot{q}_n^{(2)}(t) \; \frac{(EI)_2}{l_2^3} \; k_n^4 \; q_n^{(2)}(t) + \frac{\lambda_4}{l_2} \phi'_n(0) = 0 \qquad (313)$$

$$. \; 2 m_E \; \ddot{Z}_1(t) + \Lambda_1 = 0 \qquad (314)$$

$$. \; 2 m_E \; \ddot{Z}_2(t) + \Lambda_2 = 0 \qquad (315)$$

$$. \; 2 \; I_x \; \ddot{\alpha}_1(t) + \Lambda_3 = 0 \qquad (316)$$

$$. \; 2 \; I_x \; \ddot{\alpha}_2(t) + \Lambda_4 = 0 \qquad (317)$$

We assume harmonic motion as defined in Chapter III and introduce the following new non-dimensional parameters:

$$\mu_2^* = \frac{M_1}{2m_E} \quad ; \quad \nu_2^* = \frac{M_1 l_1^2}{2I_x}$$

$\overline{P}_n$ and $\overline{q}_n^{(2)}$ remain as defined in Chapter III, but:

$$\overline{q}_n^{(1)} = \frac{\overline{\lambda}_3\phi'_n(0) - \overline{\Lambda}_1\phi_n(\eta_1) - \overline{\Lambda}_2\phi_n(\eta_2) - \overline{\Lambda}_3\phi'_n(\eta_1) - \overline{\Lambda}_4\phi'_n(\eta_2)}{\omega^2 - k_n^4} \quad (318)$$

and

$$(\overline{Z}_i)_{i=1,2} = \frac{\mu_2^* (\Lambda_i)_{i=1,2}}{\omega^2} \quad (319)$$

$$(\overline{\alpha}_i)_{i=1,2} = \frac{\nu_2^* (\Lambda_j)_{j=3,4}}{\omega^2} \quad (320)$$

Substitution of (318), (319), (320), $\overline{P}_n$ and $\overline{q}_n^{(2)}$ into the constraint equation leads to the eigenvalue matrix and hence to the frequency equation for the new configuration.

The natural frequencies obtained in Chapter III are found as particular solutions of this frequency equation, in the case where $\eta_1 = \eta_2 = 0$, by factorising out the non-identically zero determinant.

3. Effect of the engines on the pitching natural frequencies

The problem is slightly more complex in this case because additional degrees of freedom have to be allowed for the engines, namely rotations about the y-axis.

Let

I_y : mass moment of inertia of each engine about the y-axis

$\beta_1(t), \beta_2(t)$: angular rotations of the engines about the y-axis.

The presence of the engines corresponds to an additional term in the kinetic energy:

$$T = m_E (\dot{Z}_1^2(t) + \dot{Z}_2^2(t)) + I_x(\dot{\alpha}_1(t)^2 + \dot{\alpha}_2^2(t)) +$$

$$I_y(\dot{\beta}_1^2(t) + \dot{\beta}_2^2(t)) \tag{321}$$

but the potential energy of the overall structure remains unchanged. The new additional constraint conditions are:

$$(\sum_{n=1,3}^{\infty} q_n^{(1)}(t)\phi_n(\eta_1)) - Z_1(t) = 0 \tag{322}$$

$$(\sum_{n=1,3}^{\infty} q_n^{(1)}(t)\phi_n(\eta_2)) - Z_2(t) = 0 \tag{323}$$

$$(\sum_{n=1}^{\infty} P_n^{(1)}(t)\theta_n(\eta_1)) - \beta_1(t) = 0 \tag{324}$$

$$(\sum_{n=1}^{\infty} P_n^{(1)}(t)\theta_n(\eta_2)) - \beta_2(t) = 0 \tag{325}$$

$$(\sum_{n=1}^{\infty} \frac{q_n^{(1)}(t)}{l_1} \phi'_n(\eta_1)) - \alpha_1(t) = 0 \tag{326}$$

$$(\sum_{n=1}^{\infty} \frac{q_n^{(1)}(t)}{l_1} \phi'_n(\eta_2)) - \alpha_2(t) = 0 \tag{327}$$

From this point on same procedure as previously applies, and therefore the details will be omitted.

4. Conclusion

The expected changes in the natural frequencies due to the presence of the engines can be discussed on a qualitative basis even before performing the numerical computations.

Because mass and inertia has been added to the structure, the new natural frequencies are expected to be lower than those computed in Chapter III (ef. Ref. (45), p.83)

In particular, the first natural mode of the structure was shown to be essentially a wing mode; consequently, its corresponding natural frequency is expected to change by a larger amount than the natural frequencies corresponding to modes in which the elastic behavior of the fuselage or tail is predominant.

APPENDIX VII

EVALUATION OF INTERNAL FORCES (SHEAR AND BENDING MOMENTS) ILLUSTRATED FOR A CANTILIVERED BEAM.

1. Introduction

The Rayleigh-Ritz Component Modes Method using Lagrange Multipliers is characterised by two main factors.

(1) The use, for each component, of its unconstrained modes for determining the deformation in each overall structural mode.

(2) The identification of the Lagrange Multipliers as the shear forces and bending moments at the points of constraint.

The computational advantages introduced by (1) are particularly clear at the stage in which the constraint conditions have to be written. In the one-dimensional case of beam structures for instance, the boundary conditions satisfied by the free-free modes are such that the continuity of the second and third derivatives of the bending displacement is automatically satisfied. This results from the fact that $\overline{W}''(x)$ and $\overline{W}'''(x)$ (with the notations used in Chapter II), have zero value at the points of constraint, as given by the Rayleigh-Ritz expansion. Obviously, the bending moments and shear forces which are proportional to $\overline{W}''$ and $\overline{W}'''$ should not be zero on physical grounds, and consequently the problem which arises is that of the convergence of $\overline{W}''(x)$ and $\overline{W}'''(x)$ as given by the method. This problem is also connected to (2) above.

For the sake of clarity, the author has chosen to illustrate the convergence analysis on a conceptually simple case, which is that

of a cantiliver beam. In other words, the problem is studied for one constraint point.

2. Convergence of $\overline{W}''$ and $\overline{W}'''$ illustrated for a cantiliver beam.

Consider a beam of span L, $0 \leq x \leq L$, clamped at the end $x = 0$, as shown in the figure below.

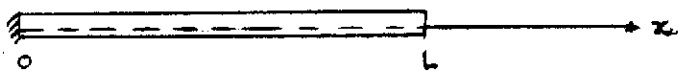

The treatment of this problem is based upon seeking mode shapes as given by the expansion:

$$\overline{W}(x) = \sum_{n=1}^{\infty} \overline{q}_n \, \phi_n(x) \qquad (328)$$

subject to the constraints:

$$\sum_{n=1}^{\infty} \overline{q}_n \, \phi_n(0) = 0 \qquad (329)$$

$$\frac{1}{L} \sum_{n=1}^{\infty} \overline{q}_n \, \phi'_n(0) = 0 \qquad (330)$$

By proceeding as stated in Chapters II - IV, the Lagrange multipliers and generalized coordinates are determined, and consequently the functions

$$\overline{W}''(x) = \sum_{n=1}^{\infty} \overline{q}_n \, \phi''_n(x)$$

and

$$\overline{W}'''(x) = \sum_{n=1}^{\infty} \overline{q}_n \, \phi_n'''(x)$$

are also determined.

The variations of $\overline{W}''(x)$ along the beam span in the fundamental mode is represented in Figure 51; the different curves correspond to the number of modes considered in the analysis which is indicated along the curve. The exact variation of $\overline{W}''(x)$ can also be seen, as given by Reference (21).

Two fundamental remarks can be made:

(a) As the number of modes considered in the analysis increases, $\overline{W}''(x)$ to the known exact result except in the neighborhood of x = 0.

(b) However, the exact value of $\overline{W}''(0)$ given by Reference (21) $\overline{W}''(0) = 0.8$), is only 8.75% higher than the value of the corresponding Lagrange Multiplier, obtained in a 40-modes analysis.

This fact is not surprising, as the value of $\overline{\lambda}_2/\overline{\lambda}_1$ (the Lagrange multipliers associated with equations (329) and (330) is precisely that of the bending moment at x=0 (up to multiplication), i.e. $\overline{\lambda}_2/\overline{\lambda}_1 = \overline{W}''(0)$.

Hence, as shown in Figure 51, the method offers a good representation of $\overline{W}''(x)$ as the number of modes increases; moreover, because the ratio $\overline{\lambda}_2/\overline{\lambda}_1$ is computed in the process, it is possible to have an insight on the convergence of $\overline{W}''$ without even having to actually evaluate $\overline{W}''(x)$ along the span. For fairly complex structures, this fact represents a significant saving in computation time and effort.

Figure 52 shows however, poor results for the convergence of $\overline{W}'''$ (as expected, the rate of convergence becomes slower as the order of the derivative of $\overline{W}$ increases), but the value of the Lagrange multiplier predicts much better the value of $\overline{W}'''(0)$ than the direct result as it can be seen in the figure. This emphasizes again the convenience of using the Lagrange multipliers in the method.

3. Generalization and conclusions

The convergence results obtained in the one-constraint point-analysis can be readily generalized for the cases in which the isoperimetric (constraint) conditions have to be applied at more than one point. A behavior of the type observed in Figure 51 is expected to occur in the neighborhood of each of the constraint points, with the values of $\overline{W}''$ and $\overline{W}'''$ at the constraint points given by the values of the Lagrange multipliers associated with the particular constraint equation.

The following picture may help illustrate this statement. This picture is drawn for the model of the rotor blade considered in Chapter II, in the fundamental mode.

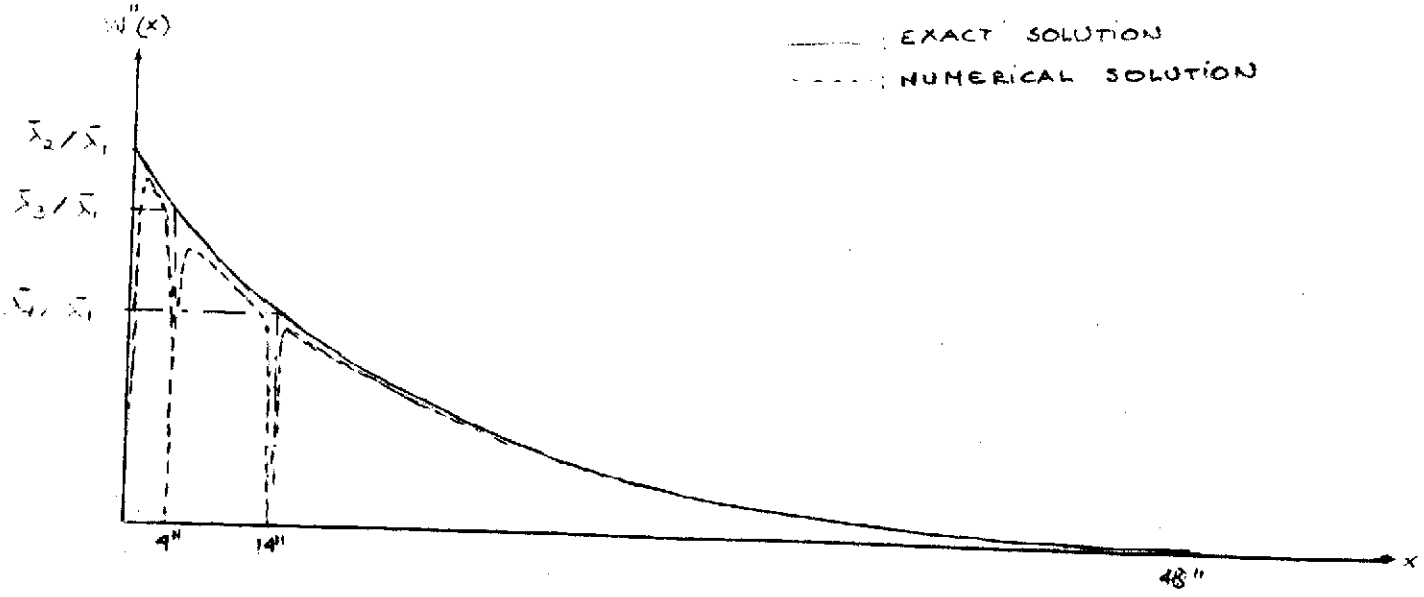

The type of behavior shown above can be explained from a mathematical point of view by the uniform convergence of the serie giving $\overline{W}(x)$ almost everywhere, i.e. except at the discrete number of constraint points. As a consequence, for example,

$$\sum_{n=1}^{N} \overline{q}_n \, \phi''_n(x) \begin{cases} \xrightarrow[N \to \infty]{} \overline{W}''(x) & \text{if } x \text{ is not a constraint point} \\ \xrightarrow[N \to \infty]{} \text{Lagrange multiplier} & \text{otherwise} \end{cases}$$

APPENDIX VIII

EFFECTS OF FINITE CROSS-SECTIONAL DIMENSIONS ON BEAM INERTIAS AND CONSTRAINT CONDITIONS

For structures of the type shown below:

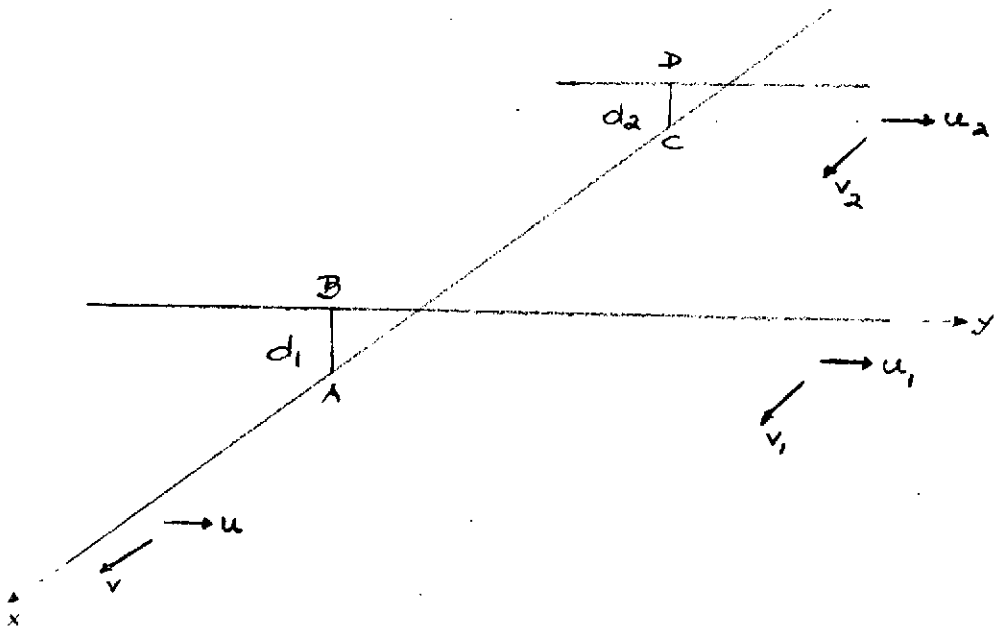

where, in contrast to the assumptions of Chapters III and IV, the points A and B, C and D do not coincide, it may be necessary to include additional (rigid) body degrees of freedom in the analysis as shown in the Figure. The corresponding additional term in the kinetic energy is:

$$T_{add} = \frac{1}{2}\left[\int_{-L}^{L}(\dot{u}^2 + \dot{v}^2)\,dm + \int_{-\ell_1}^{\ell_1}(\dot{u}_1^2 + \dot{v}_1^2)\,dm_1 + \int_{-\ell_2}^{\ell_2}(\dot{u}_2^2 + \dot{v}_2^2)\,dm_2\right]$$

and the following constraint conditions must also be included:

$$u_1(B) = u(A) - d_1\,\Theta(A)$$

$$u_2(D) = u(C) - d_2\,\Theta(C)$$

$$v_1(A) = v_1(B) + d_1\,\Theta_1(B)$$

$$v_1(C) = v_1(D) + d_2\,\Theta_2(D)$$

It could be argued that a similar treatment would be necessary also for the experimental model considered in Chapter III or for the L-100 model of the same Chapter. Although this is strictly true for the kinetic energy, such an analysis would be inconsistent with point constraint conditions.

Indeed, if we consider the experimental model recalled by the sketch which follows:

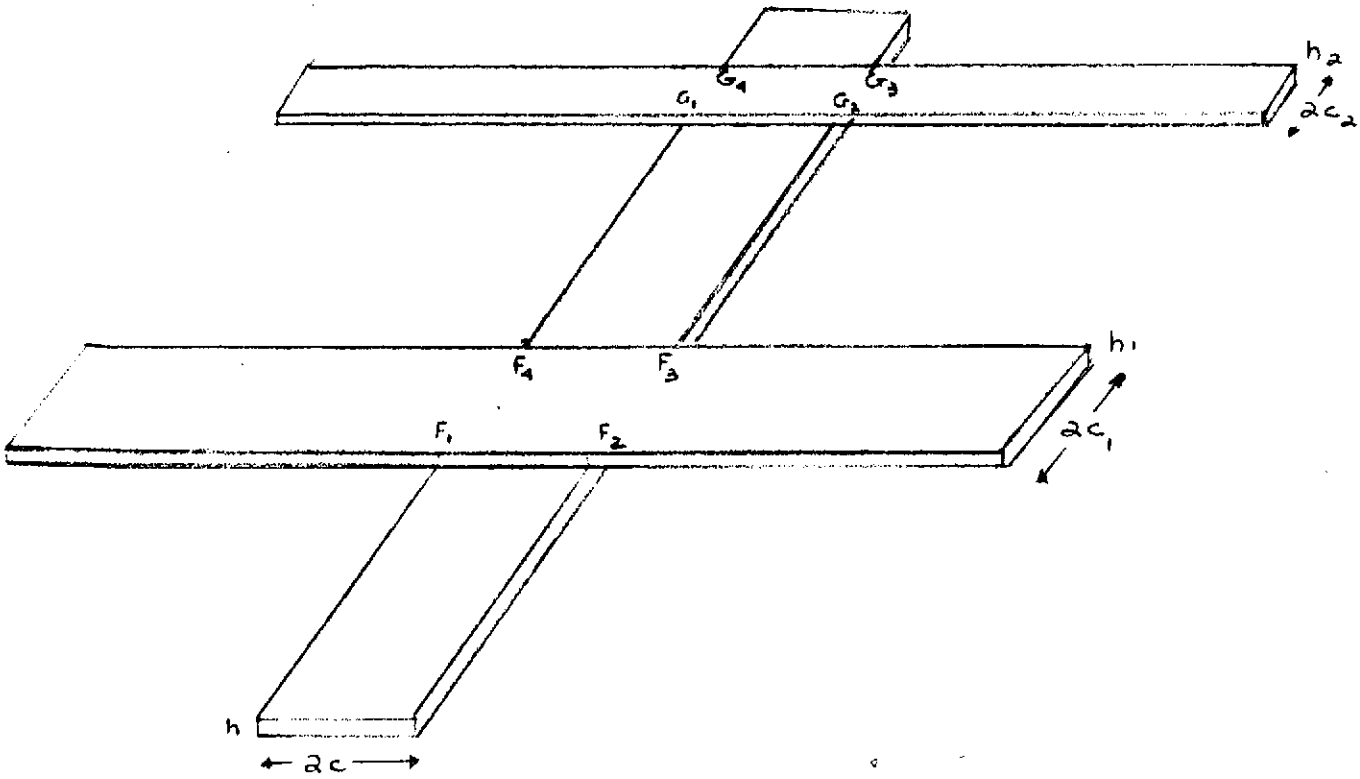

we see that $h << 2c_1$ $h_1 << 2c_1$, $h_2 << 2c_2$.

For this structure, if it is desired to include the thickness effect, then care has to be taken to express the contraint conditions consistently. Namely, the constraint conditions between beams (1) and (2) should hold on the entire area $F_1 F_2 F_3 F_4$ and similarly the constraints between beams (1) and (3) should hold at all points of the rectangle $G_1 G_2 G_3 G_4$. Of course, this induces a severe penalty on the numerical computations; the latter problem can be avoided by reducing the analysis to point contraint conditions as indicated in Chapter III.

Similarly, for the L-100 model recalled below:

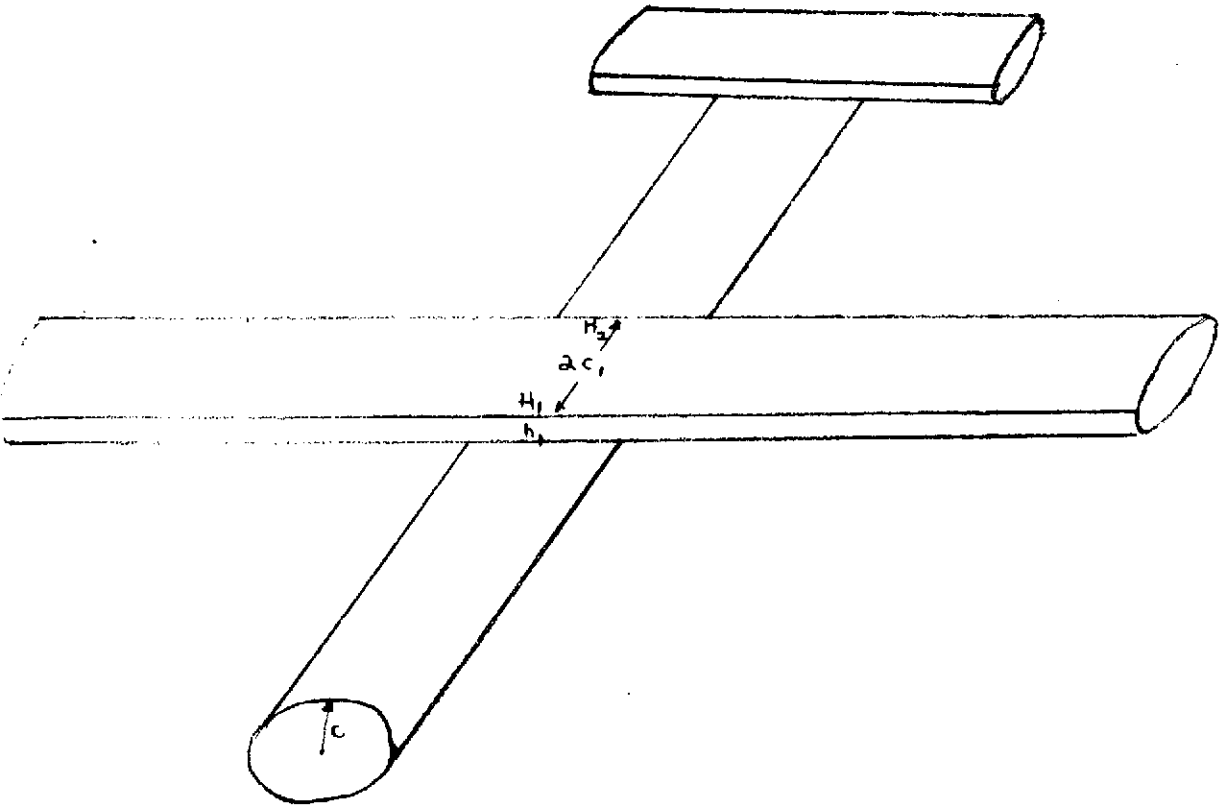

where $c + h_1$ and c_1 are of the same order of magnitude, the analysis including the cross-sectional dimensions should be applied consistent with constraint conditions formulated along the entire line $H_1 H_2$.

Among the other numerous ways in which the aforementioned structures can be modeled, very interesting alternative possibilities are:

- plate representation for all components of the experimental model
- shell representation for the fuselage of the L-100 and plate representation for the lifting surfaces.

REFERENCES

1. Holzer, H., "Die Berechnung der Drehschwingungen", J. Springer, Berlin 1921

2. Myklestad, N.O., "Vibration Analysis", McGraw-Hill, New York, 1944

3. Fettis, H.E., "The Calculation of Coupled Modes of Vibration by the Stodola Method", Journal of Aeronautical Sciences, Vol.16, No.5, p. 259, May 1949

4. White, W.T., "An Integral Equation Approach to the Problem of Vibrating Beams", Journal of the Franklin Institute, Vol.245, p. 25, Jan. 1948 and p. 117, February 1948

5. Crout, P.D., "An Application of Polynomial Approximation to the Solution of Integral Equations Arising in Physical Problems", Journal of Mathematics and Physics, Vol.19, p. 34, 1940

6. Grammel, R., "Ein Neues Verfahren zur Loesung Technischer Eigenwertprobleme", Ingenieur Archiv, Vol.10, p. 35, 1939

7. Westergaard, H.M., "On the Method of Complementary Energy", Proceedings of the American Society of Civil Engineers, Vol. 67, No.2, p.199, Feb.1941

8. Reissner, E., "Note on the Method of Complementary Energy", Journal of Mathematics and Physics, Vol. 27, p. 159, 1948

9. Duncan, W.J., "The Principles of the Galerkin Method", ARC, R&M 1848, 1939

10. Duncan, W.J., "Mechanical Admittances and their Applications to Oscillation Problems", ARC R&M 2000, March 1946

11. Duncan, W.J. and Collar, A.R., "A Method for the Solution of Oscillation Problems by Matrices", Phil. Mag., Vol.17, No.115, p.865, May 1934

12. Fox, L., "A Short Account of Relaxation Methods", Quarterly Journal of Mechanics and Applied Mathematics, Vol.I, Part 3, p.253, Sept. 1948

13. Hurty, W.C., "Vibrations of Structural Systems by Component Mode Synthesis", Proceedings of the American Society of Civil Engineers, Journal of the Engineering Mechanics Division, Vol. 86, EM4, p.51, 1960

14. Hurty, W.C., "Dynamic Analysis of Structural Systems Using Component Modes", AIAA Journal, Vol.3, No. 4, p.678, 1965

15. Gladwell, G.M.L., "Branch Mode Analysis of Vibrating Systems", Journal of Sound and Vibration, Vol.1, No.1, p.41, 1964

16. Walton, W.C., Jr., and Steeves, E.C., "A Practical Computational Method for Reducing a Dynamical System with Constraints to an Equivalent System with Independent Coordinates", Proceedings of the Second Conference on Matrix Methods in Structural Mechanics, United States Air Force, AFFDL-TR-68-150, 1969

17. Budiansky, B., Hu, P.C., and Connor, R.W., "Notes on the Lagrangian Multiplier Method in Elastic-Stability Analysis", NACA TN-1558, 1948

18. Reissner, E., "Buckling of Plates with Intermediate Rigid Supports", Journal of the Aeronautical Sciences, Vol.12, No.3, p.375, July 1945

19. Dowell, E.H., "Free Vibrations of a Linear Structure with Arbitrary Support Conditions", Journal of Applied Mechanics, Vol.38, Trans. ASME, Vol. 93, Series E, p. 595, 1971

20. Dowell, E. H., "Free Vibrations of an Arbitrary Structure in Terms of Component Modes", Journal of Applied Mechanics, Vol.29, Trans. ASME, Vol.29, Series E, p.727, Sept. 1972

21. Young, D. and Felgar, R.P., Jr., "Characteristic Functions Representing Modes of Vibration of a Beam", Report No.4913, University of Texas Publication, 1949.

22. Mabie, H. H., and Rogers, C.B., "Transverse Vibrations of Tapered Cantilever Beams with End Loads", Journal of Acoustic Society of America, Vol.36, p.463, March 1964.

23. Cranch, E.T., and Adler, A.A., "Bending Vibrations of Variable Section Beams", Journal of Applied Mechanics, Vol.23, No.1, March 1956

24. Conway, H.D. and Dubil, D.F., "Vibration Frequencies of Truncated Cone and Wedge Beams", Journal of Applied Mechanics, Trans.ASME, p.932, Dec.1965

25. Traill-Nash, R.W., "The Symmetric Vibrations of Aircraft", Aero.Quart., Vol.III, Part I, p.1, May 1951

26. Traill-Nash, R.W., "The Antisymmetric Vibrations of Aircraft", Aero. Quart., Vol.III, Part II, p.145, Sept. 1951

27. Hunn, B.A., "A Method of Calculating the Normal Modes of an Aircraft", Quarterly Journal of Mechanics and Applied Mathematics, Vol.VIII, Part 1, p.38, 1955

28. Przemieniecki, J.S. and Denke, P.H., "Joining of the Complex Structures by a Matrix Force Method", Journal of the Aircraft, Vol.3, No.3, p.236, May-June 1966

29. Schmitz, P.D., "Normal Mode Solution to the Equations of Motion of a Flexible Airplane", Journal of the Aircraft, Vol.10, No.5, p.318, May 1973

30. Jones, R.T., "Reduction of Wave Drag by Antisymmetric Arrangement of Wings and Bodies", AIAA Journal, Vol.10, No.2, p.171, Feb.1972.

31. Anon., Monthly Report No.11, NASA Contract No.NAS2-7031, July 1973.

32. Taylor, J.W. R., Editor, "Jane's All the World's Aircraft, 1967-1968", McGraw-Hill

33. Taylor, J.W.R., Editor, "Jane's All the World's Aircraft, 1971-1972, McGraw-Hill.

34. Jones, R.T., "New Design Goals and A New Shape for the S.S.T.", Aeronautics and Astronautics, p.66, Dec.1972

35. Leissa, A.W., "Vibration of Plates", NASA Report, NASA SP-160, 1969

36. Stahl, B. and Keer, L.M., "Vibration and Buckling of a Rectangular Plate With An Internal Support", Quarterly Journal of Mechanics and Applied Mathematics, Vol.XXV, Part 4, p.467, 1972

37. Wittrick, W.H. and Williams, F.W., "A General Algorithm for Computing Natural Frequencies of Elastic Structures", Quarterly Journal of Mechanics and Applied Mathematics, Vol.XXIV, Part 3, p. 263, 1971

38. Bisplinghoff, R. and Ashley, H., "Aeroelasticity", Addison Wesley, 1955

39. Anon., "The Torsion of Members Having Sections Common in Aircraft Construction", NACA Report 334

40. Anon., "Mark's Mechanical Engineers' Handbook", 6th Edition, p.5, McGraw-Hill, New York 1958

41. Daněk, O., "Application de la Resolvante De Green dans les Problèmes Dynamiques", Roum. Sci. Techn - Mec. Appl., Tome 16, No.3, p.499, Bucharest, 1971

42. Hallquist, J. and Snyder, V.W., "Linear Damped Vibrating Structures with Arbitrary Support Conditions", Journal of Applied Mechanics, Vol. 40, No.1, Trans. ASME Vol.95, Series E, p.312, March 1973

43. Kana, D.D. and Huzar, S., "Synthesis of Shuttle Vehicle Damping Using Substructural Test Results", AIAA Paper No.73-400, presented at AIAA/ASME/SAE 14th Structures, Structural Dynamics and Materials Conference, Williamsburg, Virginia, March 20-22, 1973

44. Drake, J., Kang, C.K. and Dowell, E.H., "Free Vibrations of a Plate with Varying Number of Supports", A.M.S. Department Report No.1133, Princeton University, Nov. 1973

45. Bisplinghoff, R., Ashley, H. and Halfman, R.L., "Aeroelasticity", Addison-Wesley Publishing Co., Inc. 1957

46. Scanlan, R.H. and Rosembaum,R., "Aircraft Vibration and Flutter", Dover Publications, Inc., 1968.

47. Leissa, A.W., "Vibration of Shells", NASA Report, NASA SP-288, 1973.

48. Ellison, A.M., and Jones, W.E., Jr., "Modal Damping Predictions Using Substructure Testing", Paper No.720810, presented at the National Aerospace Engineering and Manufacturing Meeting, San Diego, California, October 2-5, 1972.

49. Fox. L., "The Numerical Solution of Two-point Boundary Problems in Ordinary Differential Equations", Oxford at the Clarendon Press, 1957.

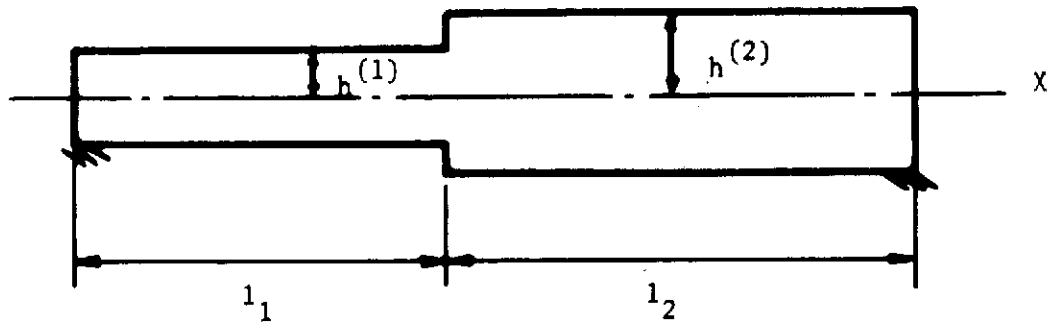

FIGURE 1 - SIMPLY SUPPORTED BEAM OF VARIABLE GEOMETRY

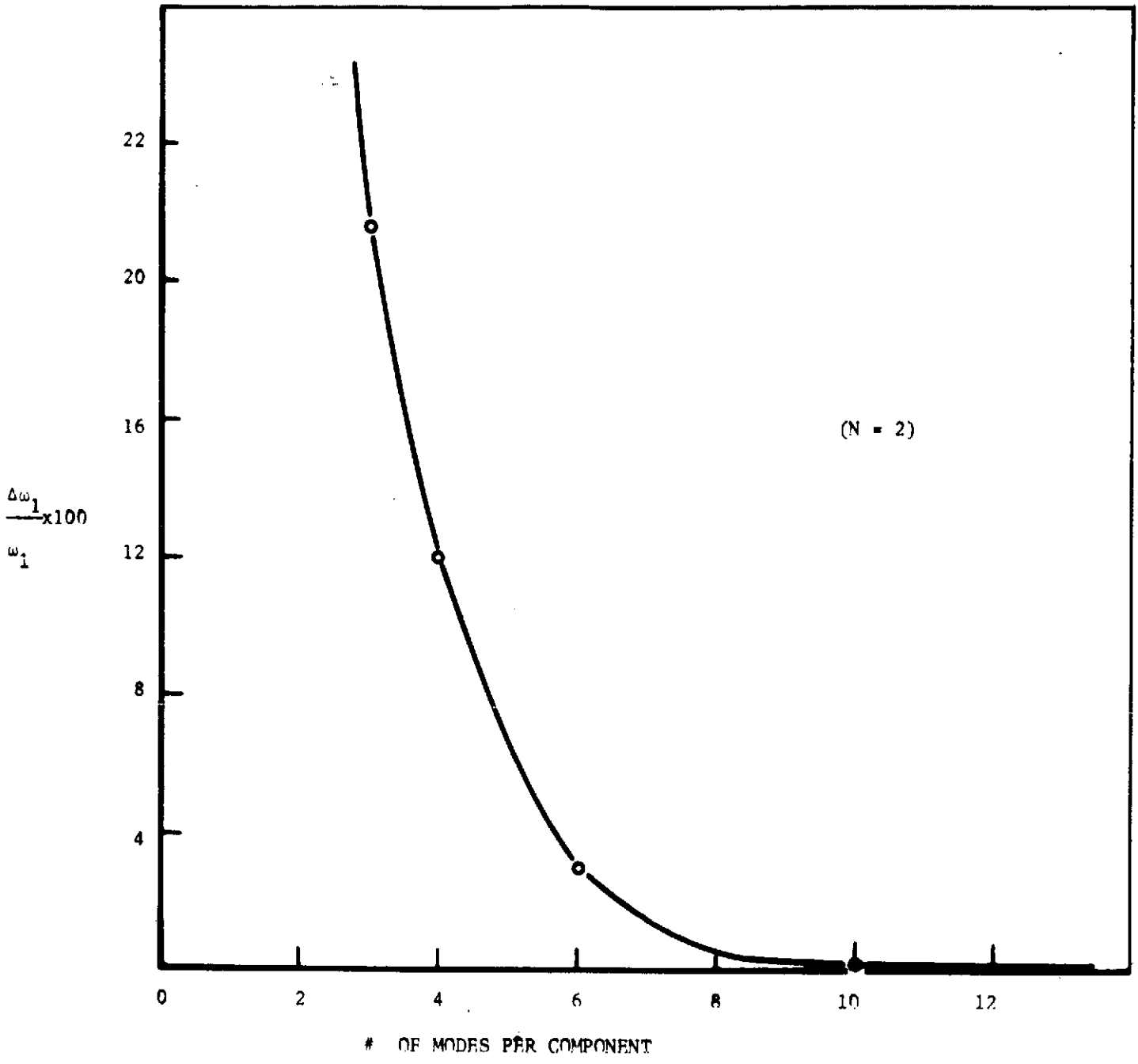

FIGURE 2. - UNIFORM BEAM, FIRST MODE, CONVERGENCE OF THE "RAYLEIGH-RITZ" TYPE

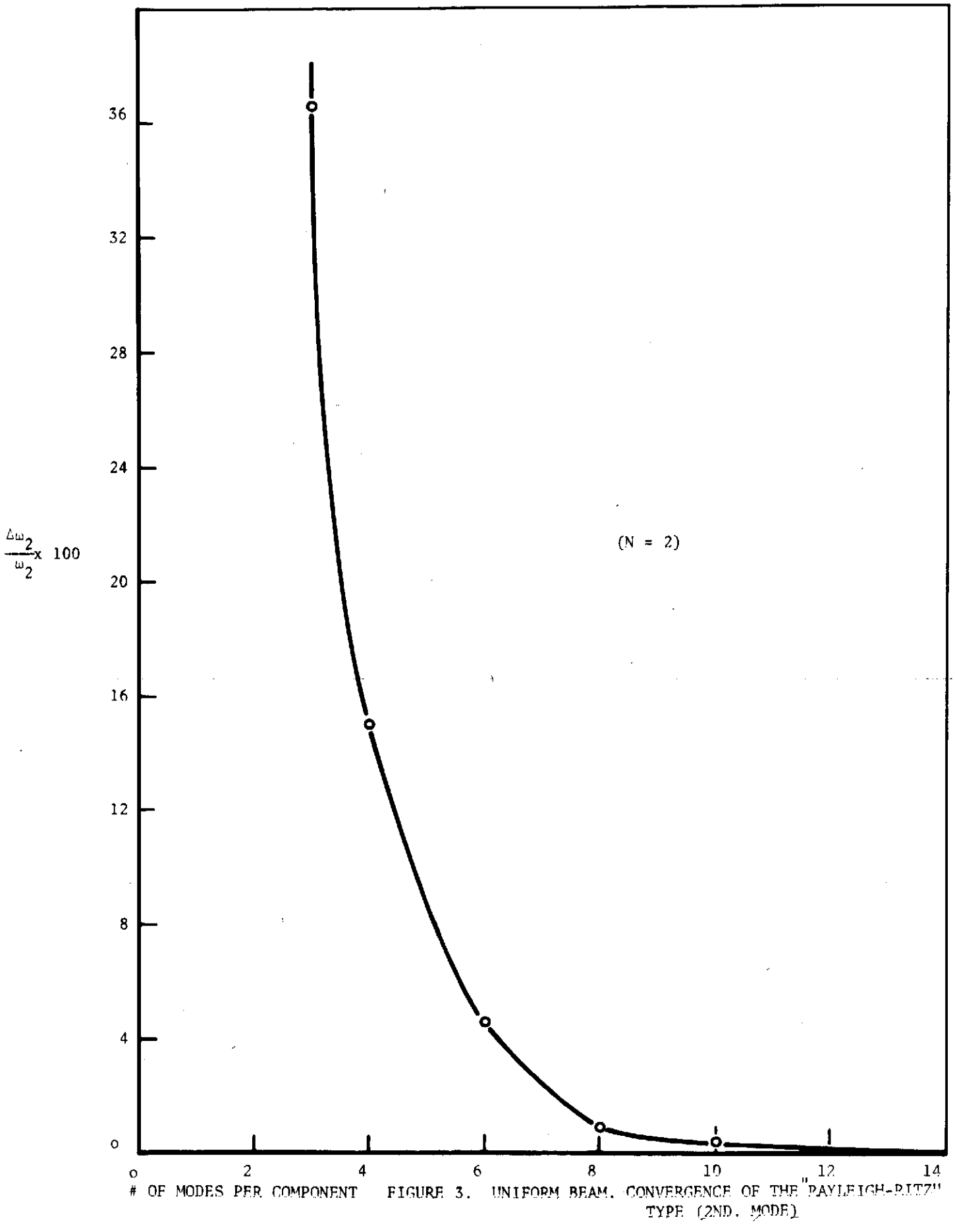

FIGURE 3. UNIFORM BEAM, CONVERGENCE OF THE "RAYLEIGH-RITZ" TYPE (2ND. MODE)

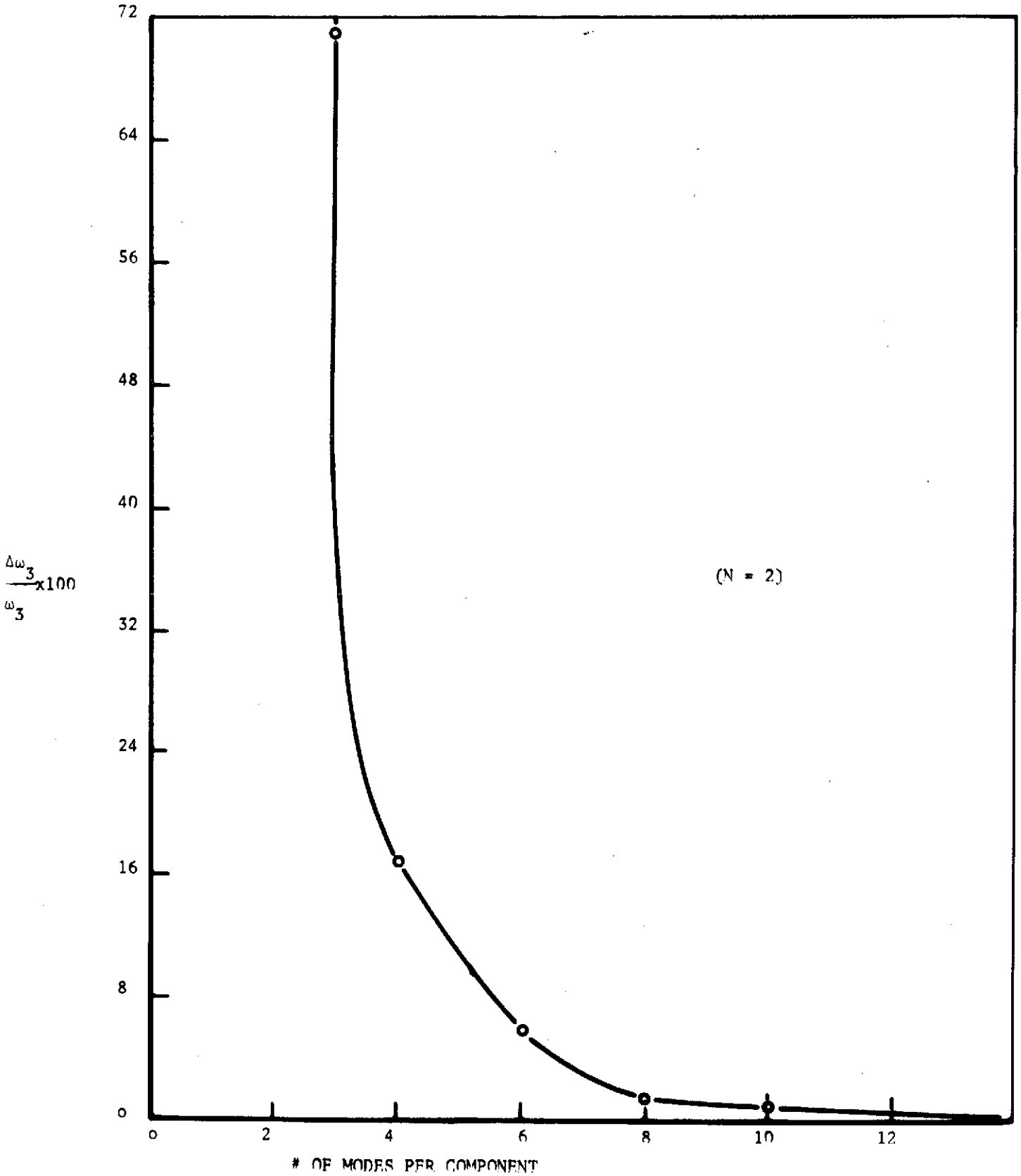

FIGURE 4.- UNIFORM BEAM, THIRD MODE.

CONVERGENCE OF THE "RAYLEIGH-RITZ" TYPE

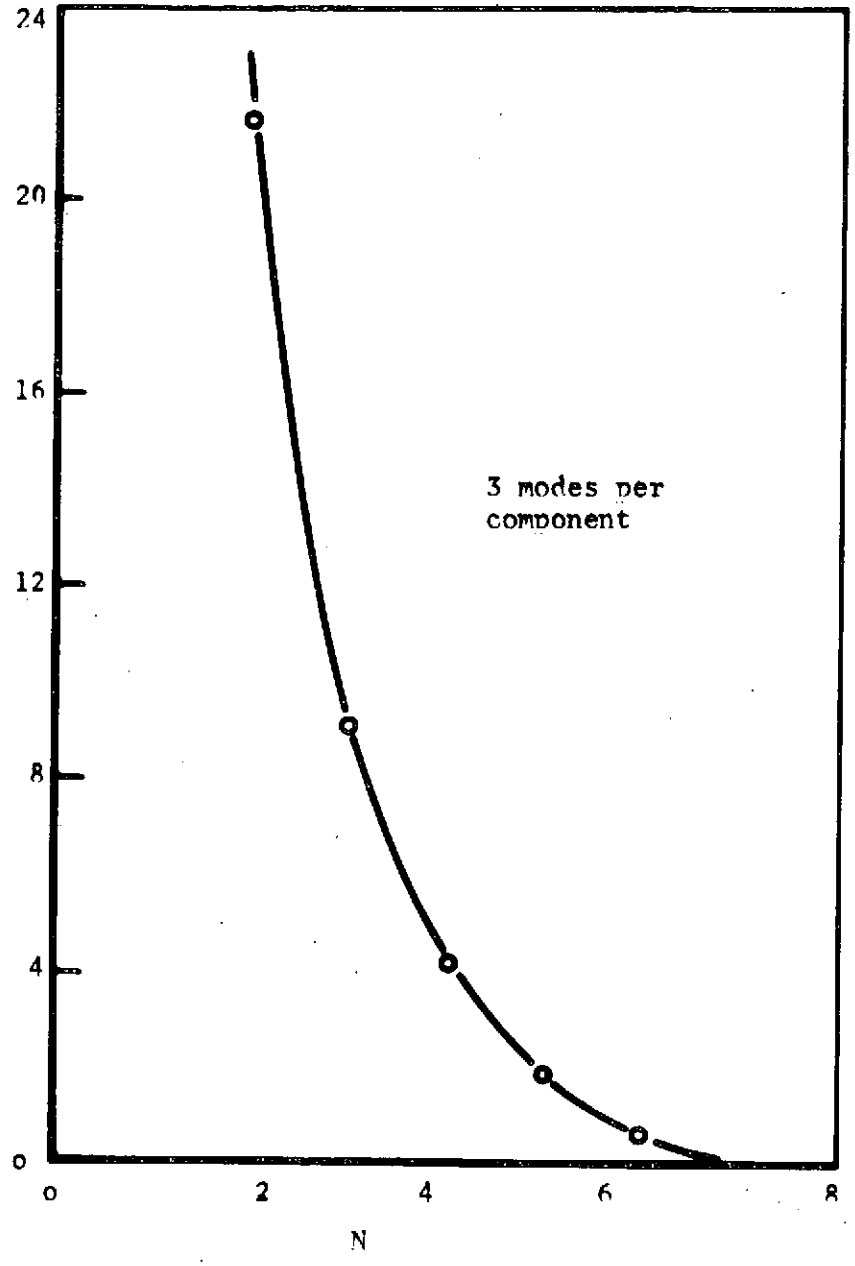

$\frac{\Delta\omega_1}{\omega_1} \times 100$

FIGURE 5. - UNIFORM BEAM
CONVERGENCE OF THE "FINITE ELEMENT" TYPE

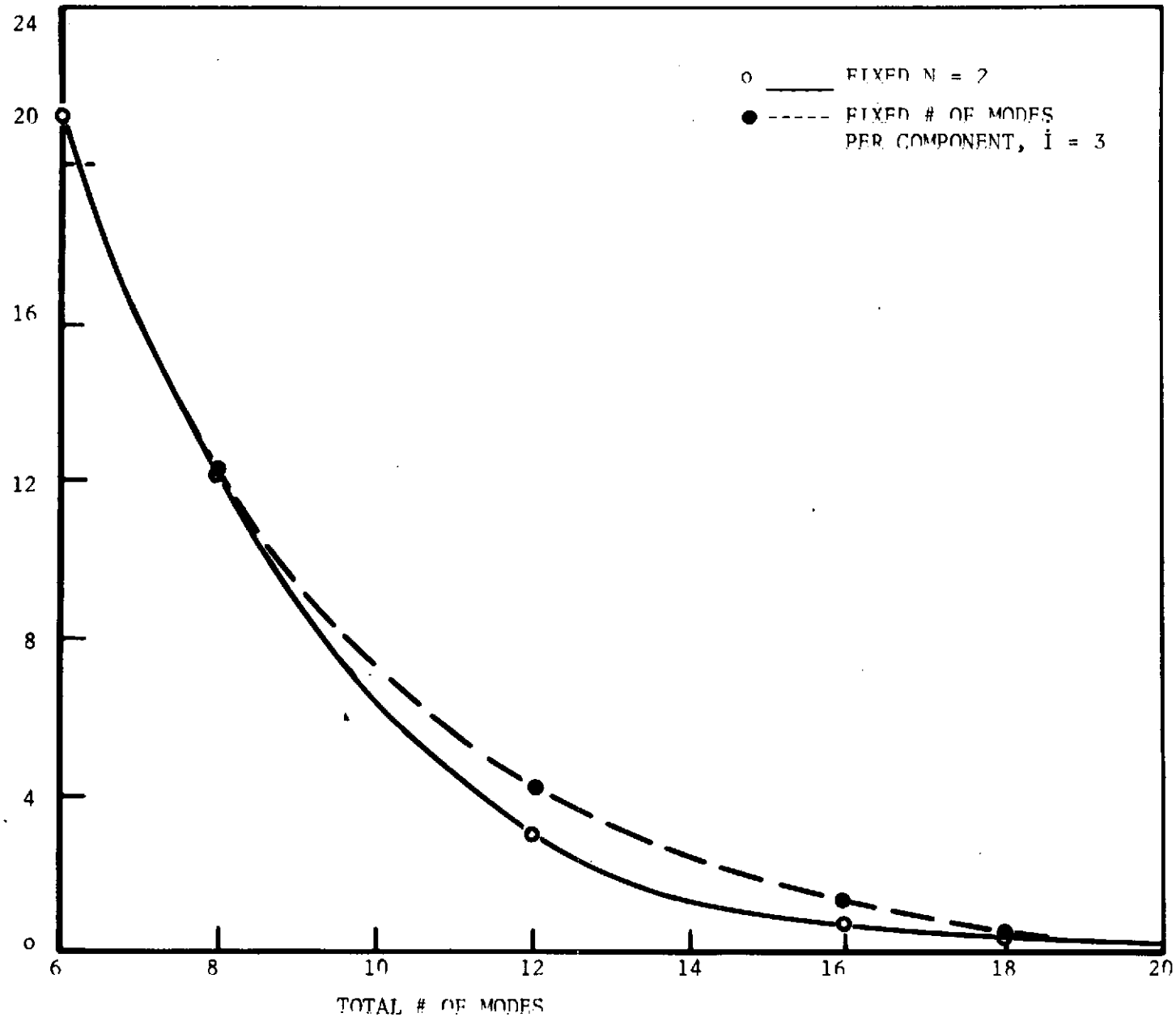

$\frac{\Delta\omega_1}{\omega_1}$ x100

FIGURE 6. - UNIFORM BEAM

COMPARATIVE CONVERGENCE IN THE FUNDAMENTAL MODE

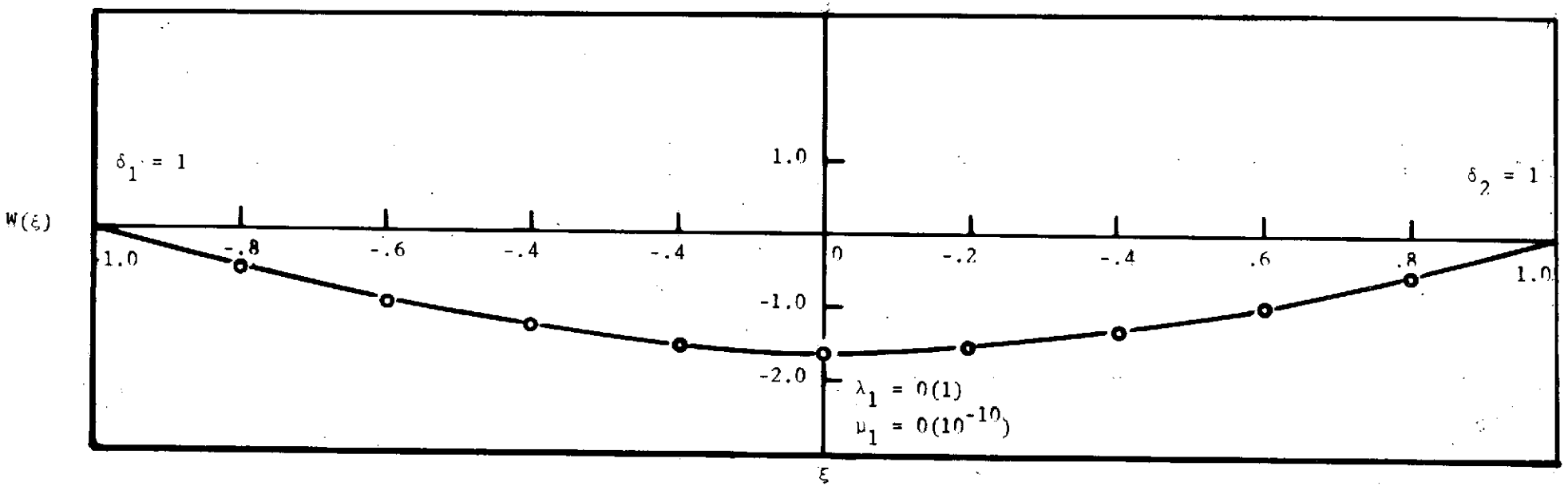

FIGURE 7. - SIMPLY SUPPORTED UNIFORM BEAM

BEAM DEFLECTION IN THE FUNDAMENTAL MODE

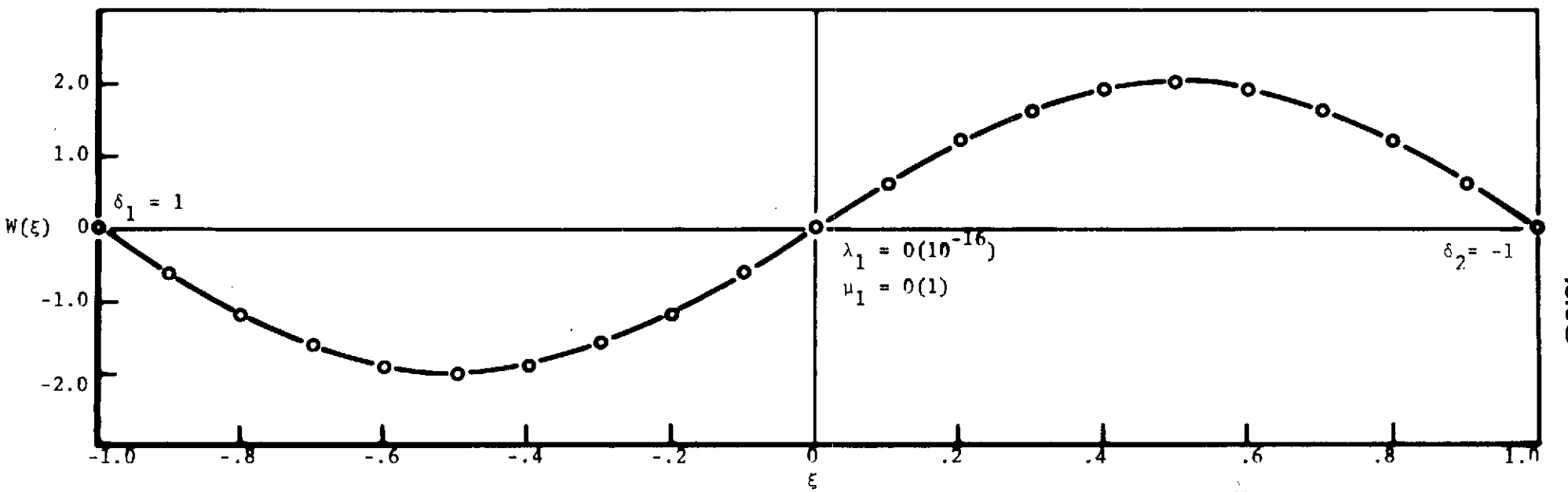

FIGURE 8. - SIMPLY SUPPORTED UNIFORM BEAM

BEAM DEFLECTION IN THE SECOND MODE

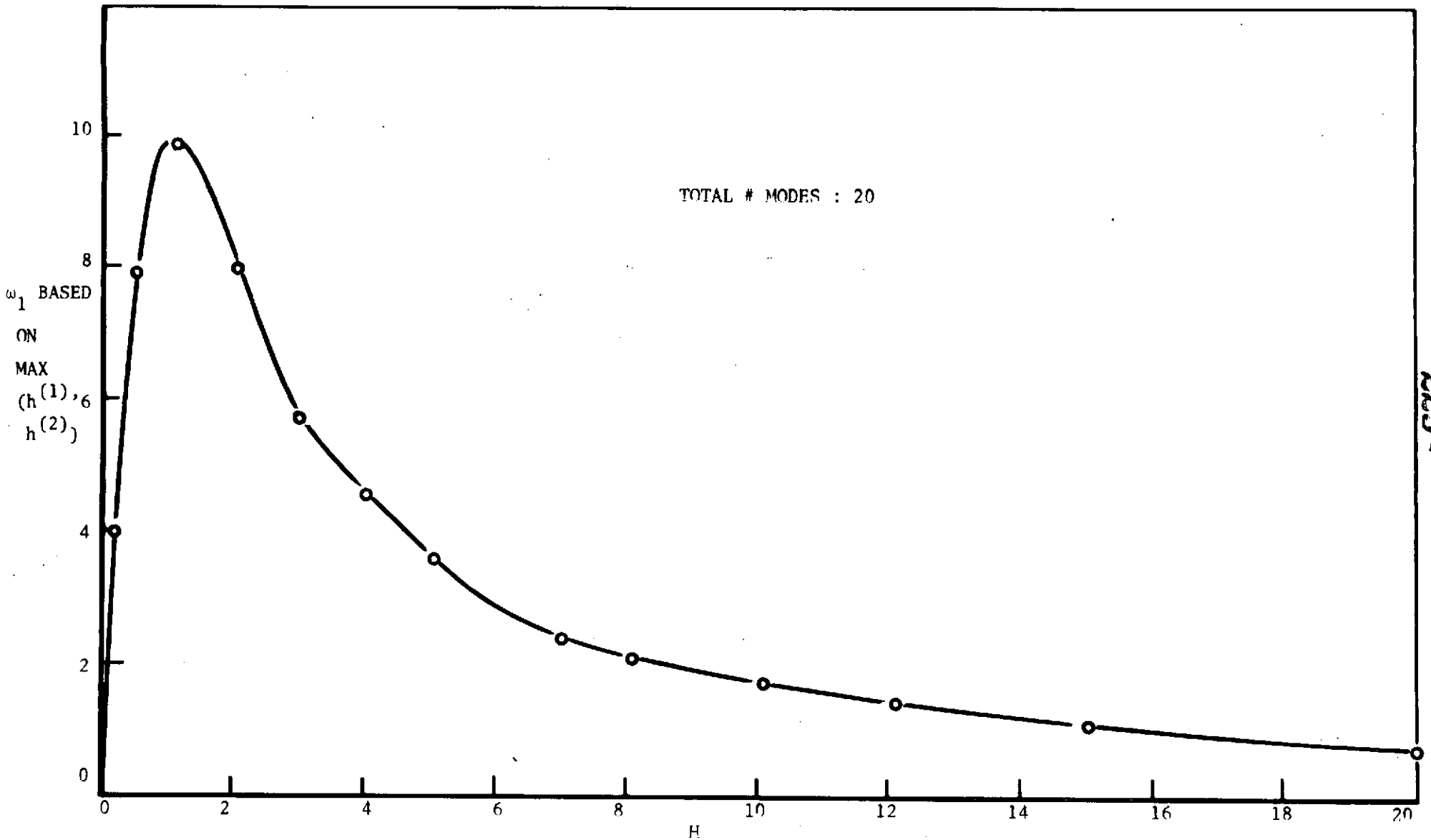

FIGURE 9. - STEPPED BEAM SIMPLY SUPPORTED AT BOTH ENDS

VARIATION IN THE FUNDAMENTAL FREQUENCY WITH THE THICKNESS RATIO

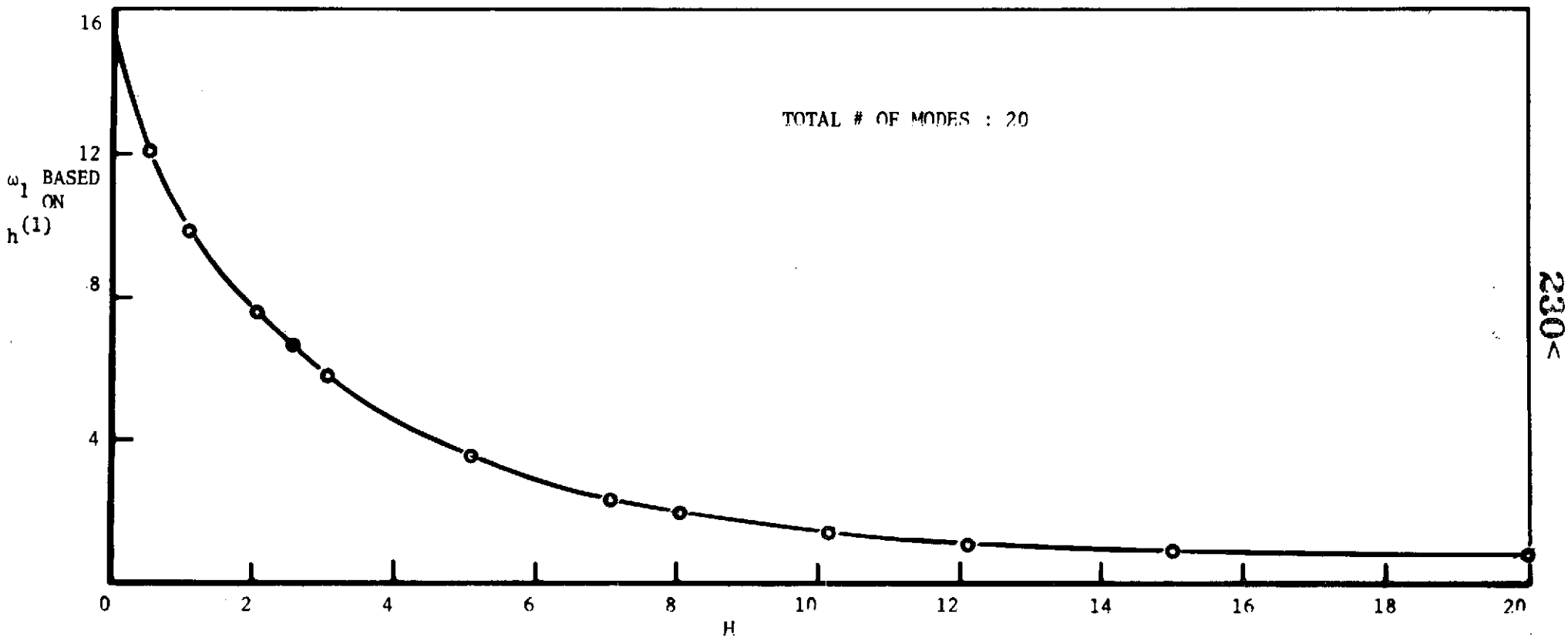

FIGURE 9. bis - STEPPED BEAM SIMPLY SUPPORTED AT BOTH ENDS

VARIATION IN THE FUNDAMENTAL FREQUENCY WITH THE THICKNESS RATIO

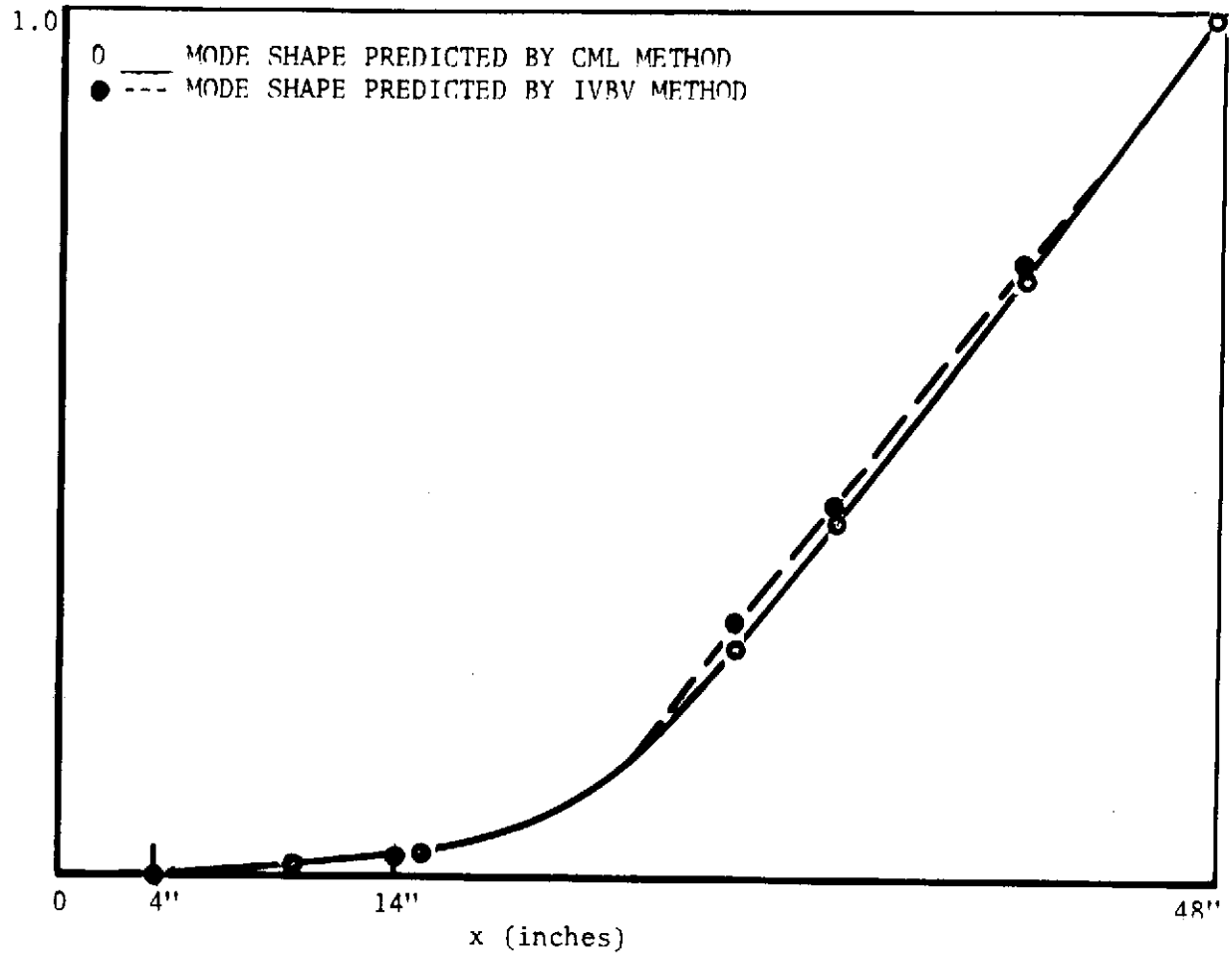

FIGURE 10. - NON-UNIFORM, CANTILIVERED HELICOPTER BLADE

FUNDAMENTAL MODE $\omega_1 = 4.4$ cps

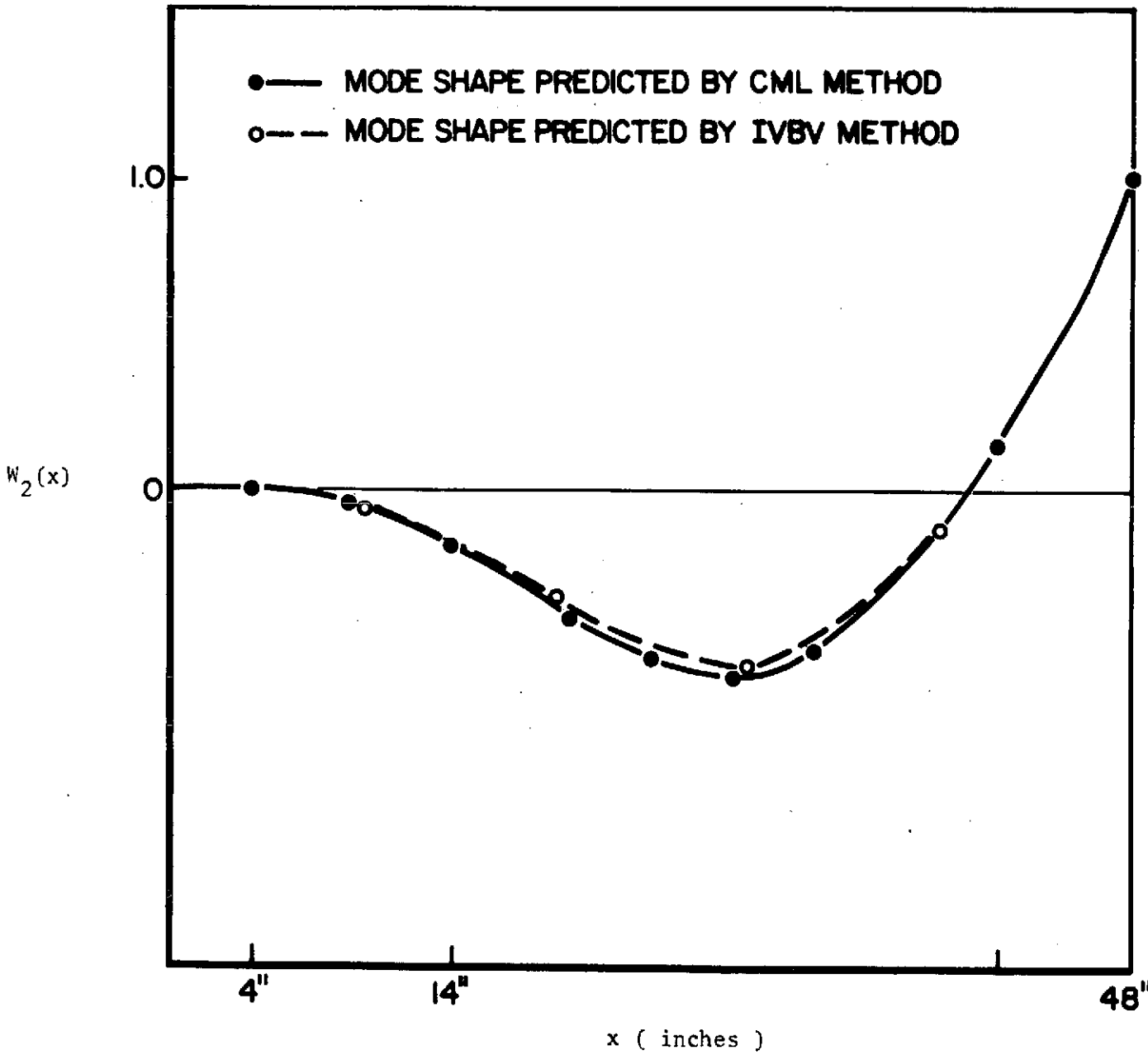

FIGURE 11 · NON UNIFORM, CANTILEVERED HELICOPTER BLADE SECOND MODE ω_2=24.6 cps

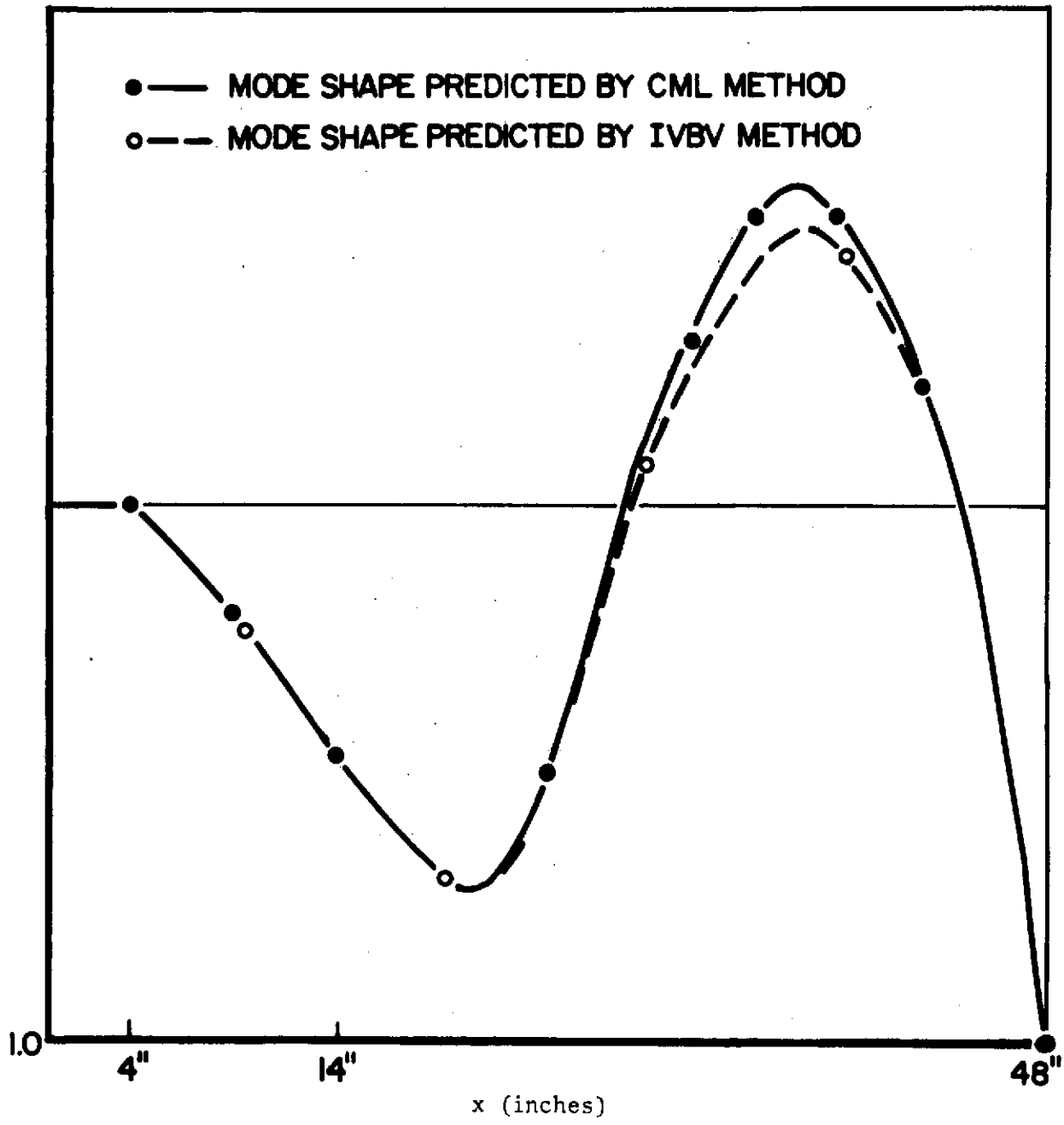

FIGURE 12 · NON UNIFORM, CANTILEVERED HELICOPTER BLADE THIRD MODE $\omega_3 = 61$ cps

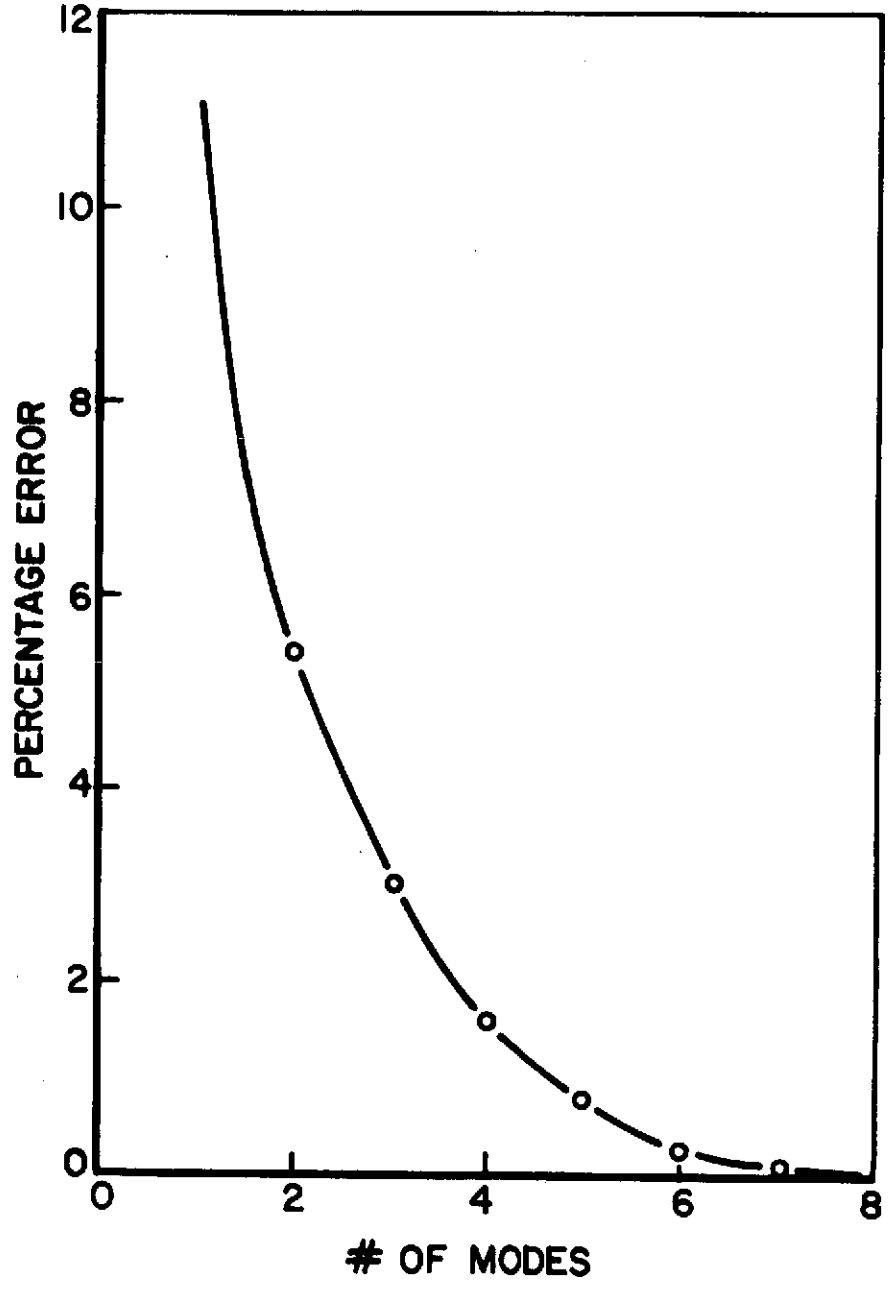

FIGURE 13 · CHECK CASE OF A CANTILEVERED BEAM, ANTISYMMETRIC VIBRATIONS. CONVERGENCE IN THE FUNDAMENTAL FREQUENCY VERSUS NB. OF MODES USED

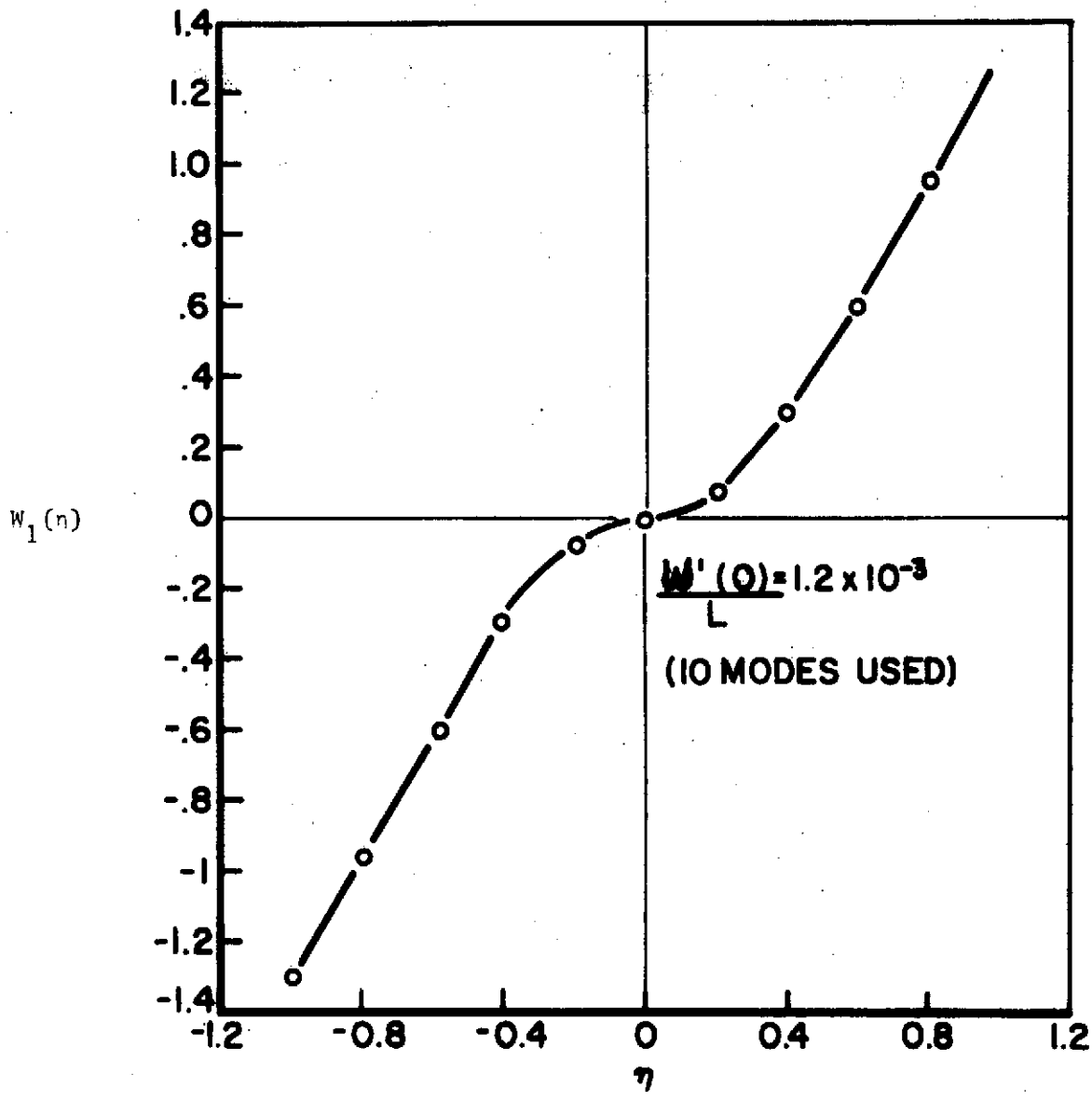

FIGURE 14 · LIMITING CASE $\nu_1 = 0$ $3.49 \leq \omega_1 \leq 3.66$
FIRST BENDING MODE

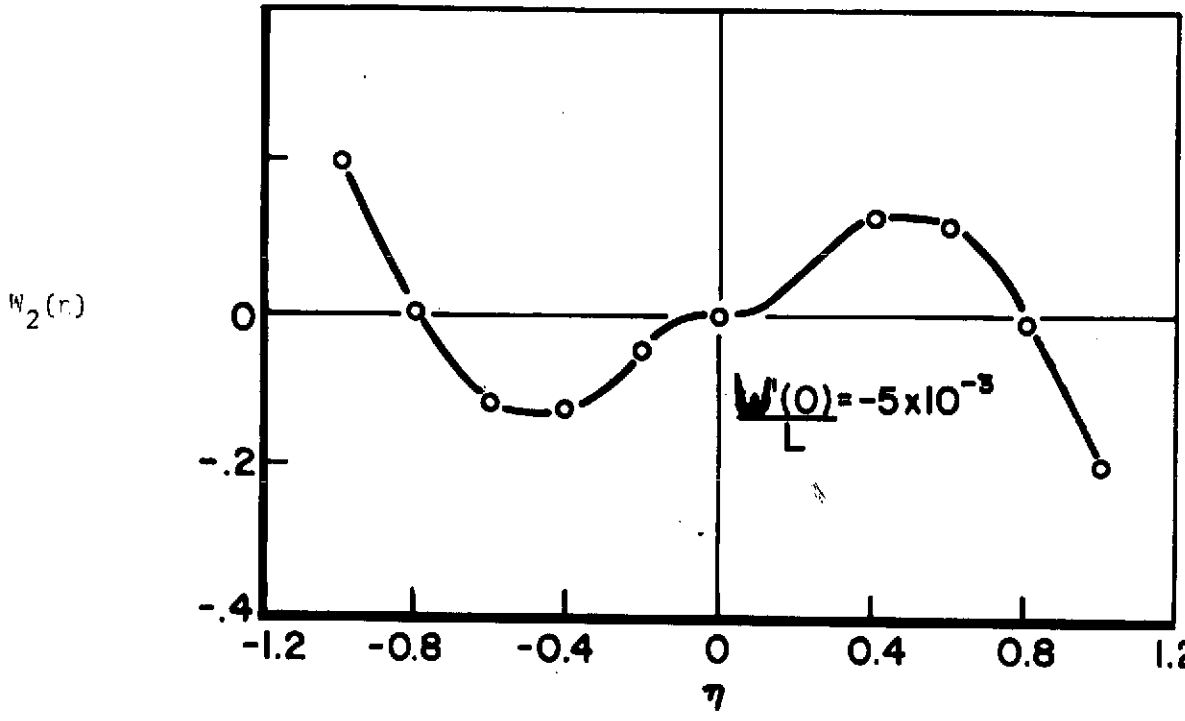

FIGURE 15 · LIMITING CASE $\nu_1 = 0$ $22.11 \leq \omega_2 \leq 22.97$
SECOND BENDING MODE

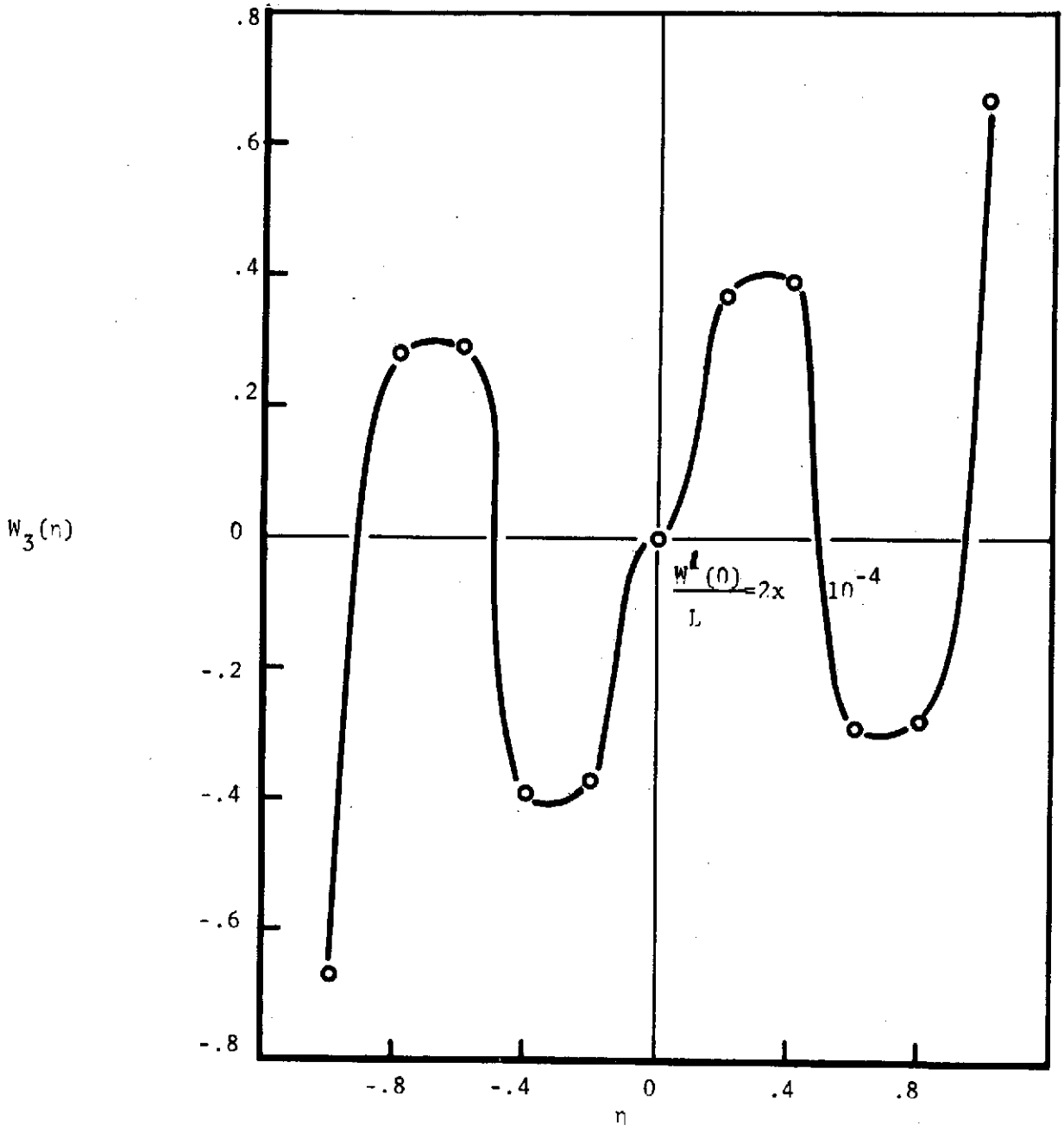

FIGURE 16. - LIMITING CASE $\nu_1 = 0$ $61.63 \leq \omega_3 \leq 64.5$

THIRD BENDING MODE.

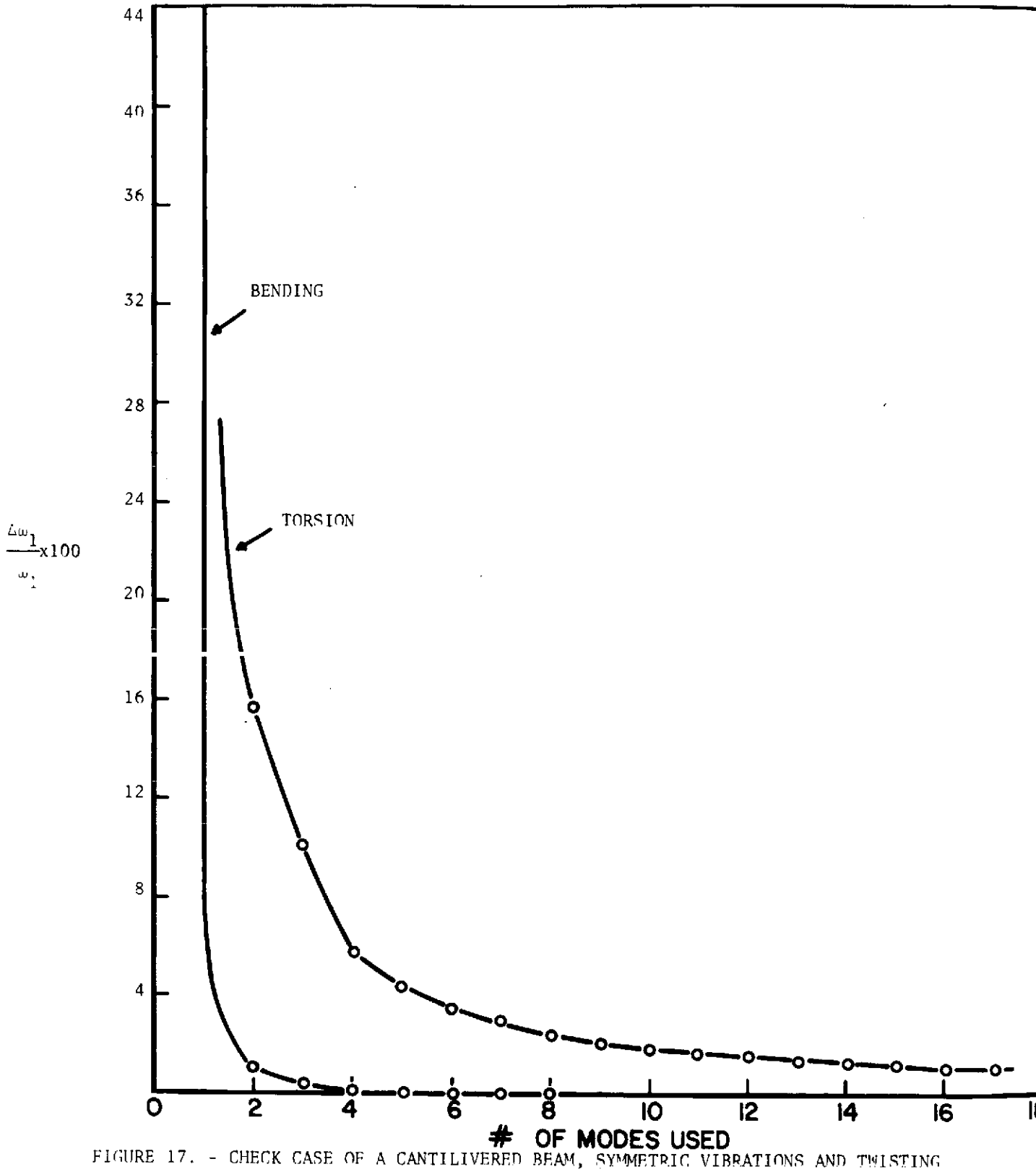

FIGURE 17. - CHECK CASE OF A CANTILIVERED BEAM, SYMMETRIC VIBRATIONS AND TWISTING CONVERGENCE IN THE FUNDAMENTAL MODE

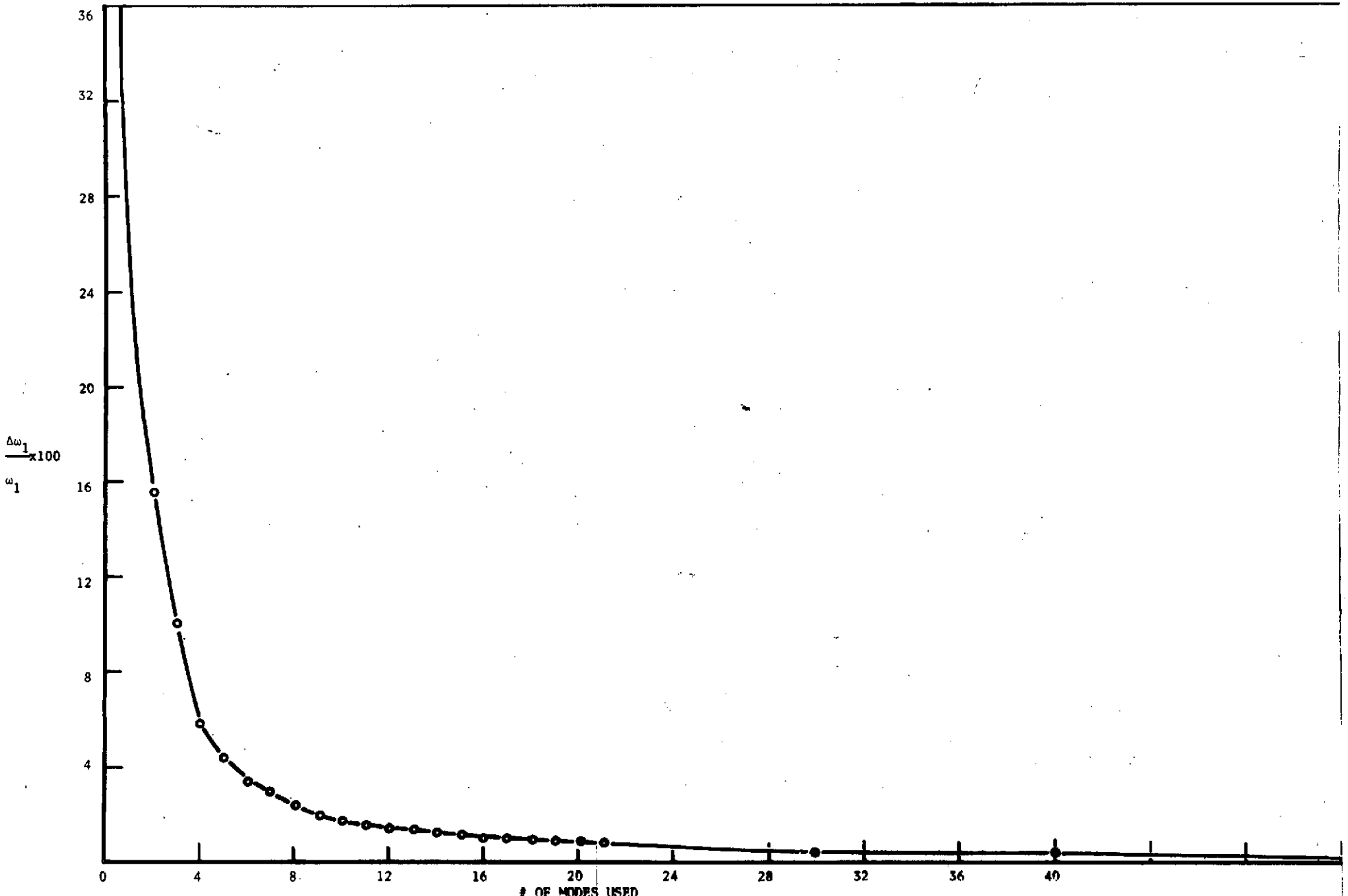

FIGURE 18. - CHECK CASE OF A CANTILIVER BEAM IN TWISTING, CONVERGENCE IN THE FUNDAMENTAL MODE (EXTENDED)

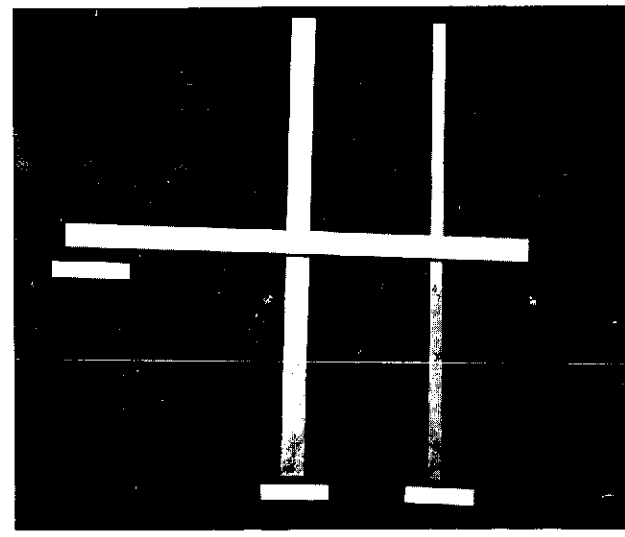

FIGURE 19. - EXPERIMENTAL MODEL

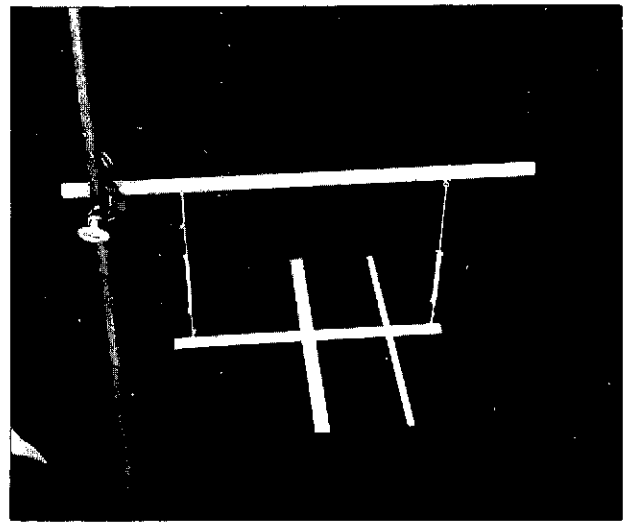

FIGURE 20. - EXPERIMENTAL MODEL WITH SUPPORTS.

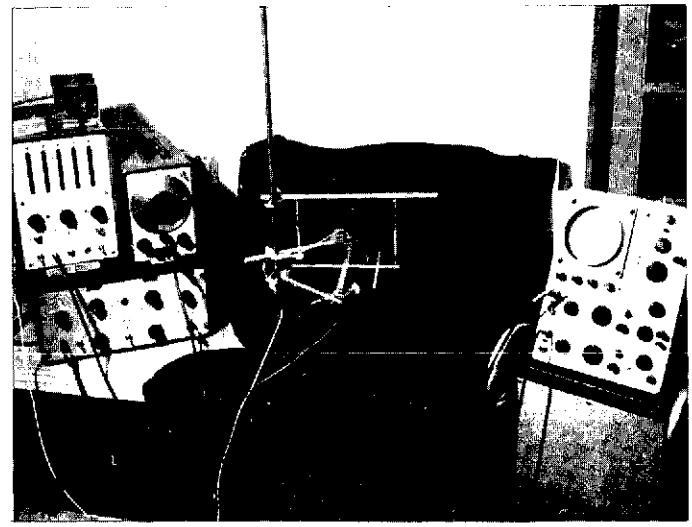

FIGURE 21. - EXPERIMENTAL APPARATUS

input ——→

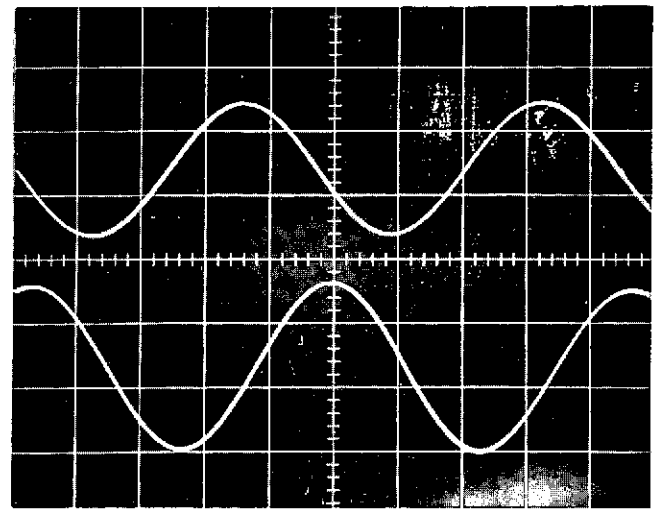

Resonance detected for ω = 264 cps

input ——→

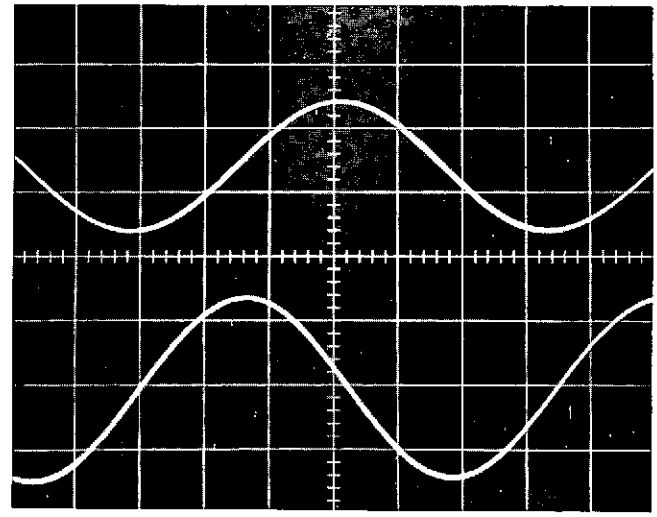

Resonance detected for ω = 112 cps

FIGURE 22. - TYPES OF OSCILLATIONS α AND β

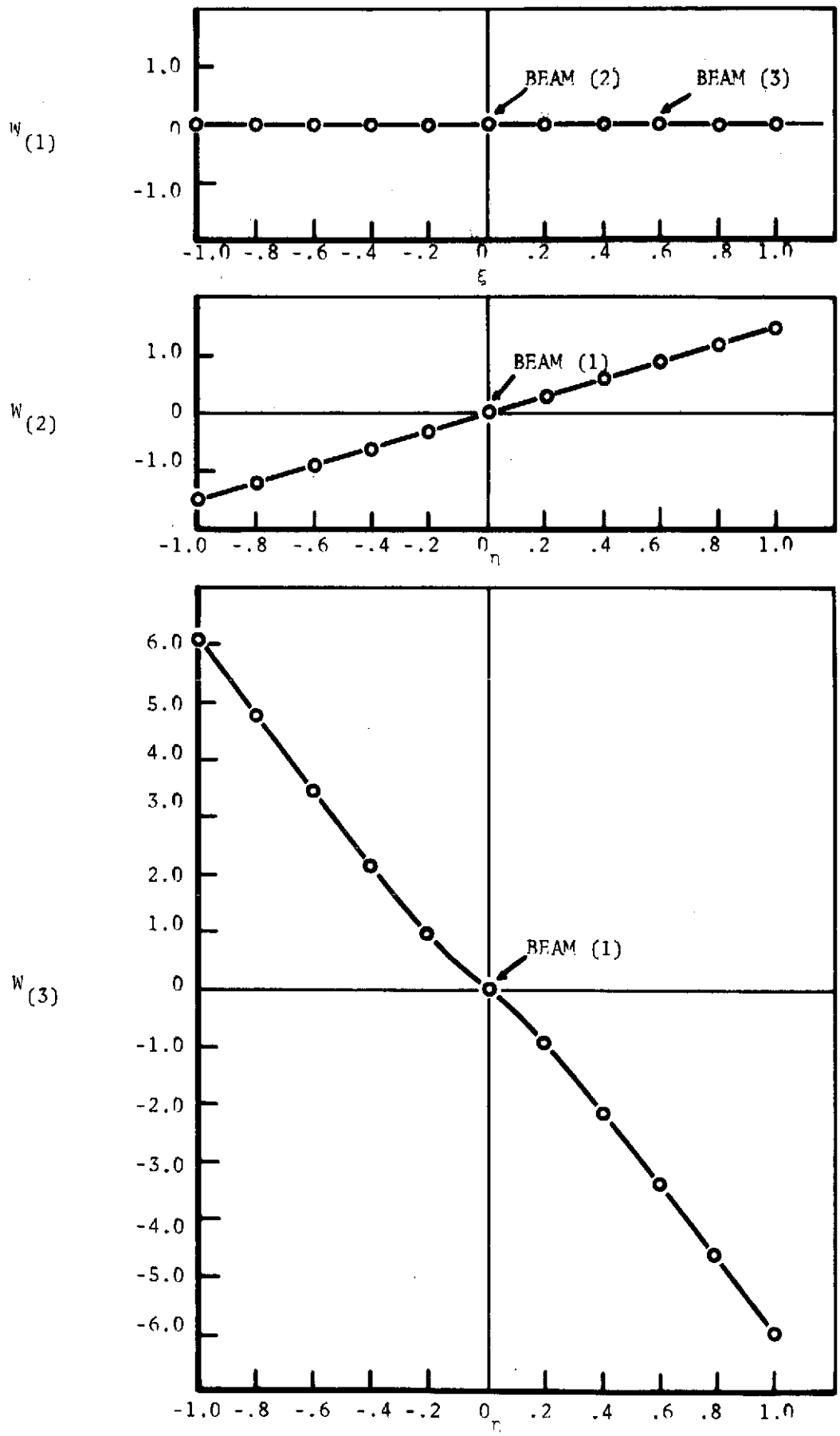

FIGURE 23. - THEORETICAL RESULTS FOR THE EXPERIMENTAL MODEL
ω = 36.7 cps PHYSICAL DISPLACEMENTS OF THE COMPONENTS

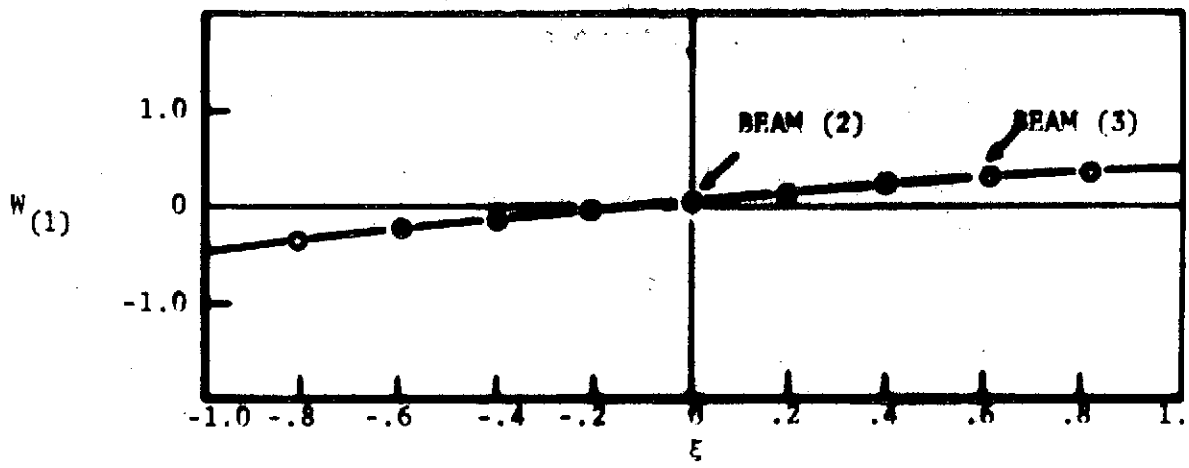

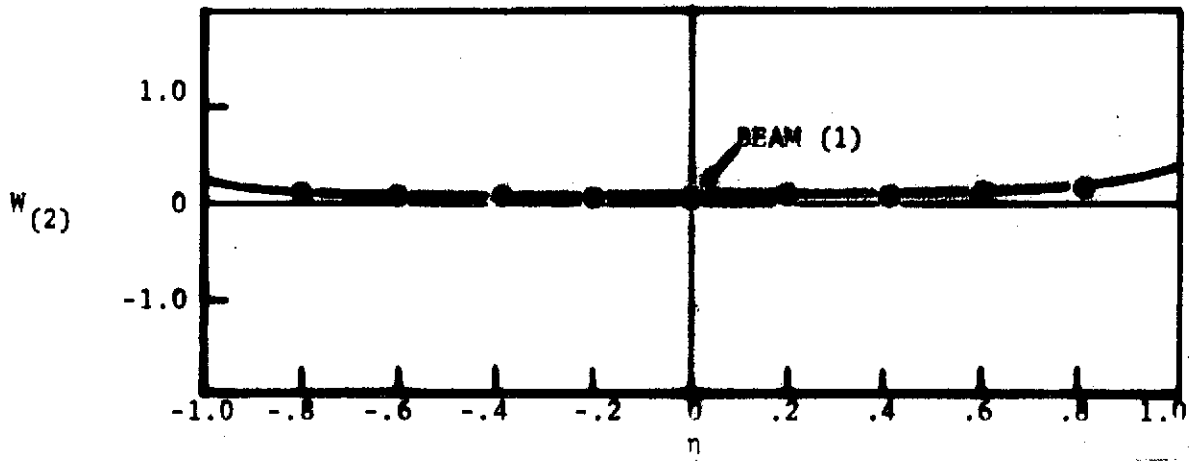

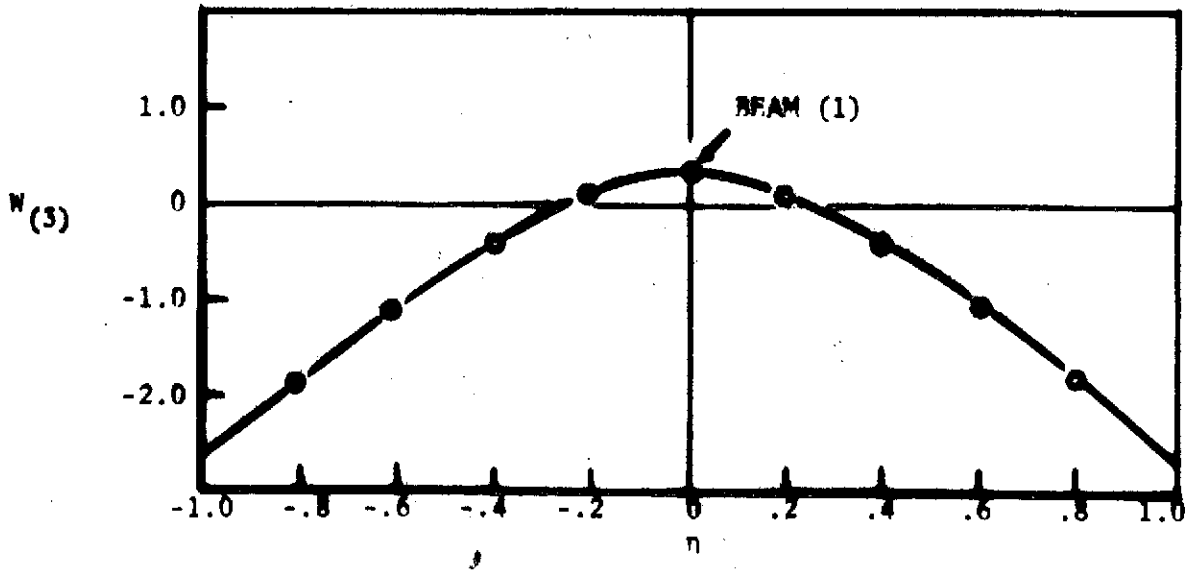

FIGURE 24. - THEORETICAL RESULTS FOR THE EXPERIMENTAL MODEL

ω = 69 cps PHYSICAL DISPLACEMENTS OF THE COMPONENTS

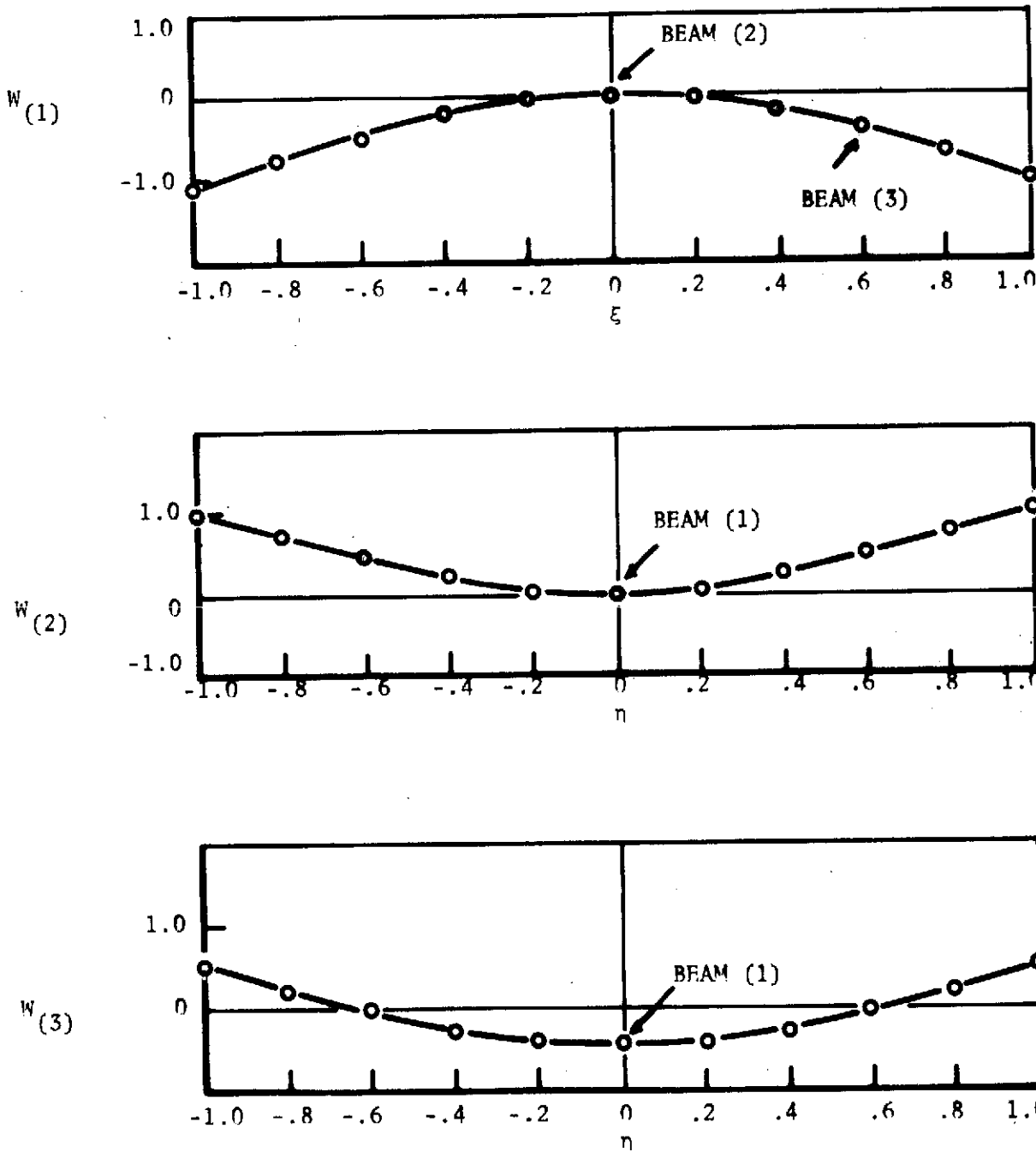

FIGURE 25. - THEORETICAL RESULTS FOR THE EXPERIMENTAL MODEL
ω = 125.6 cps PHYSICAL DISPLACEMENTS OF THE COMPONENTS

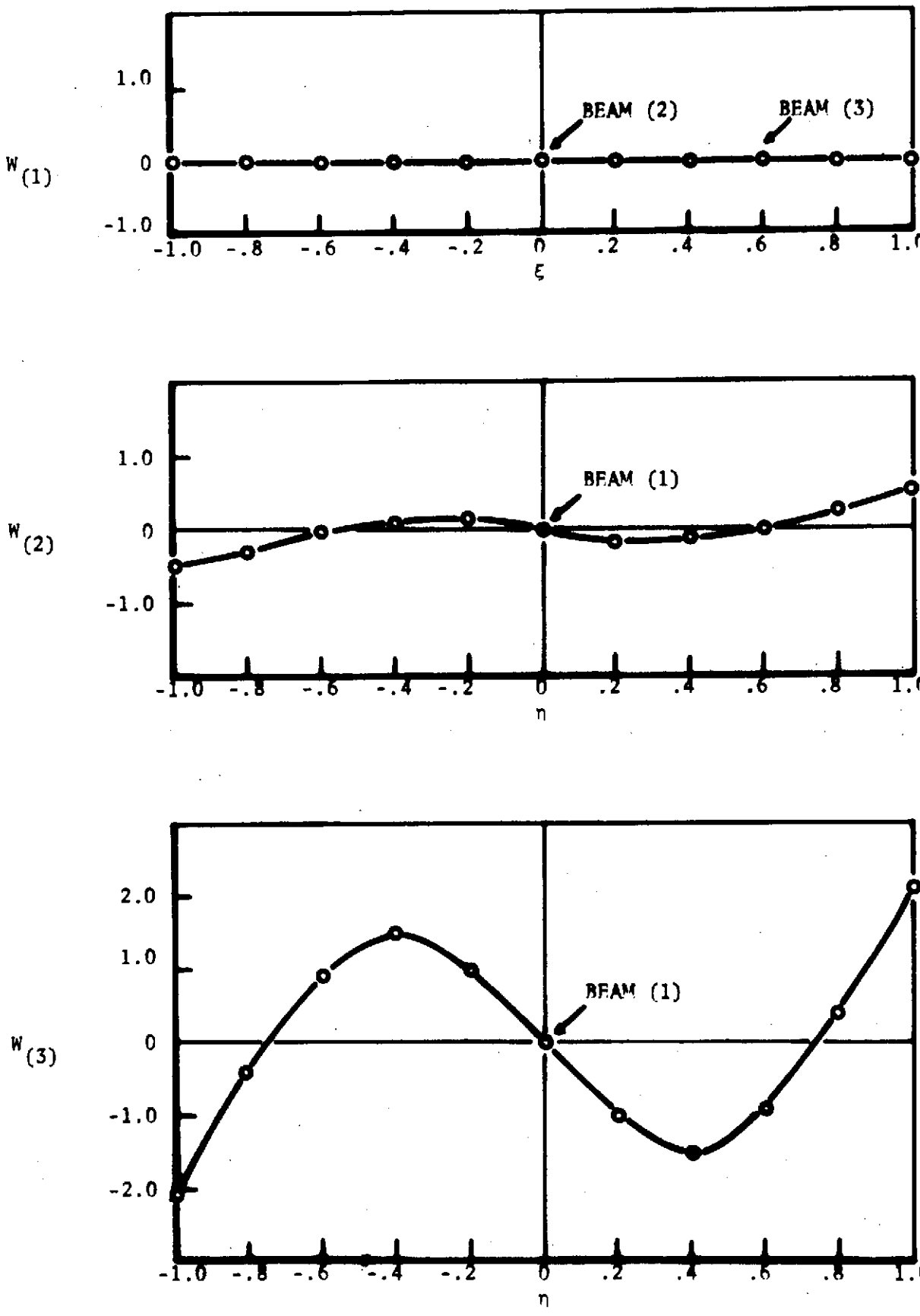

FIGURE 26. - THEORETICAL RESULTS FOR THE EXPERIMENTAL MODEL
ω = 295.5 cps PHYSICAL DISPLACEMENTS OF THE COMPONENTS

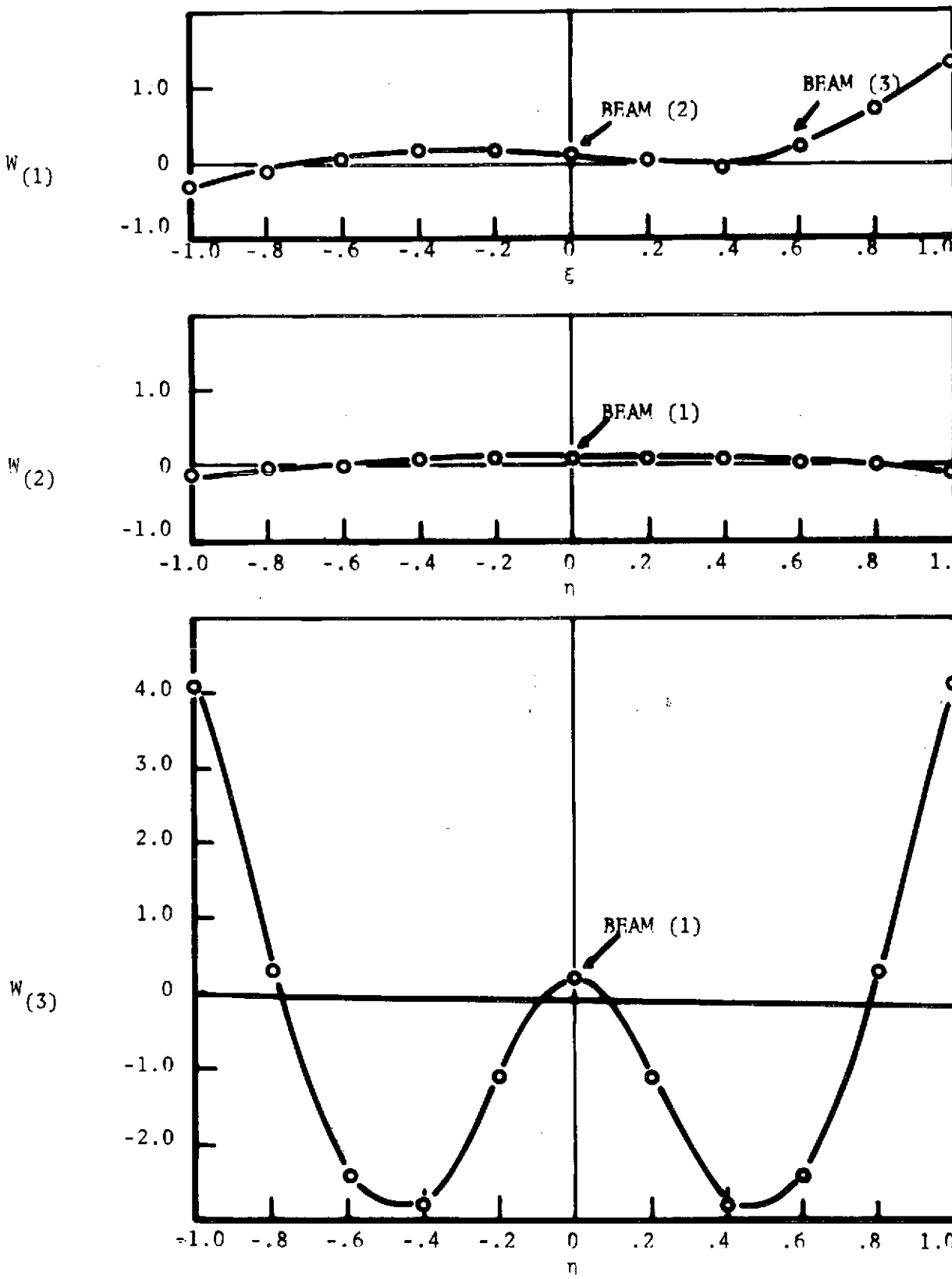

FIGURE 27. - THEORETICAL RESULTS FOR THE EXPERIMENTAL MODEL
ω = 404.8 cps PHYSICAL DISPLACEMENTS OF THE COMPONENTS

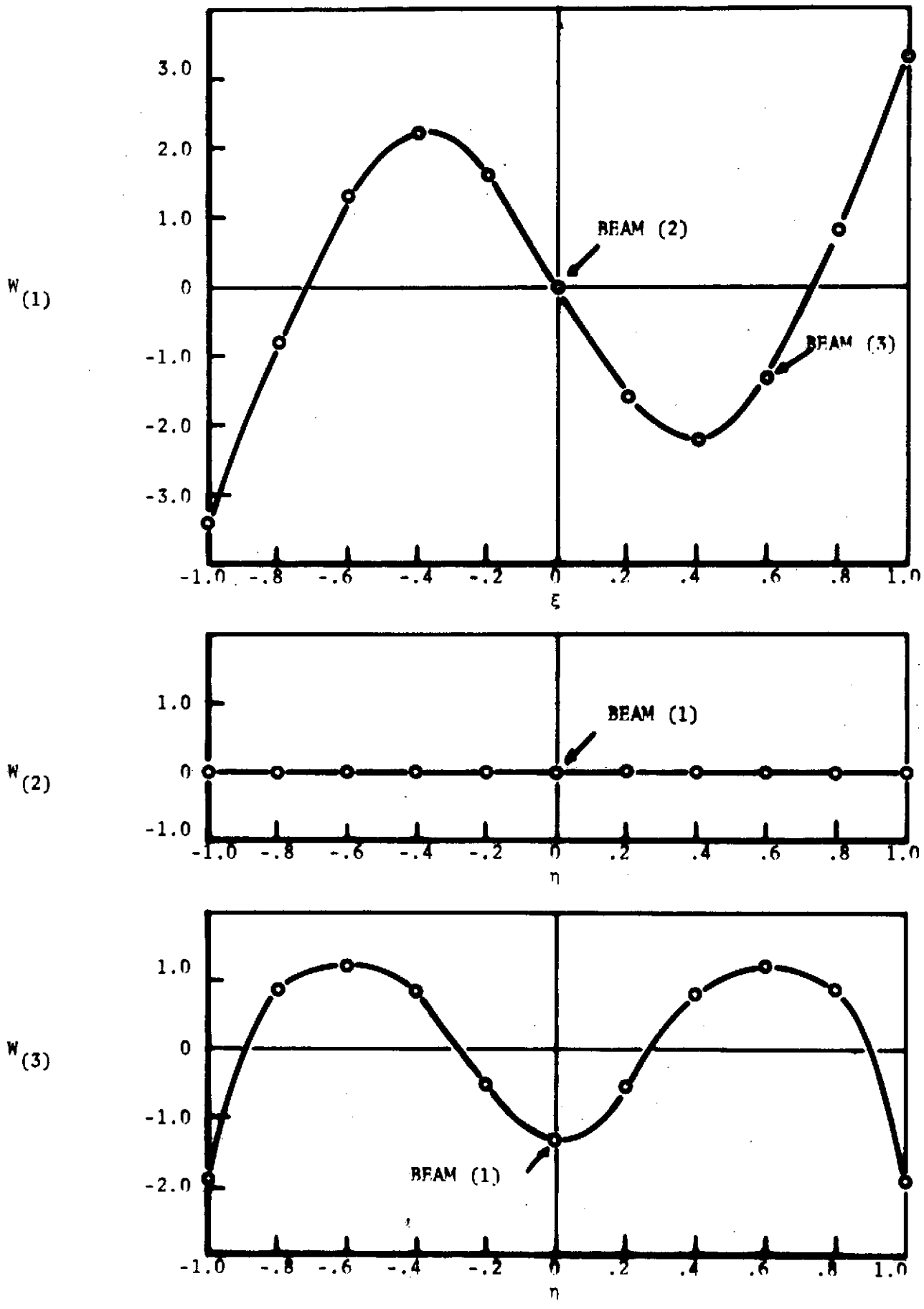

FIGURE 28. - THEORETICAL RESULTS FOR THE EXPERIMENTAL MODEL

ω = 536.2 cps PHYSICAL DISPLACEMENTS OF THE COMPONENTS

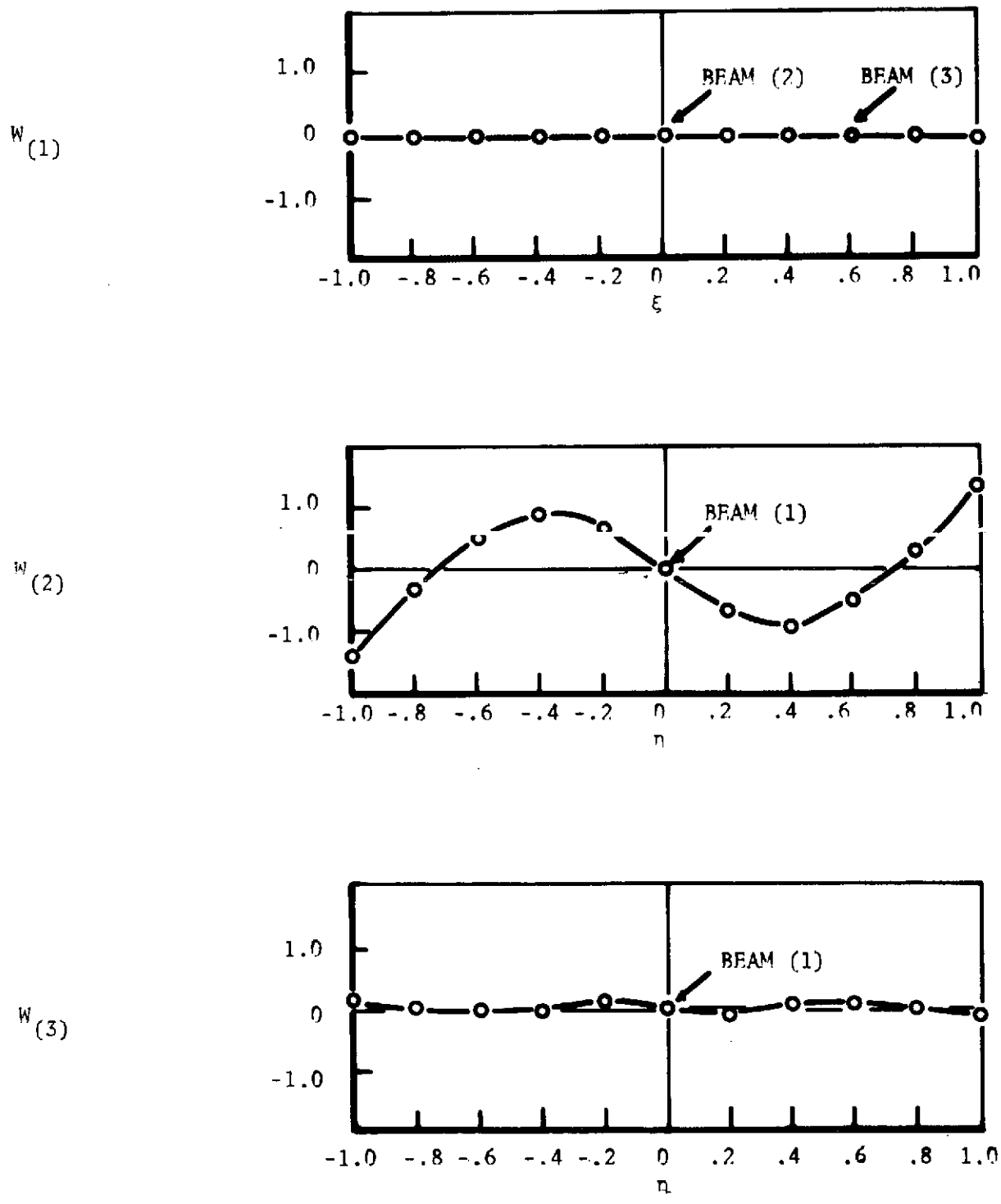

FIGURE 29. - THEORETICAL RESULTS FOR THE EXPERIMENTAL MODEL

ω = 546.5 cps PHYSICAL DISPLACEMENTS OF THE COMPONENTS

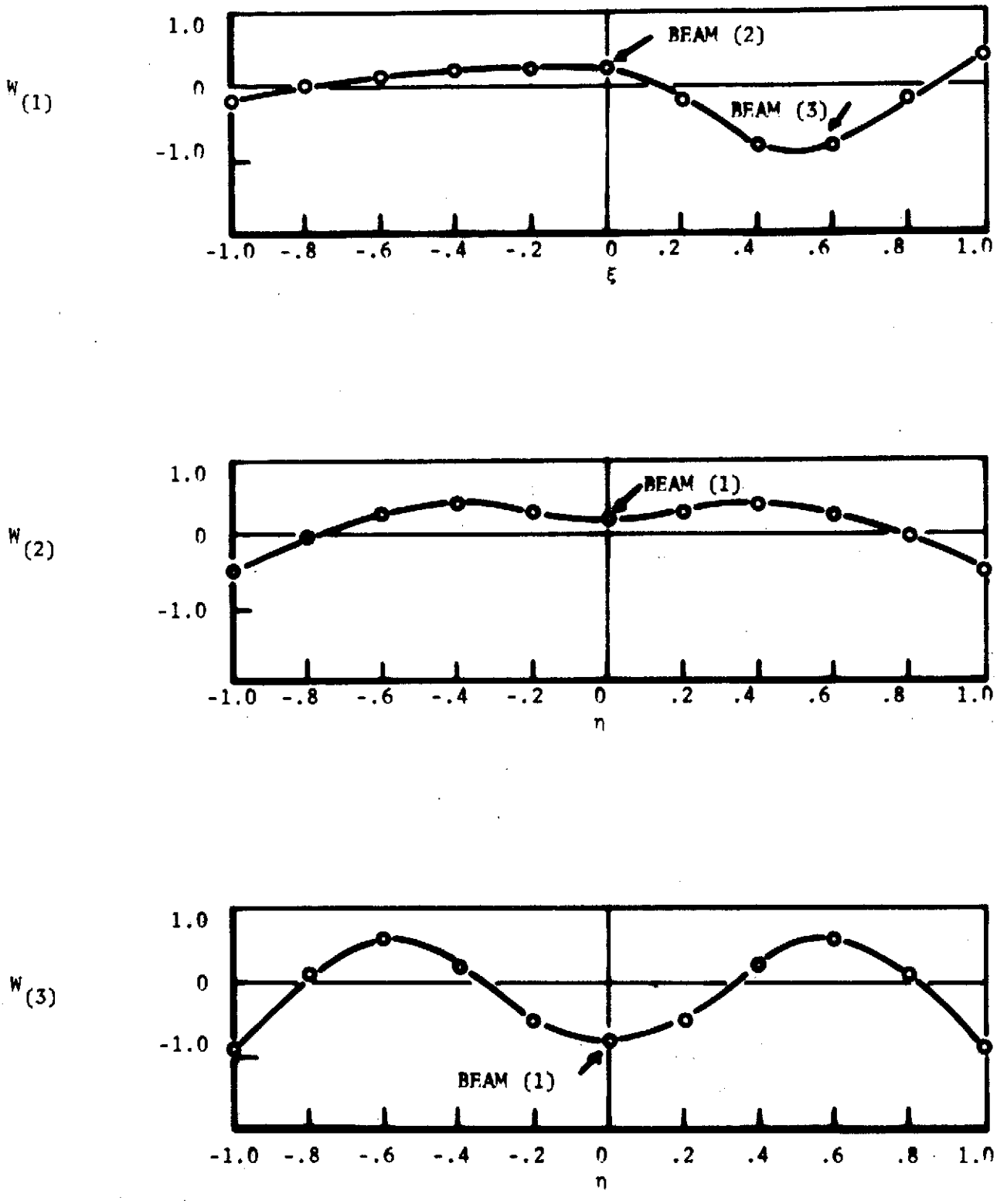

FIGURE 30. - THEORETICAL RESULTS FOR THE EXPERIMENTAL MODEL
ω = 643.3 cps PHYSICAL DISPLACEMENTS OF THE COMPONENTS

$W_{(1)}$

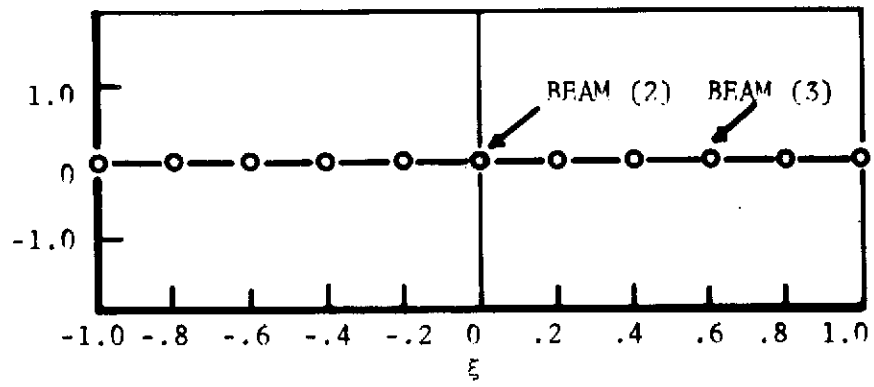

$W_{(2)}$

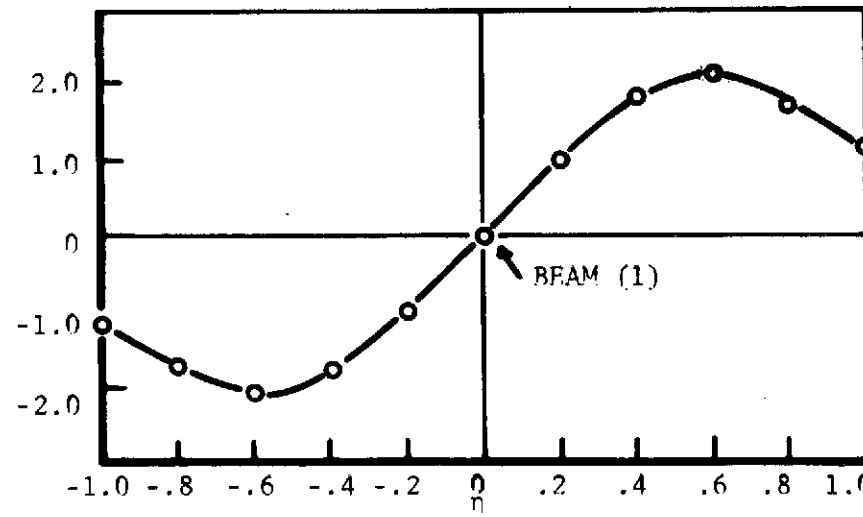

$W_{(3)}$ IS NOT DETERMINED ACCURATELY AT THIS STEP IN THE COMPUTATION

FIGURE 31. - THEORETICAL RESULTS FOR THE EXPERIMENTAL MODEL
ω = 648.2 cps PHYSICAL DISPLACEMENTS OF THE COMPONENTS

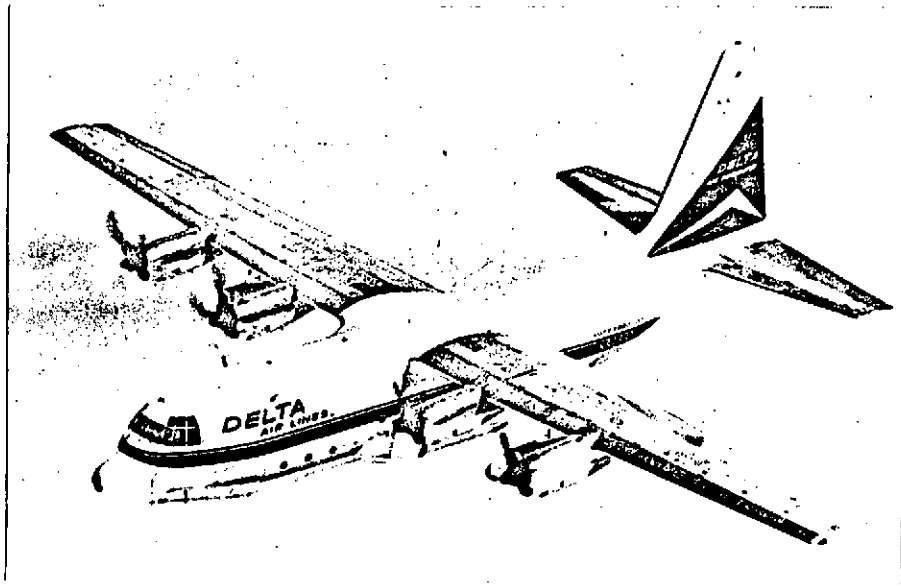

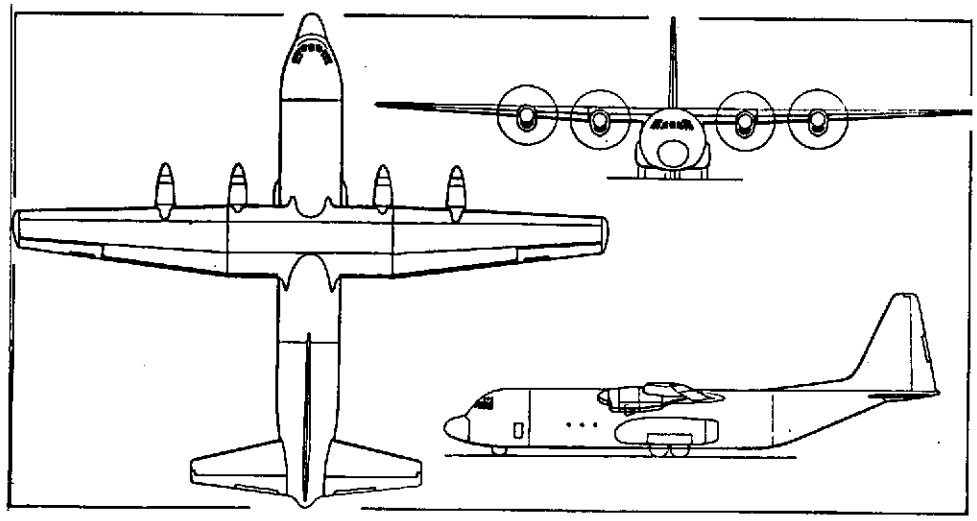

FIGURE 32. - LOCKHEED L-100 (CIVIL HERCULES)

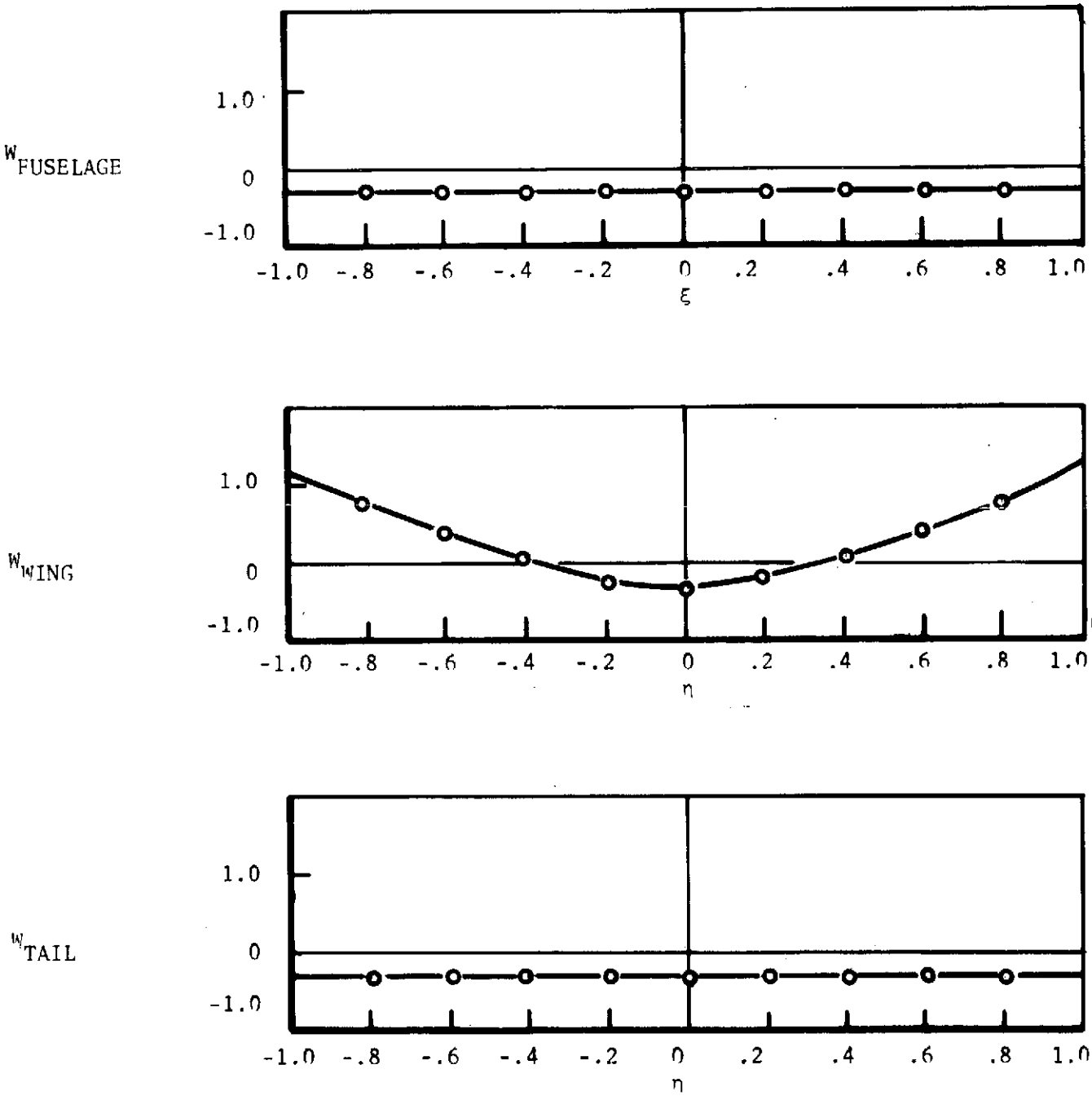

FIGURE 33. - LOCKHEED L-100 HERCULES

PHYSICAL DEFORMATIONS OF THE COMPONENTS IN THE FIRST MODE

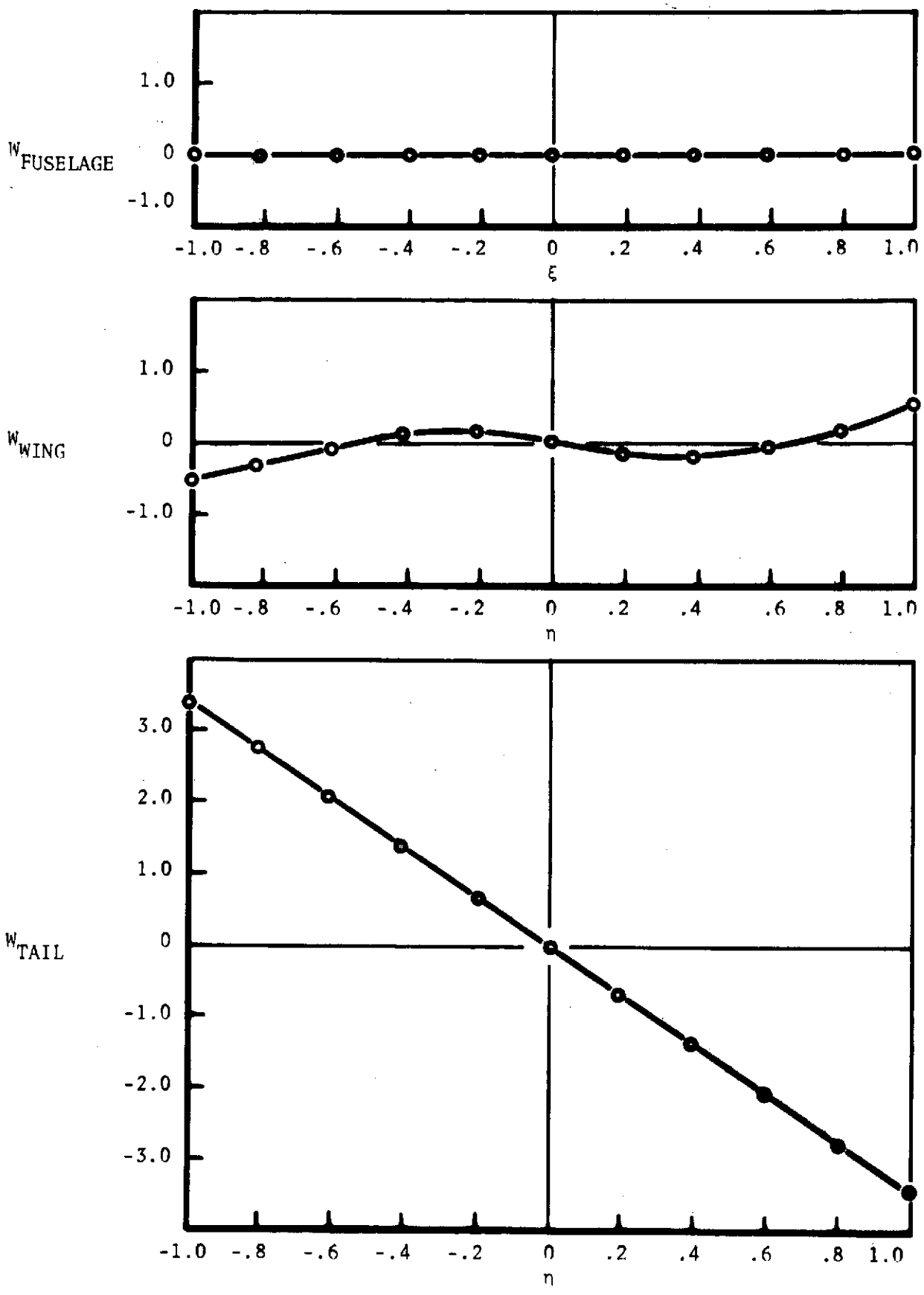

FIGURE 34. - LOCKHEED L-100 HERCULES

PHYSICAL DEFORMATIONS OF THE COMPONENTS IN THE SECOND MODE

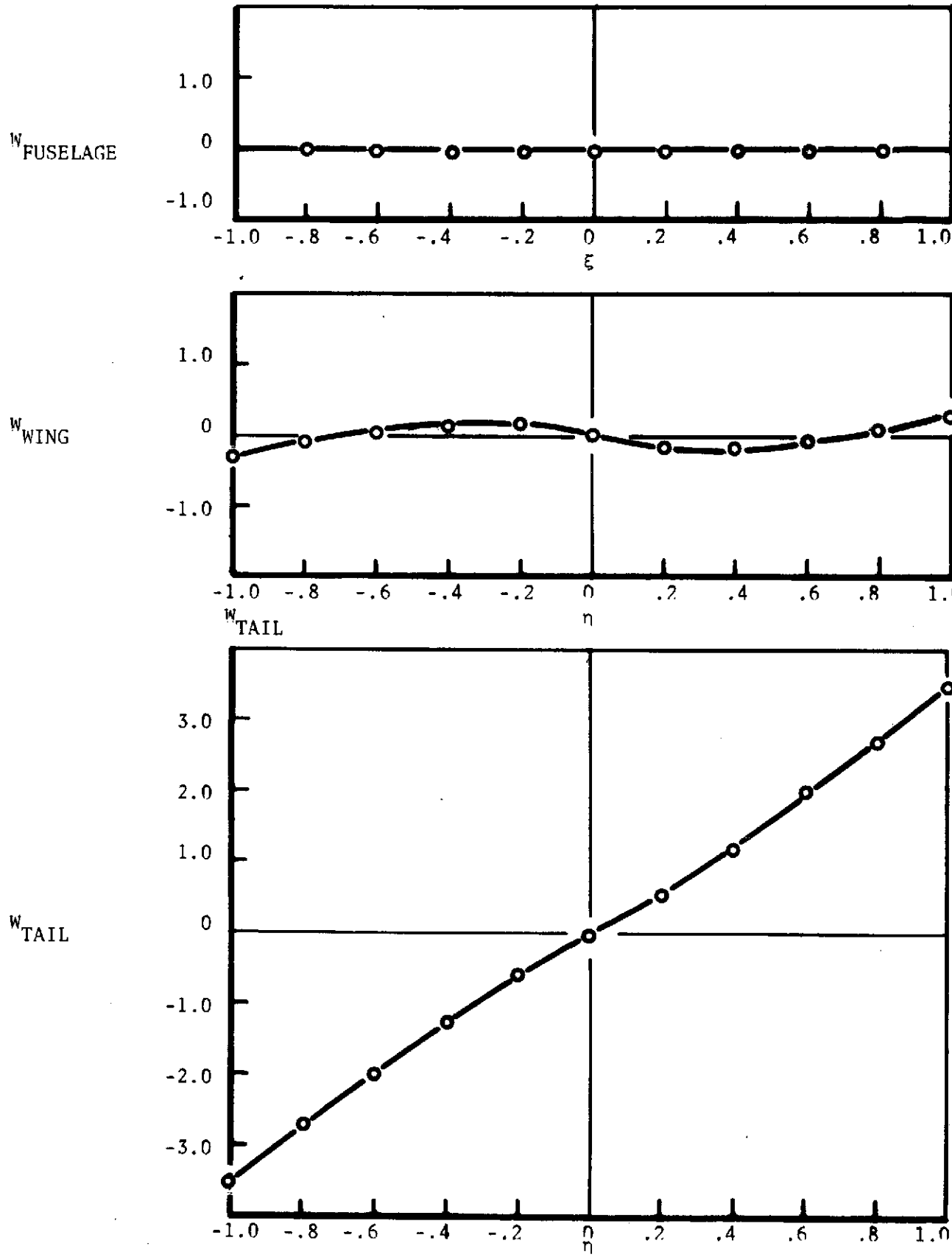

FIGURE 35. - LOCKHEED L-100 HERCULES
PHYSICAL DEFORMATIONS OF THE COMPONENTS IN THE THIRD MODE

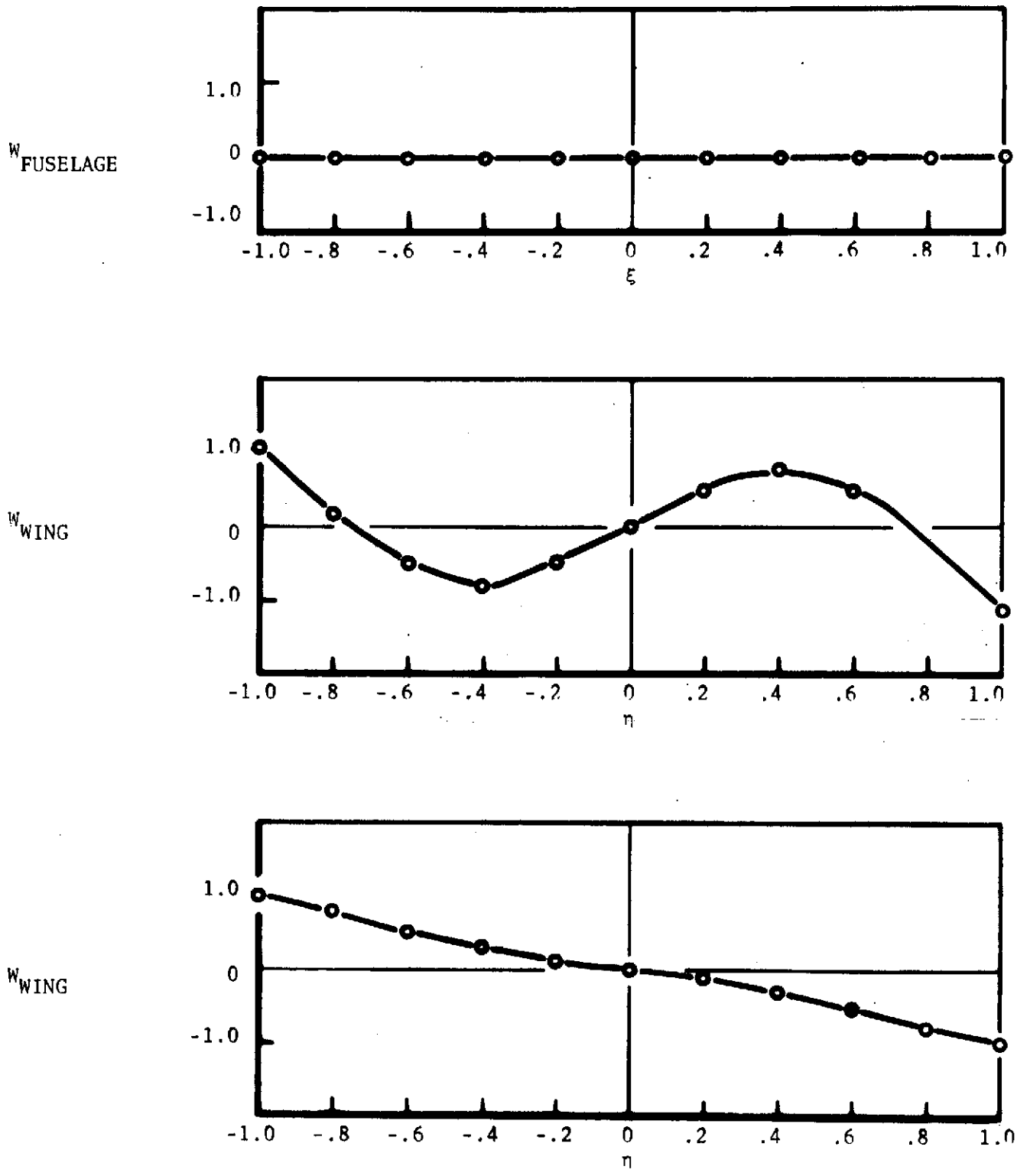

FIGURE 36. - LOCKHEED L-100 HERCULES
PHYSICAL DEFORMATIONS OF THE COMPONENTS IN THE FOURTH MODE

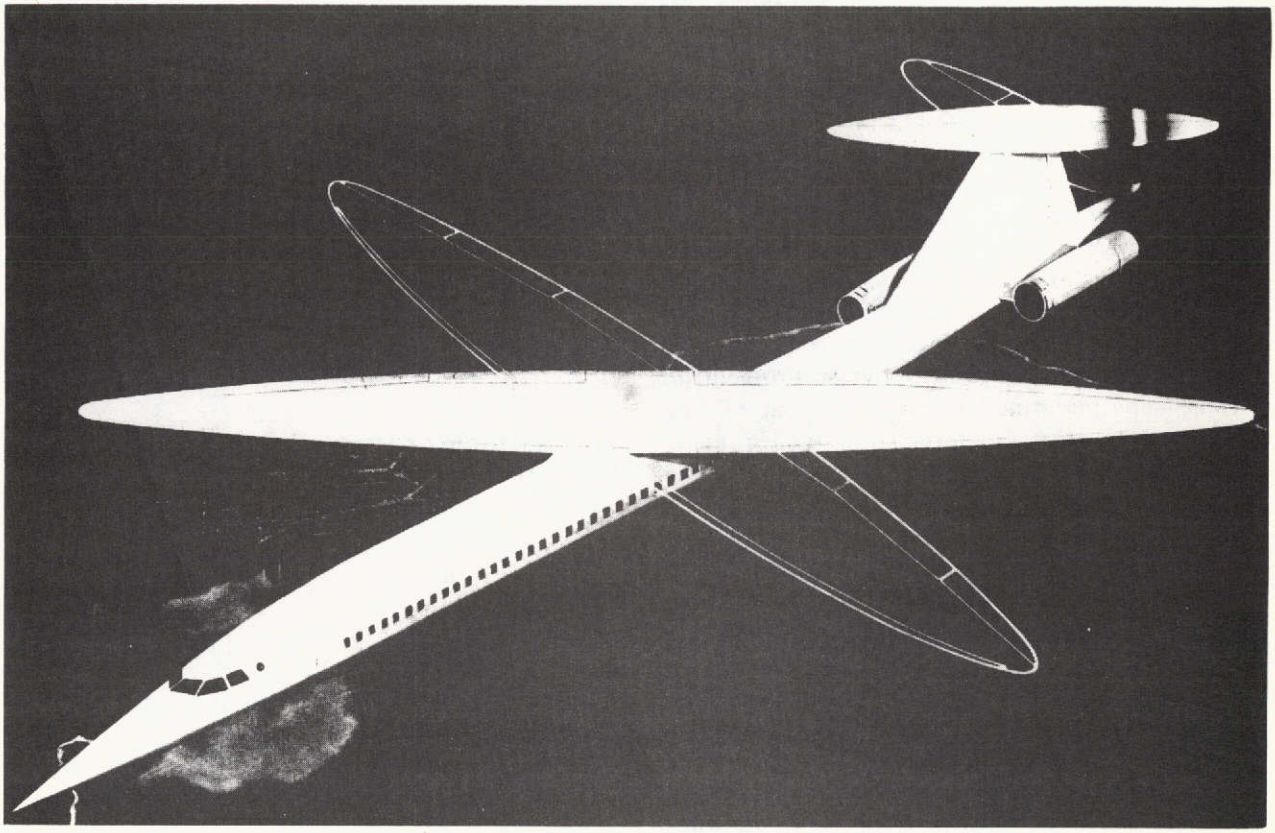

FIGURE 37. - CONCEPT OF A PIVOTING-WING SST FOR COMMERICAL OPERATIONS

5) shows the model in flight with the wing at 45 deg. Burnett L. Gadeberg of Ames controlled the model.

Variations of wing angle up to and beyond 45 deg produced no apparent changes in stability and only a slight change in lateral trim—requiring a 1- or 2-deg offset of the ailerons. Elevator and aileron effectiveness remained normal and we observed no change in longitudinal trim.

Ordinary maneuvers such as loops and rolls were performed without difficulty at wing angles of 45 deg. Coupling between longitudinal and lateral motions did not appear in aileron rolls, but was quite apparent in the response to elevator control. Thus loops performed with the wing at 45 deg appeared to take the form of a 45-deg helix, indicating that the rotation produced by the elevator tends to align with the long axis of the wing. With the left tip forward, use of the elevator in a left turn tended to steepen the bank angle. Analysis shows that in this case a certain amount of aileron deflection must be employed with the elevator to prevent banking toward the forward tip.

Varying the sweep by turning the wing as a whole has several practical advantages over the usual "swing wing" design. It keeps the wing structure continuous across the pivot and makes the primary load on the pivot tension. With separate wing panels pivoted at the root, however, much greater loads develop on the pivots (F-6). Also, sweeping the wing panels back for high-speed flight displaces the center of lift rearward, compounding the normal rearward center-of-pressure shift at

F-6 CONTINUOUS WING STRUCTURE; NO BENDING LOAD ON PIVOTS

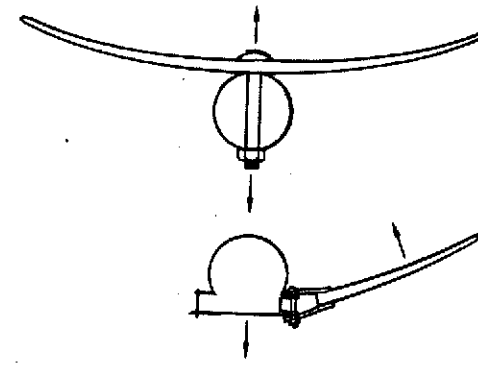

F-7 CENTROID OF LIFTING AREA NOT DISPLACED BY ROTATION

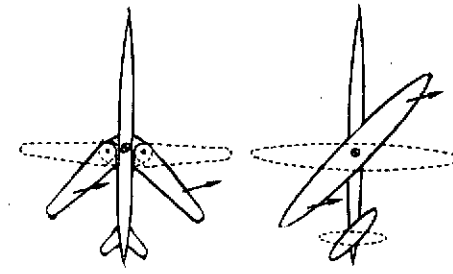

F-8 STRAIGHT-BEAM STRUCTURE.

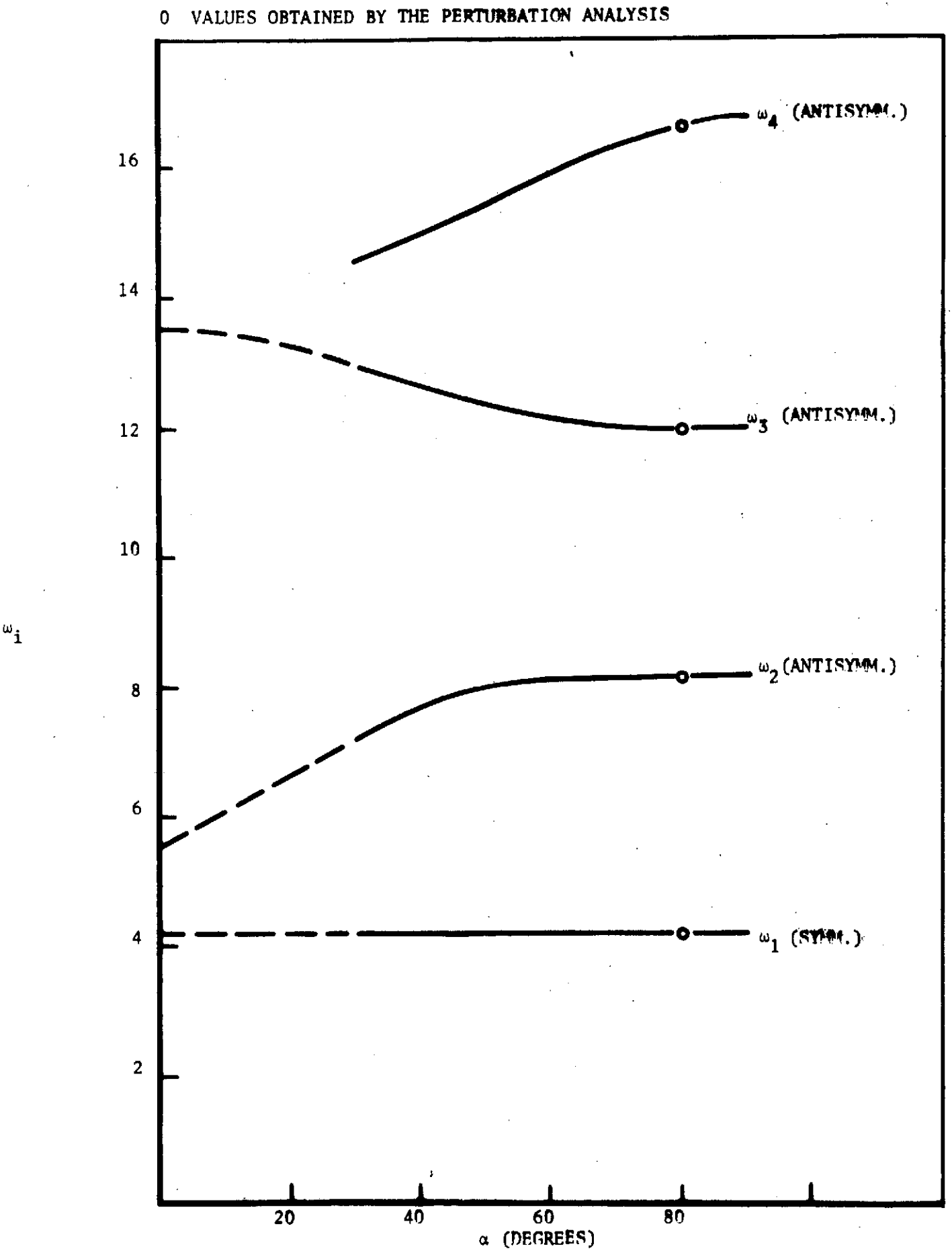

FIGURE 38. - PIVOTING-WING VERSION OF THE LOCKHEED L-100 HERCULES CHANGE IN THE NATURAL FREQUENCIES VERSUS OBLICITY ANGLE α

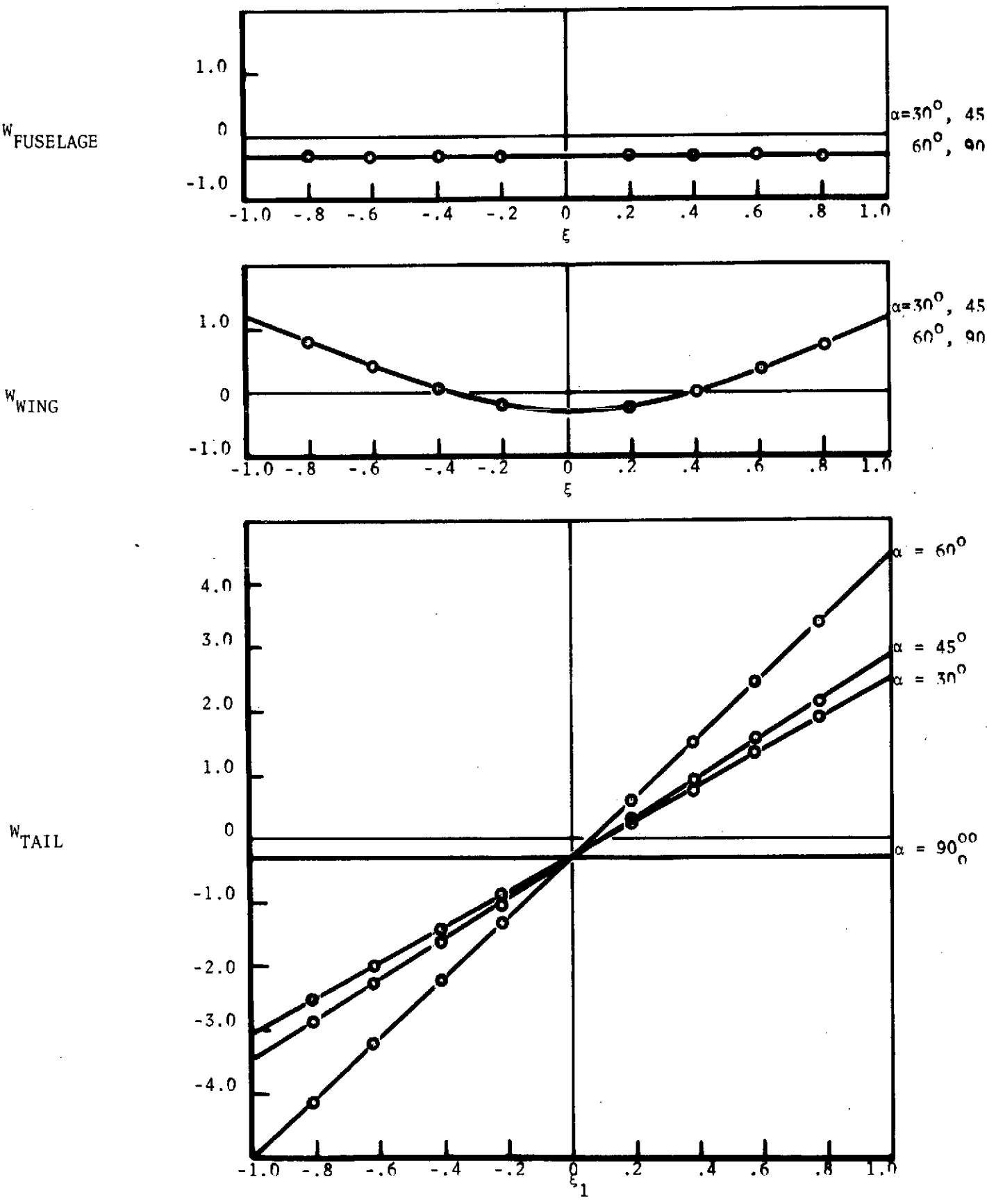

FIGURE 39. - PIVOTING-WING VERSION OF THE L-100 HERCULES
PHYSICAL DISPLACEMENTS IN THE FUNDAMENTAL MODE

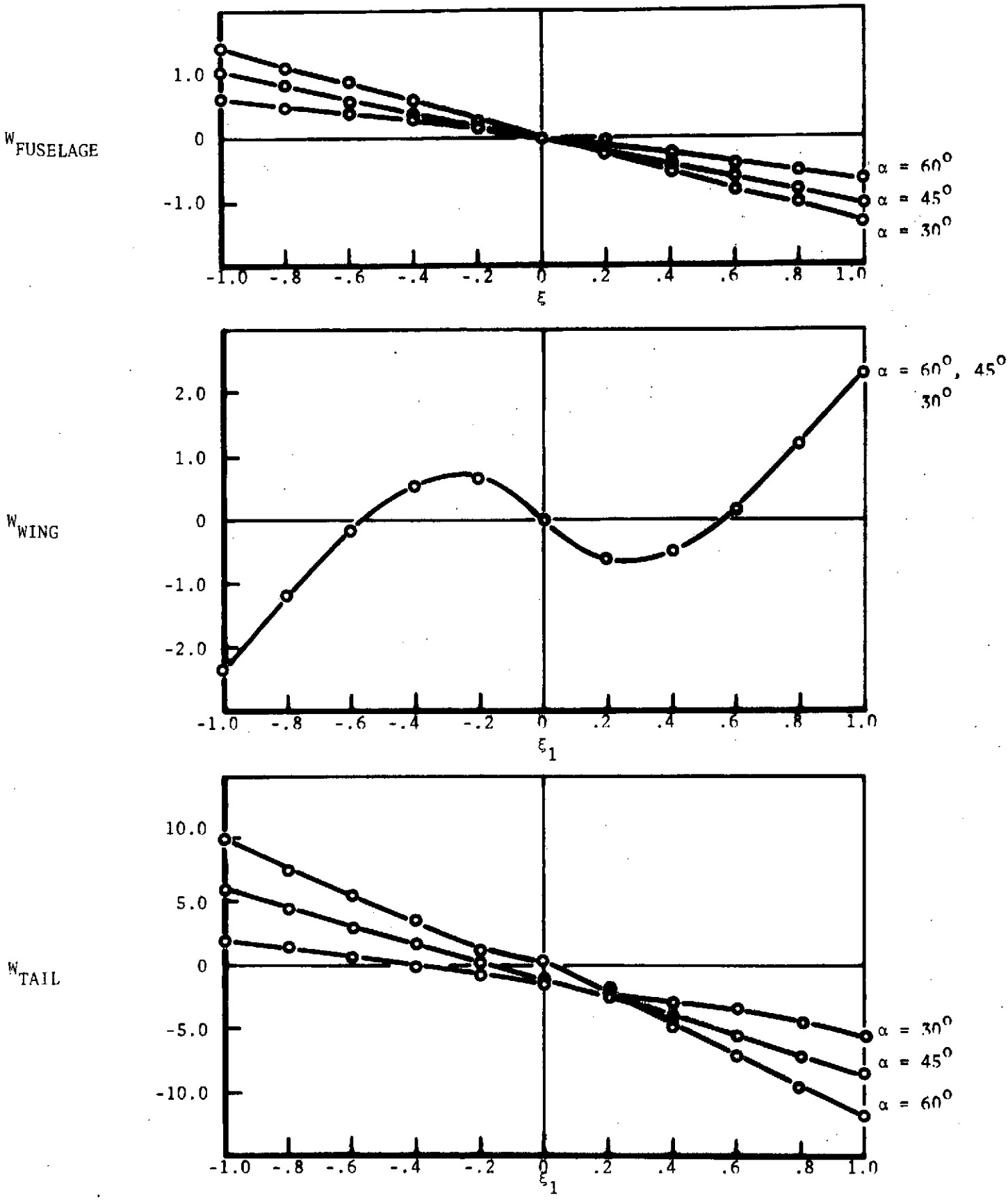

FIGURE 40. - PIVOTING-WING VERSION OF THE L-100 HERCULES , SECOND MODE CHANGE IN THE PHYSICAL DEFORMATIONS WITH THE ANGLE α

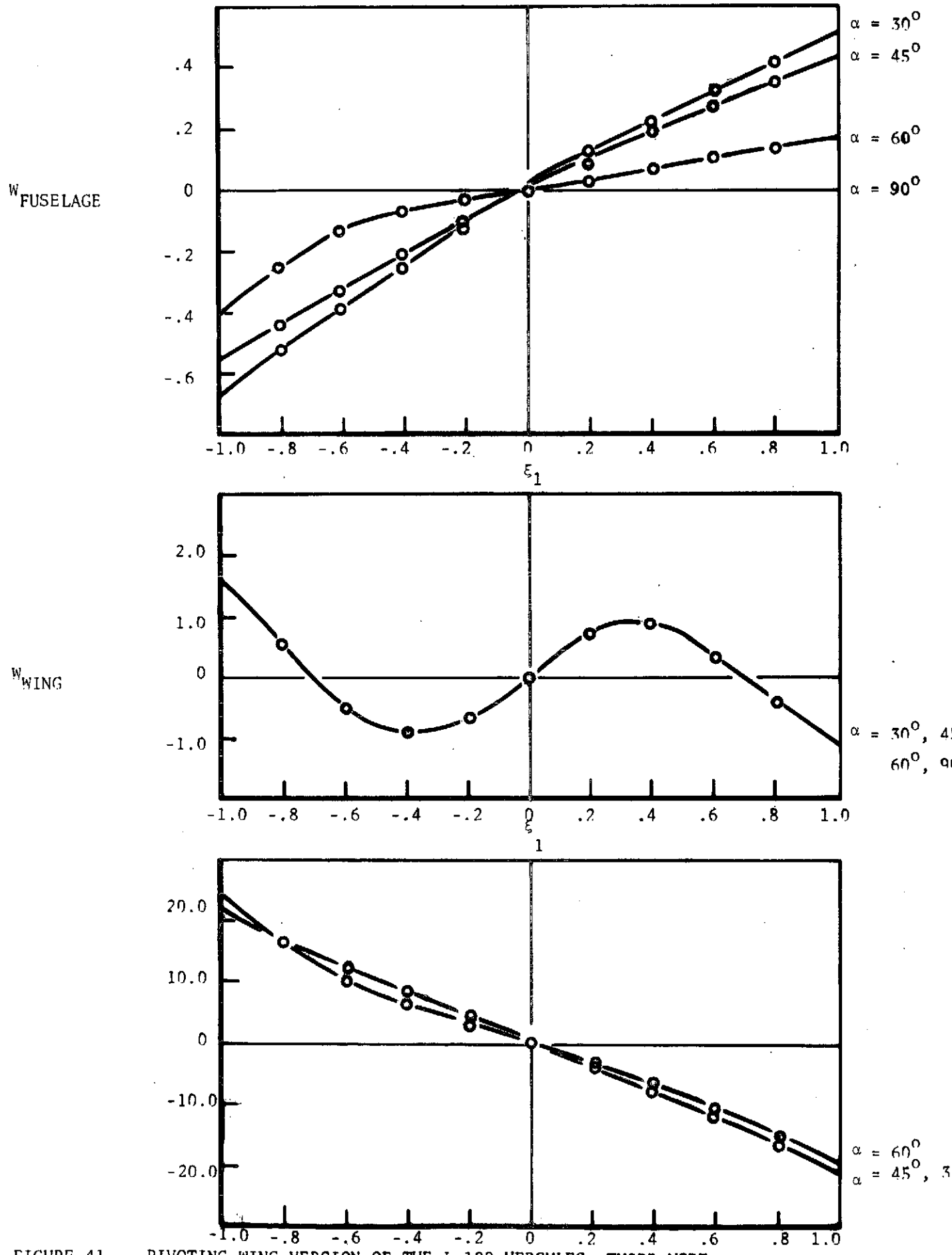

FIGURE 41. - PIVOTING-WING VERSION OF THE L-100 HERCULES, THIRD MODE

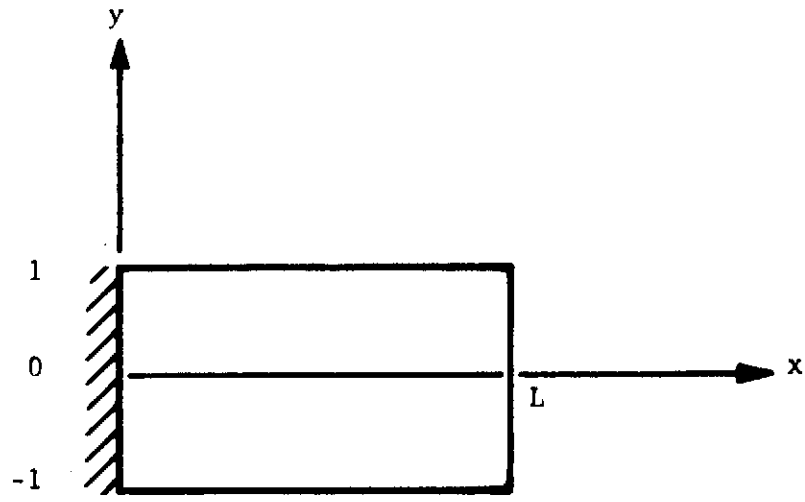

INITIAL CANTILIVERED PLATE

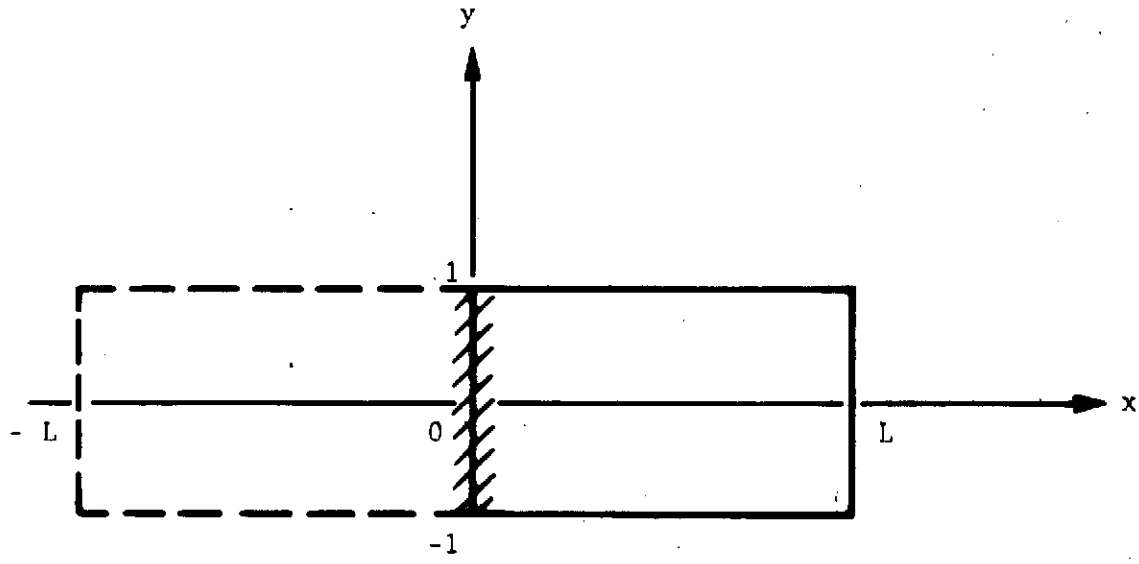

TREATMENT OF THE PROBLEM BY SYMMETRY

FIGURE 42. - CANTILIVERED PLATE IN TRANSVERSE VIBRATIONS

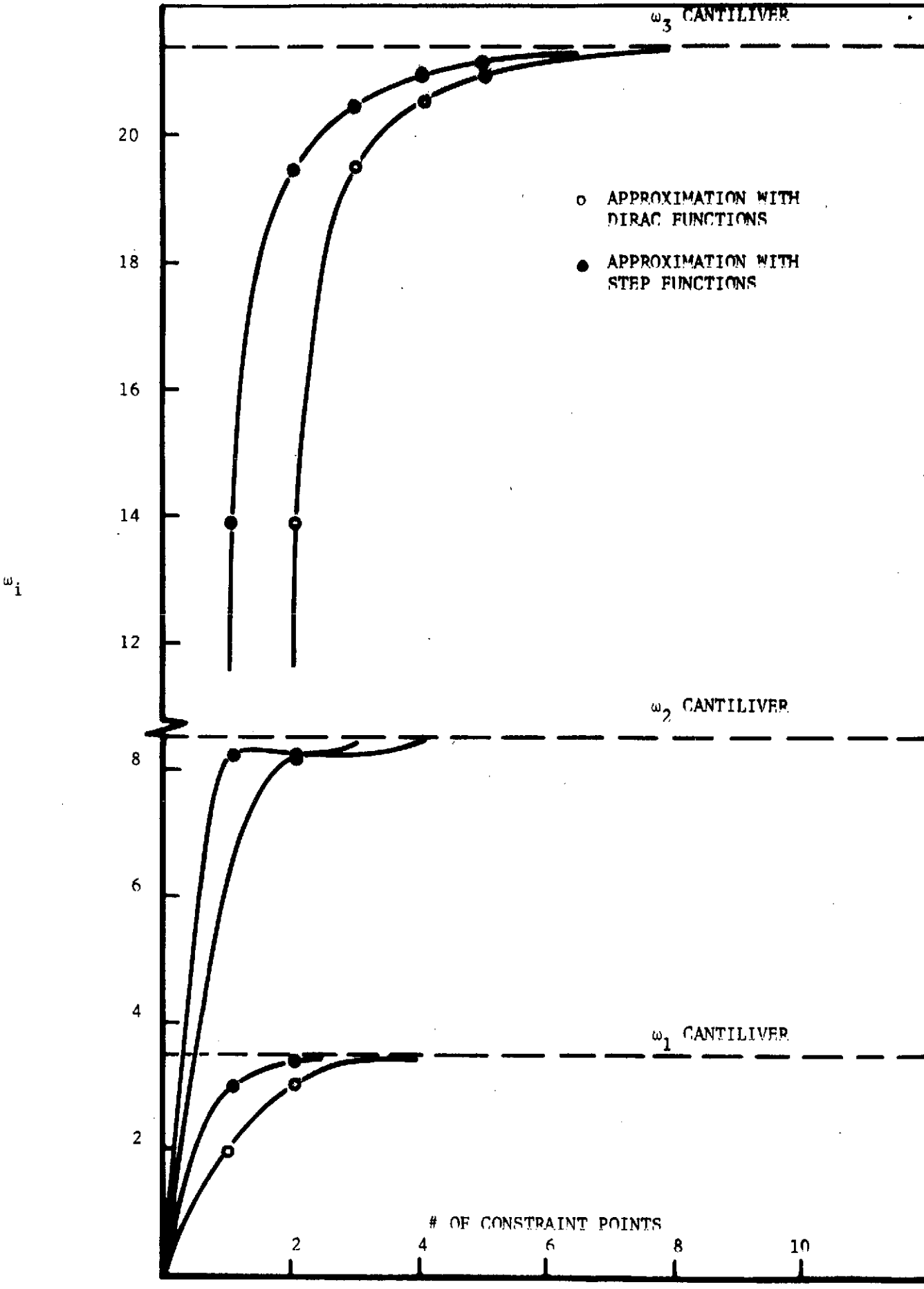

FIGURE 43. - POINT ‹ CLAMPED SQUARE PLATE. CONVERGENCE OF THE NATURAL FREQUENCIES TOWARDS THOSE OF A CANTILIVER PLATE

$\Phi_{1_{CANTIL.}}(x,y) = Y_{o_{FREE}}(y)\ X_{1_{CANTIL.}}(x)$ (Reference (35))

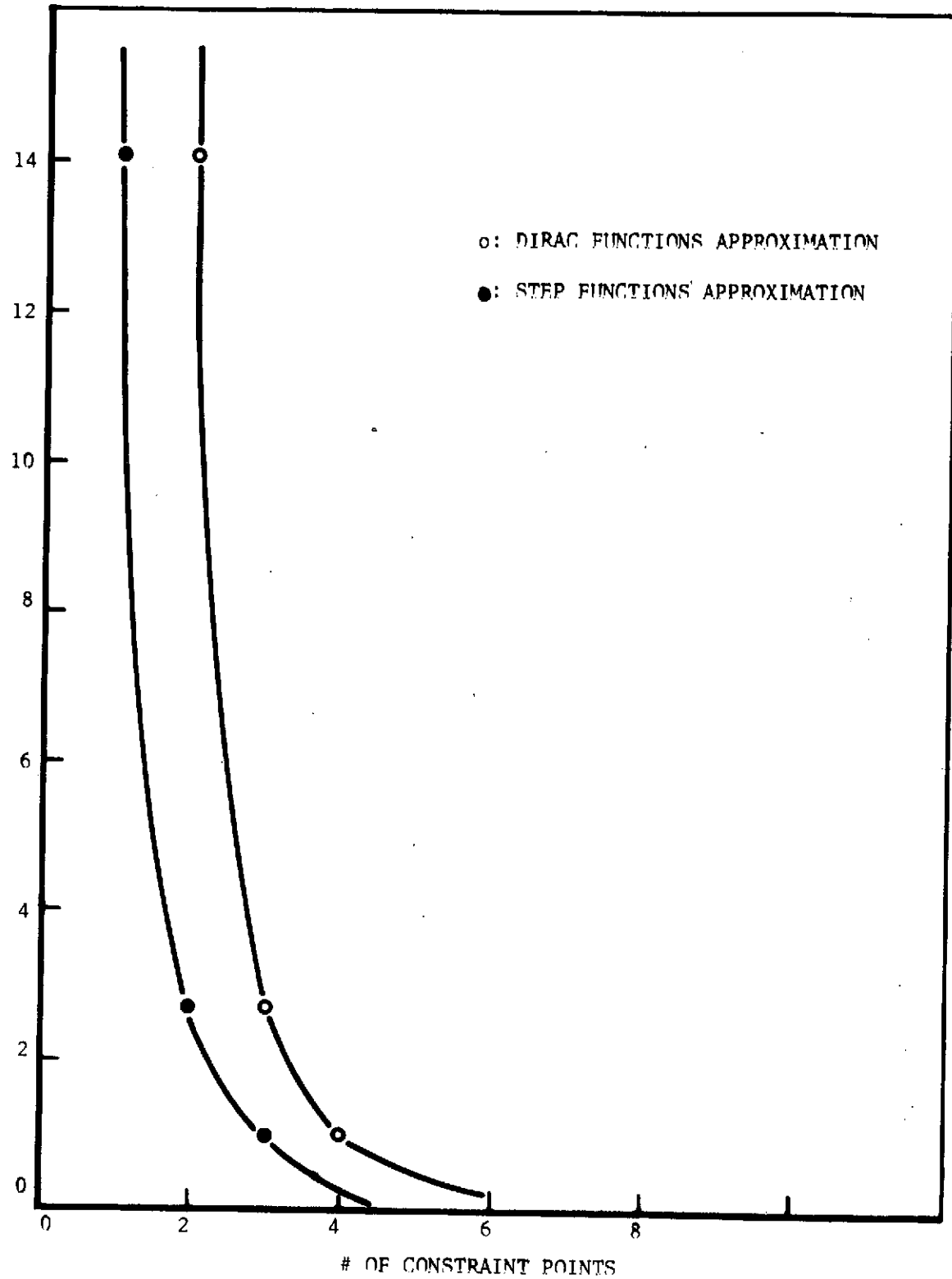

FIGURE 44. - POINT CLAMPED SQUARE PLATE, CONVERGENCE OF THE FUNDAMENTAL NATURAL FREQUENCY TOWARDS THAT OF A CANTILIVERED PLATE

$$\Phi_{2_{CANTIL}}(x,y) = X_{2_{CANTIL}}(x)\ [Y_{0_{FREE}}(y) + 0.12\ Y_{1_{FREE}}(y)\ ]$$

(Reference (3

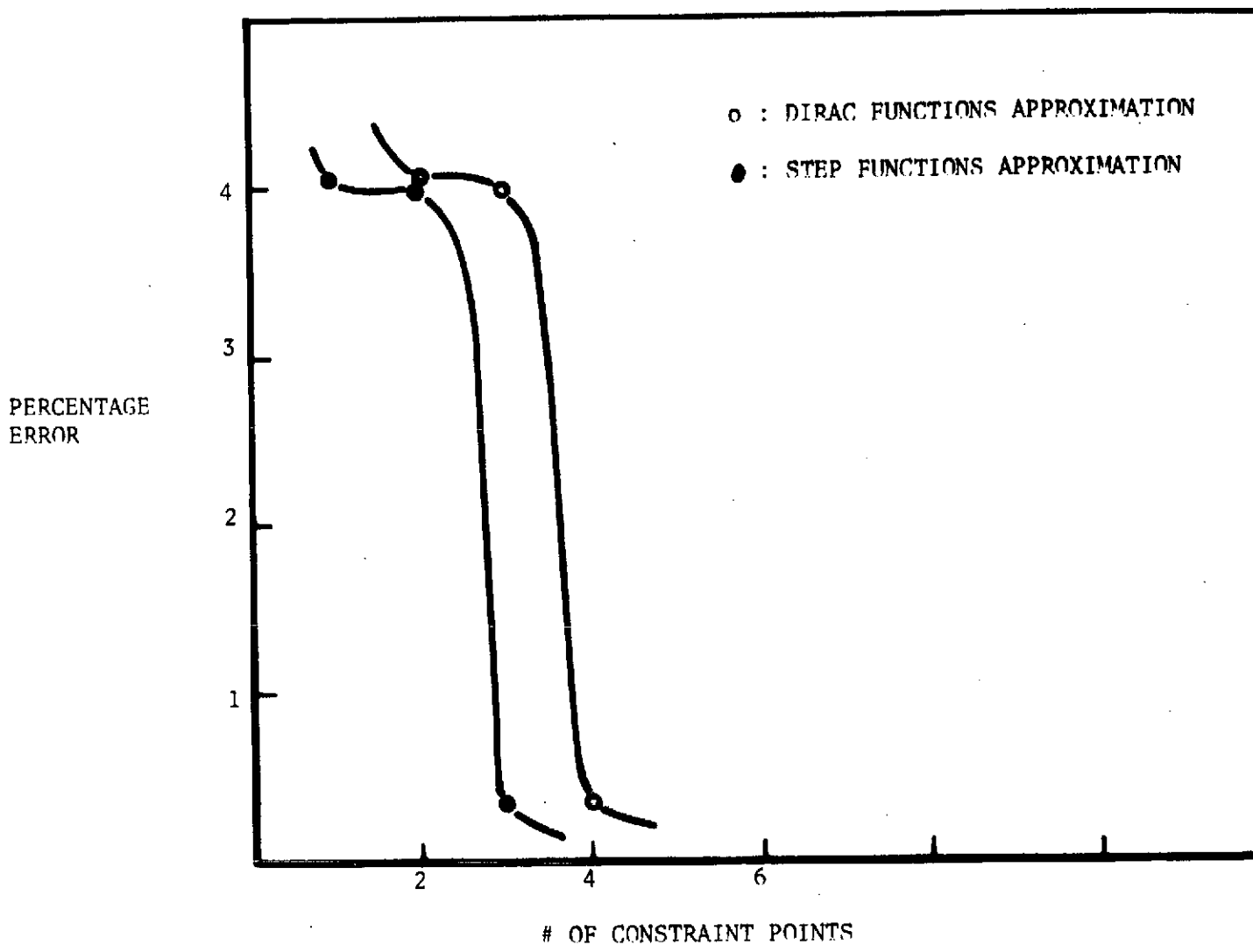

FIGURE 45. - POINT CLAMPED SQUARE PLATE.

CONVERGENCE OF THE SECOND NATURAL FREQUENCY TOWARDS THAT OF A CANTILIVERED PLATE

$$\Phi_{3_{CANTIL.}}(x,y) = Y_{2_{FREE}}(y)\ X_{1_{CANTIL}}(x) + 0.3\ Y_{0_{FREE}}(y)\ X_{3_{CANTIL}}(x)$$ (Reference (35)

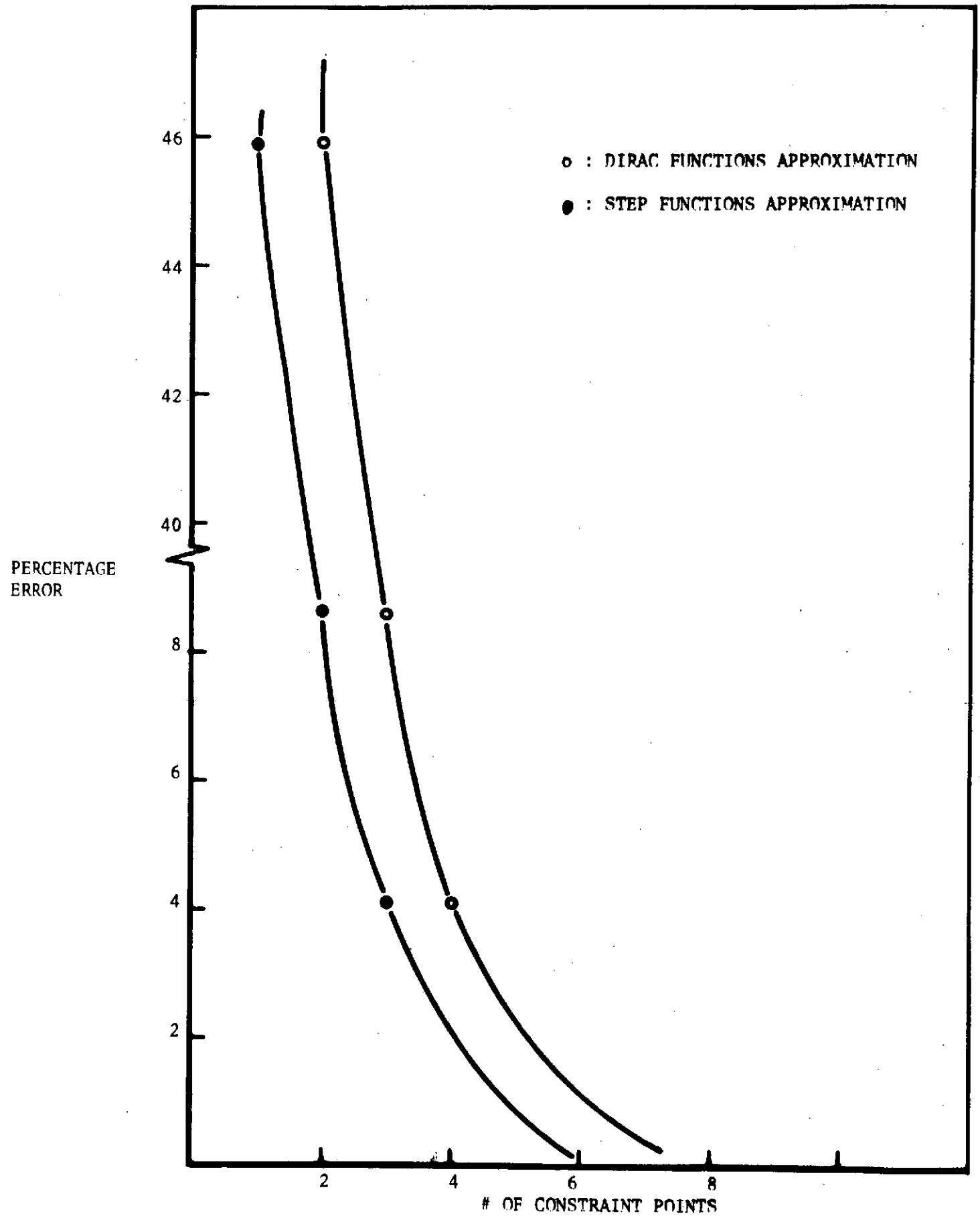

FIGURE 46. - POINT CLAMPED SQUARE PLATE, CONVERGENCE OF THE THIRD NATURAL FREQUENCY TOWARDS THAT OF A CANTILIVERED PLATE

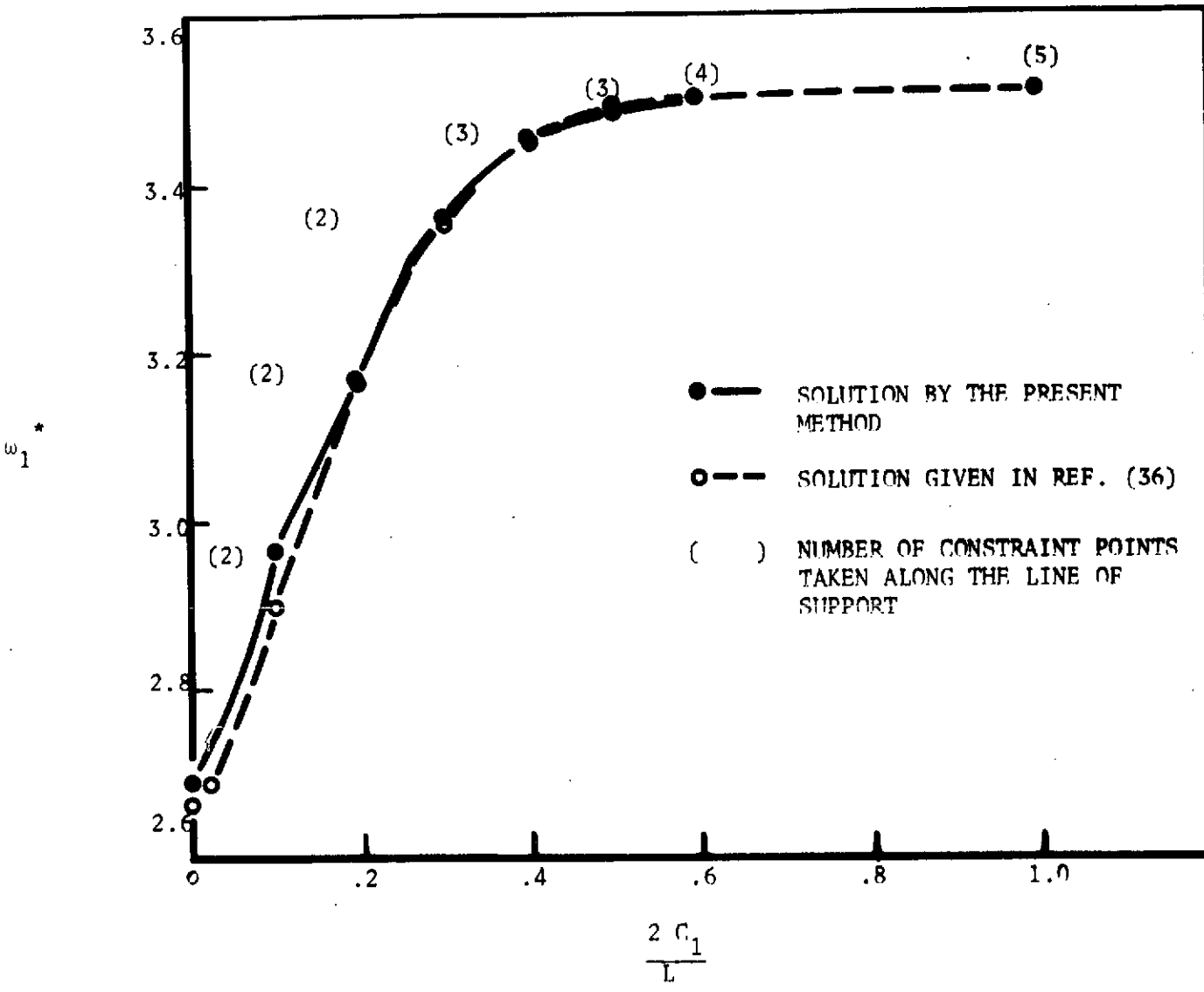

FIGURE 47. - SIMPLY SUPPORTED SQUARE PLATE WITH A LINE OF INTERNAL SUPPORT CHANGE IN THE FUNDAMENTAL FREQUENCY WITH THE SUPPORT LENGTH.

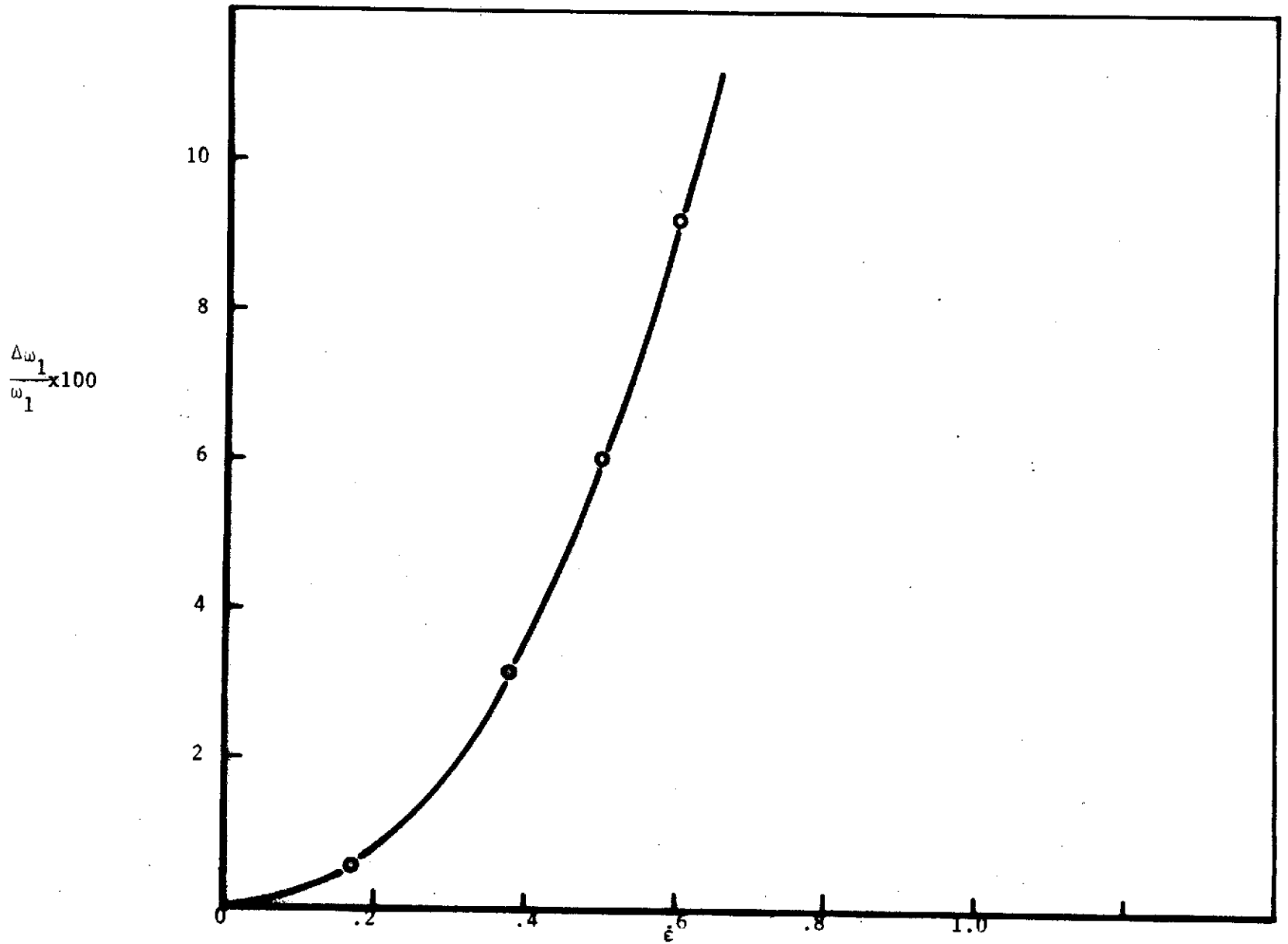

FIGURE 48. - TAPERED CANTILIVER BEAM PENCENTAGE ERROR IN THE FUNDAMENTAL NATURAL FREQUENCY VERSUS ε

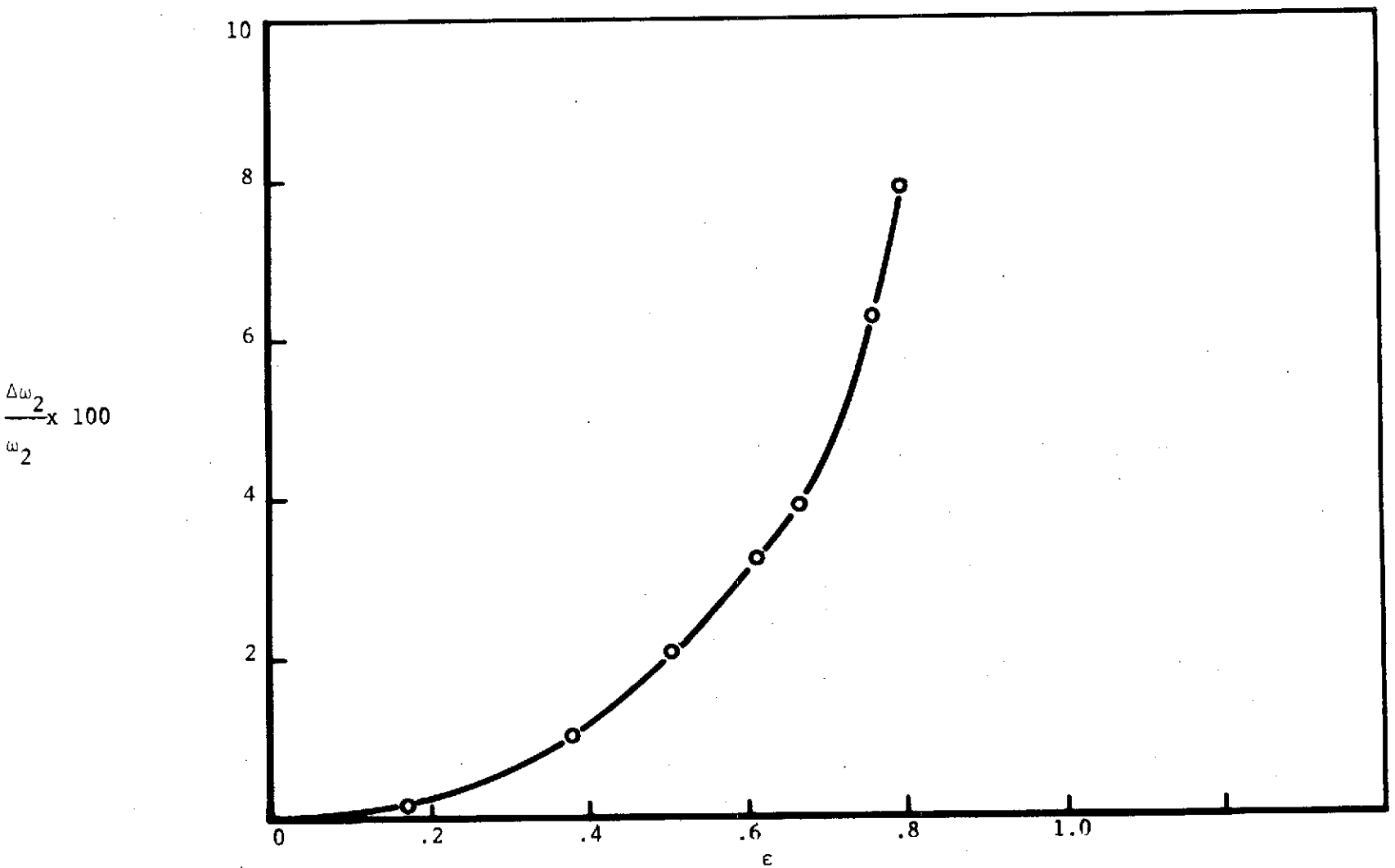

FIGURE 49. - TAPERED CANTILIVER BEAM
PERCENTAGE ERROR IN THE SECOND NATURAL FREQUENCY VERSUS ε

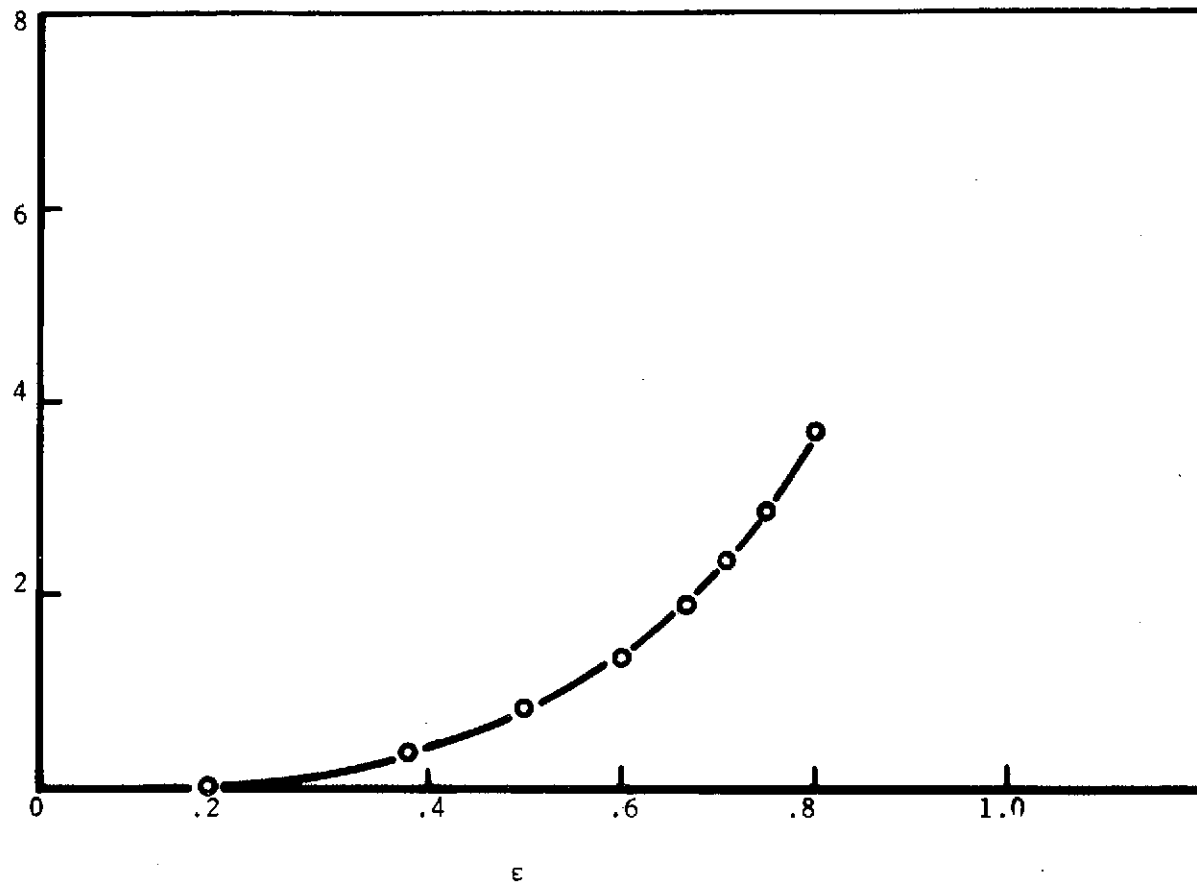

$\frac{\Delta\omega_3}{\omega_3} \times 100$

FIGURE 50. - TAPERED CANTILIVER BEAM

PERCENTAGE ERROR IN THE THIRD NATURAL FREQUENCY VERSUS ε

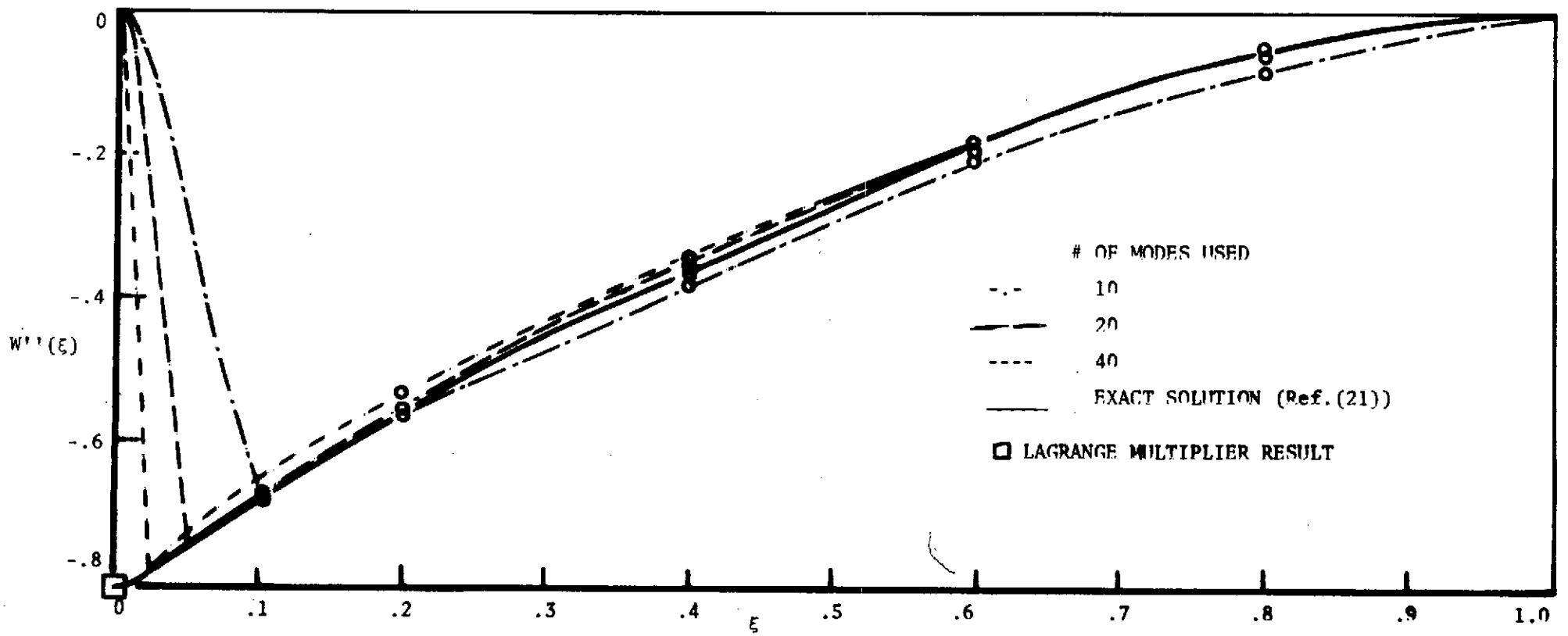

FIGURE 51. - CANTILIVERED BEAM

CONVERGENCE OF THE INTERNAL BENDING MOMENT AT THE POINT OF CONSTRAINT.

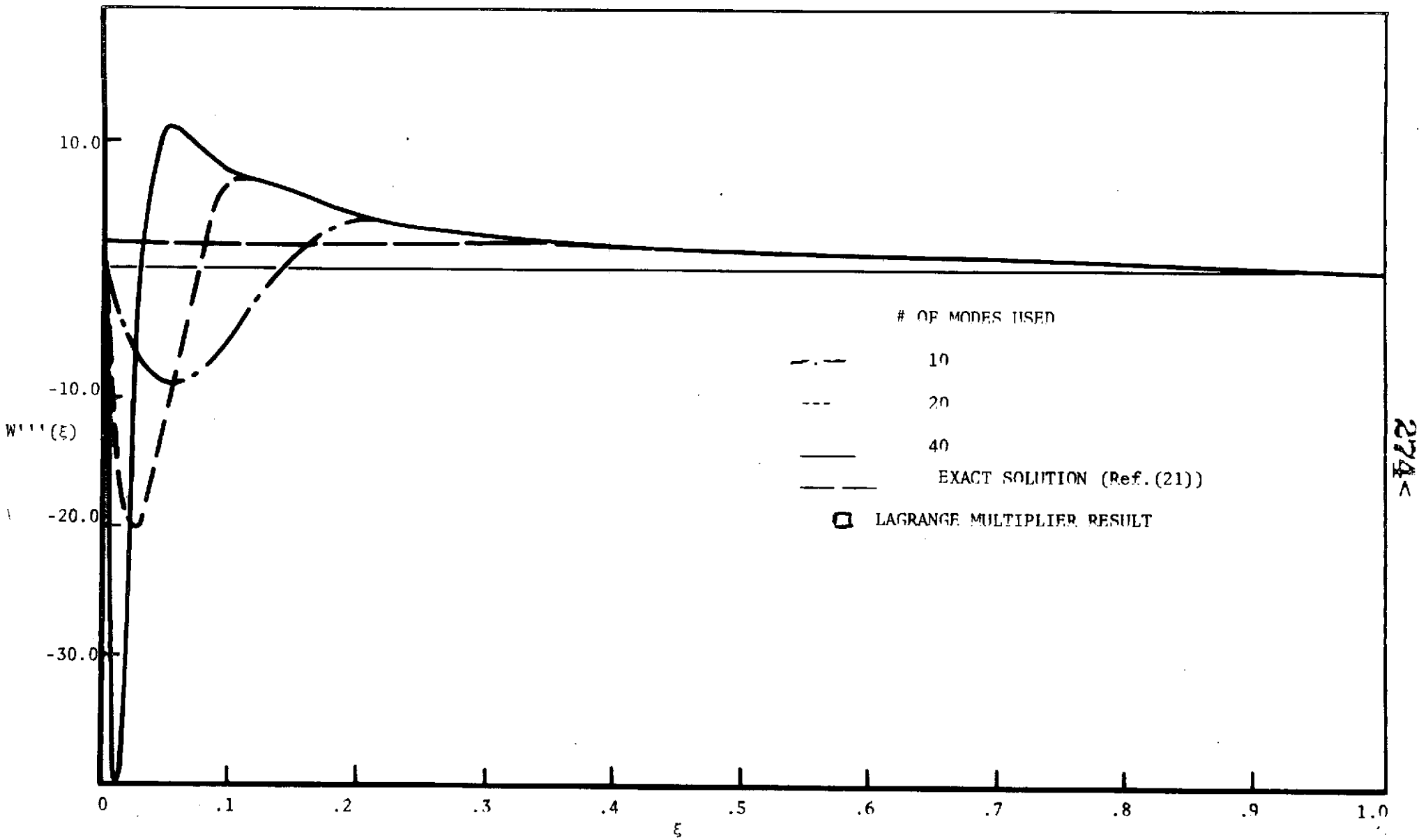

FIGURE 52. - CANTILIVER BEAM

CONVERGENCE OF THE INTERNAL SHEAR FORCE AT THE POINT OF CONSTRAINT.

ABSTRACT

The free vibrations of elastic structures of arbitrary complexity are analyzed in terms of their component modes. The method is based upon the use of the normal unconstrained modes of the components in a Rayleigh-Ritz analysis. The continuity conditions are enforced by means of Lagrange Multipliers. Examples of the structures considered are: beams with non-uniform properties, airplane structures with high or low aspect ratio lifting surface components, the oblique wing airplane as proposed by R.T. Jones, and plate structures.

The method is also applied to the analysis of modal damping of linear elastic structures. Convergence of the method versus the number of modes per component and/or the number of components is discussed; the method is compared to more conventional approaches, to ad-hoc methods for some examples, and to experimental results.